Impact fonctionnel de mutations somatiques dans le gène ERN1 (IRE1*A*LPHA) dans les glioblastomes

Stephanie Lhomond

université de BORDEAUX

THÈSE

PRÉSENTÉE A

L'UNIVERSITÉ DE BORDEAUX

ÉCOLE DOCTORALE DES SCIENCES DE LA VIE ET DE LA SANTE

Par **Stéphanie LHOMOND**

POUR OBTENIR LE GRADE DE

DOCTEUR

SPÉCIALITÉ : Biologie Cellulaire et Physiopathologie

IMPACT FONCTIONNEL DE MUTATIONS SOMATIQUES DANS LE GÈNE ERN1 (IRE1ALPHA) DANS LES GLIOBLASTOMES

Directeur de recherche : **Éric Chevet**

Soutenue le : 25 avril 2014

Devant la commission d'examen formée de :

M. MOENNER Michel	Professeur, Université de Bordeaux	Président du jury
Mme FOUFELLE Fabienne	Directrice de Recherche, INSERM	Rapporteur
M. MANIE Serge	Directeur de Recherche, CNRS	Rapporteur
M. CHEVET Eric	Directeur de Recherche, INSERM	Directeur de thèse

REMERCIEMENTS

Mes travaux de thèse ont été réalisés sous la direction d'Éric Chevet au sein de l'équipe Stress, Organites et cancer, dans l'unité INSERM U1053 dirigée par Jean Rosenbaum.

Je tiens à remercier tous les membres de l'unité INSERM U1053 de m'avoir accompagné durant ces quatre années très enrichissantes, ainsi que toutes les personnes avec qui j'ai eu le plaisir de collaborer, et en particulier Raphaël Pineau.

Je remercie plus particulièrement les membres de l'équipe Stress, Organites et cancer pour leur accueil, leur aide et leur soutien indéfectible. Un grand merci Éric, Saïd, Nicolas, Daniela, Arisa, Esther, Olivier, Néstor et Kim, ainsi que tous mes proches.

Je remercie également les membres du jury qui m'ont fait l'honneur d'évaluer ce travail.

TABLE DES MATIÈRES

TABLE DES ILLUSTRATIONS

TABLE DES ABRÉVIATIONS

α1AT	Alpha 1 anti-trypsine
ADN	Acide désoxyribonucléique
cAMP	cyclic Adenosine monophosphate
ARN	Acide ribonucléique
ARNm	ARN messager
ASK 1	Apoptosis signal-regulating kinase 1
ATF3	Activating transcription factor 3
ATF4	Activating transcription factor 4
ATF6	Activating transcription factor 6
ATG	Autophagy-related genes
ATP	Adenosine triphosphate
Bcl2	B-cell lymphoma 2
BI-1	Bax inhibitor 1
BIP	Binding immunoglobulin protein
Ca^{2+}	Calcium
CBP	CREB binding protein
CBF/NFY	CCAAT-binding factor/nuclear factor-Y
CD59	Cluster of differentiation 59
CFTR	Cystic fibrosis transmembrane conductance regulator
CHC	Carcinome hépatocellulaire
CHOP	C/EBP homologous protein
CMV	Cytomegalovirus
CNX	Calnexine
COP II	Coat protein complex II
CRE	cAMP response element
CREB	CRE binding protein
CRT	Calréticuline
CXCL3	Chemokine (C-X-C motif) ligand 3
DN	Dominant negative
DTT	Dithiothréitol
EDEM	ER degradation enhancing 1,2 mannosidase like protein
EGFR	Epidermal growth factor receptor
eIF2α	Eucaryotic initiation factor 2 α
ER	Endoplasmic reticulum
ERAD	Endoplasmic reticulum associated degradation
ERAF	Endoplasmic reticulum associated folding
Erdj	Endoplasmic reticulum dna J
ERES	Endoplasmic reticulum exit site
ERGIC	ER-golgi intermediate compartment
ERK	Extracellular-signal regulated kinase
ERN1	Endoplasmic reticulum to nucleus protein 1
ERSE	ER stress response element
FAK	Focal adhesion kinase
GADD34	Growth arrest DNA damage inducible protein 34
GAPDH	Glyceraldehyde 3-phosphate dehydrogenase

GBM	Glioblastome multiforme
GRP	Glucose related protein
HRD1	HMG-CoA reductase degradation protein 1
HSP	Heat shock protein
IDH1	Isocitrate dehydrogenase 1
IL-	Interleukine
IP3R	Inositol triphosphate receptor
IRE1α	Inositol required enzyme 1 α
JNK	c-Jun N-terminal kinase
kDa	kilo Dalton
Keap 1	Kelch-like ECH-associated protein 1
KO	Knock out
LC3	Microtubule associated protein 1 light chain 3
LMAN1	Lectine mannose-binding 1
LTP	Lipid transfert proteins
MAM	Mitochondria-associated ER membrane
MEF	Mouse embryonic fibroblast
MDM2	Mouse double minute 2 homolog
NCK1	Non catalytic region of tyrosine kinase adaptator protein 1
NF1	Neurofibromin 1
NHA-TS	Normal human astrocyte (NHA) expressing hTERT (T) and SV40ER (S)
Nrf 2	NF-E2 related factor 2
OASIS	Old astrocyte specifically induced substance
ORP150	Oxygen-regulated protein 150
OS-9	Osteosarcoma amplified 9
OST	Oligosaccharyl transferase
PDGF	Platelet derived growth factor
PDGFR	PDGF receptor
PDI	Protein disulfide isomerase
PDIA6	Protein disulfide isomerase family A, member 6
PER1	Period 1
PERK	Protein kinase (PKR)-like ER kinase
PTEN	Phosphatase and tensin homolog
QC	Quality control
REL	Réticulum endoplasmique lisse
RE	Réticulum endoplasmique
RER	Réticulum endoplasmique rugueux
RhoA	Ras homolog gene family, member A
RIDD	RNA regulated IRE1 dependent decay
RNase	Endoribonucléase
ROS	Reactive oxygen species
RyR	Ryanodine receptor
S1P	Site-1 protease
S2P	Site-2 protease
SERCA	Sarcoplasmic/endoplasmic reticulum calcium ATPase
SNP	Single nucleotide polymorphism
SPARC	Secreted protein acidic and rich in cysteine
Sp1	Stimulating protein 1
SREBP1/2	Sterol regulatory element binding protein 1 and 2
SRP	Signal recognition particle

STAT3	Signal transducer and activator of transcription 3
σ1R	Sigma-1 receptor
TBP-2	Thioredoxin binding protein-2
TMZ	Temolozomide
TP53	Tumor protein p53
TRAF2	Tumor necrosis factor (TNF) receptor associated factor 2
TRAM	Translocation associated membrane protein
TRAP	Translocon associated protein
TXNIP	Thioredoxin-interacting protein
uORF	Upstream open reading frames
UPR	Unfolded protein response
UPRE	UPR response element
UPS	Ubiquitin/proteasome system
VCP	Valosin-containing protein
VDAC	Voltage dependant anion channel
VDUP1	Vitamin-D3 upregulated protein-1
VEGF	Vascular endothelial growth factor
XBP-1	X-box binding protein 1
XBP1s	Spliced form of XBP1

RÉSUMÉ

Titre: IMPACT FONCTIONNEL DE MUTATIONS SOMATIQUES DANS LE GÈNE ERN1 (IRE1ALPHA) DANS LES GLIOBLASTOMES

Dans les cellules eucaryotes, des altérations du microenvironnement cellulaire ou des mutations des protéines de la voie de sécrétion induisent un stress du RE et activent une réponse adaptative nommée UPR. Les signaux intracellulaires associés à l'UPR sont transmis de la lumière du RE vers le noyau par trois protéines transmembranaires dont IRE1α aussi appelée ERN1. Lors d'un stress du RE, IRE1α s'oligomérise, activant ses domaines kinase et endoribonucléase desquelles découle une signalisation intracellulaire complexe. De nombreuses études reliant l'UPR au cancer désignent IRE1α comme un acteur majeur de la tumorigenèse, en particulier dans la croissance et la vascularisation des glioblastomes (GBM), bien que les mécanismes précis mis en jeu restent à déterminer. Des études menées dans notre laboratoire ont identifié deux cibles de l'activité endoribonucléase d'IRE1α (RIDD) : SPARC et PER1, comme effecteurs respectifs des effets pro-migratoire, pro-angiogénique et pro-prolifératif d'IRE1α dans les GBM. De plus, ces dernières années, le séquençage d'IRE1α a permis d'identifier environ cinquante mutations, dont quatre non silencieuses ont été identifiées dans des biopsies de GBM. L'expression de ces quatre mutations, dont A414T identifiée dans le laboratoire, dans les cellules U-87 MG, et l'implantation de ces cellules dans le cerveau de souris a permis de mettre en évidence le rôle pro tumoral de la mutation A414T et le rôle anti-tumoral de la mutation P336L. A414T stabilise les oligomères d'IRE1α, sur-activant les voies de signalisation en aval et conduisant à une croissance plus rapide et une vascularisation plus importante des tumeurs. Ainsi, nos travaux confirment qu'IRE1α est un régulateur central du développement des GBM et pourrait constituer un marqueur pronostic et une cible thérapeutique des GBM.

Mots clés: réticulum endoplasmique, stress, IRE1α, ERN1, cancer, glioblastome

ABSTRACT

Title: IMPACT OF FUNCTIONAL SOMATIC MUTATIONS IN THE GENE ERN1 (IRE1ALPHA) IN GLIOBLASTOMAS

In eukaryotic cells, alterations in the cellular microenvironment or mutations in the protein secretory pathway induce ER stress and activate an adaptive response termed UPR. The intracellular signals associated with UPR are transmitted from the ER lumen to the nucleus by three transmembrane proteins among which IRE1α also called ERN1. During ER stress, IRE1α oligomerizes, activating its kinase and endoribonuclease domains and a downstream complex intracellular signaling. Many studies linking the UPR to cancer point to IRE1α as a major player in tumorigenesis, particularly in the growth and vascularization of glioblastomas (GBM), although the precise mechanisms involved remain to be determined. Studies led in our laboratory have identified two targets of IRE1α endoribonuclease activity (RIDD): SPARC and PER1 as respective effectors of pro–angiogenic, pro-migratory and pro-proliferative effects of IRE1α in GBM. In addition, in recent years, IRE1α sequencing identified around fifty mutations, four of which have been identified in GBM biopsies. The expression of these four mutations, including A414T identified in the laboratory, in the U-87 MG cells, and implantation of these cells into mouse brain has highlighted the pro-tumoral role of the A414T mutation and the anti-tumor role of the P336L mutation. A414T oligomers stabilize IRE1α, over-activating downstream signaling pathways and leading to a faster growth and greater tumor vascularization. Thus, our work confirms that IRE1α is a central regulator of GBM development and may be a prognostic marker and therapeutic target in GBM.

Keywords: endoplasmic reticulum, stress, IRE1α, ERN1, cancer, glioblastoma

INTRODUCTION

I. Introduction générale

A. La voie de sécrétion chez les eucaryotes

La cellule eucaryote est une unité complexe intégrée au sein d'un organisme multicellulaire. Face à des sollicitations extérieures (variations du microenvironnement) ou face à des modifications intrinsèques (différentiation cellulaire), les cellules mettent en jeu de nombreuses voies de signalisation dont l'activation leur permet de s'adapter et ainsi de conserver un équilibre fonctionnel, appelé homéostasie cellulaire [10]. Une des clés du maintien de l'homéostasie des cellules eucaryotes est la compartimentation cellulaire en organites. Ces organites aux propriétés et aux fonctions distinctes augmentent l'éventail de réponses dont la cellule dispose, ce qui lui permet de survivre à un grand nombre de perturbations intracellulaires ou extracellulaires. Parmi ces compartiments le réticulum endoplasmique (RE) joue un rôle central dans le maintien de l'homéostasie cellulaire: en plus d'être le premier compartiment de la voie de sécrétion des protéines, le RE régule les homéostasies calcique, lipidique et redox

Dès les années 1960, la voie de sécrétion a été étudiée chez la levure et les mammifères [10], permettant d'identifier les compartiments qui la compose et leur hiérarchie: la voie de sécrétion débute avec le RE (**Figure 1**, (1)), où les protéines néosynthétisées sont maturées (repliement, N-glycosylation, formation de ponts disulfures intramoléculaires et intermoléculaires, isomérisation de résidus proline). Lorsque ces protéines atteignent une conformation correcte et peuvent échapper aux mécanismes de contrôle-qualité du RE, elles sont exportées vers des compartiments plus tardifs de la voie de sécrétion par l'intermédiaire de vésicules (COPII) (**Figure 1**, (2)). Elles sont alors exportées notamment vers l'appareil de Golgi (**Figure 1**, (3)), où elles finissent leur maturation (N/O-glycosylation, clivage) puis sont amenées par des vésicules de transport jusqu'à leur destination finale (**Figure 1**, (4)).

Dans certains cas, comme lors de carences en nutriments ou en acides gras [11], les protéines de la voie de sécrétion peuvent être dégradées sélectivement par macro-autophagie, fournissant des acides aminés et des acides gras réutilisables par la cellule pour générer de l'ATP et produire de nouvelles protéines [12]. L'autophagie est médiée par l'activation de

protéines ATG (Autophagy related genes), qui permettent l'invagination de membranes en phagophore jusqu'à former des vésicules appelés autophagosomes autour des protéines à dégrader (**Figure 1**, (5)). Les autophagosomes fusionnent ensuite avec les lysosomes (**Figure 1** (6)) dans lesquels les protéines sont hydrolysées [13, 14].

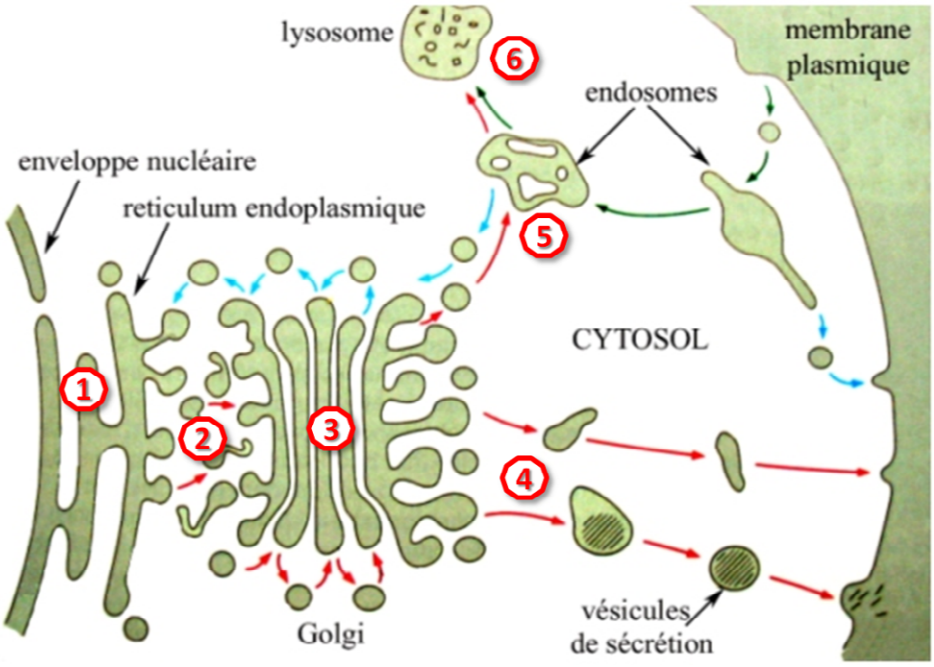

Figure 1: Représentation schématique de la voie de sécrétion chez l'Homme
Adapté d'Alberts et al. 2002.
La voie de sécrétion est constituée du réticulum endoplasmique (RE), de l'appareil de Golgi, des vésicules de sécrétion et des lysosomes. La communication entre ces compartiments est assurée par des vésicules de transport. Les protéines sont synthétisées à la membrane du RE, maturées et repliées dans la lumière du RE puis exportées vers l'appareil de Golgi où elles finissent leur maturation. Elles sont alors exportées vers leur localisation finale, soit par un flux rétrograde vers le RE ou les vésicules, soit vers la membrane plasmiques *via* les vésicules de sécrétion, soit vers les lysosomes pour dégradation.

B. Le RE, premier compartiment de la voie de sécrétion

La membrane du RE, en continuité avec la membrane nucléaire, constitue un réseau de tubules et de saccules arrangés en domaines ayant des fonctions distinctes, dont les principaux sont le REL (Réticulum Endoplasmique Lisse) et le RER (Réticulum Endoplasmique Rugueux).

Bien que tous les domaines du RE contiennent globalement les mêmes protéines, ils sont enrichis spécifiquement en protéines leur permettant d'assurer leurs fonctions propres soit la biosynthèse protéique, la biosynthèse lipidique, la détoxification des substances hydrophobes et le stockage du calcium [15]. Cette sous-compartimentalisation dépend de l'adressage spécifique à ces domaines, par des mécanismes encore inconnus, de protéines capables d'assurer les fonctions de chacun de ces domaines [16]. Elle dépend également du positionnement de ces domaines par rapport aux autres organites de la cellule tels que le noyau **(Figure 2** (1)), la mitochondrie (**Figure 2** (2)), les lysosomes, l'appareil de Golgi (**Figure 2** (3)), et la membrane plasmique (**Figure 2** (4)), avec lesquels le RE interagit étroitement (**Figure 2**).

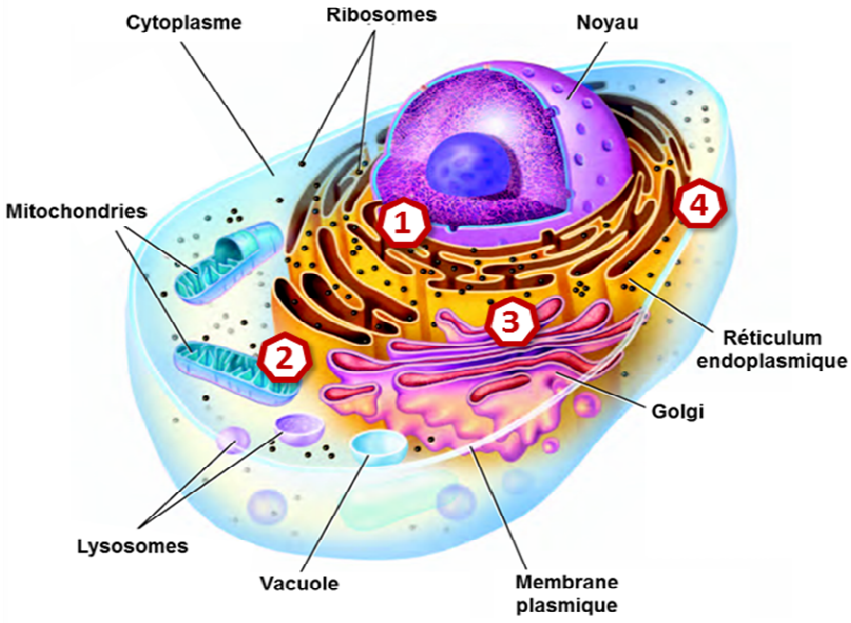

Figure 2 : Représentation schématique des organites d'une cellule humaine.
Position centrale du RE par rapport aux autres organites.

II. Les machines moléculaires du RE

A. Les principales fonctions du RE

1. Stockage du calcium

Le calcium (Ca^{2+}) est un ion intracellulaire essentiel à la physiologie humaine, qui est impliqué dans de nombreuses fonctions biologiques, notamment dans la régulation du développement embryonnaire ou de la contractilité cardiaque, dans l'apprentissage et la mémoire [17]. La concentration calcique doit pour cela être contrôlée de façon très précise, dans le temps et dans l'espace. Ainsi la signalisation calcique met en jeu un nombre important de protéines capables de fixer le Ca^{2+}, de pompes et d'échangeurs qui agissent en synergie [18].

Le RE est le compartiment principal de stockage du calcium intracellulaire: pour une concentration calcique moyenne de 0,1 µM dans le cytosol, le RE à une concentration calcique moyenne de 300 - 400 µM, qui peut atteindre 1 mM [19]. Dans la lumière du RE, ce Ca^{2+} est majoritairement lié à des protéines (calréticuline, calnexine, GRPs (Glucose related protein)), qui ont une grande capacité à lier le Ca^{2+} malgré une affinité relativement faible [20]. Cette différence de concentration en Ca^{2+} entre le RE et le reste de la cellule est essentielle au bon fonctionnement de nombreuses protéines du cytosol et du RE, et permet le relargage rapide et modulable du Ca^{2+} dans le cytosol en réponse à des stimuli. Ainsi, l'homéostasie calcique du RE est primordiale pour de nombreuses fonctions cellulaires telles que la transduction des signaux, la sécrétion et la motilité. En outre, le RE collabore étroitement avec les mitochondries pour le contrôle de l'apoptose et de la survie cellulaire au niveau de sous-domaines du RE appelés « mitochondria-associated ER membranes » (MAM) (**Figure 3**): le rapprochement physique entre ces deux compartiments assure une entrée rapide et durable de Ca^{2+} dans la mitochondrie, principalement via la pompe calcique VDAC (Voltage-dependent anion channel) et le recepteur σ1R (Sigma-1 receptor) [21, 22].

Le relargage de Ca^{2+} dans le cytosol est contrôlé par l'activation de deux récepteurs canaux: le récepteur à la ryanodine (RyR) et le récepteur à l'inositol triphosphate (IP3R) [23]. Au contraire, l'entrée de Ca^{2+} dans le RE est assurée par l'action de pompes ioniques SERCA (Sarcoplasmic/endoplasmic reticulum calcium ATPase) [24]. L'utilisation de drogues inhibant

les pompes SERCA, telles que la thapsigargine, empêche la recapture du Ca^{2+} présent dans le cytosol, provoquant de graves dysfonctions cellulaires.

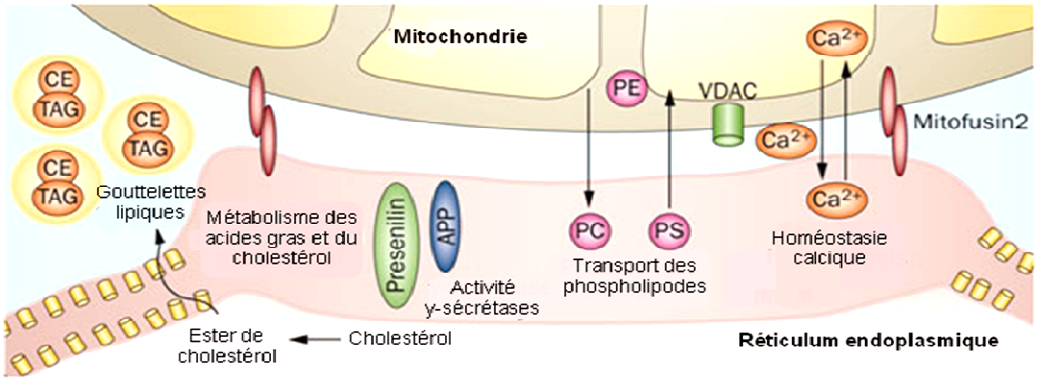

Figure 3 : Représentation schématique des MAM
Adapté de DiMauro et al, 2013 [4]
Le RE communique avec les mitochondries via des zones de rapprochement membranaire: les MAM (mitochondria-associated ER membrane). Ce sous-domaine du RE a des caractéristiques particulières, comme des radeaux lipidiques ou des protéines de rapprochement à la mitochondrie telles que la mitofusine 2 et le récepteur σ1R. Ces caractéristiques font des MAM des zones de régulation de la synthèse de lipides (cholestérol, phospholipides) et d'échanges calciques entre le RE et la mitochondrie.
PC, phosphatidylcholine; PE, phosphatidylethanolamine; PS, phosphatidylserine; TAG, triacylglycerol, VDAC, voltage-dependent anion-selective channel.

2. Biosynthèse des lipides et dérivés lipidiques

Le REL est le sous-compartiment du RE impliqué dans la biosynthèse des phospholipides qui constituent les membranes internes de la cellule et la membrane plasmique, en association avec l'appareil de Golgi. Les précurseurs cytosoliques solubles sont assemblés au niveau de la couche cytosolique de la membrane du REL puis des enzymes de transfert, appelées flippases, permettent aux phospholipides synthétisés de basculer d'un feuillet membranaire à l'autre, jusqu'à former une bicouche lipidique au niveau du REL [25].

Les membranes ainsi synthétisées, contenant par exemple des sphingolipides et des glycérophospholipides, forment des vésicules de transport qui leur permettent d'être transportées sur de longues distances, vers les organites de destination (appareil de Golgi, endosomes, lysosomes, membrane plasmique) [26, 27].

Il existe un deuxième système de transport qui concerne les sites de contacts membranaires entre le RE et les compartiments voisins, comme par exemple les MAM **(Figure 3)**: les lipides néosynthétisés ont alors pour destination une membrane jouxtant le RE, distante de moins de 10 nm [28-30]. Ces lipides sont rapidement transférés entre les deux membranes juxtaposées à l'aide de protéines capables de distinguer la membrane donneuse de la membrane réceptrice: les LTP (Lipid transfer proteins) [31].

Dans le cas des cellules sécrétrices de dérivés lipidiques tels que les hormones stéroïdiennes (cellules cortico-surrénaliennes ou les cellules endocrines des gonades, etc.), le REL est abondant et assure une synthèse *de novo* de cholestérol, notamment *via* l'activation des facteurs de transcription SREBP (Sterol regulatory element binding proteins). Ces facteurs de transcription sont synthétisés sont forme de précurseurs inactifs car ancrés dans la membrane du RE par des complexes protéiques capables de lier les stérols (SCAP, INSIG1, INSIG2) [32-36]. Lors d'une déplétion en cholestérol, le complexe SCAP/SREBP est pris en charge par les vésicules COPII et exporté vers l'appareil de Golgi où SREBP est clivé par les protéases S1P et S2P [35], libérant la partie cytosolique du précurseur, qui constitue le facteur de transcription actif [32, 33]. La libération de SREBP peut également être induit par l'intervention des caspases 3 et 7 [37, 38]. SREBP active alors la transcription de gènes cibles impliqués dans la lipogenèse, à l'aide de co-activateurs tels que CBP (CREB binding protein), CBF/NFY (CCAAT-binding factor/nuclear factor-Y) et Sp1 (Stimulating protein 1) [39, 40].

Dans ces cellules, le cholestérol synthétisé dans le RE est alors exporté vers la membrane interne de la mitochondrie qui contient des cytochromes de la famille P450 capables d'hydroxyler le cholestérol en prégnénolone [41]. Le prégnénolone est le précurseur commun aux cinq classes d'hormones stéroïdiennes (œstrogène, progestérone, androgènes, minéralocorticoïdes (aldostérone) et glucocorticoïdes (cortisol)) [42]. Une fois synthétisé dans la mitochondrie, ce précurseur est ensuite maturé soit dans la mitochondrie soit dans le RE [43].

Une fonction ubiquitaire du cholestérol est également de modifier les caractéristiques des membranes cellulaires, que ce soit leur fluidité ou le positionnement des protéines dans le feuillet membranaire. Ainsi, lorsque le cholestérol poursuit sa route dans la voie de sécrétion jusqu'à la membrane plasmique, il peut être impliqué dans la signalisation cellulaire par la formation des radeaux lipidiques propices à la concentration de récepteurs membranaires [44]. Des boucles de rétrocontrôle entre la membrane plasmique et le RE régulent alors la

production de cholestérol, une diminution du cholestérol au niveau des membranes ayant pour conséquence d'activer SREBP et la production de cholestérol.

3. Fonctions spécialisées du RE

Du fait de son rôle central dans la physiologie de la cellule, le RE est un compartiment adaptatif dynamique, dont l'homéostasie est finement régulée. Ainsi, selon la spécialisation fonctionnelle de la cellule et/ou son activité métabolique, les composants du RE peuvent varier. C'est le cas notamment du RE dans les cellules sécrétrices (lymphocytes B, cellules β pancréatiques) qui peut représenter jusqu'à 60% de la surface membranaire de la cellule [11].

Le RE des cellules musculaires, appelé réticulum sarcoplasmique, a une capacité de mobilisation du calcium très développée. Ceci permet d'assurer une signalisation calcique rapide et réversible indispensable à la contraction et à la décontraction des cellules musculaires [45].

De même, les cellules rénales ou les hépatocytes ont un REL performant pour la détoxification par hydroxylation de composés organiques très divers (métabolites cytosoliques, xénobiotiques). Un système d'oxygénases, qui comprend notamment la famille des cytochromes P450, hydroxyle ces composés ce qui augmente leur solubilité et permet ainsi leur élimination [46].

4. Biogenèse des protéines de la voie de sécrétion

Les protéines qui transitent par la voie de sécrétion représentent environ 30% des protéines produites par la cellule [14]. Ces protéines sont traduites au niveau de ribosomes attachés à la face cytosolique de la membrane du RE et pénètrent, au cours de leur synthèse, dans la lumière du RE via un canal protéique appelé translocon.

Une fois entrées dans le RE, les protéines sont prises en charges par des machineries protéiques qui assurent leur bon repliement (**Figure 4**: ERAF) puis leur export vers les compartiments suivants de la voie de sécrétion (**Figure 4**: Export), ou à défaut vers le protéasome pour dégradation (**Figure 4**: ERAD).

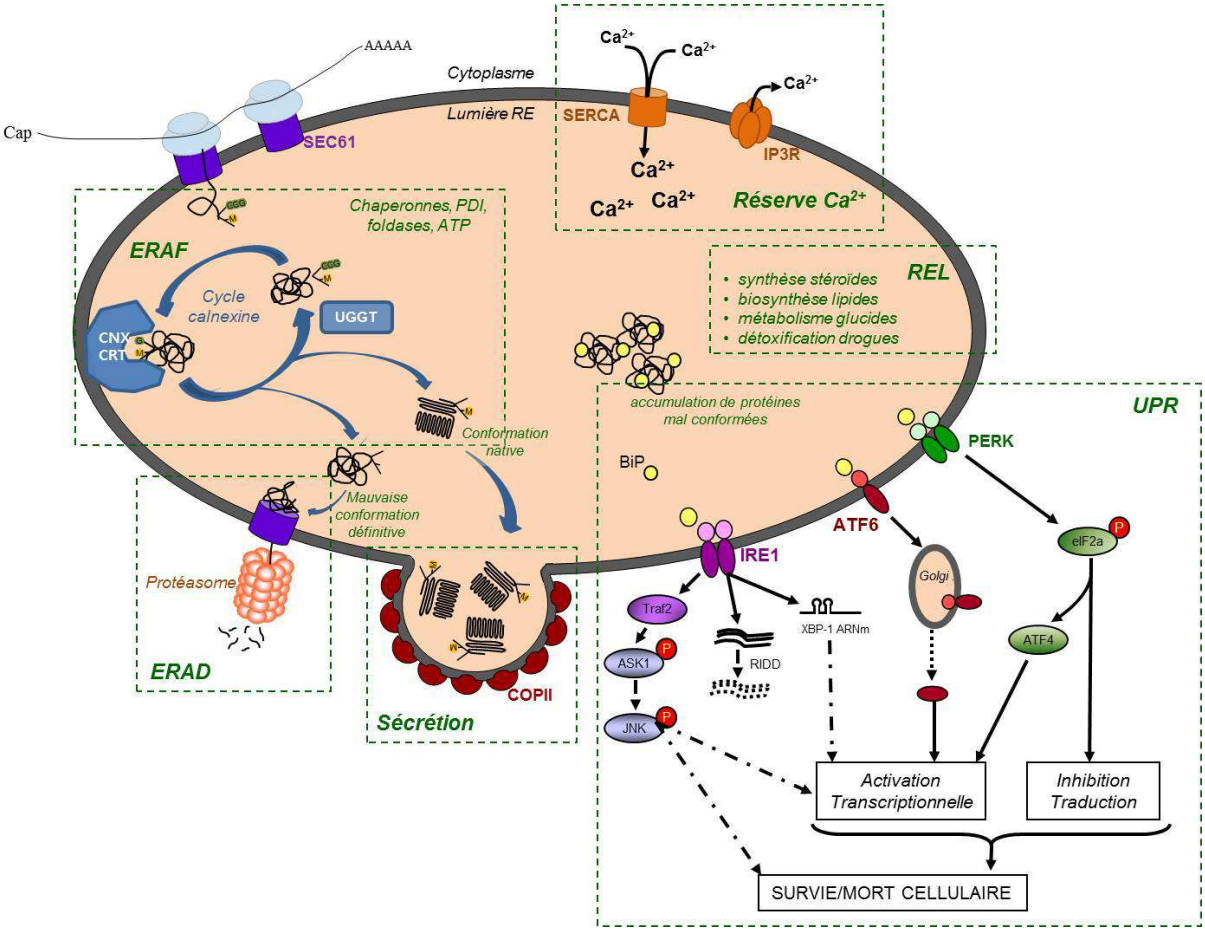

Figure 4: Les fonctions principales du réticulum endoplasmique (RE)

Le RE assure la synthèse de lipides et de stéroïdes dans le REL (RE lisse), le stockage de calcium grâce aux pompes calciques SERCA et la synthèse de protéines dans le RER (RE rugueux). Dans le RER, les protéines néosynthétisées entrent dans la lumière du RE à travers un translocon, puis sont prises en charge par le système de repliement des protéines (ERAF: ER associated folding). Les protéines correctement conformées sont acheminées vers le reste de la voie de sécrétion grâce à des vésicules, tandis que les protéines mal conformées sont prises en charge par le système ERAD (ER associated degradation). Une défaillance de ce système de synthèse, de repliement et d'export des protéines aboutit à l'accumulation de protéines mal conformées dans la lumière du RE et déclenche l'UPR (Unfolded protein response), soit l'activation d'une ou plusieurs des protéines PERK, ATF6 et IRE1. L'UPR résorbe l'accumulation des protéines mal conformées ou, le cas échéant, conduit à la mort de la cellule.

B. La maturation des protéines dans le RE

1. Translocation des protéines dans le RE

Les protéines entrant dans la voie de sécrétion possèdent pour la plupart en début de séquence, un signal d'adressage au RE: le peptide signal. Dès la synthèse de ce peptide, une protéine vient s'y fixer et ainsi arrêter la traduction : la « Signal Recognition Particule » (SRP). Le complexe ARNm/SRP/ribosome/chaîne polypeptidique naissante s'attache à la face cytosolique de la membrane du RE en interagissant avec des protéines membranaires telles que le récepteur à la SRP ou le complexe « Translocation associated proteins » (TRAP). Un canal protéique appelé translocon se forme alors et permet l'entrée dans la lumière du RE du polypeptide en cours de synthèse (**Figure 5**). Le translocon est un canal aqueux principalement composé des complexes Sec61 impliqués dans l'ancrage des ribosomes à la membrane du RE [47-51]. Selon que les protéines synthétisées sont solubles ou membranaires, leur translocation diffère: les domaines hydrophobes des protéines transmembranaires sont insérés dans la membrane du RE au fur et à mesure de la synthèse de la protéine, grâce à une ouverture du translocon vers la bicouche lipidique. Les séquences dont les caractéristiques (longueur, hydrophobicité) sont adéquates, s'ancrent par affinité dans la membrane du RE [52, 53]. La sous-unité 28S des ribosomes est séparée d'environ 1,5 nm de la partie cytosolique du complexe Sec61. C'est cet espace qui permet le passage des domaines cytosoliques qui jouxtent les domaines hydrophobes des protéines transmembranaires.

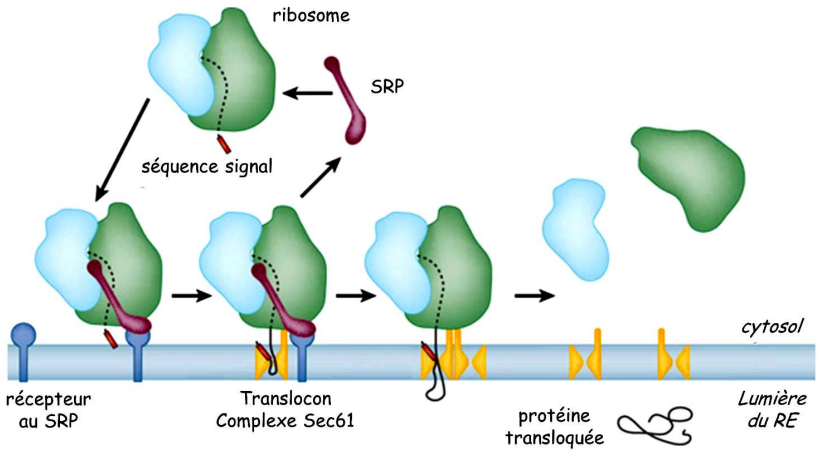

Figure 5 : Schéma de translocation d'une protéine naissante soluble.

2. Maturation et repliement des protéines dans le RE

L'ERAF (Endoplasmic reticulum associated folding) représente l'ensemble des acteurs impliqués dans le repliement des protéines néosynthétisées. Il comprend le translocon, canal protéique par lequel les polypeptides en cours de synthèse pénètrent dans la lumière du RE, les enzymes qui se lient à la protéine néosynthétisée (oligosaccharyl-transférase, protein-disulfure isomérases, etc.) ainsi que les enzymes de repliement ou foldases (calnexine, calréticuline). Lors de sa translocation, après clivage du SRP, la protéine naissante est prise en charge par des enzymes de modification post-traductionnelle comme l'OST (Oligosaccharyl-transferase) qui transfère des sucres sur les groupements amine libres (N-glycosylation) et les PDI (Protein disulfide isomerase) qui forment des ponts disulfures.

Ces modifications post-traductionnelles, qui concernent la majorité des protéines de la voie de sécrétion, permettent aux protéines d'être correctement repliées, c'est-à-dire d'acquérir une conformation tridimensionnelle de moindre énergie. Ce repliement peut s'effectuer spontanément ou nécessiter l'aide de foldases (calnexine, calréticuline) ou de chaperonnes (BiP, GRPs, HSPs (Heat Shock Proteins), oxydoréductases), qui, en se liant aux protéines néosynthétisées, fournissent un environnement favorable à leur repliement, notamment en masquant des séquences hydrophobes qui provoqueraient autrement l'agrégation des protéines ou en les rapprochant des protéines de modification post-traductionnelle.

Les protéines néosynthétisées sont retenues dans lumière du RE jusqu'à ce que le contrôle qualité (QC ; Quality control) l'étiquette comme protéine ayant atteint sa conformation de moindre énergie et l'envoie vers la machinerie d'export (

Figure 6). Si la protéine est étiquetée comme mal conformée, elle sera au contraire adressée à la machinerie de dégradation ERAD (Endoplasmic reticulum associated degradation), afin de limiter la production de macromolécules aberrantes. Il existe deux systèmes de contrôle qualité: un qui prend en charge les protéines glycosylées et fait intervenir les foldases à site lectine (calnexine et calréticuline), et un qui prend en charge les protéines non-glycosylées [54]. Si le premier système est bien connu [55], peu d'informations sont disponibles sur le fonctionnement du deuxième, qui implique probablement des chaperonnes comme GRP94 ou BiP [56].

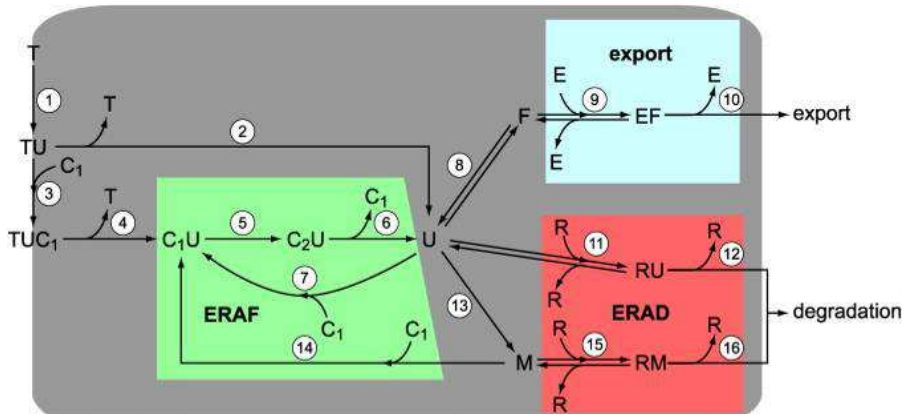

Figure 6: Modélisation des protéines dans le RE
Wiseman et al. 2007 [5].
L'homéostasie des protéines présentes dans la lumière du RE (gris) résulte d'un équilibre énergétique définissant les interactions entre la machinerie de repliement des protéines (ERAF, vert), et les machineries d'export (ERAD, rouge et Export, bleu).

3. Export des protéines hors du RE

a) Export des protéines bien conformées dans la voie de sécrétion

Lorsque les protéines échappent au QC, elles se concentrent dans des sous-domaines du RE appelés ERES (Endoplasmic reticulum exit site) [57]. Les protéines bien conformées ou "cargo" sont exportées vers l'appareil de Golgi avant d'être adressées à leur compartiment de destination. Pour cela, elles interagissent avec le système d'export, qui comprend des protéines chaperonnes, des protéines récepteurs de cargo et des protéines impliquées dans le bourgeonnement des vésicules de transport (COPII, Coat protein complex II) [10, 57, 58], comme schématisé sur la **Figure 7** ci-après.

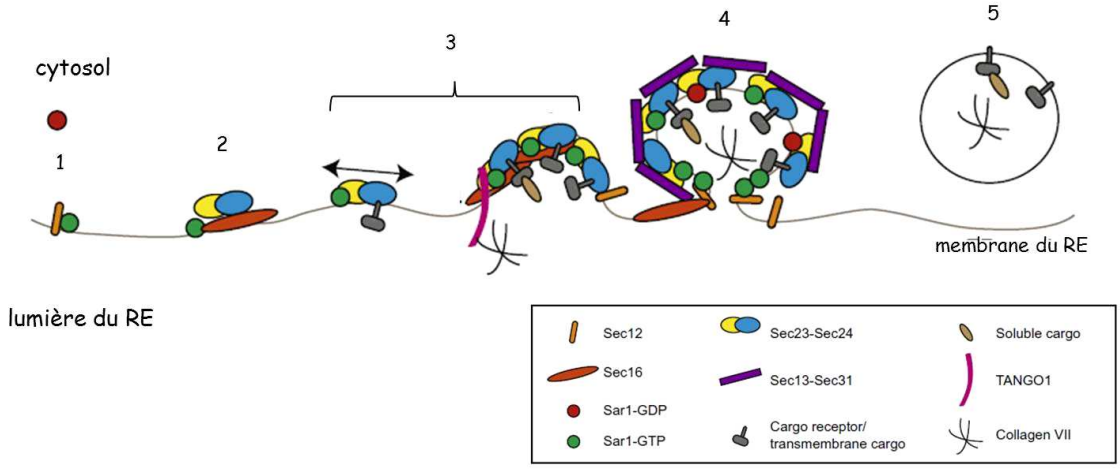

Figure 7: Représentation schématique de la formation des vésicules COPII
Adapté de Budnik and Stephens 2009 [3].

b) Export et dégradation des protéines définitivement mal conformées

Au contraire, si la protéine ne peut atteindre sa conformation native, elle est dite définitivement mal conformée, et spécifiquement adressée à un système de dégradation, ce qui évite l'accumulation de protéines mal conformées dans la lumière du RE, accumulation qui pourrait compromettre la fonction de l'organite. Les protéines mal conformées semblent majoritairement dégradées par le système ERAD, mais certains complexes comme les agrégats protéiques peuvent être dégradés par macro-autophagie: les protéines se regroupent au niveau d'un sous-domaine du RE: l'omégasome, à partir duquel elles sont dirigées vers les phagophores qui maturent en autophagosomes. Les autophagosomes fusionnent ensuite avec les lysosomes pour former des autophagolysosomes où les protéines sont dégradées.

La machinerie ERAD est, comme les autres machines moléculaires du RE, finement régulée par de nombreuses protéines du RE ou du cytosol, afin de maintenir l'homéostasie du RE. Elle est principalement constituée de chaperonnes et de protéines du RE mais aussi de protéines membranaires ou cytoplasmiques qui contrôlent le rapatriement des protéines à dégrader vers le cytosol, et en particulier vers le système principal d'élimination des protéines de la cellule: l'« Ubiquitin/proteasome system » (UPS) [59, 60]. Cette dégradation des protéines mal conformées passe par quatre étapes successives (**Figure 8**).

La première étape est la reconnaissance du substrat, qui fait intervenir les lectines OS-9 et XTP3B capables de se lier aux protéines à dégrader, soit par reconnaissance des protéines chaperonnes associées à la protéine mal conformée (BiP, GRP94), soit par reconnaissance de motifs de glycosylation spécifiques [2, 61, 62]. Le complexe contenant la protéine à dégrader, OS-9 et XTP3B est alors dirigé vers un canal protéique appelé dislocon, qui permet à la protéine d'être exportée vers le cytosol et rapidement dégradée.

Puisque la majorité des protéines à dégrader présentent des zones hydrophobes, il est important que leur dégradation se fasse aussitôt après leur translocation. Pour cela, les complexes d'ubiquitination sont directement associés au dislocon et les protéines mal conformées sont très rapidement ubiquitinées et prises en charge par la chaperonne cytosolique p97, dont le rôle est central puisqu'elle fournit l'énergie nécessaire à la dislocation de la protéine puis guide celle-ci lors de sa dislocation et de son ubiquitination et enfin la dirige vers le protéasome [2].

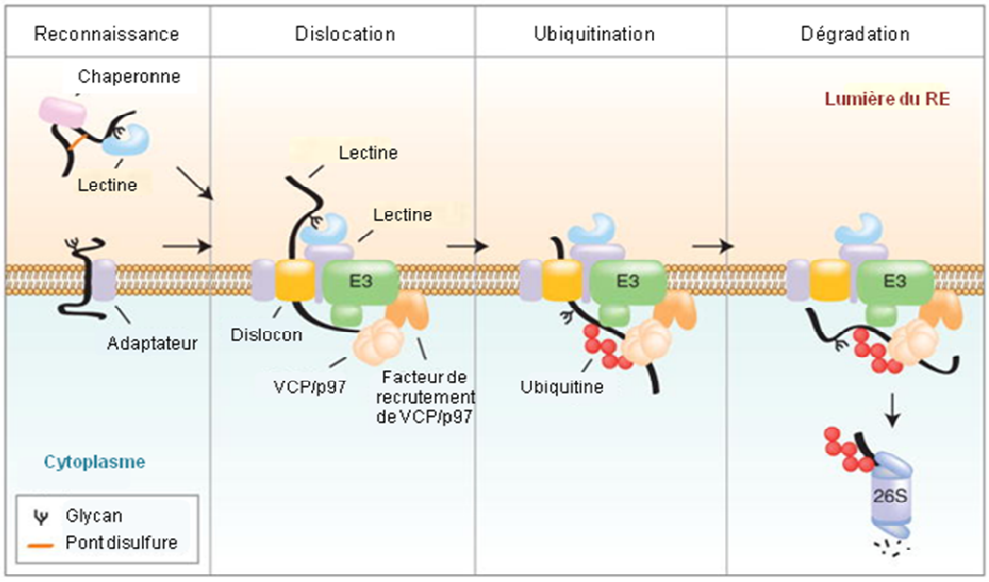

Figure 8 : Schéma récapitulatif des différentes étapes du système ERAD
Adapté de Olzmann JA, Kopito RR, Christianson JC, 2013 [2].
Les protéines reconnues comme mal conformées par le QC sont adressées au complexe de dislocation (1), exportées vers le cytosol (2), ubiquitinées (3) puis reconnues et dégradées par le protéasome (4).

Comme nous l'avons vu précédemment, les capacités de repliement des protéines du RE dépendent de l'activité des protéines composant les machineries de repliement (ERAF, QC, ERAD et export). Ainsi, l'état oxydant du RE, donc le statut redox de la cellule, et la quantité d'oxygène, de glucose, de calcium et d'ATP disponibles, sont autant de paramètres qui affectent la formation des ponts disulfures ou des N-glycans, donc les capacités du RE à replier correctement les protéines de la voie de sécrétion [15]. Si un de ces paramètres change, l'homéostasie du RE est perturbée, ce qui déclenche des voies de signalisation adaptatives depuis la lumière du RE, qui visent à rétablir cette homéostasie. Une des réponses adaptatives du RE est l'UPR, détaillée ci-après. Cette réponse est médiée par trois protéines transmembranaires: IRE1α, PERK et ATF6 (**Figure 9**).

C. Signalisation émanant du RE: l'UPR (Unfolded Protein Response)

L'UPR est une réponse adaptative de la cellule, déclenchée par l'accumulation de protéines mal conformées au sein du RE. Cette accumulation de protéines mal conformées génère un stress appelé stress du RE, qui découle d'un déséquilibre entre la quantité de protéines à replier et la capacité du RE à replier ou à exporter ces protéines. Ce stress dépend ainsi de quatre paramètres: **i)** la quantité de protéines à replier qui dépend des besoins en protéines de la cellule ou de la présence de mutations conformationnelles; **ii)** l'efficacité de la machinerie de repliement (ERAF), dépendant de la quantité et l'efficacité des protéines chaperonnes, du statut redox et des taux de glucose et d'oxygène; mais aussi **iii)** de la machinerie d'export des protéines correctement repliées, dépendant des protéines et des membranes des vésicules d'export; et **iv)** de la machinerie de dégradation des protéines associée au RE (ERAD), dépendant des molécules d'export et de dégradation.

Ces paramètres peuvent être altérés dans de nombreuses conditions physiologiques (cicatrisation, production d'insuline) ou pathologiques (infection virale, chimiothérapies). En effet, l'accroissement des besoins, en énergie, en acides aminés ou en protéines, mais aussi les modifications du milieu extracellulaire, dues à une hypoxie, une inflammation, ou la présence de virus ou d'agents de chimiothérapie sont autant de situations suscitant un stress du RE et déclenchant ainsi l'UPR. Les voies de signalisation alors activées visent à rétablir l'homéostasie du RE notamment en atténuant la traduction générale de protéines et en activant spécifiquement la transcription de protéines impliquées dans le repliement des protéines (**Figure 9**). Lorsque l'homéostasie du RE ne peut être rétablie, l'UPR bascule d'une réponse de survie cellulaire à une réponse de mort cellulaire (II**.C.3** ci-dessous).

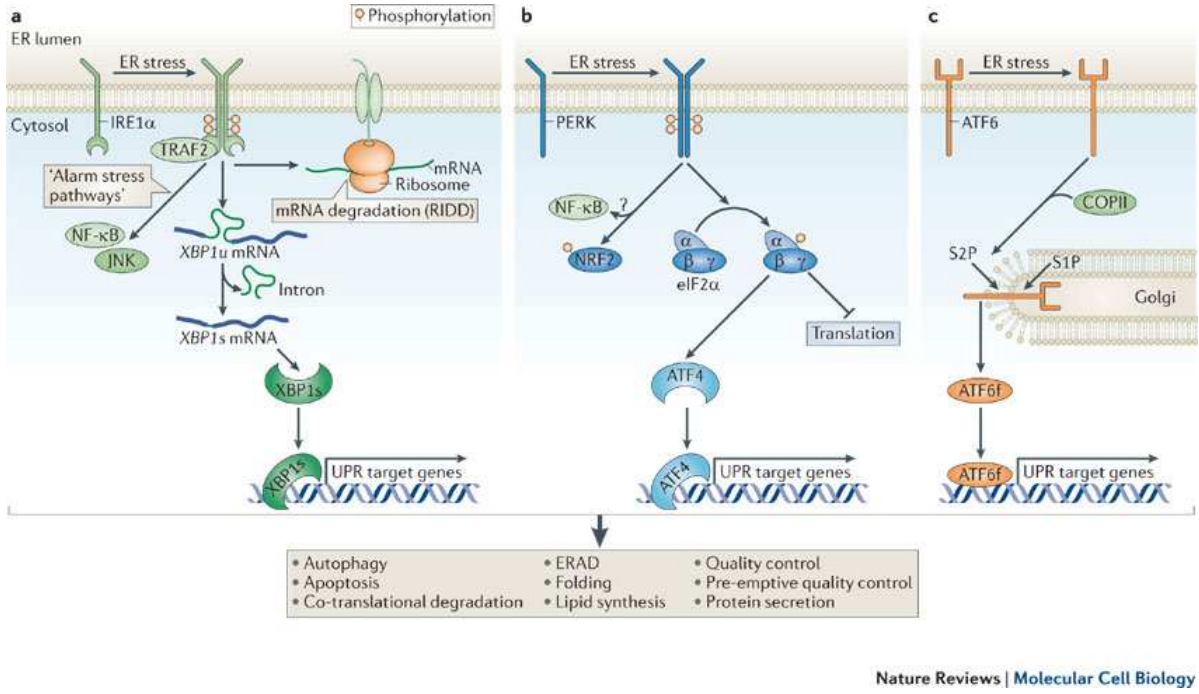

Figure 9 : Schématisation des principaux acteurs de l'UPR
Hetz, 2012 [6].
Le stress du RE déclenche une réponse adaptative, l'UPR, en activant trois protéines transmembranaires du RE: IRE1α, PERK et ATF6. Les conséquences de l'UPR sont principalement l'induction de l'expression de nombreux gènes qui sont notamment impliqués dans les machines moléculaires du RE (ERAF, QC, ERAD, export, synthèse de lipides et sécrétion de protéines) et dans le contrôle de la mort cellulaire (autophagie, apoptose).

1. Les effecteurs de l'UPR: PERK, ATF6 et IRE1α

L'UPR est initiée par trois protéines transmembranaires du RE: la protéine kinase PERK (PKR-like ER kinase), le facteur de transcription ATF6 (Activating transcription factor 6) et la protéine IRE1α (Inositol requiring enzyme 1 α) aussi appelé ERN1 (Endoplasmic reticulum to nucleus signaling 1). Chez les mammifères, en condition de stress, certains de leurs partenaires luminaux (par exemple BiP (Binding immunoglobulin protein)) se dissocient de ces trois protéines, permettant ainsi leur activation. Les trois voies de l'UPR sont redondantes pour l'expression de certaines protéines cibles comme les protéines chaperonnes BiP et GRP94 (Glucose-regulated protein of 94 kDa), et elles sont coopératives pour d'autres, comme par exemple pour l'activation de XBP1 (X-box binding protein 1), dont la transcription dépend d'ATF6 et la maturation d'IRE1α. De plus, ces trois voies sont activées à

une vitesse et pour une durée différentes ce qui permet, chez les mammifères, d'avoir une réponse intégrée très finement régulée [6, 8].

La protéine serine/thréonine kinase PERK est une protéine transmembranaire monomérique. En réponse à un stress du RE, plusieurs protéines PERK s'assemblent ce qui permet le rapprochement de leurs domaines et ainsi leur trans-autophosphorylation. L'oligomérisation et la phosphorylation de PERK entraînent la phosphorylation de ses substrats, dont le principal est la sous-unité régulatrice du facteur d'initiation de la traduction: eIF2α (eucaryotic Initiation Factor 2α). eIF2α phosphorylé ne peut plus s'intégrer dans le complexe d'initiation de la traduction, atténuant instantanément la synthèse de la majorité des protéines, celles dont la synthèse dépend de la coiffe [63]. Cette inhibition rapide de la traduction est la première phase de l'UPR et permet de réduire le flux de protéines entrant dans la lumière du RE. En conséquence de cette inactivation globale de la synthèse protéique, il y a une activation ciblée de la traduction de certains ARN messagers (ARNm), comme par exemple l'ARNm du facteur de transcription ATF4 (Activating transcription factor 4) [64]. ATF4 va ensuite activer la transcription de nombreux gènes codant pour des protéines qui vont à leur tour réguler l'homéostasie du RE, dont par exemple CHOP (C/EBP homologous protein), ATF3 (Activating transcription factor 3) [65] et GADD34 (Growth arrest DNA damage inducible protein 34) [66]. L'activation de GADD34 va déclencher une boucle de rétrocontrôle négatif en activant la déphosphorylation d'eIF2α. Il y a alors blocage de la voie PERK/eIF2α/ATF4 et reprise de la traduction globale des ARNm [66]. PERK active également une réponse anti-oxydante *via* la phosphorylation et donc la translocation nucléaire de Nrf2 (NF-E2 related factor 2) [67-69].

ATF6 est une glycoprotéine transmembranaire dont le domaine luminal est doté de sites de localisation à l'appareil de Golgi, et dont le domaine cytosolique contient une activité de facteur de transcription (motif leucine zipper) [70]. Comme toutes les protéines de la famille des facteurs de transcription membranaires, ATF6 est localisée au RE en conditions basales et donc inactive (cf. SREBP, **II.A.2**), alors qu'un stress du RE déclenche son export vers l'appareil de Golgi. Cette localisation spécifique d'ATF6 dépend de deux mécanismes: en conditions basales, ATF6 interagit avec BiP qui masque les séquences de localisation au Golgi [71], et ATF6 est dans une conformation "non native" comprenant des ponts disulfures [72, 73]. La présence de protéines mal conformées, substrat préférentiel de BiP, ou les modifications du statut redox, changent l'accessibilité d'ATF6 notamment à la protéine

PDIA5, qui réduit ses ponts disulfures (**cf. annexe: ARTICLE 6**). Les changements de conformation qui en résultent rendent la séquence d'export au Golgi accessible aux molécules du système d'export des protéines (COPII) [71-74]. ATF6 peut alors être exportée vers l'appareil de Golgi ou deux protéases, les protéases S1P (Site-1-protease) et S2P (Site-2-protease), clivent ATF6 au niveau de sites de son domaine transmembranaire. Ce clivage libère le fragment cytosolique, qui correspond à la forme active d'ATF6. Cette protéine mature est à son tour exportée vers le noyau, où elle active la transcription de ses gènes cibles [75-77] dont les chaperonnes BiP, GRP94 et calréticuline, mais aussi les facteurs de transcription CHOP et XBP1 [78-80].

Il existe deux isoformes de la protéine ATF6: ATF6α et ATF6β. L'extinction de chacune de ces deux isoformes ne compromet pas le développement chez la souris [81], alors que l'extinction simultanée des deux isoformes (double knockout (KO)) entraîne une mortalité embryonnaire. Le phénotype observé chez ces souris double KO est similaire au phénotype observé chez les souris KO pour XBP1 [82] ou IRE1α [83, 84]. Au contraire, il est intéressant de noter que l'extinction de la voie de signalisation de PERK, par un KO de PERK, ATF4 ou CHOP ne provoque pas de létalité embryonnaire même s'ils sont à l'origine de désordres variés tels que des dysfonctions pancréatiques et métaboliques et des défauts de développement du squelette (cf. **III.A**) [85-88].

IRE1α est une protéine transmembranaire comportant deux activités enzymatiques dans son domaine cytosolique: une activité kinase et une activité de clivage d'ARNm dite endoribonucléase (RNase). Les voies de signalisation découlant de l'activation de cette protéine et son mode d'activation sont détaillées dans le paragraphe suivant. Bien qu'IRE1α soit très conservée, il semble que son rôle diffère d'un organisme à l'autre étant donné que la signalisation UPR elle-même diffère d'un organisme à l'autre. Par exemple, la réponse UPR est constituée de la seule protéine Ire1p chez la levure, et de deux ou trois effecteurs chez la drosophile, le nématode ou les mammifères [89]. Ainsi, les caractéristiques d'Ire1p ou de ces homologues chez le nématode ou la drosophile ne sont qu'en partie transposables à IRE1α chez l'Homme. Sauf mention contraire, les chapitres suivant sont détaillés pour l'UPR chez les mammifères.

2. La voie de signalisation d'IRE1α

IRE1α est une protéine de 110 kDa comprenant 977 acides aminés [90]. Le domaine luminal d'IRE1α contient, comme ceux de PERK ou d'ATF6, des sites de liaison à des

protéines du RE. En réponse à un stress du RE, le domaine luminal d'IRE1α perdrait son interaction avec BiP [91] et lierait des protéines mal conformées [92], induisant des changements conformationnels nécessaires à son oligomérisation, et ainsi son activation [92-94]. L'oligomérisation par les domaines luminaux d'IRE1α entraîne la juxtaposition de ses domaines cytosoliques, leur trans-autophosphorylation et l'activation de ses deux activités enzymatiques: son activité kinase et son activité RNase (**Figure 10** : Représentation schématique de la protéine IRE1α, aussi appelée ERN1).

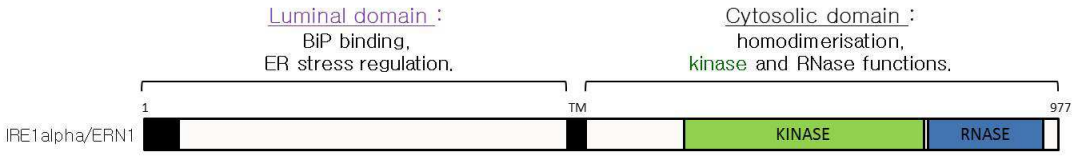

Figure 10 : Représentation schématique de la protéine IRE1α, aussi appelée ERN1
IRE1α ou ERN1 est une protéine de 977 acides aminés contenant trois domaines: un domaine luminal, un domaine transmembranaire (TM) et un domaine cytosolique. Le domaine luminal est la partie impliquée dans la liaison d'IRE1α avec ses partenaires du RE (ex: BiP), qui est activée lors d'un stress du RE. La partie cytosolique d'IRE1α contient quant à elle les domaines à activité kinase (en vert) et à activité RNase (en bleu).

IRE1α s'associe également à des protéines cytosoliques qui vont moduler ses activités: lorsqu'IRE1α est activée, elle recrute et phosphoryle, *via* son domaine kinase, la protéine adaptatrice TRAF2 (TNF receptor associated factor 2) entrainant la phosphorylation de la protéine kinase ASK1 (Apoptosis signal regulating kinase 1) et l'activation de la protéine c-Jun N-terminal kinase (JNK), un facteur impliqué dans le processus d'apoptose [83].

D'autres protéines telles que les protéines NCK1 (Non catalytic region of tyrosine kinase adaptator protein 1), BI-1 (Bax inhibitor 1) et les chaperonnes HSP90 (Heat-shock protein of 90 kDa) et HSP72 (Heat-shock protein of 72 kDa) se lient à IRE1α en absence de stress du RE. La modulation de nombreuses voies de signalisation passe par ces interactions. Par exemple, en piégeant BI-1, IRE1α empêche l'inhibition de Bcl-2 (B-cell lymphoma 2) et module ainsi l'apoptose. De même, la liaison entre IRE1α et NCK1 inhibe la voie dépendante de la protéine kinase ERK (Extracellular signal-regulated kinase). De plus, les chaperonnes HSP90 et HSP72 stabilisent IRE1α, et contribueraient à la régulation de l'UPR [95]. Deux autres rôles d'IRE1α passent par son activité RNase: la dégradation d'ARNm cibles ou RIDD (RNA regulated IRE1 dependent decay) et l'épissage non-conventionnel de l'ARNm de

XBP1. L'épissage de l'ARNm de XBP1 a été identifié dans les cellules mammifères du fait de son analogie fonctionnelle avec l'ARNm de Hac1 épissé par l'homologue d'IRE1α, Ire1p, chez la levure *S. cerevisiae* [96].

Chez les mammifères, l'ARNm de XBP1 est recruté au niveau du domaine RNase d'IRE1α, ce qui entraîne le clivage de cet ARNm au niveau de deux séquences consensus portées sur des structures tige-boucle, aboutissant à l'épissage d'un intron de 26 nucléotides chez l'Homme (**Figure 11A**). Cet épissage est suivi d'une ligation, par une ligase encore non caractérisée [97], et le décalage du cadre de lecture subséquent permet l'expression d'un facteur de transcription de type leucine zipper nommé XBP1s (spliced form of XBP1). Le rôle de la protéine XBP1 synthétisée à partir de l'ARNm non épissé de XBP1 est à ce jour mal connu, bien qu'il soit considéré comme inhibiteur de la voie IRE1α/XBP1s. En effet, la liaison de cette protéine XBP1 avec la protéine XBP1s forme un complexe dégradé par le protéasome, déstabilisant ainsi la protéine XBP1s [98]. XBP1s appartient à la famille ATF/CREB (cAMP response element binding proteins) et se fixe, après translocation nucléaire, sur des séquences CRE (cAMP response element), ERSE (ER stress response element) ou UPRE (UPR response element) présentes sur les régions promotrices de ces cibles transcriptionnelles. XBP1s induit ainsi l'expression de nombreuses chaperonnes et co-chaperonnes (BiP, ERp57, ERdj4) mais aussi de facteurs de transcription (CHOP), d'oxydoréductases (PDI, ERp57) et de protéines de la voie ERAD (EDEM, HRD1, OS-9) [99, 100]. L'ensemble de ces protéines permet d'augmenter les capacités de prise en charge des protéines par le RE et ainsi d'atténuer l'accumulation de protéines mal conformées à l'origine de l'activation de l'UPR et donc de la voie IRE1α/XBP1. Cette voie IRE1α/XBP1 est essentielle lors du développement embryonnaire chez la souris et seuls des KO conditionnels ont permis de déterminer le rôle physiologique de XBP1 [8, 82].

La deuxième activité d'IRE1α dépendante de son domaine RNase est le RIDD. Des ARNm cibles sont recrutés, par des mécanismes encore méconnus, à proximité du domaine RNase d'IRE1α. Il sont ensuite clivés au niveau de séquences consensus portées sur des structures tige-boucle ([101], **Figure 11B**).

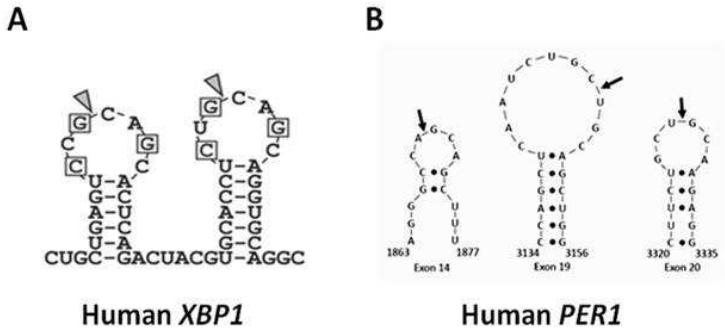

Figure 11 : Séquences et structure des sites de clivages par le domaine RNase d'IRE1α.
A. Représentation des séquences consensus de clivage de l'ARNm de XBP1 par IRE1α, localisées au sommet de structures tige-boucle.
B. Représentation des trois sites de clivage de l'ARNm de PERIOD1 (PER1), également au sommet de structures tige-boucle.

L'identification de cette activité RIDD chez la drosophile [102] puis chez la souris [103, 104], a permis de mettre en évidence des cibles potentielles du RIDD chez l'Homme comme par exemple l'insuline, le PDGFR (PDGF (Platelet Derived Growth Factor) receptor) ou CD59 (cluster of differentiation 59). De plus, par cette activité, IRE1α contrôle la stabilité de son propre ARNm, en le clivant [103-105]. Grâce à la dégradation sélective d'ARNm, IRE1α pourrait réduire les protéines à synthétiser et ainsi réduire la charge protéique du RE pour favoriser la traduction des protéines dont l'expression est spécifiquement induite par l'UPR telles que les chaperonnes BiP et GRP94. En plus des ARNm, IRE1α est également capable de dégrader directement des micro-ARN (miR) comme les miR-17, -34a, -96 ou -125b [106, 107] ou le miR-1291 [108].

3. UPR: pro-survie ou pro-mort

En réponse à un stress protéotoxique, l'UPR active tout d'abord des voies permettant à la cellule de s'adapter temporairement face à des situations de stress. En effet, ces voies cytoprotectrices permettent de diminuer la charge protéique du RE (inhibition de la traduction, dégradation d'ARNm) tout en augmentant les capacités de repliement du RE (expression/activation des acteurs des machineries du RE). Toutefois, lorsque le stress est trop intense ou lorsqu'il se prolonge, les dommages subis par la cellule peuvent être nocifs pour les cellules voisines. L'UPR active alors des voies de mort cellulaire, par autophagie ou par apoptose (**Figure 12**), par exemple par l'activation des protéines pro-apoptotiques CHOP [85]

et JNK [83]. L'activation de CHOP par la voie PERK favorise tout d'abord l'expression de GADD34, levant ainsi l'inhibition de traduction due à eIF2α. Il en résulte un afflux de protéines néosynthétisées au niveau de la lumière du RE, ce qui accentue le stress du RE. De plus, CHOP favorise l'expression du facteur pro-apoptotique Bim [109].

Il existe de nombreux liens entre la voie de signalisation IRE1α et la mort cellulaire, qui montrent tantôt le rôle d'IRE1α pro mort cellulaire et tantôt un rôle anti mort cellulaire. Dans ces fonctions pro-mort, en plus d'activer JNK, le complexe IRE1α/TRAF2 induit l'apoptose chez la souris par le clivage de la pro-caspase 12 et l'activation en cascade de la caspase 12 puis des caspases 9 et 3 [110, 111], bien que chez l'Homme il semble que la caspase-12 soit exprimée sous une forme tronquée dont l'activation ne dépend pas du stress du RE [112]. En outre, le clivage par IRE1α de miR inhibiteurs permet de stabiliser leurs ARNm cibles tels que celui de la caspase 2, une protéine pro-apoptotique, ou encore, dans le cas du miR-17, celui du facteur pro-inflammatoire TXNIP (Thioredoxin-interacting protein) aussi connu sous le nom de TBP-2 (Thioredoxin binding protein-2) et VDUP1 (vitamin-D3 upregulated protein-1) [113, 114]. Cependant, d'autres études montrent que lorsqu'IRE1α s'oligomérise, il libère le facteur anti-apoptotique BI-1. De plus, de récentes études ont montré que la voie IRE1α/JNK peut promouvoir la survie cellulaire en activant la transcription de facteurs de croissance tels que l'épiréguline [115]. Cette implication d'IRE1α dans la survie des cellules est étayée par le fait qu'une surexpression d'IRE1α peut augmenter la résistance à la mort de lignées cellulaires [116, 117], tout comme un épissage maintenu de l'ARNm de XBP1 [118]. Ce double rôle d'IRE1α dans la mort cellulaire se retrouve également dans sa fonction RIDD, qui a été montré comme réponse pro-survie en diminuant la charge protéique du RE [103], mais aussi pro-mort en dégradant des facteurs de survie [7]. Ceci souligne combien la balance entre UPR pro-survie et UPR pro-mort est finement régulée, par des régulations dont une partie nous échappe encore.

Une des clés de cette régulation réside peut-être dans les systèmes de contrôle de la durée de l'activation d'IRE1α. Parmi ceux-là, on peut citer la protéine chaperonne PDIA6, capable de lier la cystéine 148 oxydée présente dans la partie luminale des oligomères actifs d'IRE1α, ce qui entraîne la dissociation des oligomères et ainsi l'atténuation de la signalisation IRE1α [119].

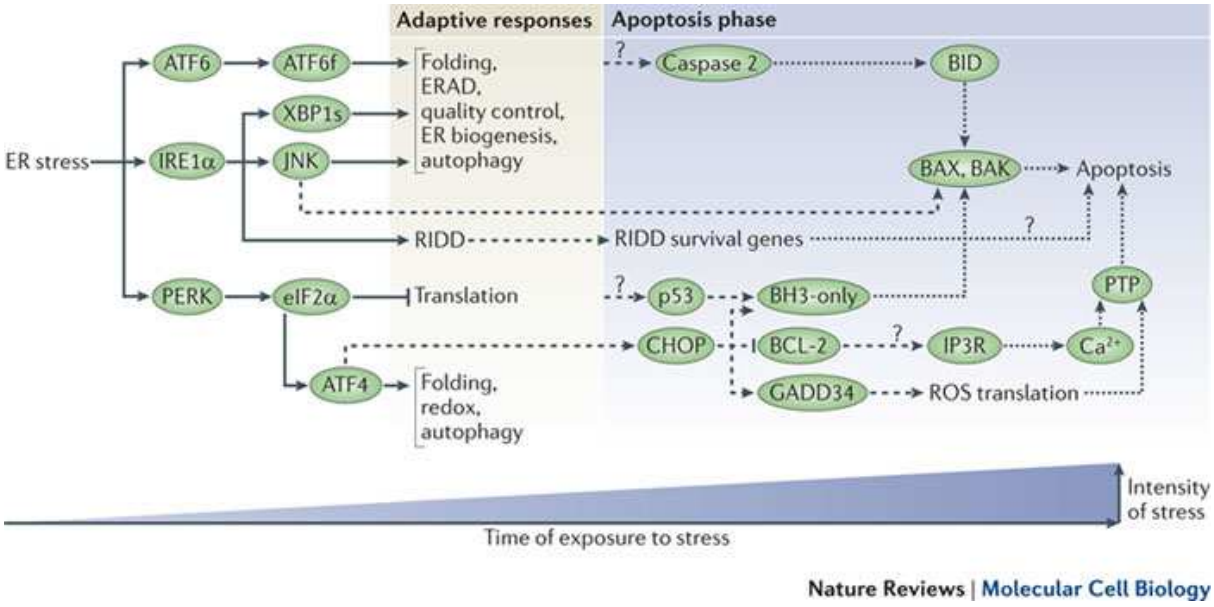

Figure 12 : Représentation des voies de signalisation pro-apoptotiques de l'UPR.
Hetz, 2012 [6].

L'UPR induite par le stress du RE est une réponse adaptative qui promeut la survie de la cellule lorsque le stress du RE initial est transitoire et/ou peu intense.

Au contraire, lors d'un stress intense et/ou prolongé les voies de signalisation de l'UPR qui sont activées deviennent des réponses de mort cellulaire, par l'activation de l'autophagie ou de l'apoptose. Les médiateurs de l'apoptose ainsi activés sont principalement les facteurs pro-apoptotiques de la famille de Bcl-2.

III. Réticulum Endoplasmique et pathologies

A. Généralités

De nombreuses pathologies ont pour origine des mutations qui altèrent le repliement de protéines. Ces maladies peuvent affecter les composants des machines de repliement ou d'export (LMAN1 (Lectine Mannose-binding 1) MCFD2 (Multiple Coagulation Factor Deficiency 2) [120], BAP [121, 122], l'α-glucosidase I [123]) ou peuvent affecter directement les propriétés de la protéine à replier et ainsi la prise en charge de ces protéines par le QC. Les maladies où les protéines à replier sont mutées, comme les maladies neurodégénératives ou la mucoviscidose, sont dites maladies conformationnelles. Elles se caractérisent par la dégradation de la protéine mutée ou son accumulation dans la lumière du RE, ce qui peut entraîner un stress du RE.

Ainsi, dans le cas de la mucoviscidose, ce sont des mutations de la protéine CFTR (Cystic fibrosis transmembrane conductance regulator) qui sont à l'origine de la pathologie, en conduisant à sa dégradation [124, 125]. En effet, CFTR étant une glycoprotéine complexe, son repliement est long, ce qui conduit 75% des protéines synthétisées à la dégradation. Toute mutation ralentissant son repliement provoque l'adressage de la totalité des protéines CFTR à l'ERAD, et ainsi une absence totale de la protéine à la membrane donc une perte de fonction de CFTR [126, 127].

De même, plusieurs mutations de l'α-1-antitrypsine (α1AT) ont été associées à une pathologie appelée ATD (Alpha 1 Antitrypsine Deficiency). Ces mutations peuvent stimuler la formation d'oligomères s'agrégeant en inclusions insolubles et s'accumulant dans le RE des hépatocytes dans lesquels elle est synthétisée [128]. Cette accumulation a deux conséquences majeures : tout d'abord, elle peut entraîner une dysfonction du RE et ainsi être toxique pour les cellules hépatiques voire pour le foie (apparition de cancer [129]) et, d'autre part, elle abroge la sécrétion de l'α1AT, ce qui fait de l'agrégation une cible thérapeutique pertinente [130]. D'autres mutations de l'α1AT entraînent la production d'une protéine tronquée retenues dans le RE puis dégradée par l'ERAD [131]. L'absence d'α1AT sécrétée est responsable des symptômes de l'ATD [132], qui sont des dommages importants au niveau des tissus, notamment pulmonaires, soumis à l'action des élastases [129]. En effet, l'α1AT a un

effet protecteur sur les tissus en inhibant l'élastase leucocytaire, une protéase activée en cas d'infection pulmonaire ou d'irritation chronique.

Parmi les mutations affectant les protéines des machines moléculaires du RE, on peut noter la mutation de la protéine BAP, partenaire qui déstabilise l'interaction de BiP avec les protéines mal conformées, à l'origine du syndrome de Marinesco-Sjoegren [121]. Ce syndrome, caractérisé par des retards de développement, des cataractes et des myopathies [122], est dû à une dysfonction ou une absence de production de la chaperonne BiP qui compromet le repliement des protéines voire de leur entrée dans le RE [133]. De même, des mutations de l'α-glucosidase I peuvent aboutir à une pathologie allant de l'atteinte neurologique sévère associée à un retard mental et à une hypotonie axiale à des atteintes multi viscérales graves [134].

Des mutations peuvent également affecter les effecteurs de l'UPR, et par conséquence, les voies de signalisation qui en découlent. C'est le cas par exemple du syndrome Wolcott-Rallison associant un diabète néonatal permanent, une dysplasie épiphysaire multiple et d'autres manifestations dont des épisodes d'insuffisance hépatique aiguë. Cette pathologie découle de mutations de PERK inhibant son activité kinase [135, 136] et aboutissant à une accumulation toxique de protéines dans le RE des cellules pancréatiques notamment [137, 138].

La pathogénicité de nombreuses maladies peut être due à une dysfonction cellulaire voire à la mort cellulaire induite par un stress chronique du RE, et toute dérégulation des voies cytoprotectrices de l'UPR peut accroître cette pathogénicité, comme le soulignent les modèles murins de KO d'ATF6, de PERK, d'IRE1α, d'ATF4, de XBP1 ou de CHOP [139]. Ces dérégulations peuvent, à titre d'exemple, être observées dans le cas des maladies métaboliques (obésité, diabète, stéatose hépatique) [140] ou inflammatoires (maladie de Crohn, iléite, colite) [141]. Dans le cas des maladies neurodégénératives telles que la maladie de Parkinson, la maladie d'Alzheimer, ou de la maladie de Huntington, il a également été montré que la mort des neurones peut être due à un défaut du système de dégradation qui maintien le stress du RE et une UPR pro-apoptotique [142].

B. Voie de sécrétion et cancer

La voie de sécrétion est un processus cellulaire dynamique hautement régulée qui permet la sécrétion de protéines dans le milieu extracellulaire et l'acheminement des protéines membranaires vers leur destination finale. La sécrétion de protéines dans le milieu extracellulaire, telles que les facteurs diffusibles ou des composants de la matrice extracellulaire, permet à la cellule de communiquer avec les cellules voisines ou de modifier son microenvironnement. Ainsi, chez l'Homme, la voie de sécrétion est essentielle à de nombreuses fonctions biologiques (sécrétion d'insuline, production d'anticorps, libération de neurotransmetteurs et d'hormone) et toute condition biologique, physique ou chimique qui perturbe cette voie finement régulée déclenche des réponses adaptatives dont l'UPR. Lorsque l'activation de cette signalisation de stress ne suffit pas à rétablir le bon fonctionnement de la voie de sécrétion, sa dérégulation chronique peut conduire à des pathologies comme le diabète, certaines maladies neurodégénératives ou l'hémophilie.

Certaines pathologies, comme le cancer, entraînent une augmentation des besoins métaboliques, de la demande en protéines sécrétées et de la prolifération ce qui sollicite anormalement les acteurs de la voie de sécrétion et en particulier le RE [9] (**Figure 13**).

De plus, les cellules cancéreuses sont des cellules qui peuvent survivre dans des conditions difficiles, comme l'hypoxie, ce qui implique que cette importante sollicitation s'accompagne, dans ces cellules, d'une augmentation des capacités de la voie de sécrétion. Bien que les mécanismes d'adaptation mis en jeu ne soient pas encore entièrement décryptés, il semblerait que des mutations ou tout autre système de levée des points critiques (check point) de contrôle de mort induite soit un mécanisme oncogénique répandu [143].

Dans cette idée, de nombreux acteurs de l'UPR ont été impliqués dans la progression tumorale (cf. **III.C**: UPR in cancer).

Il a également été montré que le développement de certaines tumeurs ou l'échappement aux traitements anticancéreux semblent favorisés par la sécrétion de facteurs pro-oncogéniques, tels que des facteurs de croissance ou d'angiogenèse, ou de molécules modulatrices de la matrice extracellulaire, tels que les métalloprotéases [144, 145]. Outre cet effet direct des protéines sécrétées, la voie de sécrétion peut affecter le développement de cancers par le fait qu'une altération de l’homéostasie protéique du RE peut augmenter la production de ROS (Reactive oxygen species), ce qui entraîne un stress oxydatif qui à son tour favorise l’instabilité génomique [146, 147]. Enfin des dérégulations de la voie de sécrétion peuvent favoriser la protéolyse anormale de protéines du RE telles que la famille des

facteurs de transcription liés à la membrane (CREB, OASIS, SREBP1/2, et ATF6) [35] et la calnexine (CNX) [148], ce qui permet aux cellules cancéreuses de respectivement augmenter la résistance au stress protéotoxique [35] ou de suractiver des voies de signalisation pro-tumorales telles que celles de l'EGFR et de STAT3 [148]. Ainsi, de nombreuses mutations affectant des protéines du RE ou des protéines sécrétées (BiP, GRP94, CRT, ERp29, PDIA6, CNX, CREB, etc.) ont été identifiées dans le cancer.

Cette relation étroite entre voie de sécrétion et cancer peut être exploitée pour la recherche de nouvelles thérapies, par exemple en ciblant les protéines anormalement présentes à la surface des cellules cancéreuses voire responsables de l'immunogénicité des tumeurs (calréticuline) [150, 151], ou en perturbant suffisamment les machineries de la voie de sécrétion pour rétablir les mécanismes d'induction de mort cellulaire.

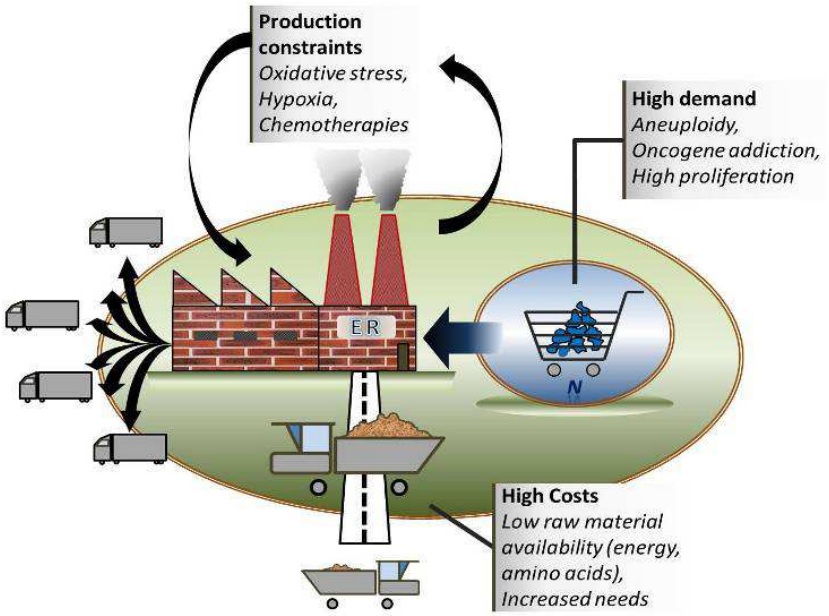

Figure 13 : Représentation schématique des contraintes imposées au RE des cellules cancéreuses.
Dejeans et al, 2014 [9].

C. UPR et cancer

Comme nous l'avons vu précédemment, les cellules sont soumises à de nombreux stress (protéotoxique, oxydatif, hypoxique, etc.) qui sollicitent le RE et déclenchent des réponses adaptatives telles que l'UPR. Toutefois, les cellules cancéreuses survivent alors qu'elles subissent un stress aigu qui devrait suffire à faire basculer l'UPR d'une réponse pro-survie à une réponse pro-mort. On comprend dès lors que l'évitement de la mort programmée est un enjeu majeur des cellules cancéreuses et que comprendre ces mécanismes d'échappement est un enjeu thérapeutique tout aussi important.

Souvent, ces mécanismes résultent de l'instabilité génomique des cellules cancéreuses ou de modifications importantes du microenvironnement. C'est le cas des mutations initiatrices de tumeurs, qui affectent des protéines centrales dont la dérégulation déstabilisent des systèmes clés de surveillance, tels que l'UPR, et permettent aux cellules cancéreuses de survivre.

La revue qui suit liste les acteurs de l'UPR dont des dérégulations ont été identifiées dans le cancer. Elle souligne en particulier l'importance de la signalisation IRE1α dans la progression tumorale, et plus particulièrement dans la migration des cellules cancéreuses et la vascularisation de la tumeur.

De récentes données confortent ce rôle central de l'UPR, et en particulier de la voie PERK, dans la survie des cellules cancéreuses. En effet, ces travaux montrent que la voie PERK/ATF4/CHOP est une voie de résistance au développement tumoral, qui peut être atténuée dans les cellules cancéreuses pulmonaires par la surexpression de la chaperonne $p58^{IPK}$ en réponse à un stress chronique [143]. Ce détournement du stress chronique, induit par une carence en glucose au sein de la tumeur, en réponse cytoprotectrice fait de $p58^{IPK}$ une cible thérapeutique pertinente.

Des études pré-cliniques prometteuses étayent également le potentiel thérapeutique de la voie PERK, cependant dans ce cas le traitement anticancéreux consiste à inhiber totalement cette voie [149]. Ces données soulignent donc une fois de plus le rôle dual que l'UPR peut avoir dans le cancer.

ARTICLE 1: Signaling the UPR in cancer

Signaling the Unfolded Protein Response in cancer

Stéphanie Lhomond and Eric Chevet

Contents

Abstract

Cancer cells present a deregulated replication cycle and are able to grow quickly in hostile environments. These cells can be subjected to many environmental challenges such as hypoxia, nutrient deprivation, remodeling of the environmental space or presence of chemotherapeutic agents. Moreover cancer cells also

E. Chevet (✉) · S. Lhomond
Inserm U1053, Université Bordeaux Segalen, 146 rue Léo Saignat, 33076, Bordeaux, France
e-mail: eric.chevet@u-bordeaux2.fr

E. Chevet · S. Lhomond
GREF, Université Bordeaux Segalen, Bordeaux, France

P. Agostinis, A. Samali (eds.), *Endoplasmic Reticulum Stress in Health and Disease*, 357
DOI 10.1007/978-94-007-4351-9_16, © Springer Science+Business Media Dordrecht 2012

have to cope with elevated oxidative stress, high DNA replication and protein synthesis rates. As a consequence cancer cells must show high adaptive capabilities in order to cope with such stresses. In the past couple of years, the Unfolded Protein Response (UPR) has emerged as an important adaptive response for cancer cells to manage these stresses and to survive under challenging conditions. Although the UPR is primarily a pro-survival response, it can also induce cell death if the stress is not alleviated. In addition to presenting enhanced adaptive capacity, cancer cells have also developed strategies to get around UPR-induced death signals. In the present chapter, we describe how cancer cells use the UPR or have altered the UPR signaling machinery to gain selective advantage over surrounding cells. We also discuss how UPR signaling is connected to classical carcinogenic pathways. Finally, we will focus our attention in particular on IRE1 signaling pathways. Collectively these elements constitute an integrated adaptive system in cancer and therefore open the way to new potential anticancer therapeutic avenues.

Keywords

UPR signaling · Cancer · Mutations · BiP/GRP78 · IRE1/ERN1 · ATF6 · PERK · XBP1 · NRF2 · NFkappaB · p53

Abbreviations

ARE	antioxidant responsive element
ATF4	activating transcription factor-4
ATF6	activating transcription factor-6
ASK1	apoptosis signal-regulating kinase-1
BI1	BAX inhibitor-1
BiP	immunoglobulin heavy chain-binding protein
CHOP	C/EBP-homologous protein
EDEM1	ER degradation enhancing mannosidase-like protein-1
eIF2α	alpha-subunit of the eukaryotic translation initiation factor-2
ER	endoplasmic reticulum
ERAD	ER-associated degradation
ERdj	ER DNAJ like
Ero1	ER oxidoreductin 1
ERSE	ER stress-response element
GADD34	growth arrest and DNA damage 34
GRP78	78 kDa glucose-regulated protein
GRP94	94 kDa glucose-regulated protein
IRE1	inositol-requiring protein-1
IP_3R1	inositol 1,4,5-trisphosphate receptor 1
JNK	c-Jun N-terminal kinase
Keap1	Kelch-like ECH-associated protein-1

MAP	mitogen-activated protein
MAPK	MAP kinase
MAPKK	MAP kinase kinase
MAPKKK	MAP kinase kinase kinase
Nrf2	nuclear factor-E2-related factor-2
PERK	protein kinase RNA-like ER kinase
PI3 K	phosphoinositide-3-kinase
PDI	protein disulfide isomerase
RIDD	regulated IRE1-dependent mRNA decay
ROS	reactive oxygen species
sXBP1	spliced form of XBP1
S1P and S2P	site-1 and site-2 proteases
TNF	tumor necrosis factor
TRAF2	TNF receptor-associated factor-2
UPR	unfolded protein response
XBP1	X-box binding protein-1

1 Introduction

Cancer cells, particularly solid tumors, are often exposed to adverse stressful conditions that should normally lead to cell death. Moreover these cells often elicit metabolic specificities that place them in high energetic demand. To cope with these challenging conditions, cancer cells have not only modulated their adaptive capacity but also reduced their sensitivity to stress-mediated cell death. For instance, these cells can grow on very little oxygen, nutrient or calcium, despite an oxidative environment or even in the presence of chemotherapeutic agents (Fig. 1). These conditions, combined with cancer cells' high replicative rates, lead to the primary activation of adaptive cellular responses such as the UPR. The recent demonstration of the important role of the UPR in tumor growth has led one to address the pro-oncogenic role of this signaling pathway. In particular, major objectives have been set to identify the mechanisms involved and those that have been altered to allow such events to happen in cancer cells. Many studies carried out in human cancer tissues or cell lines and/or in animal models have tried to identify key regulators of UPR involved in cancer development and progression (Table 1). In the present chapter, we will list the components of the UPR and precisely describe their role in cancer cells as well as the conditions in which the UPR is activated. Moreover, we will provide information on how the UPR connects with canonical oncogenic pathways. Finally, we will more precisely focus on the role of IRE1 and the alteration of its downstream signaling pathways in cancer.

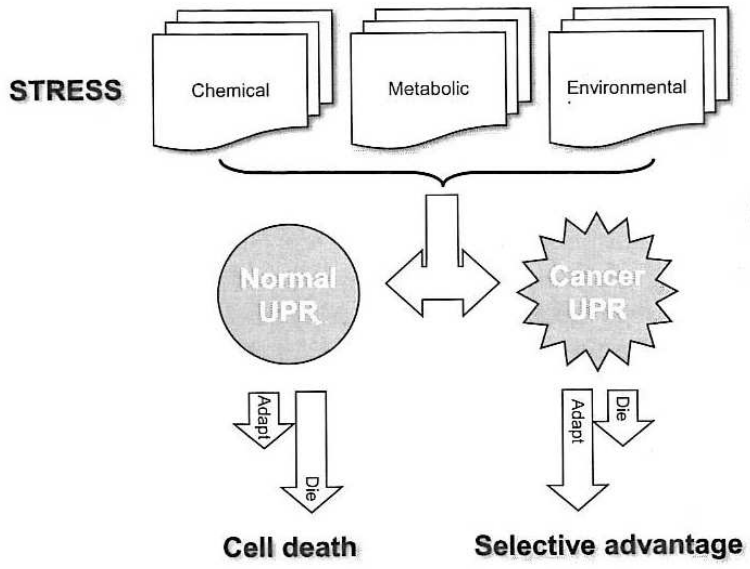

Fig. 1 Contribution of the UPR to the response to various stresses in normal and cancer cells

2 Principal components of the UPR in cancer cells

The Endoplasmic Reticulum (ER) is an organelle involved in calcium homeostasis, lipid biosynthesis and is an essential compartment for the synthesis of secreted and trans-membrane proteins (see Chap. 1). Following translocation into the ER, newly synthesized proteins are supported by ER chaperones and are subjected to a quality control system. Proteins can then be targeted to their compartment of destination or be degraded by the ER-Associated Degradation (ERAD) system. Under basal conditions, there is a balance between the amount of newly synthesized proteins entering the ER and that of proteins exported to more distal compartments of the secretory pathway. However, under ER stress conditions this balance is disrupted which leads to accumulation of proteins in the ER. This increased ER protein load triggers Unfolded Protein Response (UPR) which aims to restore ER balance or, if this is not possible, to kill the cell (see Chap. 3 for full detail). The intracellular signals involved in the UPR are transmitted from the ER lumen to the rest of the cell by three trans-membrane proteins of the ER: PERK (protein kinase (PKR)-like ER kinase), IRE1 (Inositol Requiring Enzyme 1) and ATF6 (Activating Transcription Factor 6).

2.1 ER lumen resident UPR sensors

2.1.1 BiP (immunoglobulin heavy chain-Binding Protein)

BiP, also named GRP78 (Glucose-Related Protein 78) is a soluble protein chaperone of the ER lumen and belongs to the Hsp70 family. It contains two major domains:

Table 1 UPR signaling actors mutated in human cancers. ×, +and – represent mutations of proteins involved in UPR signaling (columns) found in human cancer tissues or cell lines (lines). + corresponds to positive mutations (over- expression or activation of these proteins). – corresponds to negative mutations (under- expression or activation of these proteins). × represents positive or negative mutations

	IRE1	ATF6	PERK	BiP	GRP94	ERAD	KEAP1	NRF2	ATF4	GSK3b	JNK	TRAF2	XBP1	BI-1	p53	PKB/PI3K	PTEN	NFkB	MAPKs
Bone															–	×			×
Breast				+		±						×	+	+	–	×	–	×	×
Brain	×			±		–		+	+		×				–	+	–		
Endometrium															–	+	–		
Esophagus				–	+			+							–				
Hematopoietic, lymph. tissue				+		+									–	+	–		
Kidney	×										×			–	–				
Large intestine														–	–	+			
Liver	+	×		+		±	–								–				
Lung	×			-		–	–	+		×	×	×	+		–	×			
Ovary	×	×	×	+		–					×	×		+	–	+		×	
Pancreas													+		–				
Prostate				+			–							+	–	+	–		×
Skin				+		+		+				×			–	×			×
Stomach	×			+	+									–	–				
Thyroid															–	+	–		×
Upper aerodigestive tract							–	+							–	+			
Urinary tract															–	×			
Uterus														+					

a N-terminal ATP dependent domain and a C-terminal domain, which binds hydrophobic patches within proteins [1]. BiP has different functions in the ER: it regulates ER Ca^{2+} levels through binding to Inositol 3 Phosphate Receptor (IP3R) channels and plays an important chaperone role for the nascent polypeptides translocated into the ER and for misfolded proteins. Surprisingly, BiP was also found to associate with cytosolic, mitochondrial and extracellular partners that not only make it a key factor in cellular stress response [2, 3, 4, 5], but also the physiological relevance of these interactions remains to be demonstrated. BiP is also the first and major sensor of the UPR. Indeed, under basal conditions, BiP binds to hydrophobic segments of neo-synthesized and unfolded proteins present in ER lumen, but is also bound to the three trans-membrane proteins PERK, ATF6 and IRE1, the initial UPR transducers. Seeing as BiP has a greater affinity for misfolded proteins, BiP will be titered away from those three transducers following the accumulation of misfolded proteins in the ER, leading to the activation of UPR signaling. Moreover, in response to ER stress, BiP expression is up-regulated by a selective increase in transcription and translation [6, 7], thus enhancing ER folding capacities, as explained further below.

2.1.2 Glucose Regulated Proteins (GRP) family chaperones

Three major chaperoning systems define the ER folding capacity: the Protein Disulfide Isomerases (PDI), the lectin chaperones including calnexin and calreticulin, and the GRP chaperones. Similar to BiP, GRP94, also called gp96, is part of the latter chaperone group and belongs to the Hsp90 family. GRP94 and BiP show many common targets and GRP94 expression is increased in response to BiP silencing, suggesting a tight cooperation between those proteins and compensatory (but not replacement) mechanisms [1]. GRP170 is a nucleotide exchange factor of BiP and thereby modulates BiP activities such as binding with ERdj (ER DNAJ like) proteins and regulation of Ca^{2+} [8]. GRP94 and GRP170, two proteins that participate in the regulation of calcium homeostasis, are involved in supporting and folding numerous secretory proteins alongside BiP and are essential for expression of integrins and Toll-like receptors on the cell surface [9, 10]. The perturbation of the Ca^{2+} homeostatic balance, tightly regulated particularly by GRP chaperones, has been shown to lead to caspase-7 and caspase-4 activation and subsequently apoptosis upon activation of ER stress [11]. Furthermore, the expression of GRP94 and GRP170 is up-regulated upon ER stress.

2.1.3 Chaperones and cancer

Over expression of BiP has been associated with poor diagnostic cancers such as castration-resistant prostate cancers [12], some aggressive breast cancers [13], gastric cancers with lymph node metastasis, hepatocellular carcinoma with tumor venous infiltration [14] and glioblastoma [15]. In the case of the latter two, high BiP expression levels are correlated with less overall survival and resistance to chemotherapeutic agents. BiP has even been thought to be used as a tumor biomarker for poor prognosis melanoma [16]. However, clinical studies showed cancers with negative correlation between the level of expression of BiP and poor diagnosis: in lung cancers [5], esophagus adenocarcinoma [17] and neuroblastoma [18]. These results

confirm data obtained in mouse models heterozygous for BiP, which show no effect of lower BiP levels on organ development but an impediment in tumor angiogenesis [19]. Over expression of BiP is not restricted to the ER only. Indeed, upon severe ER stress, BiP is strongly up-regulated and it is possible that BiP will be located in mitochondria or the plasma membrane. Moreover, presence of BiP at cancer cell surface tightly regulated their fate for survival or death, as shown in ovarian cancer [20], prostate cancer [21], melanoma [22] and gastric cancer [23]. When extracellular elements like α_2-microglobuline, Cripto or T-cadherin bind to the N-terminal or C-terminal domain of BiP they can promote PI3K Akt/PKB and MAPK signaling pathways leading to the activation of proliferative and pro-life pathways and positive feedback loops increasing BiP expression, which allows cancer cells to survive ER stress [1]. GRP94, similar to BiP, has been found mutated in aggressive gastric carcinoma and esophagus adenocarcinoma and is linked to poor prognosis [24, 25].

2.2 The transmembrane UPR transducers

2.2.1 PERK (protein kinase (PKR)-like ER kinase)

PERK is a 125-kDa type I transmembrane kinase activated by ER stress. Upon accumulation of un/misfolded proteins in the lumen of the ER, BiP dissociates from PERK allowing oligomerization and trans-autophosphorylation of PERK, leading to its activation. PERK then activates two major cytosolic signaling pathways of the UPR. Firstly, PERK phosphorylates the eukaryotic translation initiation factor 2 α (eIF2α), leading to its inhibition and to translation attenuation and consequently to a decrease in the amount of newly synthesized proteins entering the ER (ER load) [26]. Moreover, translation attenuation causes a decrease of cyclin D1 pool triggering cell cycle arrest in G1 [27, 28]. Phosphorylation of eIF2α leads to ATF4 (activating transcription factor 4) translation. Indeed under basal conditions, ATF4 mRNA translation is prevented by the presence of a micro open reading frame in 5' of ATF4 ATG and elevated concentrations of eIF2-GTP. The translation inhibition caused by eIF2α phosphorylation leads to a decrease in eIF2-GTP amounts thus allowing for the bypass of the micro-ORF and ATF4 translation [29, 30]. ATF4 translocates to the nucleus and subsequently promotes transcription of genes with CRE (Cyclic AMP Response Element) such as CHOP (C/EBP homologous protein), ATF3 (Activating Transcription Factor 3) and GADD34 (Growth Arrest DNA Damage inducible protein 34) [31, 32, 33] (Fig. 2). CHOP is a transcription factor that decreases the transcription of the anti-apoptotic factor BCL-2 (B-Cell Lymphoma 2) [34] and enhances transcription of the pro-apoptotic factors BIM (B-cell lymphoma 2 Interacting Mediator of cell death), BAK (Bcl-2 homologous Antagonist-Killer) and BAD (Bcl-2-Associated Death promoter). Furthermore, CHOP promotes the expression of TRB3 (Tribbles Related Protein 3), which can bind to Akt/PKB (Protein Kinase B) preventing its activation (phosphorylation) and its anti-apoptotic function [35]. GADD34 is the mediator of a negative feedback loop on eIF2α phosphorylation, as GADD34, which is activated in response to eIF2α phosphorylation, is the regulatory subunit of the eIF2α phosphatase Protein Phosphatase 1 (PP1) [36]. Secondly,

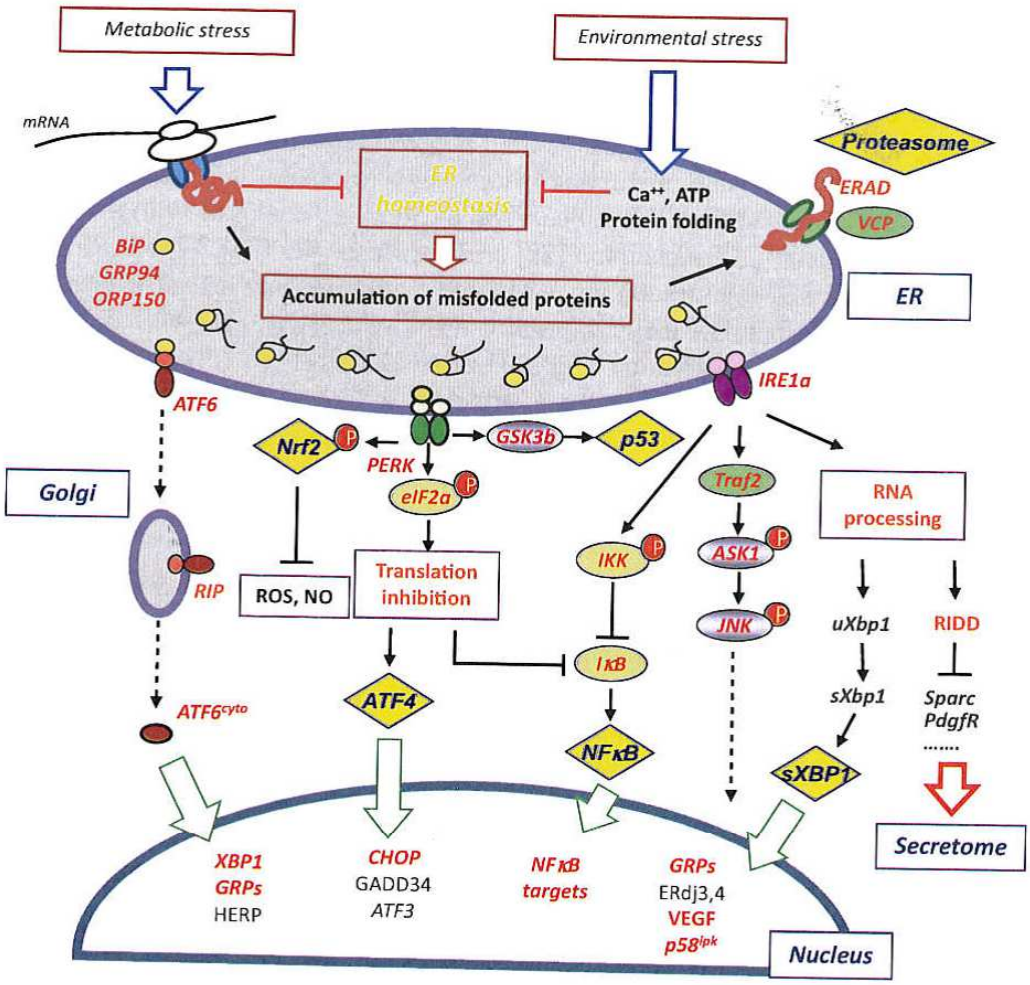

Fig. 2 Global representation of UPR signaling and major alterations in cancer. *Circled P*: phosphorylation events; *blue arrows*: stress actions; *green arrows*: transcriptional activation; *red arrow*: inhibition of the secretome; *yellow diamonds*: major actors in cancers; the main UPR actors deregulated in cancer are colored in red

PERK directly phosphorylates NRF2 (NF-E2 Related Factor 2), releasing NRF2 from its cytosolic partner KEAP1 (Kelch-like ECH-Associated Protein 1) and promoting its nuclear translocation [37]. NRF2 is a basic leucine zipper transcription factor which can then regulate transcription of genes with ARE (Antioxidant Response Element) in their promoter that are able to regulate ROS (Reactive Oxygen Species) cellular levels [38] and the Nitric Oxide pathway [39] (Fig. 2).

Studies were carried out to determine the impact of PERK on cancer development. Transformed MEF (Mouse Embryonic Fibroblasts) from mice deficient for PERK generate smaller tumors, less vascularized and less resistant to hypoxia than tumors from transformed wild type MEF [40]. Another study performed using animal models of mammary carcinoma showed the importance of PERK in cancer cells to decrease ROS cellular levels and so to avoid cell cycle slow-down due to DNA damage and active DNA damage checkpoints [41]. Moreover, cancer cell

lines such as HT29 (colorectal adenocarcinoma), dominant-negative for PERK, have worse survival rates under hypoxia compared to cancer cells expressing PERK [42]. Additionally, over activation of PERK/eIF2α signaling has been involved in tumor dormancy of squamous carcinoma cells [43]. Recently, activating mutations of ATF4 have been reported in neuroectodermal tumor cells [44] and it was seen that ATF4 expression was increased upon anoxia in cancer cells through mechanisms independent of hypoxia inducible factor-1α (HIF-1α) [45]. In the same line of evidence, NRF2 is over activated in squamous cell carcinoma such as lung, skin, head and neck, larynx and esophagus cancers [46, 47] with mutations in the KEAP1 binding domain. KEAP1 is inactivated in adenocarcinoma such as lung, gallbladder, liver and prostate cancers [48, 49], increasing NRF2 stability in these cancer cells. However, studies in mice deficient for KEAP1 demonstrated that KEAP1 inactivation and NRF2 over expression are not sufficient to promote spontaneous cancer formation [49, 50]. These mutations only confer a selective advantage and increased chemotherapy resistance to cancer cells.

2.2.2 ATF6 (Activating Transcription Factor 6)

ATF6α is a 90 kDa-type II trans-membrane protein activated upon ER stress, it belongs to a larger family of trans-membrane transcription factors that also comprises proteins such as ATF6α, OASIS, or CREBH [51]. As it is a basic leucine zipper transcription factor located in the ER upon basal conditions, ATF6α must relocate to the nucleus to achieve its biological functions [52, 53, 54]. Upon ER stress, ATF6α undergoes modifications of its disulfide bridges and dissociates from BiP, which allows separation of ATF6α oligomers into monomers [55]. ATF6α is then exported to the Golgi apparatus through COPII vesicles and cleaved by two proteases: S1P (Site-1 Protease) and S2P (Site-2 Protease). This enables the release of the cytoplasmic N-terminal part of ATF6α, containing its transcription factor activity and which is approximately 50 kDa in size. As a consequence, nuclear ATF6α regulates the transcription of genes encoding ATF/CRE or ERSE (Endoplasmic Reticulum Stress Response Element) promoting sequences [56]. For instance, ATF6α increases the transcription of ER chaperones (BiP/GRP78, GRP94, GRP170/ORP150, calreticulin), and UPR actors such as CHOP and XBP1 (X-box Binding Protein 1) [57]. Over expression of ATF6α has been shown to contribute to liver carcinogenesis [58, 59]. Moreover, several studies have reported mutations in ATF6α in human ovarian cancer tissues (COSMIC database). However, the ATF6α pathway is linked to cancer development through mutations of downstream targets of ATF6α, mainly the GRPs chaperones and XBP1.

2.2.3 IRE1 (Inositol Requiring Enzyme 1)

IRE1α (Inositol Requiring Enzyme 1 α), also named ERN1 (Endoplasmic Reticulum to Nucleus signaling 1), is a 110 kDa-type I trans-membrane protein activated by ER stress and the most conserved UPR transducer. IRE1α has a close homolog in mammals, which presents a sequence conservation of 51% and is named IRE1β [60]. IRE1β expression is restricted to cells from the gastro-intestinal tract and this protein presents a spectrum of activity slightly different from that of IRE1α [60,

61]. It has been involved in mesoderm formation in *Xenopus laevis* [62] and in the regulation of chylomicron formation in primary mouse enterocytes [63].

IRE1α contains two separated enzymatic activities in its C-terminal cytosolic region: a kinase domain and an endoribonuclease domain. Activation of IRE1α upon ER stress has not yet been fully decrypted, but it is known that dissociation of BiP is part of the activation process [64]. When IRE1α is activated, it forms oligomers and, similar to PERK, is trans-autophosphorylated and adopts a suitable conformation for its endoribonuclease activity [65]. IRE1α activates three distinct signaling pathways: 1) a phosphorylation cascade signaling pathway by its kinase domain, whereas the activated endoribonuclease domain leads to two additional signaling pathways: 2) XBP1 splicing and 3) RIDD for Regulated IRE1-Dependent Decay.

1) IRE1α, *via* its kinase domain, triggers a phosphorylation reaction chain initiated by the recruitment of TRAF2 (Tumor Necrosis Factor Receptor-Associated Factor 2) to IRE1α [66]. The adaptor TRAF2 recruits and activates ASK1 (Apoptosis Signal regulating Kinase 1). Furthermore, TRAF2 activates caspase 4, which leads to an apoptotic response. When ASK1 is phosphorylated, it in turn phosphorylates JNK (c-Jun N-terminal kinase), which also leads to an apoptotic response [67]. JIK (c-Jun N-terminal inhibitory kinase) binds activated IRE1α and modulates ASK1/JNK activation [68]. Moreover, activated IRE1α dissociates from the oncogene NCK (Non Catalytic region of tyrosine Kinase adaptor protein), leading to the subsequent activation of a MAPK pathway: the ERK (Extracellular signal-Regulated Kinase) pathway [69]. IRE1α also leads to phosphorylation of IκK (Inhibitor of NF-κB (IκB)-Kinase) (Fig. 2). IkappaK activation leads to IκB inactivation and so promotes NF-κB activity. NF-κB is a transcription factor enhancing the transcription of many genes involved in cell proliferation, apoptosis, inflammation, immunity, plus negative regulators of NFkappaB itself. For instance, NFkappaB increases transcription of anti-apoptotic genes like BCL2A1 (Bcl-2 related protein A1) and cIAP1/2 (c- Inhibitor of Apoptosis Protein 1 and 2) [70] and of the pro-inflammatory protein Tumor Necrosis Factor α (TNFα; [67]).

2) IRE1α, *via* its endoribonuclease domain, is responsible for the atypical cytosolic splicing of XBP1 mRNA. Indeed, IRE1α cleaves a non-conventional 26-nucleotides intron from human XBP1 mRNA [71], which is then re-ligated by an as of yet unknown ligase in human. This leads to a change in XBP1 open reading frame, translation of which generates an active leucine zipper transcription factor termed XBP1s (spliced XBP1). XBP1s binds to CRE, ERSE or UPRE (UPR Response Element) promoters, thereby enhancing transcription of ER chaperones (such as BiP, PDI, ERp57, ERdj4), ERAD components (EDEM (ER degradation enhancer mannosidase α-like protein), HRD1, OS-9, XTP3-B, Derlin 2/3) and CHOP [72, 73].

3) RIDD allows the selective degradation of mRNA, encoding mostly secretory proteins, which results in a decrease in ER load. Some targets of RIDD have been identified as SPARC (Secreted Protein Acidic and Rich in Cysteine), CD59 (Cluster of Differentiation 59), insulin or PDGFR (Platelet Derived Growth Factor Receptor) [74,75,76].

Following the first report of the modulation of IRE1α signaling by BAX (Bcl-2-Associated X protein) and BAK [77], IRE1α activity was found inhibited by BI-1

(Bax Inhibitor-1) [78]. BI-1 is an anti-apoptotic protein related to BCL-2 and the activation of these two proteins depends on calcium concentration. But BI-1 interacts with many proteins such as IRE1α, G-actin, NADPH (Nicotinamide Adenine Dinucleotide Phosphate)-P450 reductase and of course BAX. Through these interactions, BI-1 enhances actin polymerization, decreases ROS production and inhibits BAX-mediated and IRE1α-mediated pro-apoptotic responses [78]. The links existing between IRE1 and cancer will be described in the last section of the chapter.

2.3 ER-Associated Degradation (ERAD)

As mentioned before, ER stress is the consequence of the accumulation of un/misfolded proteins in the ER lumen. As part of the mechanisms set in place to attenuate the stress, cells have developed a mechanism to reduce the load of proteins accumulated in the ER. This mechanism consists of trafficking properly folded proteins to their correct localization or in directing proteins recognized as misfolded proteins towards ERAD. Indeed, when proteins cannot fold properly, they are handled by protein chaperones that will retro-translocate them into the cytosol. Depending whether proteins are glycosylated or not, their spectrum of chaperones can differ. The N-glycosylated proteins are handled by EDEM (ER Degradation Enhancer Mannosidase α-like protein), OS-9 (OSteosarcoma amplified 9), XTP3-B and other chaperones that bind SEL1L (sel-1 homolog 1), a cofactor of the transmembrane protein HRD1, that retro-translocate the misfolded proteins to the cytosol [79, 80]. This retro-translocation pathway is accompanied by a cytosolic deglycosylation of glycoproteins, which is mediated by N-glycanase (RE) [81], and binding to cytosolic segregases such as the AAA+ATPase p97/VCP [82], which allows for protein ubiquitination and the subsequent targeting to the proteasome leading to their proteolytic degradation [83, 84]. The non-glycosylated proteins are handled by BiP and addressed to trans-membrane proteins like HERP (Homocysteine-induced Endoplasmic Reticulum Protein) and DER1 (Degradation in Endoplasmic Reticulum protein1, homolog of Derlin1) [79, 80]. The misfolded proteins are thus retro-translocated to the cytosol where they are ubiquitinated by E3-ubiquitin ligases such as synoviolin (synovial apoptosis inhibitor 1, homolog of HRD1) and degraded by the proteasome. Many ubiquitin ligases are mutated in cancers [85]. Moreover gp78, an E4-ubiquitin ligase involved in ubiquitination and degradation of many proteins such as mutant CFTR (Cystic Fibrosis Trans-membrane conductance Regulator) [86] and the metastasis suppressor KAI1 [87]. Gp78 is over expressed in human sarcoma and has been shown to inhibit metastasis formation (at least) by inducing the degradation of KAI1 [87]. Gp78 expression is partially regulated by synoviolin, as well as P53, which makes synoviolin an interesting protein in cancer as described further below. Moreover, the ubiquitin-ligase RNF5 is over expressed in breast cancer, melanoma, and associated with metastasis formation [88], whereas another ubiquitin-ligase, Parkin, well known as a tumor suppressor, is under expressed in breast, lung and ovarian cancer, glioblastoma and hepatocellular carcinoma [89, 90, 91, 92, 93, 94, 95]. Finally, high expression levels of p97/VCP in liver cancer have

associated with high levels of recurrence and poor prognosis [96] and the targeting of VCP/p97 in hematological cancer cells has lead to promising results in anti-cancer therapies [97].

3 Connection between the UPR and canonical cancer signaling pathways

Cancerous cells that have acquired the capacity to bypass all the cellular proliferation and/or replication fidelity checkpoints are highly resistant against both environmental and internal death signals. Many studies have highlighted the key mechanisms of cancer formation, development, progression to metastasis and resistance to anti-cancer therapies and identified canonical signaling pathways involved in these processes. Here, we list the connections between UPR signaling and major cancer signaling pathways (Fig. 2).

3.1 p53

P53 was discovered in 1979 [98] as a transcription factor that binds to promoters containing p53 Responsive Element (p53RE; [99]). This is true for the majority of P53 targets but P53 can also bind non-canonical promoter sequences [100]. The targeting of non-conventional DNA sequences by P53 may principally result from the abnormal accumulation of P53 in the cell. This could instance occur when there is a stabilization of p53 by its natural antisense transcript Wrap53 [101]. P53 thus regulates the transcription of a large number of genes involved in mitosis or programmed cell death such as miR-34a, miR-34b and miR-34c [102], p21, HDM2 (Human Double Minute 2), PUMA (P53 Up-regulated Modulation of Apoptosis), Noxa or BAX (Bcl-2-Associated X protein).

Thus far, P53 has been shown to control many pathways regulating protein translation, apoptosis, senescence, DNA damage repair capacities, cell cycle arrest and differentiation [103], thereby indicating that this protein is a major regulator of cell fate. In normal cells, this key role needs to be tightly regulated by P53 modulators such as HDM2, ATR (Ataxia Telangiectasia and Rad3-related protein), CHK1 and CHK2 (Checkpoint Kinase 1 and 2) or otherwise cells may die prematurely and unnecessarily (cell cycle arrest followed by apoptosis). In contrast, in numerous cancers, P53 mutations allow the cells to escape from death (Table 1). For example, HDM2 is an E3 ubiquitin ligase able to inactivate P53 by promoting its nuclear export and thus its ubiquitination and degradation by the proteasome [104]. This role of HDM2 on P53 seems to be potentiated by MDM 4 binding to HDM2. P53 is activated by a lot of factors such as oncogene activation (MYC, E2F1, Ras, BCR-ABL), DNA damage, ribosomal stress and developmental defects. Thus, P53 activity is regulated by post-translational modifications like phosphorylation, acetylation, sumoylation or ubiquitination, which control localization, stability, activity and

half-life of P53. P53 localization in the cell is important for its activation because as a transcription factor it is active only in the nucleus and will be inactivated upon relocalization in the cytosol. Many links connect the UPR to p53 down-regulation but also to p53 up-regulation. It has been demonstrated that GSK3β for instance can phosphorylate P53 on serine 315 and 376 and consequently promotes P53 transport from the nucleus to the cytoplasm. P53 is thus ubiquitinated by synoviolin or HDM2 and degraded by the proteasome [105]. Other phosphorylations of the P53 amino terminal domain can stabilize this protein by disrupting the HDM 2-P53 interaction [104, 106]. PERK activates GSK3β, and synoviolin has been demonstrated to be up-regulated upon activation of the UPR [107, 108]. Indeed, synoviolin is a double agent: it is part of the ERAD system and it retains P53 in the cytosol under basal conditions. Upon light stress, P53 is still retained by synoviolin and trafficked to the proteasome, but upon more acute stresses synoviolin binds to unfolded proteins rather than to P53. P53 is then freed to travel to the nucleus [107]. Eventually, chronic and prolonged UPR leads to the up-regulation of two targets of P53: PUMA and Noxa [109], two pro-apoptotic molecules, emphasizing the fact that P53 activity is tightly linked to the UPR.

3.2 PKB (Akt)/PI3K – NF-κB

The PI3K/PKB(Akt)/NFκB pathway comprises a phosphorylation cascade resulting in control of cell cycle progression and cell proliferation, and it is globally an anti-apoptotic pathway. Among other things, it inhibits the TSC1/TSC2 (Tuberous Sclerosis 1 and 2) complex, thus enhancing cell proliferation *via* activation of the mTOR (mammalian Target Of Rapamycin) pathway. TSC1/TSC2 have both been connected to the UPR recently [110]. Additionally, it accelerates the cell cycle progression by promoting the G1/S phase transition, and inhibits GSK3β, resulting in the increased stability of crucial protein of the cell cycle [111, 112, 113]. PI3Ks (PhosphatidylInositide-3-Kinases), first actors of this signaling pathway, are lipid kinases activated by a large range of extracellular signals such as interferon, growth factors (EGF (epidermal growth factor) PDGF (platelet-derived growth factor), FGF (fibroblast growth factor), IGF (insulin-like growth factor), VEGF), and interleukins but also by activated intracellular proteins like Rac, Rho (Ras homolog gene family), Src, SHP1 (Src-Homology domain-containing protein tyrosine Phosphatase 1) and PKC (Protein Kinase C) [114].

Activation of PI3K induces phosphorylation of PIP2 (phosphatidylinositol-3,4-diphosphate) giving birth to PIP3 (phosphatidylinositol-3,4,5-triphosphate). PIP3 recruits the serine/threonine kinases PDK1 (phosphoinositide-dependent kinase 1) and Akt/PKB (Protein Kinase B), this complex then relocates to the plasma membrane where PDK1 is able to phosphorylate Akt/PKB. This PDK1 activation by PIP3 can be blocked by the phosphatase PTEN (Phosphatase and TENsin homolog), which dephosphorylates PIP3 to form PIP2. PKB, best known as Akt, is a serine/threonine kinase and it is the major target of PI3K. It regulates cell cycle progression and proliferation, migration, metabolism, apoptosis, angiogenesis and tumor

growth [112, 115, 116]. Among other things, phosphorylated Akt/PKB activates the mTOR pathway, inhibits the pro-apoptotic ASK1/JNK pathway and enhances activation of the pro-angiogenic factors VEGF and HIF-1 [112]. Moreover, it promotes cell survival as it enhances anti-apoptotic proteins like BCL-2, IκK and HDM2 and it inhibits pro-apoptotic proteins such as BAD and FOXO [112, 117]. Similar to p53, this important role in cellular regulation indicates that PI3K and Akt/PKB may actually be seen as oncogenes. Indeed, several studies have shown that Akt/PKB and PI3K were up-regulated in human cancers like thyroid cancer, ovarian cancer, malignant glioma and oral squamous cell carcinoma [111, 118, 119, 120], supporting results obtained in colorectal cancer cell lines [121]. PTEN for its part is a tumor suppressor down-regulated in lymphoma, leukemia, cancers of the prostate, breast, thyroid and endometrium and in glioblastoma multiforme [122, 123, 124].

3.3 Mitogen/Stress-Activated Protein Kinases pathways

The MAPK pathway includes about 14 serine/threonine kinases, which are phosphorylated in a cascade leading to activation of a transcription factor modulating different cellular functions and responses such as survival, apoptosis, proliferation and differentiation, by acting on mitosis, metabolism, motility, cell cycle progression, cellular proliferation, survival and growth, gene expression and protein synthesis. These kinases are separated in two groups named conventional and unconventional MAPKs. The conventional MAPKs are ERK1/2/5 (Extracellular signal-Regulated Kinase 1, 2 and 5), p38 isoforms and JNK1/2/3. These kinases are groups of three successive kinases: a MAPK, activated by a MAPK kinase (MAPKK or MAP2K), itself activated by a MAPKK kinase (MAPKKK or MAP3K). For instance, the MAPKs ERK1/2 are phosphorylated and activated by the MAPKKs MEK1/2, who are in turn phosphorylated and activated by the MAPKKKs A-Raf, B-Raf and Raf-1. The MAPKKKs are phosphorylated in response to extracellular signals and by the activation of small GTPases, and the MAPKs activation, which can be emphasized by others kinases named MK (MAPK-activated protein Kinases). This leads to transcriptional inductions. The unconventional kinases are not activated by phosphorylation cascades and little is known about their activation mechanisms [125], but all the MAPK kinases participate in the cellular responses cited above, and their activation is provoked by extracellular signals such as exposure to growth factors (PDGF (Platelet-Derived Growth Factor), EGF (Epidermal Growth Factor), NGF (Nerve Growth Factor)), insulin, cytokines, osmotic stress, microtubule disorganization and ligands for GPCR (heterodimeric G Protein Coupled Receptors). Environmental stresses (oxidative stress, hypoxia, growth factor deprivation, ischemia, heat shock, ionizing radiations, UV irradiation, DNA-damaging agents, DNA and protein synthesis inhibitors) and inflammatory cytokines (TNFα and Interleukin-1 (IL1)) promote TRAF, Rac1 (Ras-related C3 botulinum toxin substrate) or CDC42 (Cell Division Cycle 42) activation and subsequent activation of the MAPKs p38 and JNK (MAPKK=ASK1/2 among others). It leads to the phosphorylation of many targets in the cytoplasm (c-PLA2 (cytosolic phospholipase A2), MNK1/2,

MK2/3, HuR (Hu antigen R), BAX and Tau) and in the nucleus (ATF1/2, MEF2, Elk-1 (E twenty-six (ETS)-like transcription factor 1), NF-ATc1 (nuclear factor of activated T-cells, cytoplasmic, calcineurin-dependent 1), Ets1 (v-ets erythroblastosis virus E26 oncogene homolog 1), MSK1/2, HSF1 (Heat shock factor protein 1), STAT3 (Signal Transducer and Activator of Transcription 3), c-Myc, JunB and more importantly for this chapter: p53, NFκB, c-Jun, CHOP and ATF6α) [126, 127, 128]. Similar to p53, MAPKs control a large range of cellular responses and thus are prime candidates for cancer development. They are often mutated in cancers like thyroid follicular cell-derived neoplasm [111], skin, prostate, breast and bone cancers.

4 IRE1α pathway components involved in cancer promotion

IRE1α activity (activation of at least three downstream signaling pathways) in various pathophysiological situations supports the idea that IRE1α is a key regulator of cell fate upon ER stress. Moreover, recent reports have demonstrated that IRE1α plays a key regulatory role in cancer initiation and development. Some mutations in the IRE1α gene found in human cancer samples (ovary, lung, kidney, brain and stomach) have reinforce the idea of IRE1α as being a potential actor in tumor initiation and growth [129, 130] (Fig. 3). In addition to mutations present in IRE1α itself, many mutations have also been discovered in IRE1α downstream targets, which in turn could contribute to cancer development, as described below.

4.1 IRE1α kinase activity and cancer

The IRE1α mediated recruitment of TRAF2 and subsequent JNK activation is linked to pro-apoptotic responses. The ability of cancer cells to avoid cell death can occur for instance through the inhibition of this pathway. In this line of evidence, TRAF2 mutations have been found in breast, lung, ovary and skin cancers. Similarly JNK mutations were found in kidney, ovary, lung and central nervous system cancers (COSMIC database). Although these mutations do not directly involve IRE1α signaling, they certainly may contribute to alter UPR signaling in cancer.

4.2 XBP1 splicing and cancer [131]

Some target genes activated (over expressed) by XBP1 transcription factor activity are EDEM and PDI. Globally, $XBP1^{-/-}$ mice cannot survive more than two weeks and show increased apoptosis particularly in the liver at the embryonic stage [132]. These mice also present defects in pancreas morphology and function [133]. Moreover, XBP1 has been involved in plasma cell differentiation [134] and regulation of the cellular changes associated with specialized secretory cells [135, 136].

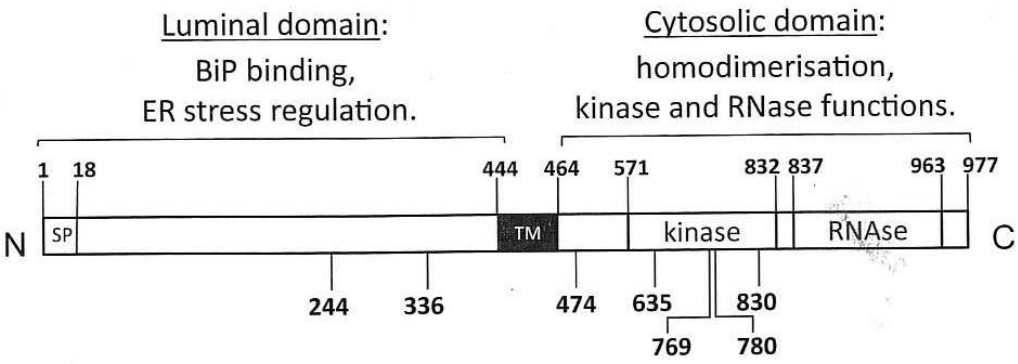

Aminoacids	Cancer	
244: Asn > Ser	Kidney	*Greenman, Nature, 2007*
336: Pro > Leu	Glioma	*Parsons, Science, 2008*
474: Leu > Arg	Lung	*Greenman, Nature, 2007*
635: Arg > Trp	Stomach	*Greenman, Nature, 2007*
769: Ser > Phe	Glioma	*Greenman, Nature, 2007*
780: Gln > STOP	Glioma	*Greenman, Nature, 2007*
830: Pro > Leu	Ovary	*Greenman, Nature, 2007*

Fig. 3 Schematic representation of IRE1 structure and mutations found in cancer. *SP*: signal peptide; *TM*: trans-membrane domain; *kinase*: kinase domain; *RNAse*: endoribonuclease domain. The numbers represent the position of the amino-acids bordering IRE1alpha domains (top of IRE1alpha representation) or the amino-acids mutated in cancers (bottom of IRE1alpha representation)

Furthermore, the direct interaction of BAX and BAK with IRE1α is essential for XBP1 splicing [77, 137].

The importance of XBP1 in cancer biology has been clearly illustrated in many cases. Indeed, transformed MEF cells with a deletion of the XBP1 gene cannot form tumors in SCID mice, contrary to transformed MEF expressing functional XBP1 [138]. These results have been confirmed in human cancers with an over expression of XBP1 in breast, lung and pancreas cancers [58, 131, 139] and by the fact that inhibitors of IRE1α endoribonuclease activity appeared to act as anti-cancer drugs as demonstrated in mouse models [140] and on multiple myeloma [141]. Moreover, animal studies demonstrated that expression of a dominant negative construct of IRE1α in a glioblastoma cell line (U87) impairs angiogenesis of xenograft tumors derived from these cells and that rescue of the IRE1α/XBP1 pathway by expressing the spliced form of XBP1 is sufficient to restore angiogenesis [142, 143].

4.3 RIDD and cancer

IRE1α endoribonuclease activity has been demonstrated to degrade many mRNA encoding secretory proteins, which allows a decrease of ER protein load [76]. This IRE1-mediated mRNA decay pathway (RIDD) may also be involved in tumor development since some of its targets are essential for cancer formation, cancer

development and metastasis. This is the case for Secreted Protein Acid Rich in Cysteine (SPARC), and Target of Methylation-induced Silencing (TMS1) [144, 145].

4.4 Involvement of IRE1 modulators in cancer

BI-1 has a double role (tissue specific) in cancer as it is over expressed in prostate, breast, uterus and ovary cancers [146, 147] but under expressed in kidney, stomach and colon cancers [147]. Collectively, these elements strongly suggest that IRE1 and its downstream signaling pathways might represent important actors in cancer development and progression.

5 Conclusion

This book chapter is a non-exhaustive review of the literature for the existing links between UPR and major cancer signaling pathways. We can note the particular involvement of the three UPR trans-membrane sensors, ATF6, IRE1 and PERK in regulating many cellular responses and particularly cancer cell fate. We can see that many links exist between the well-characterized cancer signaling pathways and the UPR signaling. Thus, major oncogenes such as Akt/PKB, or tumor suppressor genes, like p53, or pro-inflammatory pathways, like the NKkB pathway, can be modulated by these three ER stress sensors and are often deregulated in cancer. That is why an understanding of the UPR signaling is important in deciphering cancer biology. IRE1α is one of the most promising element for which functional characterization can lead to major advances in the understanding and the treatment of many human cancers due to the major role of this protein in controlling many cellular responses that are mis-regulated in cancer cells. To this end, recent studies focused on IRE1α mutants in human cancer cell lines or patient samples to decipher the precise mechanisms of IRE1α activation in cancer, especially in lung carcinoma, ovarian cancer, gliomas, kidney cancer and gastric cancer.

References

1. Zhang LH, Zhang X (2010) Roles of GRP78 in physiology and cancer. J Cell Biochem 110(6):1299–1305
2. Sun FC, Wei S, Li CW, Chang YS, Chao CC, Lai YK (2006) Localization of GRP78 to mitochondria under the unfolded protein response. Biochem J 396(1):31–39
3. Philippova MD, Ivanov MB, Joshi E, Kyriakakis K, Rupp T, Afonyushkin V, Bochkov P. Erne TJ, Resink (2008) Identification of proteins associating with glycosylphosphatidylinositol- anchored T-cadherin on the surface of vascular endothelial cells: role for Grp78/BiP in T-cadherin-dependent cell survival. Mol Cell Biol 28(12):4004–4017

4. Shani G, Fischer WH, Justice NJ, Kelber JA, Vale W, Gray PC (2008) GRP78 and Cripto form a complex at the cell surface and collaborate to inhibit transforming growth factor beta signaling and enhance cell growth. Mol Cell Biol 28(2):666–677
5. Misra UK, Deedwania R, Pizzo SV (2005) Binding of activated a2-macroglobulin to its cell surface receptor GRP78 in 1-LN prostate cancer cells regulates PAK-2-dependent activation of LIMK. J Biol Chem 280(28):26278–26286
6. Yoshida H, Haze K, Yanagi H, Yura T, Mori K (1998) Identification of the cis-acting endoplasmic reticulum stress response element responsible for transcriptional induction of mammalian glucose-regulated proteins. Involvement of basic leucine zipper transcription factors. J Biol Chem 273(50):33741–33749
7. Gülow K, Bienert D, Haas IG (2002) BiP is feed-back regulated by control of protein translation efficiency. J Cell Sci 115(Pt 11):2443–2452
8. Weitzmann A, Volkmer J, Zimmermann R (2006) The nucleotide exchange factor activity of Grp170 may explain the non-lethal phenotype of loss of Sil1 function in man and mouse. FEBS Lett. 580(22):5237–5240
9. Nicchitta C (2006) http://www.signaling-gateway.org. GRP94, UCSD Nature Molecule Pages. doi:10.1038/mp.a000645.01
10. Ogawa S (2003) ORP150 (150 kDa oxygen regulated protein) suppressed neuronal cell death. Nippon Yakurigaku Zasshi 121(1):43–48
11. Nakagawa T, Zhu H, Morishima N, Li E, Xu J, Yankner BA, Yuan J (2000) Caspase-12 mediates endoplasmic-reticulum-specific apoptosis and cytotoxicity by amyloid-beta. Nature 403(6765):98–103
12. Daneshmand S, Quek ML, Lin E, Lee C, Cote RJ, Hawes D, Cai J, Groshen S, Lieskovsky G, Skinner DG, Lee AS, Pinski J (2007) Glucose-regulated protein GRP78 is up-regulated in prostate cancer and correlates with recurrence and survival. Hum Pathol 38(10):1547–1552
13. Lee E, Nichols P, Spicer D, Groshen S, Yu MC, Lee AS (2006) GRP78 as a novel predictor of responsiveness to chemotherapy in breast cancer. Cancer Res 66:7849–7853
14. Su R Z, Li H, Li H, Song C, Bao J, Wei L, Cheng (2010) Grp78 promotes the invasion of hepatocellular carcinoma. BMC Cancer 10:20
15. Pyrko P, Schonthal AH, Hofman FM, Chen TC, Lee AS (2007) The unfolded protein response regulator GRP78/BiP as a novel target for increasing chemosensitivity in malignant gliomas. Cancer Res 67:9809–9816
16. Zhuang L, Scolyer RA, Lee CS, McCarthy SW, Cooper WA, Zhang XD, Thompson JF, Hersey P (2009) Expression of glucose-regulated stress protein GRP78 is related to progression of melanoma. Histopathology 54:462–470
17. Langer R, Feith M, Siewert JR, Wester HJ, Hoefler H (2008) Expression and clinical significance of glucose regulated proteins GRP78 (BiP) and GRP94 (GP96) in human adenocarcinomas of the esophagus. BMC Cancer 8:70
18. Weinreb I, Goldstein D, Irish J, Perez-Ordonez B (2009) Expression patterns of Trk-A, Trk-B, GRP78, and p75NRT in olfactory neuroblastoma. Hum Pathol 40:1330–1335
19. Dong D, Ni M, Li J, Xiong S, Ye W, Virrey JJ, Mao C, Ye R, Wang M, Pen L, Dubeau L, Groshen S, Hofman FM, Lee AS (2008) Critical role of the stress chaperone GRP78/BiP in tumor proliferation, survival, and tumor angiogenesis in transgene-induced mammary tumor development. Cancer Res 68(2):498–505
20. Chinni SR, Falchetto R, Gercel-Taylor C, Shabanowitz J, Hunt DF, Taylor DD (1997) Humoral immune responses to cathepsin D and glucose-regulated protein 78 in ovarian cancer patients. Clin Cancer Res 3:1557–1564
21. Gonzalez-Gronow M, Cuchacovich M, Llanos C, Urzua C, Gawdi G, Pizzo SV (2006). Prostate cancer cell proliferation in vitro is modulated by antibodies against glucose-regulated protein 78 isolated from patient serum. Cancer Res. 66:11424–11431

22. Papalas JA, Vollmer RT, Gonzalez-Gronow M, Pizzo SV, Burchette J, Youens KE, Johnson KB, Selim MA (2010) Patterns of GRP78 and MTJ1 expression in primary cutaneous malignant melanoma. Mod Pathol 23:134–143
23. Rauschert N, Brandlein S, Holzinger E, Hensel F, Muller-Hermelink HK, Vollmers HP (2008) A new tumor-specific variant of GRP78 as target for antibody-based therapy. Lab Invest 88:375–386
24. Chen X, Ding Y, Liu CG, Mikhail S, Yang CS (2002) Overexpression of glucose-regulated protein 94 (Grp94) in esophageal adenocarcinomas of a rat surgical model and humans. Carcinogenesis 23(1):123–130
25. Zheng HC, Takahashi H, Li XH, Hara T, Masuda S, Guan YF, Takano Y (2008) Overexpression of GRP78 and GRP94 are markers for aggressive behavior and poor prognosis in gastric carcinomas. Hum Pathol 39(7):1042–1049
26. Harding HP, Zhang Y, Ron D (1999) Protein translation and folding are coupled by an endoplasmic-reticulum-resident kinase. Nature 397(6716):271–274
27. Brewer JW, Hendershot LM, Sherr CJ, Diehl JA (1999) Mammalian unfolded protein response inhibits cyclin D1 translation and cell-cycle progression. Proc Natl Acad Sci U S A 96(15):8505–8510
28. Brewer JW, Diehl JA (2000) PERK mediates cell-cycle exit during the mammalian unfolded protein response. Proc Natl Acad Sci U S A 97(23):12625–12630
29. Harding HP, Novoa I, Zhang Y, Zeng H, Wek R, Schapira M (2000) Regulated translation initiation controls stress-induced gene expression in mammalian cells. Mol Cell 6(5):1099–1108
30. Vattem KM, Wek RC (2004) Reinitiation involving upstream ORFs regulates ATF4 mRNA translation in mammalian cells. Proc Natl Acad Sci U S A 101(31):11269–11274
31. Fawcett TW, Martindale JL, Guyton KZ, Hai T, Holbrook NJ (1999) Complexes containing activating transcription factor (ATF)/cAMP-responsive-element-binding protein (CREB) interact with the CCAAT/enhancer-binding protein (C/EBP)-ATF composite site to regulate Gadd153 expression during the stress response. Biochem J 339:135–141
32. Ma Y, Brewer JW, Diehl JA, Hendershot LM (2002) Two distinct stress signaling pathways converge upon the CHOP promoter during the mammalian unfolded protein response. J Mol Biol 318(5):1351–1365
33. Jiang HY, Wek SA, McGrath BC, Lu D, Hai T, Harding HP, Wang X, Ron D, Cavener DR, Wek RC (2004) Activating transcription factor 3 is integral to the eukaryotic initiation factor 2 kinase stress response. Mol Cell Biol 24(3):1365–1377
34. McCullough KD, Martindale JL, Klotz LO, Aw TY, Holbrook NJ (2001) Gadd153 sensitizes cells to endoplasmic reticulum stress by down-regulating Bcl2 and perturbing the cellular redox state. Mol Cell Biol 21(4):1249–1259
35. Ohoka N, Yoshii S, Hattori T, Onozaki K, Hayashi H (2005) TRB3, a novel ER stress-inducible gene, is induced via ATF4-CHOP pathway and is involved in cell death. Embo J 24(6):1243–1255
36. Novoa I., Zeng H, Harding HP, Ron D (2001) Feedback inhibition of the unfolded protein response by GADD34-mediated dephosphorylation of eIF2alpha. J Cell Biol 153(5):1011–1022
37. Cullinan SB, Diehl JA (2006) Coordination of ER and oxidative stress signaling: the PERK/Nrf2 signaling pathway. Int J Biochem Cell Biol 38(3):317–332
38. Harding HP, Zeng H, Zhang Y, Jungries R, Chung P, Plesken H, Sabatini DD, Ron D (2001) Diabetes mellitus and exocrine pancreatic dysfunction in perk-/- mice reveals a role for translational control in secretory cell survival. Mol Cell 7(6):1153–1163
39. Dhakshinamoorthy S, Porter AG (2004) Nitric oxide-induced transcriptional up-regulation of protective genes by Nrf2 via the antioxidant response element counteracts apoptosis of neuroblastoma cells. J Biol Chem 279(19):20096–20107

40. Blais JD, Addison CL, Edge R, Falls T, Zhao H, Wary K, Koumenis C, Harding HP, Ron D, Holcik M, Bell JC (2006) Perk-dependent translational regulation promotes tumor cell adaptation and angiogenesis in response to hypoxic stress. Mol Cell Biol 26(24):9517–9532
41. Bobrovnikova-Marjon E, Grigoriadou C, Pytel D, Zhang F, Ye J, Koumenis C, Cavener D, Diehl JA (2010) PERK promotes cancer cell proliferation and tumor growth by limiting oxidative DNA damage. Oncogene 29(27):3881–3895
42. Little JL, Wheeler FB, Fels DR, Koumenis C, Kridel SJ (2007) Inhibition of fatty acid synthase induces endoplasmic reticulum stress in tumor cells. Cancer Res 67(3):1262–1269
43. Ranganathan AC, Zhang L, Adam AP, Aguirre-Ghiso JA (2006) Functional coupling of p38-induced up-regulation of BiP and activation of RNA-dependent protein kinase-like endoplasmic reticulum kinase to drug resistance of dormant carcinoma cells. Cancer Res 66(3):1702–1711
44. Armstrong JL, Flockhart R, Veal GJ, Lovat PE, Redfern CP (2010) Regulation of endoplasmic reticulum stress-induced cell death by ATF4 in neuroectodermal tumor cells. J Biol Chem 285(9):6091–6100
45. Ameri K, Lewis CE, Raida M, Sowter H, Hai T, Harris AL (2004) Anoxic induction of ATF-4 through HIF-1-independent pathways of protein stabilization in human cancer cells. Blood 103(5):1876–1882
46. Shibata T, Ohta T, Tong KI, Kokubu A, Odogawa R, Tsuta K, Asamura H, Yamamoto M, Hirohashi S (2008) Cancer related mutations in NRF2 impair its recognition by Keap1-Cul3 E3 ligase and promote malignancy. Proc Natl Acad Sci U S A 105(36):13568–13573
47. Kim YR, Oh JE, Kim MS, Kang MR, Park SW, Han JY, Eom HS, Yoo NJ, Lee SH (2010) Oncogenic NRF2 mutations in squamous cell carcinomas of oesophagus and skin. J Pathol 220(4):446–451
48. Shibata T, Kokubu M, Gotoh M, Ojima H, Ohta T, Yamamoto M, Hirohashi S (2008) Genetic alteration of Keap1 confers constitutive Nrf2 activation and resistance to chemotherapy in gallbladder cancer. Gastroenterology 135(4):1358–1368, 1368 e1–e4
49. Taguchi K, Maher JM, Suzuki T, Kawatani Y, Motohashi H, Yamamoto M (2010) Genetic analysis of cytoprotective functions supported by graded expression of Keap1. Mol Cell Biol 30(12):3016–3026
50. Taguchi K, Motohashi H, Yamamoto M (2011) Molecular mechanisms of the Keap1-Nrf2 pathway in stress response and cancer evolution. Genes Cells 16(2):123–140
51. Asada R, Kanemoto S, Kondo S, Saito A, Imaizumi K (2011) The signalling from endoplasmic reticulum-resident bZIP transcription factors involved in diverse cellular physiology. J Biochem 149(5):507–518
52. Haze K, Yoshida H, Yanagi H, Yura T, Mori K (1999) Mammalian transcription factor ATF6 is synthesized as a transmembrane protein and activated by proteolysis in response to endoplasmic reticulum stress. Mol Biol Cell 10(11):3787–3799
53. Ye J, Rawson RB, Komuro R, Chen X, Davé UP, Prywes R, Brown MS, Goldstein JL (2000) ER stress induces cleavage of membrane-bound ATF6 by the same proteases that process SREBPs. Mol Cell 6(6):1355–1364
54. Chen X, Shen J, Prywes R (2002) The luminal domain of ATF6 senses endoplasmic reticulum (ER) stress and causes translocation of ATF6 from the ER to the Golgi. J Biol Chem 277(15):13045–13052
55. Nadanaka S, Yoshida H, Mori K (2006) Reduction of disulfide bridges in the lumenal domain of ATF6 in response to glucose starvation. Cell Struct Funct. 31(2): 127–134
56. Yoshida H, Okada T, Haze K, Yanagi H, Yura T, Negishi M, Mori K (2000) ATF6 activated by proteolysis binds in the presence of NF-Y (CBF) directly to the cis-acting element responsible for the mammalian unfolded protein response. Mol Cell Biol 20(18):6755–6767

57. Yoshida H, Matsui T, Yamamoto A, Okada T, Mori K (2001) XBP1 mRNA is induced by ATF6 and spliced by IRE1 in response to ER stress to produce a highly active transcription factor. Cell 107(7):881–891
58. Shuda M, Kondoh N, Imazeki N, Tanaka K, Okada T, Mori K, Hada A, Arai M, Wakatsuki T, Matsubara O, Yamamoto N, Yamamoto M (2003) Activation of the ATF6, XBP1 and grp78 genes in human hepatocellular carcinoma: a possible involvement of the ER stress pathway in hepatocarcinogenesis. J Hepatol 38(5):605–614
59. Arai M, Kondoh N, Imazeki N, Hada A, Hatsuse K, Kimura F, Matsubara O, Mori K, Wakatsuki T, Yamamoto M (2006) Transformation-associated gene regulation by ATF6alpha during hepatocarcinogenesis. FEBS Lett 580:184–190
60. Imagawa Y, Hosoda A, Sasaka S, Tsuru A, Kohno K (2008) RNase domains determine the functional difference between IRE1alpha and IRE1beta. FEBS Lett 582(5):656–660
61. Bertolotti A, Wang X, Novoa I, Jungreis R, Schlessinger K, Cho JH, West AB, Ron D (2001) Increased sensitivity to dextran sodium sulfate colitis in IRE1beta-deficient mice. J Clin Invest 107(5):585–593
62. Yuan L, Cao Y, Oswald F, Knöchel W (2008) IRE1beta is required for mesoderm formation in Xenopus embryos. Mech Dev 125(3–4):207–222
63. Iqbal J, Dai K, Seimon T, Jungreis R, Oyadomari M, Kuriakose G, Ron D, Tabas I, Hussain MM (2008) IRE1beta inhibits chylomicron production by selectively degrading MTP mRNA. Cell Metab 7(5):445–455
64. Bertolotti A, Zhang Y, Hendershot LM, Harding HP, Ron D (2000) Dynamic interaction of BiP and ER stress transducers in the unfolded-protein response. Nat Cell Biol 2(6):326–332
65. Lee KP, Dey M, Neculai D, Cao C, Dever TE, Sicheri F (2008) Structure of the dual enzyme Ire1 reveals the basis for catalysis and regulation in nonconventional RNA splicing. Cell 132(1):89–100
66. Urano F, Wang X, Bertolotti A, Zhang Y, Chung P, Harding HP, Ron D (2000) Coupling of stress in the ER to activation of JNK protein kinases by transmembrane protein kinase IRE1. Science 287(5453):664–666
67. Nishitoh H, Matsuzawa A, Tobiume K, Saegusa K, Takeda K, Inoue K, Hori S, Kakizuka A, Ichijo H (2002) ASK1 is essential for endoplasmic reticulum stress-induced neuronal cell death triggered by expanded polyglutamine repeats. Genes Dev 16(11):1345–1355
68. Yoneda T, Imaizumi K, Oono K, Yui D, Gomi F, Katayama T, Tohyama M (2001) Activation of caspase-12, an endoplastic reticulum (ER) resident caspase, through tumor necrosis factor receptor-associated factor 2-dependent mechanism in response to the ER stress. J Biol Chem 276(17):13935–13940
69. Nguyên DT, Kebache S, Fazel A, Wong HN, Jenna S, Emadali A, Lee EH, Bergeron JJ, Kaufman RJ, Larose L, Chevet E (2004) Nck-dependent activation of extracellular signal-regulated kinase-1 and regulation of cell survival during endoplasmic reticulum stress. Mol Biol Cell 15(9):4248–4260
70. Pahl HL (1999) Activators and target genes of Rel/NF-kappaB transcription factors. Oncogene 18(49):6853–6866
71. Uemura A, Oku M, Mori K, Yoshida H (2009) Unconventional splicing of XBP1 mRNA occurs in the cytoplasm during the mammalian unfolded protein response. J Cell Sci 122(Pt 16):2877–2886
72. Lee AH, Iwakoshi NN, Glimcher LH (2003) XBP-1 regulates a subset of endoplasmic reticulum resident chaperone genes in the unfolded protein response. Mol Cell Biol 23(21):7448–7459
73. Yoshida H, Matsui T, Hosokawa N, Kaufman RJ, Nagata K, Mori K (2003) A time-dependent phase shift in the mammalian unfolded protein response. Dev Cell 4(2):265–271
74. Hollien J, Weissman JS (2006) Decay of endoplasmic reticulum-localized mRNAs during the unfolded protein response. Science 313(5783):104–107

75. Oikawa D, Tokuda M, Iwawaki T (2007) Site-specific cleavage of CD59 mRNA by endoplasmic reticulum-localized ribonuclease, IRE1. Biochem Biophys Res Commun 360(1):122–127
76. Hollien J, Lin JH, Li H, Stevens N, Walter P, Weissman JS (2009) Regulated Ire1-dependent decay of messenger RNAs in mammalian cells. J Cell Biol 186(3):323–331
77. Hetz C, Bernasconi P, Fisher J, Lee AH, Bassik MC, Antonsson B, Brandt GS, Iwakoshi NN, Schinzel A, Glimcher LH, Korsmeyer SJ (2006) Proapoptotic BAX and BAK modulate the unfolded protein response by a direct interaction with IRE1alpha. Science 312(5773):572–576
78. Henke N, Lisak DA, Schneider L, Habicht J, Pergande M, Methner A (2011) The ancient cell death suppressor BAX inhibitor-1. Cell Calcium. PMID:21663964
79. Ye Y, Shibata Y, Yun C, Ron D, Rapoport TA (2004) A membrane protein complex mediates retro-translocation from the ER lumen into the cytosol. Nature 429(6994):841–847
80. Oda Y, Okada T, Yoshida H, Kaufman RJ, Nagata K, Mori K (2006) Derlin-2 and Derlin-3 are regulated by the mammalian unfolded protein response and are required for ER-associated degradation. J Cell Biol 172(3):383–393
81. Katiyar S, Joshi S, Lennarz WJ (2005) The retrotranslocation protein Derlin-1 binds peptide:N-glycanase to the endoplasmic reticulum. Mol Biol Cell 16(10):4584–4594
82. Ballar P, Pabuccuoglu A, Kose FA (2011) Different p97/VCP complexes function in retrotranslocation step of mammalian ER-associated degradation (ERAD). Int J Biochem Cell Biol 43(4):613–621
83. Jarosch E, Lenk U, Sommer T (2003) Endoplasmic reticulum-associated protein degradation. Int Rev Cytol 223:39–81
84. McCracken AA, Brodsky JL (2005) Recognition and delivery of ERAD substrates to the proteasome and alternative paths for cell survival. Curr Top Microbiol Immunol 300:17–40
85. Tsai YC, Weissman AM (2010) The Unfolded Protein Response, Degradation from Endoplasmic Reticulum and Cancer. Genes Cancer 1(7):764–778
86. Morito D, Hirao K, Oda Y, Hosokawa N, Tokunaga F, Cyr DM, Tanaka K, Iwai K, Nagata K (2008) Gp78 cooperates with RMA1 in endoplasmic reticulum-associated degradation of CFTRDeltaF508. Mol Biol Cell 19(4):1328–1336
87. Tsai YC, Mendoza A, Mariano JM, Zhou M, Kostova Z, Chen B, Veenstra T, Hewitt SM, Helman LJ, Khanna C, Weissman AM (2007) The ubiquitin ligase gp78 promotes sarcoma metastasis by targeting KAI1 for degradation. Nat Med 13(12):1504–1509
88. Bromberg KD, Kluger HM, Delaunay A, Abbas S, DiVito KA, Krajewski S, Ronai Z (2007) Increased expression of the E3 ubiquitin ligase RNF5 is associated with decreased survival in breast cancer. Cancer Res 67(17):8172–8179
89. Cesari R, Martin ES, Calin GA, Pentimalli F, Bichi R, McAdams H, Trapasso F, Drusco A, Shimizu M, Masciullo V, D'Andrilli G, Scambia G, Picchio MC, Alder H, Godwin AK, Croce CM (2003) Parkin, a gene implicated in autosomal recessive juvenile parkinsonism, is a candidate tumor suppressor gene on chromosome 6q25-q27. Proc Natl Acad Sci U S A 100(10):5956–5961
90. The Cancer Genome Atlas (TCGA) Research Network (2008) Comprehensive genomic characterization defines human glioblastoma genes and core pathways. Nature 455(7216):1061–1068
91. Denison SR, Wang F, Becker NA, Schüle B, Kock N, Phillips LA, Klein C, Smith DI (2003) Alterations in the common fragile site gene Parkin in ovarian and other cancers. Oncogene 22(51):8370–8378
92. Fujiwara M, Marusawa H, Wang HQ, Iwai A, Ikeuchi K, Imai Y, Kataoka A, Nukina N, Takahashi R, Chiba T (2008) Parkin as a tumor suppressor gene for hepatocellular carcinoma. Oncogene 27(46):6002–6011

93. Wang F, Denison S, Lai JP, Philips LA, Montoya D, Kock N, Schüle B, Klein C, Shridhar V, Roberts LR, Smith DI (2004) Parkin gene alterations in hepatocellular carcinoma. Genes Chromosomes Cancer 40(2):85–96
94. Yamamoto S, Tomita Y, Nakamori S, Hoshida Y, Nagano H, Dono K, Umeshita K, Sakon M, Monden M, Aozasa K (2003) Elevated expression of valosin-containing protein (p97) in hepatocellular carcinoma is correlated with increased incidence of tumor recurrence. J Clin Oncol 21(3):447–452
95. Picchio MC, Martin ES, Cesari R, Calin GA, Yendamuri S, Kuroki T, Pentimalli F, Sarti M, Yoder K, Kaiser LR, Fishel R, Croce CM (2004) Alterations of the tumor suppressor gene Parkin in non-small cell lung cancer. Clin Cancer Res 10(8):2720–2724
96. Yamamoto S, Tomita Y, Nakamori S, Hoshida Y, Nagano H, Dono K, Umeshita K, Sakon M, Monden M, Aozasa K (2003) Elevated expression of valosin-containing protein (p97) in hepatocellular carcinoma is correlated with increased incidence of tumor recurrence. J Clin Oncol 21(3):447–452
97. Wang Q, Shinkre BA, Lee JG, Weniger MA, Liu Y, Chen W, Wiestner A, Trenkle WC, Ye Y (2010) The ERAD inhibitor Eeyarestatin I is a bifunctional compound with a membrane-binding domain and a p97/VCP inhibitory group. PLoS One 5(11):e15479
98. DeLeo AB, Jay G, Appella E, Dubois GC, Law LW, Old LJ (1979) Detection of a transformation-related antigen in chemically induced sarcomas and other transformed cells of the mouse. Proc Natl Acad Sci U S A 76(5):2420–2424
99. Wang B, Xiao Z, Ren EC (2009) Redefining the p53 response element. Proc Natl Acad Sci U S A 106(34):14373–14378
100. Goldstein I, Marcel V, Olivier M, Oren M, Rotter V, Hainaut P (2011) Understanding wild-type and mutant p53 activities in human cancer: new landmarks on the way to targeted therapies. Cancer Gene Ther 18(1):2–11
101. Mahmoudi S, Henriksson S, Corcoran M, Méndez-Vidal C, Wiman KG, Farnebo M (2009) Wrap53, a natural p53 antisense transcript required for p53 induction upon DNA damage. Mol Cell 33(4):462–471
102. Kumamoto K, Spillare EA, Fujita K, Horikawa I, Yamashita T, Appella E, Nagashima M, Takenoshita S, Yokota J, Harris CC (2008) Nutlin-3a activates p53 to both down-regulate inhibitor of growth 2 and up-regulate mir-34a, mir-34b, and mir-34c expression, and induce senescence. Cancer Res 68(9):3193–3203
103. Vousden KH, Lu X (2002) Live or let die: the cell's response to p53. Nat Rev Cancer 2(8):594–604
104. Michael D, Oren M (2002) The p53 and Mdm2 families in cancer. Curr Opin Genet Dev 12(1):53–59
105. Qu L., Huang S, Baltzis D, Rivas-Estilla AM, Pluquet O, Hatzoglou M, Koumenis C, Taya Y, Yoshimura A, Koromilas AE (2004) Endoplasmic reticulum stress induces p53 cytoplasmic localization and prevents p53-dependent apoptosis by a pathway involving glycogen synthase kinase-3beta. Genes Dev 18(3):261–277
106. Wahl GM, Carr AM (2001) The evolution of diverse biological responses to DNA damage: insights from yeast and p53. Nat Cell Biol 3(12):E277–E286
107. Yamasaki S, Yagishita N, Nishioka K, Nakajima T (2007) The roles of synoviolin in cross-talk between endoplasmic reticulum stress-induced apoptosis and p53 pathway. Cell Cycle 6(11):1319–1323
108. Baltzis D, Pluquet O, Papadakis AI, Kazemi S, Qu LK, Koromilas AE (2005) The eIF2alpha kinases PERK and PKR activate glycogen synthase kinase 3 to promote the proteasomal degradation of p53. J Biol Chem 282(43):31675–31687
109. Li J, Lee B, Lee AS (2006) Endoplasmic reticulum stress-induced apoptosis: multiple pathways and activation of p53-up-regulated modulator of apoptosis (PUMA) and NOXA by p53. J Biol Chem 281(11):7260–7270

110. Wouters BG, Van Den Beucken T, Magagnin MG, Koritzinsky M, Fels D, Koumenis C (2005) Control of the hypoxic response through regulation of mRNA translation. Semin Cell Dev Biol 16(4–5):487–501
111. Brzezianska E, Pastuszak-Lewandoska D (2011) A minireview: the role of MAPK/ERK and PI3 K/Akt pathways in thyroid follicular cell-derived neoplasm. Front Biosci 16:422–439
112. Jiang BH, Liu LZ (2009) PI3 K/PTEN signaling in angiogenesis and tumorigenesis. Adv Cancer Res 102:19–65
113. Blanco-Aparicio C, Renner O, Leal JF, Carnero A (2007) PTEN, more than the AKT pathway. Carcinogenesis 28(7):1379–1386
114. Hennessy BT, Smith DL, Ram PT, Lu Y, Mills GB (2005) Exploiting the PI3 K/AKT pathway for cancer drug discovery. Nat Rev Drug Discov 4(12):988–1004
115. Adjei AA, Hidalgo M (2005) Intracellular signal transduction pathway proteins as targets for cancer therapy. J Clin Oncol 23(23):5386–5403
116. Shinohara M, Chung YJ, Saji M, Ringel MD (2007) AKT in thyroid tumorigenesis and progression. Endocrinology 148(3):942–947
117. Zhao L, Vogt PK (2008) Class I PI3 K in oncogenic cellular transformation. Oncogene 27(41):5486–5496
118. Nakayama K, Nakayama N, Kurman RJ, Cope L, Pohl G, Samuels Y, Velculescu VE, Wang TL, Shih Ie.M (2006) Sequence mutations and amplification of PIK3CA and AKT2 genes in purified ovarian serous neoplasms. Cancer Biol Ther 5(7):779–785
119. Iamaroon A, Krisanaprakornkit S (2009) Overexpression and activation of Akt2 protein in oral squamous cell carcinoma. Oral Oncol 45(10):e175–e179
120. Mure H, Matsuzaki K, Kitazato KT, Mizobuchi Y, Kuwayama K, Kageji T, Nagahiro S (2010) Akt2 and Akt3 play a pivotal role in malignant gliomas. Neuro Oncol 12(3):221–232
121. Samuels Y, Diaz LA Jr., Schmidt-Kittler O, Cummins JM, Delong L, Cheong I, Rago C, Huso DL, Lengauer C, Kinzler KW, Vogelstein B, Velculescu VE (2005) Mutant PIK3CA promotes cell growth and invasion of human cancer cells. Cancer Cell 7(6):561–573
122. Abbott RT, Tripp S, Perkins SL, Elenitoba-Johnson KS, Lim MS (2003) Analysis of the PI-3-Kinase-PTEN-AKT pathway in human lymphoma and leukemia using a cell line microarray. Mod Pathol 16(6):607–612
123. Terakawa N, Kanamori Y, Yoshida S (2003) Loss of PTEN expression followed by Akt phosphorylation is a poor prognostic factor for patients with endometrial cancer. Endocr Relat Cancer 10(2):203–208
124. Sansal I, Sellers WR (2004) The biology and clinical relevance of the PTEN tumor suppressor pathway. J Clin Oncol 22(14):2954–2963
125. Cargnello M, Roux PP (2011) Activation and function of the MAPKs and their substrates, the MAPK-activated protein kinases. Microbiol Mol Biol Rev 75(1):50–83
126. Cuadrado A, Nebreda AR (2010) Mechanisms and functions of p38 MAPK signalling. Biochem J 429(3):403–417
127. Bogoyevitch MA, Ngoei KR, Zhao TT, Yeap YY, Ng DC (2010) c-Jun N-terminal kinase (JNK) signaling: recent advances and challenges. Biochim Biophys Acta 1804(3):463–475
128. Raman M, Chen W, Cobb MH (2007) Differential regulation and properties of MAPKs. Oncogene 26(22):3100–3112
129. Greenman C, Stephens P, Smith R, Dalgliesh GL, Hunter C, Bignell G, Davies H, Teague J, Butler A, Stevens C, Edkins S, O'Meara S, Vastrik I, Schmidt EE, Avis T, Barthorpe S, Bhamra G, Buck G, Choudhury B, Clements J, Cole J, Dicks E, Forbes S, Gray K, Halliday K, Harrison R, Hills K, Hinton J, Jenkinson A, Jones D, Menzies A, Mironenko T, Perry J, Raine K, Richardson D, Shepherd R, Small A, Tofts C, Varian J, Webb T, West S, Widaa S, Yates A, Cahill DP, Louis DN, Goldstraw P, Nicholson AG, Brasseur F, Looijenga L, Weber BL, Chiew YE, DeFazio A, Greaves MF, Green AR, Campbell P, Birney E, Easton DF, Chenevix-Trench G, Tan MH, Khoo SK, Teh BT, Yuen ST, Leung SY, Wooster R, Futreal

PA, Stratton MR (2007) Patterns of somatic mutation in human cancer genomes. Nature 446(7132):153–158
130. Parsons DW, Jones S, Zhang X, Lin JC, Leary RJ, Angenendt P, Mankoo P, Carter H, Siu IM, Gallia GL, Olivi A, McLendon R, Rasheed BA, Keir S, Nikolskaya T, Nikolsky Y, Busam DA, Tekleab H, Diaz LA Jr., Hartigan J, Smith DR, Strausberg RL, Marie SK, Shinjo SM, Yan H, Riggins GJ, Bigner DD, Karchin R, Papadopoulos N, Parmigiani G, Vogelstein B, Velculescu VE, Kinzler KW (2008) An integrated genomic analysis of human glioblastoma multiforme. Science 321(5897):1807–1812
131. Koong AC, Chauhan V, Romero-Ramirez L (2006) Targeting XBP-1 as a novel anti-cancer strategy. Cancer Biol Ther. 5(7):756–759
132. Reimold AM, Etkin A, Clauss I, Perkins A, Friend DS, Zhang J, Horton HF, Scott A, Orkin SH, Byrne MC, Grusby MJ, Glimcher LH (2000) An essential role in liver development for transcription factor XBP-1. Genes Dev 14(2):152–157
133. Hess DA, Humphrey SE, Ishibashi J, Damsz B, Lee AH, Glimcher LH, Konieczny SF (2011) Extensive Pancreas Regeneration Following Acinar-Specific Disruption of Xbp1 in Mice. Gastroenterology 141(4):1463–1472
134. Iwakoshi NN, Lee AH, Glimcher LH (2003) The X-box binding protein-1 transcription factor is required for plasma cell differentiation and the unfolded protein response. Immunol Rev 194:29–38
135. Brewer JW, Hendershot LM (2005) Building an antibody factory: a job for the unfolded protein response. Nat Immunol 6(1):23–29
136. Shaffer AL, Shapiro-Shelef M, Iwakoshi NN, Lee AH, Qian SB, Zhao H, Yu X, Yang L, Tan BK, Rosenwald A, Hurt EM, Petroulakis E, Sonenberg N, Yewdell JW, Calame K, Glimcher LH, Staudt LM (2004) XBP1, downstream of Blimp-1, expands the secretory apparatus and other organelles, and increases protein synthesis in plasma cell differentiation. Immunity 21(1):81–93
137. Romero-Ramirez L, Cao H, Nelson D, Hammond E, Lee AH, Yoshida H, Mori K, Glimcher LH, Denko NC, Giaccia AJ, Le QT, Koong AC (2004) XBP1 is essential for survival under hypoxic conditions and is required for tumor growth. Cancer Res 64(17):5943–5947
138. Spiotto MT, Banh A, Papandreou I, Cao H, Galvez MG, Gurtner GC, Denko NC, Le QT, Koong AC (2010) Imaging the unfolded protein response in primary tumors reveals microenvironments with metabolic variations that predict tumor growth. Cancer Res 70(1):78–88
139. Fujimoto T, Onda M, Nagai H, Nagahata T, Ogawa K, Emi M (2003) Upregulation and overexpression of human X-box binding protein 1 (hXBP-1) gene in primary breast cancers. Breast Cancer 10(4):301–306
140. Feldman DE, Chauhan V, Koong AC (2005) The unfolded protein response: a novel component of the hypoxic stress response in tumors. Mol Cancer Res 3(11):597–605
141. Papandreou I, Denko NC, Olson M, Van Melckebeke H, Lust S, Tam A, Solow-Cordero DE, Bouley DM, Offner F, Niwa M, Koong AC (2011) Identification of an Ire1alpha endonuclease specific inhibitor with cytotoxic activity against human multiple myeloma. Blood 117(4):1311–1314
142. Drogat B, Auguste P, Nguyen DT, Bouchecareilh M, Pineau R, Nalbantoglu J, Kaufman RJ, Chevet E, Bikfalvi A, Moenner M (2007) IRE1 signaling is essential for ischemia-induced vascular endothelial growth factor-A expression and contributes to angiogenesis and tumor growth in vivo. Cancer Res 67(14):6700–6707
143. Romero-Ramirez L, Cao H, Regalado MP, Kambham N, Siemann D, Kim JJ, Le QT, Koong AC (2009) X box-binding protein 1 regulates angiogenesis in human pancreatic adenocarcinomas. Transl Oncol 2(1):31–38
144. Nagaraju GP, Sharma D (2011) Anti-cancer role of SPARC, an inhibitor of adipogenesis. Cancer Treat Rev 37(7):559–566
145. McConnell BB, Vertino PM (2004) TMS1/ASC: the cancer connection. Apoptosis 9(1):5–18

146. Grzmil M, Thelen P, Hemmerlein B, Schweyer S, Voigt S, Mury D, Burfeind P (2003). Bax inhibitor-1 is overexpressed in prostate cancer and its specific down-regulation by RNA interference leads to cell death in human prostate carcinoma cells. Am J Pathol 163(2):543–552
147. Grzmil M, Kaulfuss S, Thelen P, Hemmerlein B, Schweyer S, Obenauer S, Kang TW, Burfeind P (2006) Expression and functional analysis of Bax inhibitor-1 in human breast cancer cells. J Pathol 208(3):340–349

IV. Signalisation IRE1α et glioblastome

A. Le glioblastome multiforme (GBM)

Les gliomes sont parmi les cancers primitifs les plus mortels. C'est le deuxième cancer le plus fréquent chez l'enfant, après la leucémie, et le troisième cancer le plus mortel chez le jeune adulte. Ces tumeurs restent rares, avec 5 cas pour 100 000 habitants, et leur pronostic est principalement lié à leur localisation ou à leur taille. Les gliomes sont classés en quatre stades selon la dernière classification de l'O.M.S. de 2007 [150], du plus bénin nommé grade I au plus grave nommé grade IV.

Les tumeurs de grade IV, aussi appelées glioblastomes multiforme (GBM) ou astrocytomes de stade IV, sont le plus souvent incurables, avec une médiane de survie inférieure à 2 ans (14,5 mois), et un taux de survie à 5 ans quasiment nul [151]. Le GBM survient principalement chez des personnes de 45 à 70 ans et représente à lui seul environ 50% des gliomes diagnostiqués. Le mauvais pronostic du GBM est majoritairement dû à : **i)** un phénotype infiltrant, avec une dissémination de cellules cancéreuses invasives dans le cerveau, ce qui les rend difficiles à atteindre par la chirurgie ou par une radiothérapie ciblée; et **ii)** la résistance aux traitements. Ces tumeurs peuvent être volumineuses et profondes, donc peu opérable, et même après une chirurgie la plus complète possible, la grande hétérogénéité de ces tumeurs, la présence de spots infiltrants et l'instabilité génétique résultant notamment des chimiothérapies, expliquent l'échappement des GBM aux traitements. L'ajout d'un agent alkylant depuis 2000, le témolozomide (TMZ - témodal), en complément de la radiothérapie puis en chimiothérapie seule, a permis une amélioration modeste de la survie des patients (de 12 à 15 mois) [152] ainsi que de leur qualité de vie. Cependant, de nombreuses résistances sont apparues suite à ce traitement, à cause d'une mutagenèse importante au niveau de la tumeur conduisant notamment à des mutations du gène MGMT (et méthylation). Une deuxième thérapie à base d'antiangiogénique (avastin) ou d'inhibiteur de topoisomérases peut être mise en place lors d'une rechute après un traitement au TMZ. Les traitements actuels ne donnant presque aucune chance de rémission, une attention particulière est apportée à la qualité de vie des patients et chaque traitement est envisagé en fonction des effets sur la tumeur mais aussi des effets sur le patient et ses capacités neurologiques. Une meilleure compréhension de la physiopathologie des GBM est essentielle pour : **i)** découvrir de nouvelles cibles thérapeutiques et développer de nouvelles thérapies, et **ii)** définir des bons

marqueurs pronostics qui permettent d'adapter au mieux les thérapies et conserver aux patients la meilleure qualité de vie possible. Afin d'identifier de nouvelles cibles thérapeutiques, de nombreuses études ont listé les gènes dont les mutations pourraient impacter des étapes clés du développement des GBM, notamment des études menées par The Cancer Genome Atlas project (TCGA) [153, 154]. Plusieurs candidats ont ainsi été mis en évidence: EGFR, PTEN, TP53, NF1 et IDH1. Cependant, un traitement ciblé du GBM par des molécules inhibant spécifiquement ces candidats, par exemple avec un inhibiteur de l'EGFR, peut être inefficace à cause de phénomènes compensatoires. Ainsi, des inhibiteurs moins spécifiques qui ciblent la famille des EGFR sont en cours d'essais cliniques, en association avec un antiangiogénique. Ceci souligne la pertinence qu'il y a à comprendre l'ensemble des voies de signalisation impliquées, afin d'avoir un large panel de chimiothérapies qui pourront permettre de contourner les multiples résistances qui sont apparues et apparaîtront. Le deuxième enjeu majeur de la recherche sur les GBM est l'identification de marqueurs pronostics qui permettent de définir des thérapies adaptées, selon par exemple les profils de mutation des tumeurs, l'âge du patient ou les réponses aux traitements.

B. Le rôle d'IRE1α dans les GBM

Le rôle de la signalisation IRE1α dans le GBM a été démontré par des approches d'extinction de la signalisation IRE1α. En effet, l'expression d'un dominant négatif (DN) [155], qui ne contient pas les domaines à activité catalytique d'IRE1α mais qui est toutefois capable de se lier aux protéines IRE1α endogènes, a pour conséquence d'inhiber l'activité d'IRE1α y compris endogène et de bloquer ainsi les voies de signalisation en aval d'IRE1α

Afin d'étudier le rôle de la signalisation IRE1α dans le développement de GBM, ce dominant-négatif (DN) a été exprimé de façon stable dans des cellules issues de glioblastome humain U-87 MG. Ces cellules U87-DN implantées sur une membrane choro-allantoïdienne de poulet [156] ou dans un cerveau de souris [157] forment des tumeurs de taille inférieure et moins vascularisées que les tumeurs issues de cellules U-87 MG contrôles (U87-EV). La perte du phénotype prolifératif et angiogénique au profit d'un phénotype avasculaire et migratoire s'explique en partie par le rôle d'IRE1α dans la production de facteurs pro-angiogéniques tels que VEGF-A, IL-1β, IL-6, et IL-8. Cependant, ces études n'ont pas permis d'établir précisément quel domaine ou quelle activité d'IRE1α est (sont) impliqué(s) dans le phénotype des tumeurs formées dans les conditions contrôles (U87-EV). Afin de déterminer

dans quelle mesure l'activité RIDD est responsable du phénotype observé dans les U87-DN, nous avons réalisé une étude comparative entre le transcriptome des U87-EV et celui des U87-DN. De façon plus générale, l'expression des mutations d'IRE1α identifiées dans des GBM humains nous a permis de comprendre comment des modifications de séquence d'IRE1α peuvent conférer des avantages sélectifs aux cellules tumorales et ainsi favoriser la progression tumorale et la résistance aux traitements anti-cancéreux.

HYPOTHESES ET OBJECTIFS DU PROJET

En 2010, date de début de mon projet de thèse, sept mutations somatiques ponctuelles avaient été identifiées dans des biopsies de patients atteints de divers cancers (glioblastomes, cancer du rein, de l'ovaire, du poumon et de l'estomac), dont six définies comme étant initiatrices de tumeur. Des travaux de séquençage effectués au sein de notre équipe, ont mis en évidence une huitième mutation, la quatrième identifiée dans une biopsie de GBM.

Nous avons fait l'hypothèse que ces mutations somatiques d'IRE1α changent les capacités de signalisation de cette protéine, modifiant de ce fait les propriétés du RE et de la voie de sécrétion et impactant ainsi sur le développement et l'agressivité des tumeurs.

Ainsi, l'objectif de ma thèse a été de définir si une ou plusieurs des mutations d'IRE1α identifiées dans des cancers humains a (ont) un impact fonctionnel dans ces cancers.

Pour cela, j'ai tout d'abord étudié l'impact fonctionnel de ces mutations sur la signalisation IRE1α, puis j'ai caractérisé l'impact de ces mutations sur le phénotype tumoral, que ce soit la tumorigenèse, la croissance tumorale, la vascularisation ou la réponse aux traitements médicaux.

Dans ce but, nous avons reproduit *in vitro* ces mutations et mis en place des outils de criblage nous permettant de sélectionner les mutations potentiellement intéressantes pour l'évolution du cancer. Nous avons ensuite validé l'intérêt de ces mutations pour le développement de la tumeur à l'aide de travaux *in vivo* réalisés chez la souris, dans un modèle de GBM.

En parallèle de cette étude, j'ai en outre pu participer aux travaux du laboratoire visant à caractériser le rôle d'IRE1α dans le GBM, travaux qui ont donné lieu aux **articles 3 et 4** présentés ci-après.

APPROCHES EXPERIMENTALES

Toutes les méthodologies utilisées durant ma thèse sont décrites dans la revue méthodologique incluse ci-après (**ARTICLE 2**) ou dans l'**article 5** figurant dans la section résultats.

ARTICLE 2

Adaptation of the secretory pathway in cancer through IRE1 signaling

Stéphanie Lhomond[1], Nestor Pallares[1], Kim Barroso[1], Nicolas Dejeans[1], Helena Falzi[1], Said Taouji[1], John B. Patterson[2] and Eric Chevet[1,3]

[1]Inserm, U1053, 33000 Bordeaux, France; Université de Bordeaux, 33000 Bordeaux, France.
[2]ManKind corporation, 28903 North Avenue Paine, Valencia, California, 91355, USA.

[3]Correspondence to EC: Inserm U1053, Université de Bordeaux, 146 rue Léo Saignat, 33000 Bordeaux, France. Phone +33(0)557579253, Fax: +33(0)556514077, email: eric.chevet@inserm.fr

Keywords: Endoplasmic Reticulum, Unfolded Protein Response, IRE1, ERN1, XBP1, IRE1 inhibitors.

Abstract

The unfolded protein response (UPR) was originally identified as a signaling network coordinating adaptive and apoptotic responses to accumulation of unfolded proteins in the endoplasmic reticulum (ER). More recent work has shown that UPR signaling can be triggered by a multitude of cellular events and that the UPR plays a critical role in the prevention of cell transformation but also in tumor development. This has been particularly well illustrated with studies on one of the three major ER stress sensors, IRE1. This ER resident type I transmembrane protein senses luminal ER stress and transduce signals through its cytosolic RNase activity. IRE1 signaling has been shown to contribute to the progression of solid tumors through pro-angiogenic mechanisms. Herein, we expose the methodologies for investigating IRE1 signaling in tumor cells and in tumors. Moreover, we show that

selective pharmacological inhibition of IRE1 RNase activity sensitizes tumor cells to ER stress.

1. Introduction

Twenty-five years ago, the existence of a signaling pathway was identified in mammalian cells to control adaptation to protein folding defect. This occurs through the transcriptional upregulation of key ER chaperones (1) mediated by three classes of ER stress sensors, namely Inositol-requiring enzyme-1 (IRE1, α and β isoforms), activating transcription factor 6 (ATF6) (α and β isoforms) and protein kinase RNA-like ER kinase (PERK) (2). PERK activation also involves its dimerization and auto-transphosphorylation (3, 4). Activated PERK phosphorylates the translation initiator factor eIF2α, inhibiting protein synthesis, and nuclear factor erythroid 2-related factor 2 (NRF2), a transcription factor involved in redox metabolism (5). This reduces the load of newly synthesized proteins entering the ER, thus having an important pro-survival effect (6). Phosphorylation of eIF2α limits the amount of active ribosomes and allows the translation of mRNAs containing short open reading frames (micro-ORFs) in their 5'-untranslated regions, including Activating Transcription Factor-4 (ATF4). ATF4 controls the expression of genes involved in redox and amino acid metabolism, in addition to ER chaperones and foldases (7, 8). ATF4 also regulates the expression of important genes involved in apoptosis including the transcription factor C/EBP-homologous protein (CHOP) and growth arrest and DNA damage-inducible-34 (GADD34) (see above). GADD34 participates on a feedback loop to dephosphorylate eIF2α by interacting with protein phosphatase 1C (PP1C), restoring protein synthesis (9). Finally, ATF6α is a type-II ER located protein that contains a bZIP transcription on its cytosolic domain. Upon ER stress ATF6α translocates to the Golgi apparatus where it is cleaved by S1P and S2P proteases to release a cytosolic fragment (ATF6c) (10, 11). ATF6c is a transcription factor that regulates the expression of genes of the ERAD pathway among other target genes (12, 13). Exclusive or combined action of ATF6c and XBP1s may also have a differential effect on gene expression (14).

Activation of IRE1α involves its oligomerization, and auto-transphosphorylation, leading to a conformational change that activates the RNase domain. IRE1α RNase excises a 26-nucleotide intron of the X-Box binding protein-1 (XBP1) encoding mRNA, which is then religated by a yet unknown RNA ligase. This changes the coding reading frame of the mRNA,

leading to the expression of an active transcription factor, termed XBP1s, for the spliced form (12, 15, 16). XBP1s trans-activates a subset of target genes involved in protein folding, endoplasmic reticulum-associated degradation (ERAD), protein translocation to the ER, and protein secretion (17, 18) (**Fig. 1**). IRE1α also signals through the scaffolding of many adapter proteins and regulators, a dynamic protein platform referred to as the UPRosome (5) (**Fig. 1**). IRE1α interacts with the adapter protein TRAF2, leading to the downstream activation of the kinase JNK (19). IRE1α RNase activity also degrades a subset of mRNA through a process known as regulated IRE1-dependent decay of mRNA (RIDD) (20-22) (**Fig. 1**). The pool of RNAs degraded by RIDD depends on the cell type affected and targets mRNAs encoding for proteins of the secretory pathway. The selectivity of IRE1α to degrade particular RIDD substrates may depend on the presence of a conserved nucleotide sequence accompanied by a defined secondary structure (20-23). Moreover, IRE1α has also been shown to cleave premature microRNAs thereby impacting on the control of apoptosis (24). Furthermore, the regulation of IRE1α expression levels by microRNAs was shown to impact on its biological functions (25-27).

The role of IRE1 in cancer has been well documented (28-30). In particular we have shown that in glioblastoma IRE1 activity contributes to tumor growth through the activation of pro-angiogenic and pro-inflammatory pathways (28-31), thereby indicating that IRE1 could represent a potentially relevant therapeutic target in this disease. Herein, we list the methodologies used in our laboratory to investigate and pharmacolocgically perturb IRE1 (32) signaling in glioblastoma cells.

2. Materials

2.1. Cell lines and mouse strains (U-87 MG, RagGamma mice)

Human glioblastoma derived cells U-87 MG were from ATCC. RagGamma mice were produced in the Bordeaux 1 University animal house (Dir. R. Pineau).

2.2. Antibodies

2.2.1. Mouse monoclonal antibodies against XBP1s (clones 2G4 and 5E4) were produced in-house and respectively used for immunohistochemistry and immunoblotting.

2.2.2. Rabbit antisera to JNK1 were from SantaCruz Biotechnologies (SantaCruz, CA, USA). Anti phospho-JNK were from Cell Signaling Technology (Danvers, MA, USA).

2.2.3. Rabbit antisera to IRE1 were from SantaCruz Biotechnologies (SantaCruz, CA, USA). Rabbit monoclonal antibodies to phospho-IRE1 (S724) were from Abcam (Cambridge, MA, USA).

2.2.4. Antibodies to Vimentin (dil. 1/400) were from Acris Antibodies (Herford, Germany) and antibodies to CD31 (dil. 1/200) were from BD Pharmingen (Franklin Lakes, NJ USA).

2.2.5. Secondary antibodies used herein were Alexia 547 (Fluoroprobes 547h Donkey Anti Rat IGG FP-SB6110) 1/200, Alexia 488 (Fluoroprobes 488h Donkei Anti Mouse IGG FP-5A4110) 1/200 or EnVision FLEX/HRP (Dako F8010/F8012/F8024). Hoechst (Molecularprobes 34580) 1/1000)) was used.

2.3. PCR primers

RT-PCR primers: hPer1 Fwd, 5'-GGGTCCTCCAGTGATAGCAA-3' ; Rev, 5'-GAGGAGGAGGCACATTTACG-3' (amplicon length: 386 bp); hGapdh Fwd, 5'-ACCACCATGGAGAAGGCTGG-3' ; Rev, 5'-CTCAGTGTAGCCCAGGATGC-3' (amplicon length: 528 bp); hPer2, Fwd, 5'-TACGCTGGCCACCTTGAAGTA-3' ; Rev, 5'-CACATCGTGAGGCGCCAGGA-3' (amplicon length: 386 bp). siRNA: GL2, 5'-CGUACGCGGAAUACUUCGA-3' ; Ire1α, 5'-UUACUGGCUUCUGAUAGGA-3' ; Xbp1, 5'-CUCAUGGCCUUGUAGUUGA-3'. For quantitative PCR the corresponding primers were used: hPER2, Fwd, 5'-TACGCTGGCCACCTTGAAGTA-3' ; Rev, 5'-CACATCGTGAGGCGCCAGGA-3' ; hPER1, Fwd, 5'-TATACCCTGGAGGAGCTGGA-3' ; Rev, 5'-AGGAAGGAGACAGCCACTGA-3' ; 18S, Fwd, 5'-GGATCCATTGGAGGGCAAGT-3' ; Rev, 5'-CCGCTCCCAAGATCCAACTA-3' .

2.4. Chemicals

IRE1 inhibitors: Irestatin (Axon Medchem, Vienna, VA, USA), Toyocamycin (Sigma-Aldrich, StLouis, MO, USA) and MKC8866 (labeled MKC; MannKind Corporation, WO 2011/127070 A2) (33). Tunicamycin was purchased from Calbiochem (Merck KGaA, Darmstadt, Germany). Acrylamide-Bis-acrylamide 30:1 was from Biorad (Hercules, CA, USA). SDS was from Thermo Fisher Scientific (Waltham, MA, USA).

2.5. SDS-PAGE and PhosTag SDS-PAGE gel components

2.5.1. Resolving buffer: 1.5 M Tris/HCl solution, pH 8.8 (4x solution for resolving gel): add about 100 mL distilled water to a 1 L graduated cylinder or a glass beaker. Weigh

181.7 g Tris and transfer to the cylinder. Add distilled water to a volume of 900 mL. Mix and adjust pH with HCl. Make up to 1 L with distilled water. Filter the solution. Store at 4°C in the dark.

2.5.2. Stacking buffer: 0.5 M Tris/HCl solution, pH 6.8 (4x solution for staking gel): add about 100 mL distilled water to a 1-L graduated cylinder or a glass beaker. Weigh 60.6 g Tris and transfer to the cylinder. Add distilled water to a volume of 900 mL. Mix and adjust pH with HCl. Make up to 1 L with distilled water. Store at 4°C.

2.5.3. 10% (w/v) SDS solution: add about 100 mL distilled water to a 1-L graduated cylinder or a glass beaker. Weigh 100 g SDS and transfer to the cylinder. Add distilled water to a volume of 1 L. Store at room temperature.

2.5.4. 5.0 mmol/L Phostag solution containing 3% (v/v) methanol: add 0.1 mL methanol to the oily product Phostag AAL-107 plastic tube (Wako Cat. No. 304-93525). Dilute the methanol solution with 3.2 mL of distilled water by pipetting. Wrap the tube with aluminum foil. Keep the solution in 2-mL microtubes at 4°C in the dark.

2.5.5. 10 mM $MnCl_2$ solution: add about 50 mL distilled water to a 500-mL graduated cylinder or a glass beaker. Weigh 0.10 g $MnCl_2$(H2O)4 (MW: 198) and transfer to the cylinder. Add distilled water to a volume of 500 mL. Mix and store at room temperature.

2.5.6. 10% (w/v) ammonium persulfate solution: weigh 500 mg (NH4)2S2O8 (MW: 228) and transfer to a 15 mL conical flask. Add distilled water to a volume of 5 mL. Mix and aliquote in 2-mL microtubes placed at -20°C for long-term storage.

2.5.7. 30% acrylamide/Bis solution (29.2:0.8 acrylamide:Bis) (Bio-Rad, Hercules, CA, USA). Store at 4°C.

2.5.8. N , N , N , N ′ -tetramethyl-ethylenediamine (TEMED) (Sigma Chemical Company, St. Louis, MO, USA). Store at 4°C.

2.5.9. Running buffer, pH 8.3 (10x solution): add about 100 mL distilled water to a 1-L graduated glass beaker. Weigh 30.2 g Tris, 10.0 g SDS and 144 g glycine and transfer to the glass beaker. Add distilled water to a volume of 500 mL. Vortex to pre-dissolve Tris, SDS and glycine then add distilled water to a volume of 900 mL. Mix and adjust pH to 8.3. Make up to 1 L with distilled water. Store at room temperature.

2.5.10. Sample buffer (3x solution): add about 1 mL distilled water to a 10-mL graduated cylinder. Weigh 1.5 mg bromophenol blue and 0.60 g SDS and transfer to the cylinder. Add 3 mL glycerol, 3.9 mL of solution b (0.5 M Tris/HCl solution, pH 6.8). Add distilled water to a volume of 8.5 mL. Mix and aliquote in 2-mL microtubes placed at -20°C

for long-term storage. Just before use, thaw the sample buffer and add 15% of 2-mercaptoethanol.

2.6. Immunoblotting components

2.6.1. PVDF membranes (Millipore, Darmstadt, Germany).

2.6.2. Western blot transfer buffer: 0.025 M Tris, 0.192 M glycine and 10% methanol.

2.6.3. Phosphate-buffered saline (PBS; 10×): 1.5 M NaCl, 0.1 M Tris–HCl, pH 7.4.

2.6.4. PBST: TBS containing 0.1% Tween-20.

2.6.5. Blocking solution: 3% bovine serum albumine (BSA) in PBS. Store at 4°C.

2.6.6. Diluent solution: 5% BSA in PBST. Store at 4°C.

2.6.7. Mini PROTEAN® 3 System glass plates (catalog number 1653311) (Bio-Rad). Medium binder clips (1¼ in.). Plastic container.

2.6.8. Wypall X-60 reinforced paper (Kimberly-Clark, Neenah, WI, USA).

2.7. RNA extraction and RT-PCR

2.7.1. RNA extraction - TRIzol® Reagent (life technologies, Ref: 15596026), chloroform (Sigma-Aldrich, Ref: C2432), isopropanol (Carlo Erba, Ref: 415156), ethanol 75%.

2.7.2. Reverse transcription - Nuclease free water, Random Hexamer 100 pmol (Thermo Scientific, Ref: SO142), dNTP Mix, 10 mM each (Thermo Scientific, Ref: R0191), 5X RT Buffer (Thermo Scientific, Ref: EP074), Ribolock™ RNase Inhibitor (Thermo Scientific, Ref: EO0381), Maxima® Reverse Transcriptase (200 Units/µL) (Thermo Scientific, Ref: EP0741).

2.7.3. PCR amplification - 10X PCR Buffer minus $MgCl_2$ (Life technologies, Ref: 18067-017), $MgCl_2$ (50 mM) (Life technologies, Ref: 18067-017), *Taq* DNA Polymerase (200 Units/µL) (Life technologies, Ref: 10342-053), dNTP Mix, 10 mM each (Life technologies, Ref: 18427013).

2.7.4. Agarose gel electrophoresis - Agarose (UltraPure™ Agarose, Ref: 16500-100), Tris base, acetic acid and EDTA buffer (TAE) (Sigma Aldrich, Ref: T9650), UltraPure™ 10mg/mL Ethidium Bromide used at 0.5 µg/mL (life technologies, 15585-011), Loading dye 5X (Quiagen, Ref: 1037649)

3. Methods

3.1. Immunoblot

3.1.1. Gel and transfer - Samples were resolved by SDS-PAGE and transferred onto PVDF membranes (EMD Millipore, Billerica, MA, USA) using liquid transfer for 40 min at 30 V using and the transfer buffer: 25 mM Tris-HCl, 192 mM glycine pH 8.8.

3.1.2. Membrane preparation - Membranes were then washed with distilled water and incubated with Ponceau S (0.1 % (x/v) Ponceau S in 1% (v/v) acetic acid) for 5 min prior extensive washing with distilled water. Membranes were then blocked using PBS, 0.1% Tween 20 (PBST) and 3% (w/v) Bovine Serum Albumin for 45 min at room temperature.

3.1.3. Incubation with antibodies – primary antibodies were diluted with PBST at the appropriate dilution (see 2.2) and incubated with the membrane overnight at 4°C. Then the membrane was washed 5x 5-10 min with PBST prior to be incubated with HRP-conjugated secondary antibodies (dil. 1/5000) for 45 min at room temperature. Membrane was then washed with PBST 5x 5-10 min (**Figs. 2, 3**).

3.1.4. Blot revealing and analysis – Membranes were incubated with chemoluminescent reagent (KPL, Gaithersburg, MD, USA) as recommended by the manufacturer and exposed to X-Ray films. Bands were quantified using the ImageJ software (NIH).

3.2. Phostag analysis

Carry out all procedures at room temperature unless otherwise specified.

3.2.1. Resolving gel - Mix 2.5 mL of resolving buffer, 3.33 mL of acrylamide mixture, 4 µL of Phostag solution, 100 µL of $MnCl_2$ solution and 3.87 mL of distilled water in a 50 mL conical flask. Add 100 µL of SDS, 50 µL of ammonium persulfate, and 10 µL of TEMED, and cast gel within a 7.25 cm × 10 cm × 1.5 mm gel cassette. Allow space for stacking the gel and gently overlay with isobutanol or water.

3.2.2. Stacking gel - Prepare the stacking gel by mixing 2.5 mL of resolving buffer, 1.5 mL of acrylamide mixture, and 5.84 mL water in a 50 mL conical flask. Add 100 µL of SDS, 50 µL of ammonium persulfate, and 10 µL of TEMED. Insert a 10-well gel comb immediately without introducing air bubbles.

3.2.3. Sample preparation and electrophoresis – U-87 MG cells were plated on 6-well plates (200000 cells/well). Twenty-four hours post seeding, cells were treated with Tunicamycin (5 µg/mL) or vehicle (DMSO) for 6 hours. Cells are lysed in RIPA buffer with

protease and phosphatase inhibitors (Roche, Basel, Switzerland). Mix 12 µL cell lysate samples (around 30 µg total proteins) with 6 µL of 2-mercaptoethanol containing sample buffer. Heat at 95°C for 5 min and centrifuge the heated samples at 3,000 × g for 30 s to bring down the condensate. Load 18 µL of each sample or 5 µL of protein standard in the gel. Electrophoresis should be performed at 10-15 mA until the dye front (from the bromophenol blue dye in the samples) has reached the bottom of the gel.

3.2.4. Gel preparation before immunoblotting - Following electrophoresis, pry the gel plates open with the use of a spatula. The gel remains on one of the glass plates. Remove the stacking gel. Rinse the gel twice with a general transfer buffer containing 10 mM EDTA for a minimum of 10 minutes with gentle agitation, to eliminate the manganese ions (Mn^{2+}) from the gel. Transfer carefully to a container with western blot transfer buffer without EDTA for 10 min.

3.2.5. Immunoblotting - Cut a PVDF membrane to the size of the gel and immerse in methanol. Rinse twice in distilled water and once with transfer buffer. Samples were transferred onto PVDF membranes (Millipore, Darmstadt, Germany) using liquid transfer for 3 hrs at 10 V at 4°C using the transfer buffer. Membranes were then washed with distilled water and incubated with Ponceau S (0.1 % (x/v) Ponceau S in 1% (v/v) acetic acid) for 5 min prior extensive washing with distilled water. Membranes were then blocked using PBS, 0.1% Tween 20 and 3% (w/v) Bovine Serum Albumin for 45 min at room temperature (**Fig. 2**).

3.3. RT-PCR for XBP1 mRNA splicing

3.3.1. mRNA extraction - mRNA extraction should be perform in a RNase-free environment. After the stress, the medium is removed from the wells and the cells are washed with PBS. Add 1 mL of TRIzol® Reagent for 10 min in each well. Lyse the cells directly in the wells by pipetting the cells up and down several times. Transfer each extract in a clean 1.5 mL tube and add 200 µL of chloroform. Vortex the tubes vigorously for 15 seconds. Incubate for 2-3 minutes at room temperature. Centrifuge the samples at 12,000 x g for 15 min at 4°C. Remove the aqueous phase of the sample by angling the tube at 45° and pipetting the solution out. Avoid drawing any of the interphase or organic layer into the pipette when removing the aqueous phase. Place the aqueous phase (about 0.4 mL) into a new tube. Add 0.4 mL of isopropanol to the aqueous phase. Incubate at -80°C for 1 hour or at -20°C overnight. Centrifuge at 12,000 x g for 10 minutes at 4°C. Remove the supernatant from the tube, leaving only the RNA pellet. Wash the pellet, with 1 mL of 75% ethanol. Vortex the sample briefly, then centrifuge the tube at 7500 x g for 5 minutes at 4°C. Discard the wash. Vacuum

or air-dry the RNA pellet for 5-10 minutes. Do not dry the pellet by vacuum centrifuge. Resuspend the RNA pellet in 20 µL of RNase-free water at 4°C for 20 min. After homogenization, dose the RNA at 260 nm. Check the 260/230 and 260/280 ratios for protein contaminant.

3.3.2. Reverse transcription - In a clean 200 µL tube, use 1 µg of RNA as template for the reaction, then add the following reaction components (manufacturer protocol, Thermo Scientific): 1 µL Random Hexamer, 1 µL dNTP Mix 10 mM, 4 µL 5X RT Buffer, 0.5 µL Ribolock™ RNase Inhibitor, 1 µL Maxima® Reverse Transcriptase Complete with RNase free Water to 20 µL. Start with 10 minutes at 25°C followed by 30 minutes at 50°C, terminate the reaction by heating at 85°C for 5 minutes.

3.3.3. XBP1 splicing Polymerase Chain Reaction - PCR reaction should be performed in a DNA-free environment. Use of "clean" dedicated automatic pipettors and aerosol resistant barrier tips are recommended. In a clean 200 µL tube, use 20 to 40 ng as template for the reaction, then add the following reaction components (manufacturer protocol, Life technologies): 0.3 µM Forward primer, 0.3 µM Reverse primer, 5 µL 10X Buffer minus $MgCl_2$, 2 µL $MgCl_2$ (50 mM), 0.5 µL *Taq* DNA Polymerase, 1 µL dNTP Mix 10 mM, Nuclease free water to 50 µL. PCR program: initial denaturation step start at 95°C for 10 minutes, followed by 40 cycles of: 30 seconds denaturation step at 95°C, 45 seconds annealing step at 60°C and 45 seconds elongation step at 72°C. The PCR reaction was finalized by 10 min elongation at 72°C.

3.3.4. Agarose gel electrophoresis - Cast a 4% agarose gel containing 0.5 µg/mL ethidium bromide in TAE buffer. Mix 10 µL of PCR reaction with 2.5 µL of 5X loading dye. Load the mix onto the gel and set the power supply at 100 V for 2 hours. Observe the result under UV light, prolong the migration time if the Xbp1 unspliced and Xbp1 spliced forms are not separated enough (**Fig. 3**).

3.4. Measure of RIDD

This protocol was designed to measure the RIDD activation of IRE1 in U-87 MG human cells and can be used to evaluate IRE1 mRNA decay activity regulators.

3.4.1. Cells preparation - Incubate 300000 cells by well in 4-well of a 6-well plate, 48 hrs. before siRNA transfection.

3.4.2. siRNA transfection - Transfect cells by using the siRNAi Max Lipofectamine reagent (Invitrogen Corp.). Briefly, for each siRNA, dilute 9 µL of RNAiMAX Reagent in 150 µL of Opti-MEM® Medium (Life technologies) and 30 pmol of siRNA in 150 µL of

Opti-MEM® Medium. Add the diluted siRNA to the diluted Lipofectamine® RNAiMAX and incubate for 5 min at room temperature. Add 250 µl of this solution to the cells and incubate for 2 to 4 days.

3.4.3. RNA extraction, reverse transcription and PCR - Perform these steps as described in the first chapter, excepted for the PCR program. Samples were denatured for 10 min at 95°C, then cycled for 30 cycles (denaturation: 95°C, 30s; annealing: 62°C, 30s; elongation: 72°C, 45s) and then subjected to a final elongation of 10 min at 72°C.

3.4.4. Gel electrophoresis -The PCR products were resolved on 2% agarose gels (see section 1).

3.4.5. Analysis - Quantify the bands using the ImageJ software (NIH). Normalize by dividing the PERIOD1 and PERIOD2 signal to the signal of the GAPDH. Normalization of each biological replicate can be performed by dividing the values by the mean of all values of the corresponding experiment or by dividing each value by the control (**Fig. 3**).

3.5. Immunohistochemistry for Vimentin/CD31 and XBP1s

The entire process for Vimentin and CD31 staining is performed at room temperature and in moist chamber.

3.5.1. Tissue preparation - Dry the sheets for 15 minutes. Fix the tissue with PAF 4%: 10 mL Formaldehyde 16 % (Elecron Microscopy Sciences 15710) plus 30 mL of 1X PBS. Wash with 1X PBS for 5 minutes. Do this process 3 times. Permeabilize with PBS-Triton 0.1% for 1 hour (add 1 mL of Triton 100% to 1 L of PBS 1x). Wash with 1X PBS 3 times for 5 minutes.

3.5.2. Blocking and antibody reaction (immunofluorescence) – Mark the area around the tissue with a Dako Pen (Dako 52002). Saturate with PBS-BSA 5% for 1 hour (add 50 mg of Albumin from bovine serum (Sigma 96%) to 1 L of 1X-PBS). Wash with 1X PBS for 5 minutes, 3 times. Primary antibody: PBS-BSA 1% with Anti-Vimentin 1/400 (Mouse IgG1) (Acris BM5050P) for 1 hour. Wash with 1X PBS 3 times for 5 minutes. Secondary antibody: PBS-BSA 1% with Alexa 488 (Fluoroprobes 488 Donkey Anti-Mouse IGG FP-5A4110), at a 1/200 dilution for 30 minutes. Wash with 1X PBS for 5 minutes, 3 times. Primary antibody: PBS-BSA 1% with Anti-CD31 Purified Rat Anti-Mouse 1/200 (BD Pharmingen 550274) for 1 hour. Wash with 1X PBS for 5 minutes, 3 times. Secondary antibody: PBS-BSA 1% with Alexa 547 (Fluoprobes 547 Donkey Anti-Rat IGG FP-SB6110) (dilution 1/200) with Hoechst (PBS BSA 1% + Hoechst (1/1000)) for 30 minutes. Wash with 1X PBS 3 times for 5 minutes. Mount with 100 µL of Interchim glue (FP-483331

Fluoromount-G Four immunofluorescent) and one coverglass (RS France Coverglass 24X60 mm 0.13-0.17 mm).

3.5.3 Antibody reaction (HRP) - Primary antibody: PBS BSA 1% with anti-XBPIs mouse monoclonal IgG1 for 2 hours. Wash with 1X PBS 3 times for 5 minutes. Secondary antibody: EnVision FLEX/HRP (Dako K8010/K8012/K8024) for 30 minutes. Wash with PBS 1x 5 minutes. Do this 3 times. Reveal with EnVision FLEX DAB+CHROMOGEN (Dako K8010/K8012/K8024). Wash with distilled water for 5 minutes. Stain with hemalun for 3 minutes. Wash with running water for 5 minutes. Wash with distilled water and 3 drops of NH3. Dehydrate by increasing battery graduation alcohol and toluene. Mount with 100 µL of mounting medium (PERTEX HistoLab F/00811) and a coverglass (RS France Coverglass 24X60mm 0.13-0.17mm) (**Fig. 4**).

3.6. Orthotopic injections and tumor collection

3.6.1. Cell culture and treatments – U-87 MG cells were plated on 75 cm^2 flasks (500000 cells/flask). Forty-four hours post seeding, cells were trypsinized, washed three times with PBS and suspend in PBS at the concentration of 10000 cells per microliter. Mice were anesthetized using ketamine and xylazine, then 1µL of U-87 solution was injected using Hamilton syringe directly into mouse brain at the bregma (length -0.1 µm; lateral 2.2 mm on the left, depth: 3 mm). Five mice are injected for each cell type. The analgesic buprenorphine is used before and after intracranial injection.

3.6.2. Tumor collection - Two to three weeks after orthotopic injections, mice are sacrificed (cervical dislocation) and brains are immediately frozen in liquid nitrogen. Mouse brain slices are obtained using a cryostat then stained as indicated below (**Fig. 4**).

3.7. Cytotoxicity assays

3.7.1. U-87 MG cells (5000 cells per well) are grown in a 96-well plate in 100 µL growth medium (DMEM, FBS 5%) in presence or absence of the indicated compounds (final concentration 4 µg/mL in 0.1% DMSO) for 24hrs or 48hrs (37°C, 5% CO_2).

3.7.2. Without removing the cell culture supernatant, gently add dropwise 50 µL of cold 50% TCA to each well, and incubate the plates at 4 °C for 1-3 hours. Note: the plates should be disturbed as little as possible during and after fixation solution step. Do not inject the water stream directly onto the bottom of the wells, as this can cause the cell monolayer to detach.

3.7.3. Remove the liquid by inverting the plate. Wash five times with water, tapping on paper towels after rinsing.

3.7.4. Air dry the plates (face up) in room temperature for 12-24 hours.

3.7.5. Cells are stained by addition of 100 µL of 0.4% sulforhodamine B (SRB)/1% glacial acetic acid to each well at room temperature for 30 min, and rinse the plates four times with 200 µL of 1% glacial acetic acid (each time), tapping on paper towels after rinsing to remove unbound dye.

3.7.6. Air dry the plates (face up) at room temperature for 12-24 hours.

3.7.7. Add 100 µl of 10 mM Tris and shake until all bound SRB is into the solution.

3.7.8. Measure absorbance at 515 nm read with a microplate reader (PerkinElmer Envision plate reader) and cell viability was calculated as a percent of control (untreated) cells (**Fig. 5**).

3.8. Statistical analyses

Non-linear regression was used to fit curves to the mean and standard deviations (N=3) calculated with GraphPad Prism^{TM} software. Statistical significance of compounds toxicity in U87 cells was determined by ANOVA and Dunnett's *post hoc* comparison test at the 0.05 confidence level.

4. Notes

4.1. For Phostag analysis gels must be ran at rather low voltage (10-15 mA/gel) to allow better resolution and sharp bands (**Fig. 2C**). For the detection of IRE1 ser724 phosphorylation using the phosphospecific antibodies, it is better to immunoprecipitate IRE1 (following cell lysis with RIPA buffer containing protease and phosphatase inhibitors (Complete and PhoSTOP; Roche, Basel, Switzerland) overnight at 4°C. Immunoprecipitates are then resolved by SDS-PAGE and transferred onto PVDF membranes prior to immunoblotting using anti p-IRE1 antibodies (**Fig. 2D**).

4.2. For quantifying the increase in XBP1s expression by immunoblot (**Fig. 3B**), the amount of basal and ER stress-induced XBP1s should be investigated in preliminary experiments and depend on the cell lines/tissues to be analyzed. Several cell lines exhibit strong basal XBP1s such as Hela cells or human hepatoma HuH7 cells.

4.3. RIDD activity: Note that if you intend to validate the ability of IRE1 to cleave an mRNA upon stress, it is necessary to block the transcriptional regulation of potential substrates in order to validate their posttranscriptional regulation by IRE1. Furthermore, in this protocol the degradation of PERIOD1 mRNA was used as a marker of IRE1 endoribonuclease basal activation (31) (**Fig. 3**). Depending of the cell type, and the expression level of PERIOD1, it could be necessary to use another previously identified substrate of IRE1 mRNA decay activity, such as GPC3 (27) or SPARC (34). The siIRE1 is used as a positive control of IRE1 modulation and PERIOD2 mRNA, a non-target of IRE1, as a negative control. The siGL2 represents a control unspecific siRNA. The siXBP1 is used to confirm that the regulation of the IRE1 mRNA target is not due to transcriptional regulation mediated by XBP1.

4.4. For immunohistochemistry experiments, all the solutions are prepared extemporaneously and conserved fresh. Hematoxylin can be used several times but the incubation time must increase with recycled solutions. Finally, the volume of each solution necessary for each slide (Dakopen-delimited area) is of about 300 µL.

4.5. For xenografts, cells must be resuspended in 100 µL (1.5 mL tubes) or 50 µL (round bottom tubes) in order for the syringe used for injection to homogenize properly the cell suspension and collect 1 µL / brain for injection. To inject more than 10000 cells is not necessary.

Acknowledgements

This work was funded by grants from INSERM, Institut National du Cancer (INCa), La Ligue Contre le Cancer to EC. S.L. was supported by a PhD scholarship from the French government and N.D. was supported by a post-doctoral fellowship from the Fondation de France.

References

1. Kozutsumi Y, Segal M, Normington K, Gething MJ, Sambrook J. The presence of malfolded proteins in the endoplasmic reticulum signals the induction of glucose-regulated proteins. Nature. 1988;332:462-4.
2. Walter P, Ron D. The unfolded protein response: from stress pathway to homeostatic regulation. Science. 2011;334:1081-6.
3. Kimata Y, Kohno K. Endoplasmic reticulum stress-sensing mechanisms in yeast and mammalian cells. Curr Opin Cell Biol. 2011;23:135-42.
4. Bertolotti A, Zhang Y, Hendershot LM, Harding HP, Ron D. Dynamic interaction of BiP and ER stress transducers in the unfolded-protein response. Nat Cell Biol. 2000;2:326-32.
5. Hetz C. The unfolded protein response: controlling cell fate decisions under ER stress and beyond. Nat Rev Mol Cell Biol. 2012;13:89-102.
6. Harding HP, Novoa I, Zhang Y, Zeng H, Wek R, Schapira M, et al. Regulated translation initiation controls stress-induced gene expression in mammalian cells. Molecular cell. 2000;6:1099-108.
7. Harding HP, Zhang Y, Zeng H, Novoa I, Lu PD, Calfon M, et al. An integrated stress response regulates amino acid metabolism and resistance to oxidative stress. Molecular cell. 2003;11:619-33.
8. Lerner AG, Upton JP, Praveen PV, Ghosh R, Nakagawa Y, Igbaria A, et al. IRE1alpha induces thioredoxin-interacting protein to activate the NLRP3 inflammasome and promote programmed cell death under irremediable ER stress. Cell Metab. 2012;16:250-64.
9. Novoa I, Zeng H, Harding HP, Ron D. Feedback inhibition of the unfolded protein response by GADD34-mediated dephosphorylation of eIF2alpha. J Cell Biol. 2001;153:1011-22.
10. Haze K, Yoshida H, Yanagi H, Yura T, Mori K. Mammalian transcription factor ATF6 is synthesized as a transmembrane protein and activated by proteolysis in response to endoplasmic reticulum stress. Mol Biol Cell. 1999;10:3787-99.
11. Asada R, Kanemoto S, Kondo S, Saito A, Imaizumi K. The signalling from endoplasmic reticulum-resident bZIP transcription factors involved in diverse cellular physiology. J Biochem. 2011;149:507-18.
12. Lee K, Tirasophon W, Shen X, Michalak M, Prywes R, Okada T, et al. IRE1-mediated unconventional mRNA splicing and S2P-mediated ATF6 cleavage merge to regulate XBP1 in signaling the unfolded protein response. Genes Dev. 2002;16:452-66.
13. Yamamoto K, Sato T, Matsui T, Sato M, Okada T, Yoshida H, et al. Transcriptional induction of mammalian ER quality control proteins is mediated by single or combined action of ATF6alpha and XBP1. Dev Cell. 2007;13:365-76.
14. Shoulders MD, Ryno LM, Genereux JC, Moresco JJ, Tu PG, Wu C, et al. Stress-Independent Activation of XBP1s and/or ATF6 Reveals Three Functionally Diverse ER Proteostasis Environments. Cell Rep. 2013.
15. Calfon M, Zeng H, Urano F, Till JH, Hubbard SR, Harding HP, et al. IRE1 couples endoplasmic reticulum load to secretory capacity by processing the XBP-1 mRNA. Nature. 2002;415:92-6.
16. Yoshida H, Matsui T, Yamamoto A, Okada T, Mori K. XBP1 mRNA is induced by ATF6 and spliced by IRE1 in response to ER stress to produce a highly active transcription factor. Cell. 2001;107:881-91.
17. Acosta-Alvear D, Zhou Y, Blais A, Tsikitis M, Lents NH, Arias C, et al. XBP1 controls diverse cell type- and condition-specific transcriptional regulatory networks. Molecular cell. 2007;27:53-66.
18. Lee A-H, Iwakoshi NN, Glimcher LH. XBP-1 regulates a subset of endoplasmic reticulum resident chaperone genes in the unfolded protein response. Mol Cell Biol. 2003;23:7448-59.
19. Urano F, Wang X, Bertolotti A, Zhang Y, Chung P, Harding HP, et al. Coupling of stress in the ER to activation of JNK protein kinases by transmembrane

protein kinase IRE1. Science. 2000;287:664-6.
20. Han D, Lerner AG, Vande Walle L, Upton J-P, Xu W, Hagen A, et al. IRE1alpha kinase activation modes control alternate endoribonuclease outputs to determine divergent cell fates. Cell. 2009;138:562-75.
21. Hollien J, Lin JH, Li H, Stevens N, Walter P, Weissman JS. Regulated Ire1-dependent decay of messenger RNAs in mammalian cells. J Cell Biol. 2009;186:323-31.
22. Hollien J, Weissman JS. Decay of endoplasmic reticulum-localized mRNAs during the unfolded protein response. Science. 2006;313:104-7.
23. Oikawa D, Tokuda M, Hosoda A, Iwawaki T. Identification of a consensus element recognized and cleaved by IRE1 alpha. Nucleic Acids Res. 2010;38:6265-73.
24. Upton JP, Wang L, Han D, Wang ES, Huskey NE, Lim L, et al. IRE1alpha cleaves select microRNAs during ER stress to derepress translation of proapoptotic Caspase-2. Science. 2012;338:818-22.
25. Dai BH, Geng L, Wang Y, Sui CJ, Xie F, Shen RX, et al. microRNA-199a-5p protects hepatocytes from bile acid-induced sustained endoplasmic reticulum stress. Cell Death Dis. 2013;4:e604.
26. Maurel M, Chevet E. Endoplasmic Reticulum stress signaling: the microRNA connection. Am J Physiol Cell Physiol. 2013;304:C1117-26.
27. Maurel M, Dejeans N, Taouji S, Chevet E, Grosset CF. MicroRNA-1291-mediated silencing of IRE1alpha enhances Glypican-3 expression. RNA. 2013;19:778-88.
28. Auf G, Jabouille A, Guerit S, Pineau R, Delugin M, Bouchecareilh M, et al. Inositol-requiring enzyme 1alpha is a key regulator of angiogenesis and invasion in malignant glioma. Proceedings of the National Academy of Sciences of the United States of America. 2010;107:15553-8.
29. Drogat B, Auguste P, Nguyen DT, Bouchecareilh M, Pineau R, Nalbantoglu J, et al. IRE1 signaling is essential for ischemia-induced vascular endothelial growth factor-A expression and contributes to angiogenesis and tumor growth in vivo. Cancer research. 2007;67:6700-7.
30. Moenner M, Pluquet O, Bouchecareilh M, Chevet E. Integrated endoplasmic reticulum stress responses in cancer. Cancer research. 2007;67:10631-4.
31. Pluquet O, Dejeans N, Bouchecareilh M, Lhomond S, Pineau R, Higa A, et al. Posttranscriptional regulation of PER1 underlies the oncogenic function of IREalpha. Cancer research. 2013;73:4732-43.
32. Hetz C, Chevet E, Harding HP. Targeting the unfolded protein response in disease. Nat Rev Drug Discov. 2013;12:703-19.
33. Volkmann K, Lucas JL, Vuga D, Wang X, Brumm D, Stiles C, et al. Potent and selective inhibitors of the inositol-requiring enzyme 1 endoribonuclease. The Journal of biological chemistry. 2011;286:12743-55.
34. Dejeans N, Pluquet O, Lhomond S, Grise F, Bouchecareilh M, Juin A, et al. Autocrine control of glioma cells adhesion and migration through IRE1alpha-mediated cleavage of SPARC mRNA. J Cell Sci. 2012;125:4278-87.

Figure Legends

Figure 1: Schematic representation of IRE1 signaling. Upon accumulation of misfolded proteins in the ER, BiP is titered away from IRE1 leading to IRE1 oligomerization and downstream signaling. Three major signaling pathways are activated downstream of IRE1 including the activation of the JNK cascade, the unconventional splicing of XBP1 mRNA and the regulated IRE1 dependent decay of mRNA (RIDD).

Figure 2: IRE1 phosphorylation analysis. (**A**) Schematic representation of Phostag-p-IRE1 interaction. (**B**) Schematic representation of the Phostag analysis protocol. (**C**) IRE1 phosphorylation analysis using Phostag. U87 cells were lysed and protein samples were resolved by SDS-PAGE and phostag. Following transfert onto PVDF membranes, IRE1 and p-IRE1 are visualized by immunoblot with anti-IRE1 antibodies. (**D**) IRE1 phosphorylation analysis by immunoblotting using anti p-IRE1 (S724). U87 cells were lysed and protein samples were immunoprecipitated with anti-IRE1 antibodies. Immunoprecipitates were resolved by SDS-PAGE, transferred onto PVDF and immunoblotted with anti-p-IRE1 or anti-IRE1 antibodies.

Figure 3: Analysis of IRE1 downstream signaling. (**A**) XBP-1 mRNA splicing. (**B**) XBP1s protein expression. U87 cells were lysed and protein samples were resolved by SDS-PAGE. Following transfert onto PVDF membranes, XBP1s is visualized by immunoblot with anti-XBP1s antibodies (**C**) Analysis of RIDD activity towards PER1 mRNA. (**D**) JNK phosphorylation in response to tunicamycin-induced ER stress. U87 cells treated with tunicamycin were lysed and protein samples were resolved by SDS-PAGE and phostag. Following transfert onto PVDF membranes, JNK1 and p-JNK1 are visualized by immunoblot with anti-JNK1 and anti-p-JNK1 antibodies

Figure 4: Orthotopic glioblastoma model in the mouse. (**A**) Schematic representation of the orthotopic graft injection of U87MG cells into immunocompromised mice. (**B**) Following injection of U87 cells and 2-3 weeks, mouse brains were collected and preserved. Sections were performed and staining with H&E, anti-XBP1s antibodies (revealed using HRP-conjugated secondary antibodies), anti-Vimentin, anti-CD31 (revealed with fluorescently labeled secondary antibodies). T: tumoral; NT: non tumoral.

Figure 5: Impact of IRE1 inhibition on U87 cells sensitivity to tunicamycin-induced ER stress. (**A**) Impact of Toyocamycin, Irestatin and MKC8866 (labeled MKC) on XBP1 mRNA splicing activity. The concentrations used are indicated in the figure. XBP1 mRNA splicing activity was evaluated in control U87 cells and in U87 cells stably overexpressing wild-type IRE1, a situation sufficient for IRE1 activation. (**B**) Toxicity of Toyocamycin, Irestatin and MKC8866 (labeled MKC) as assessed using Sulforhodamin-B staining and increasing concentrations of the compounds. (**C**) Synergistic effects of MKC8866 and tunicamycin on toxicity in U87 cells.

Figure 1

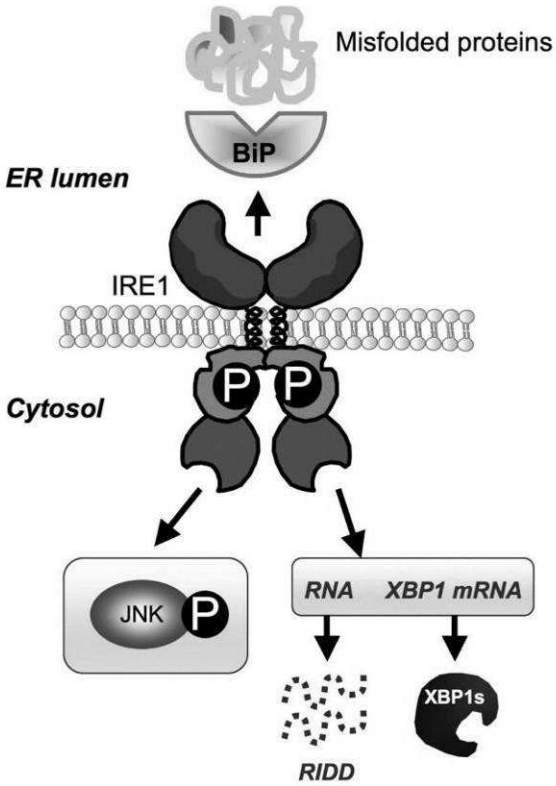
Misfolded proteins
BiP
ER lumen
IRE1
Cytosol
P
P
JNK
P
RNA
XBP1 mRNA
XBP1s
RIDD

Figure 2

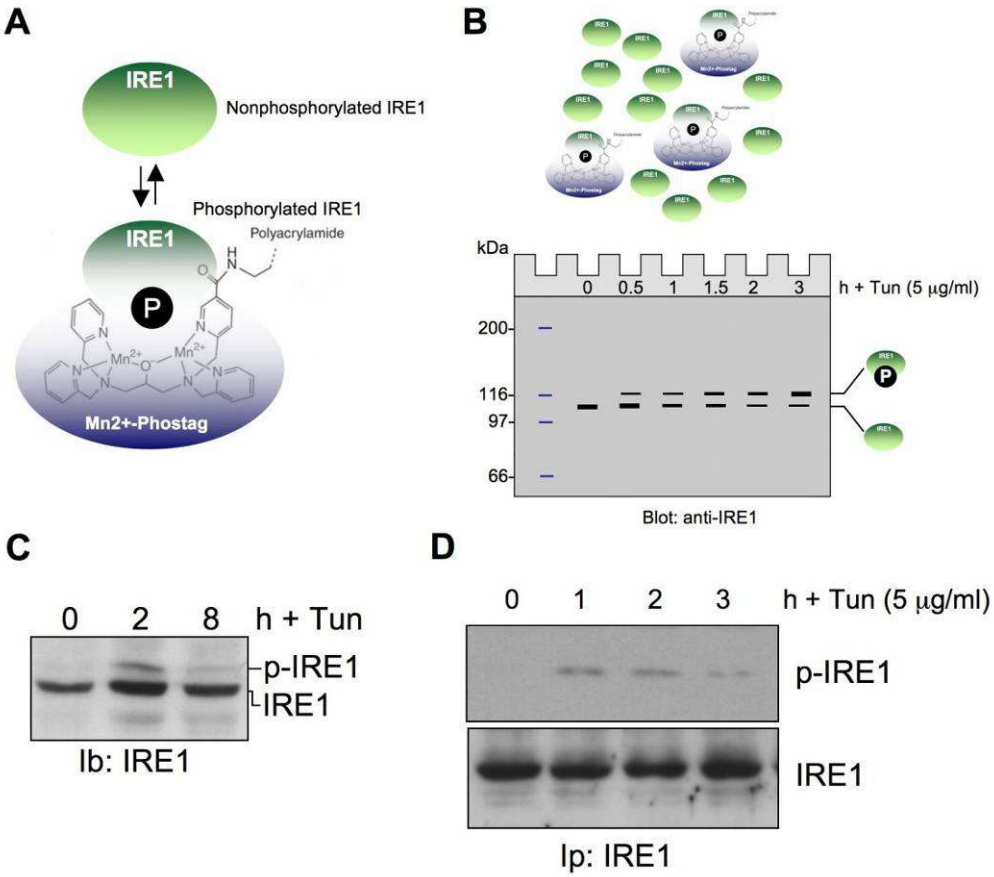
A
IRE1
Nonphosphorylated IRE1
Phosphorylated IRE1
Polyacrylamide
IRE1
P
Mn2+-Phostag
B
kDa
0 0.5 1 1.5 2 3
h + Tun (5 μg/ml)
200
116
97
66
Blot: anti-IRE1
C
0 2 8 h + Tun
p-IRE1
IRE1
Ib: IRE1
D
0 1 2 3 h + Tun (5 μg/ml)
p-IRE1
IRE1
Ip: IRE1

Figure 3

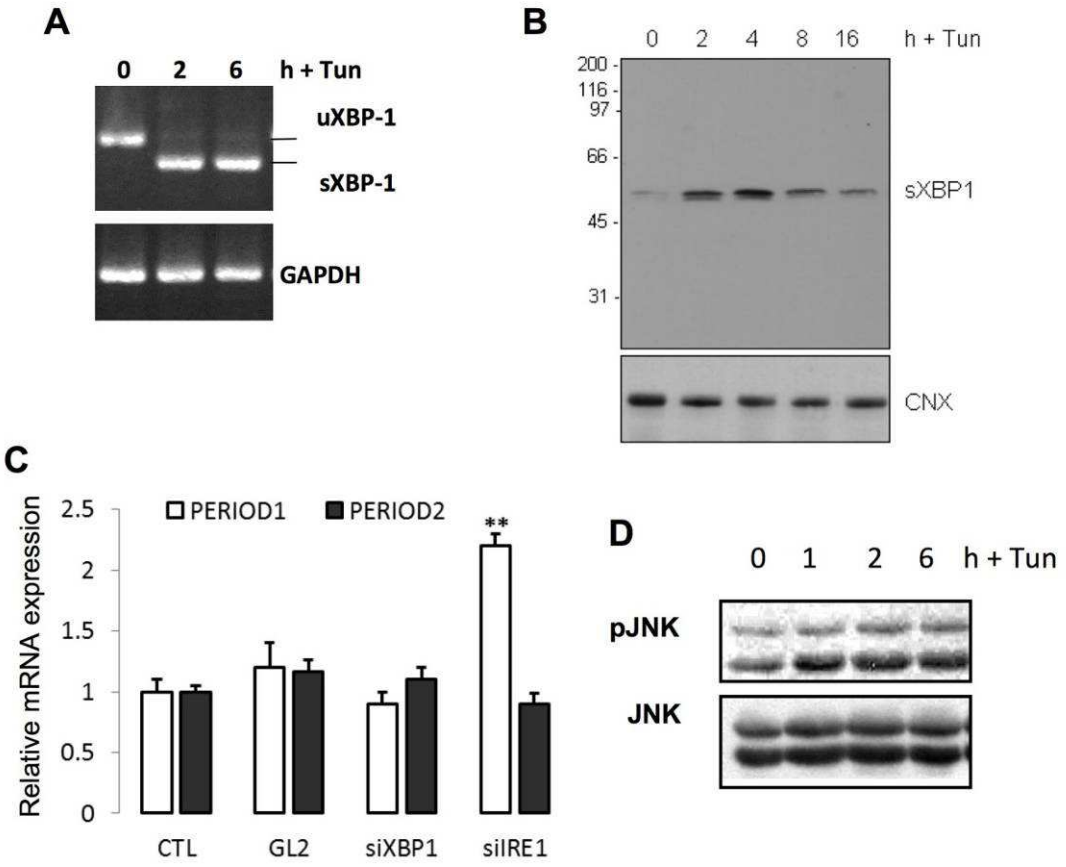
A
0 2 6 h + Tun
uXBP-1
sXBP-1
GAPDH
B
0 2 4 8 16 h + Tun
200
116
97
66
45
31
sXBP1
CNX
C
Relative mRNA expression
2.5
2
1.5
1
0.5
0
PERIOD1
PERIOD2
**
CTL
GL2
siXBP1
siIRE1
D
0 1 2 6 h + Tun
pJNK
JNK

Figure 4

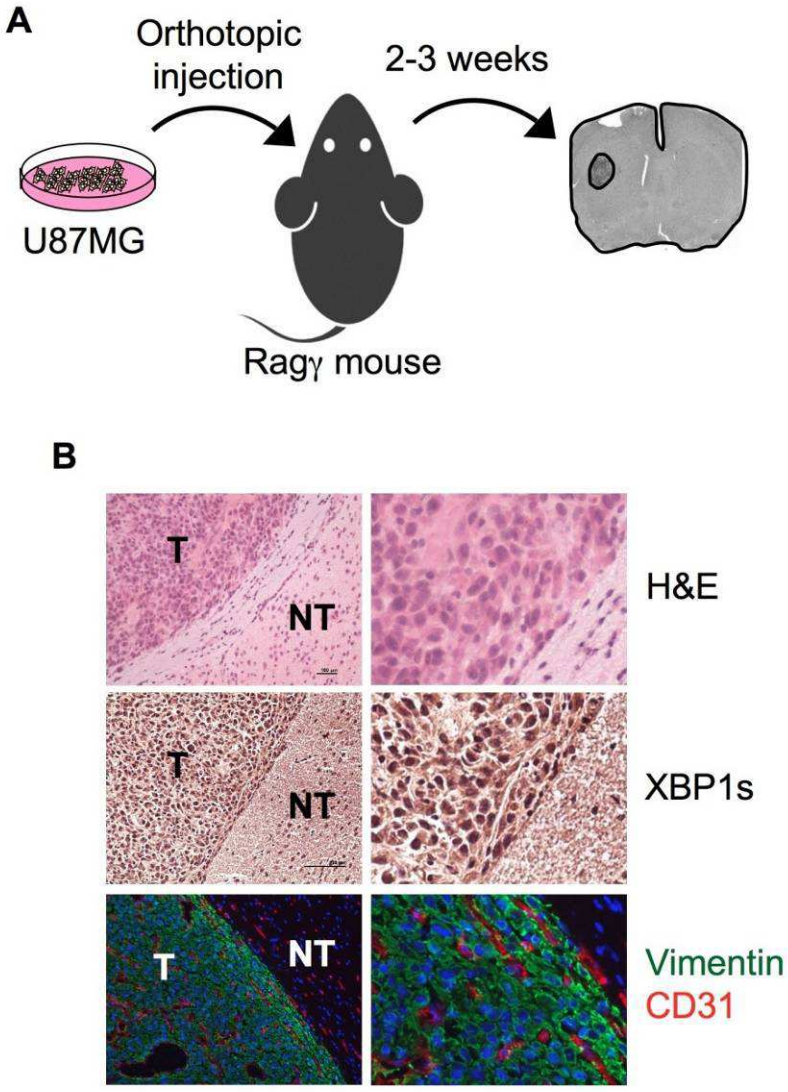
A
Orthotopic injection
2-3 weeks
U87MG
Ragγ mouse
B
T
NT
H&E
XBP1s
Vimentin
CD31

Figure 5

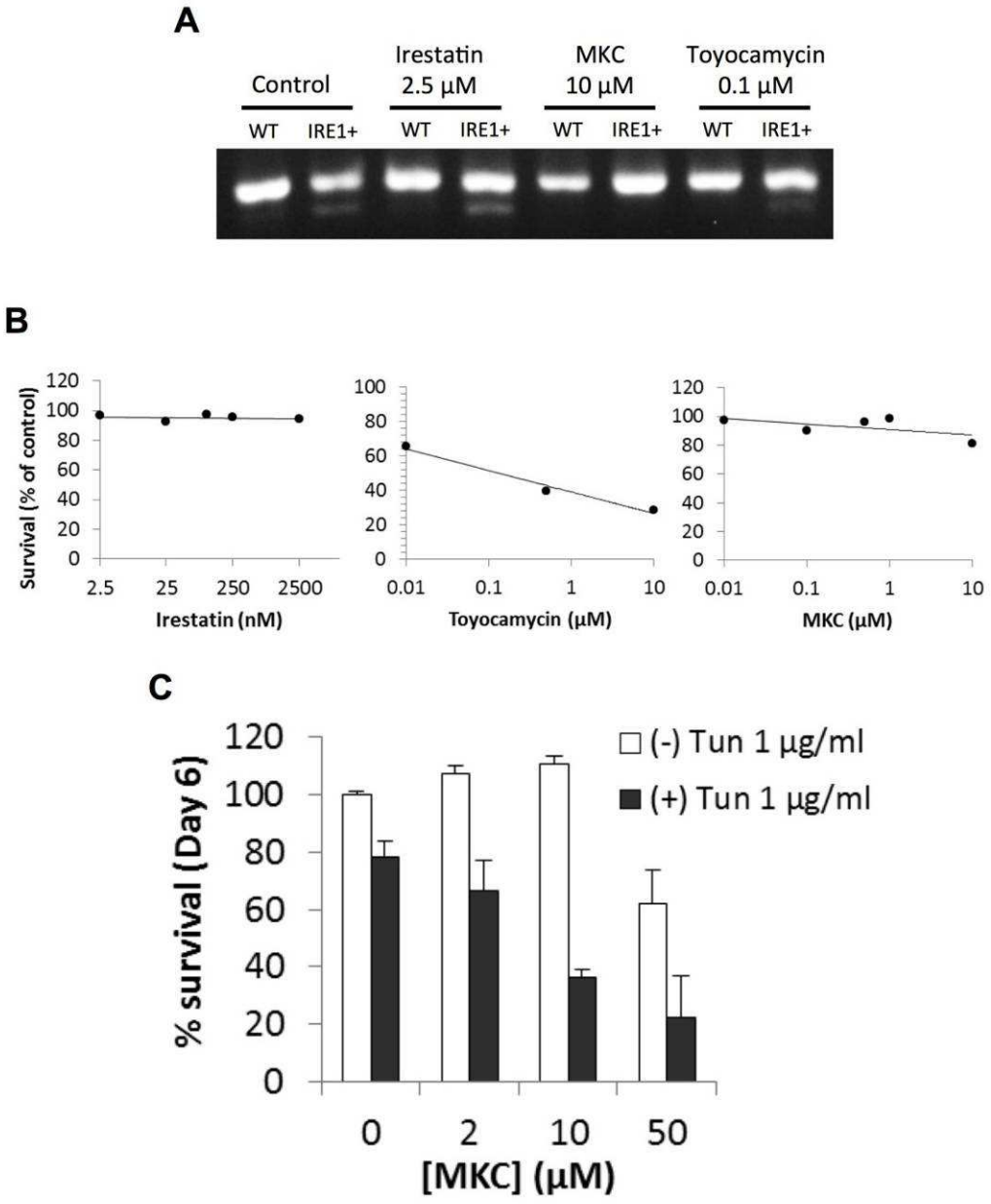
A
Control
Irestatin 2.5 µM
MKC 10 µM
Toyocamycin 0.1 µM
WT
IRE1+
B
Survival (% of control)
Irestatin (nM)
Toyocamycin (µM)
MKC (µM)
C
(-) Tun 1 µg/ml
(+) Tun 1 µg/ml
% survival (Day 6)
[MKC] (µM)

RÉSULTATS

Comme cela a été démontré dans les dix dernières années, la signalisation d'IRE1α est essentielle au développement de tumeurs cérébrales issues de glioblastome humain chez la souris [157]. Cette étude repose sur l'expression dans des cellules provenant d'un GBM, les U-87 MG, d'une protéine chimère IRE1-NCK ayant un effet dominant-négatif sur la signalisation en aval d'IRE1α [155].

Les cellules inactivées pour IRE1α, les U87-DN, forment des tumeurs plus petites, moins vascularisées mais plus invasives, ce qui globalement augmente la survie des souris. L'étude comparative des transcrits entre ces U87-DN et les U-87 contrôle (U87-EV) a mis en évidence une sous-expression dans les U87-DN de facteurs proangiogéniques tels que le VEGF-A, IL-1β, IL-6 ou IL-8, associée à une surexpression de facteurs antiangiogéniques tels que SPARC (Secreted protein acidic and rich in cystein), PER1 (period 1), la décorine ou la thrombospondine [157].

Dans les articles décrits ci-après, nous avons cherché à déterminer comment la signalisation d'IRE1α pouvait être responsable du phénotype tumoral observé, et en particulier quelle était l'implication de la fonction d'IRE1α de dégradation d'ARNm cibles: la fonction RIDD.

ARTICLE 3: AUTOCRINE CONTROL OF GLIOMA CELLS ADHESION AND MIGRATION THROUGH IRE1ALPHA-MEDIATED CLEAVAGE OF SPARC MRNA

Dans cet article, nous avons posé l'hypothèse que la signalisation IRE1α, en particulier à travers la dégradation d'ARNm, joue un rôle clé dans l'adaptation des cellules tumorales à leur microenvironnement.

Afin de tester cette hypothèse, nous avons recherché un transcrit dont l'expression est augmentée dans les U87-DN par rapport aux U87-EV, et qui puisse être impliqué dans le remaniement du microenvironnement tumoral. Ceci nous a permis d'identifier SPARC, une protéine de la matrice extracellulaire, comme cible potentielle du RIDD pouvant expliquer l'acquisition de propriétés migratoires par les cellules U87-DN.

Afin de décrypter les mécanismes moléculaires mis en jeu lors de la formation des tumeurs *in vivo*, nous avons établi un modèle mimant la formation de tumeur *in vitro*, ainsi que la migration des cellules depuis la tumeur formée. Pour cela, nous avons déposé les U-87

MG sur une surface non-adhérente (agar) et mesurer la vitesse de formation de sphéroïdes appelés ci-après neurosphères. Les capacités de migration des cellules cancéreuses à partir des sphèroïdes est ensuite évalué en transférant ces neurosphères sur une surface adhérente et en mesurant la distance parcourue depuis le sphéroïde et les caractéristiques des cellules en cours de migration. Ces méthodes, associées à des méthodes classiques de mesure d'adhésion et de migration (Transwell), ont permis de confirmer *in vitro* les résultats précédemment observés *in vivo*, c'est-à-dire l'acquisition d'un phénotype migratoire des cellules U87-DN par rapport aux U87-EV.

Des expériences de clivage *in vitro* de l'ARNm de SPARC par IRE1α, complétés par une approche d'extinction de l'expression d'IRE1α (siRNA) dans les U87-EV, ont confirmé que SPARC est une cible du RIDD. Nous avons alors utilisé une approche de siRNA ou d'anticorps bloquant pour restaurer dans les U87-DN un niveau d'expression de SPARC équivalant au niveau basal présent dans les U87-EV. Ceci nous a permis de confirmer que la stabilisation de SPARC et sa sécrétion dans le milieu extracellulaire sont impliqués dans l'acquisition d'un phénotype migratoire des cellules U87-DN. Nous avons enfin démontré que le rôle de SPARC dans l'acquisition de ce phénotype passe par son action sur le cytosquelette d'actine [158], en particulier par l'activation de la GTPase RhoA.

Dans les cellules U87-DN, la perte de l'activité d'IRE1α lève la dégradation de l'ARNm de SPARC par IRE1α, ce qui entraîne une augmentation de la sécrétion de cette protéine. SPARC peut alors activer la protéine RhoA et phosphoryler la protéine FAK, favorisant la formation de fibres de stress et d'adhésions focales et en conséquence la migration des cellules U87-DN (**Figure 14**).

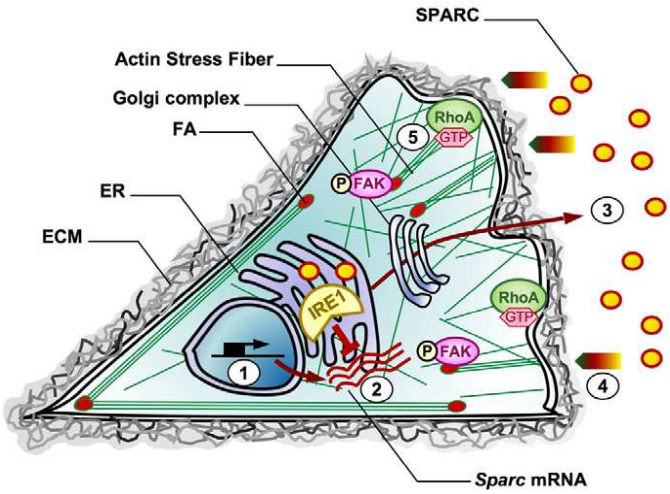

Figure 14: Schéma récapitulatif du rôle d'IRE1α et de SPARC dans les U87

J'ai participé à ce travail en testant l'impact de l'inactivation de la voie de signalisation dépendante d'IRE1α sur la migration des cellules de glioblastome ainsi que sur la formation de neurosphères.

ARTICLE 3

Autocrine control of glioma cells adhesion and migration through IRE1α-mediated cleavage of SPARC mRNA

Nicolas Dejeans[1,2,‡], Olivier Pluquet[1,2,*,‡], Stéphanie Lhomond[1,2], Florence Grise[1,2], Marion Bouchecareilh[1,2], Amélie Juin[1,2], Maud Meynard-Cadars[1,2], Aurélien Bidaud-Meynard[1,2], Catherine Gentil[3], Violaine Moreau[1,2], Frédéric Saltel[1,2] and Eric Chevet[1,2,§]

[1]INSERM U1053, 146 rue Léo Saignat, 33076 Bordeaux, France
[2]Université Bordeaux-Segalen, 146 rue Léo Saignat, 33076 Bordeaux, France
[3]TIERS-MIP, Faculté de médecine de Purpan, 37 allées Jules Guesde, 31073 Toulouse, France

*Present address: Institut de Biologie de Lille, CNRS UMR8161/Universités Lille 1 et Lille 2/Institut Pasteur de Lille, 1, rue du Pr. Calmette, BP 447, 59021 Lille, France
‡These authors contributed equally to this work
§Author for correspondence (eric.chevet@u-bordeaux2.fr)

Accepted 28 May 2012
Journal of Cell Science 125, 4278–4287

doi: 10.1242/jcs.099291

Summary

The endoplasmic reticulum (ER) is an organelle specialized for the folding and assembly of secretory and transmembrane proteins. ER homeostasis is often perturbed in tumor cells because of dramatic changes in the microenvironment of solid tumors, thereby leading to the activation of an adaptive mechanism named the unfolded protein response (UPR). The activation of the UPR sensor IRE1α has been described to play an important role in tumor progression. However, the molecular events associated with this phenotype remain poorly characterized. In the present study, we examined the effects of IRE1α signaling on the adaptation of glioma cells to their microenvironment. We show that the characteristics of U87 cell migration are modified under conditions where IRE1α activity is impaired (DN_IRE1). This is linked to increased stress fiber formation and enhanced RhoA activity. Gene expression profiling also revealed that loss of functional IRE1α signaling mostly resulted in the upregulation of genes encoding extracellular matrix proteins. Among these genes, *Sparc*, whose mRNA is a direct target of IRE1α endoribonuclease activity, was in part responsible for the phenotypic changes associated with IRE1α inactivation. Hence, our data demonstrate that IRE1α is a key regulator of SPARC expression in vitro in a glioma model. Our results also further support the crucial contribution of IRE1α to tumor growth, infiltration and invasion and extend the paradigm of secretome control in tumor microenvironment conditioning.

Key words: IRE1, Cell adhesion, cell migration, Endoplasmic reticulum, SPARC

Introduction

The endoplasmic reticulum (ER) plays an essential role in maintaining the maturation and folding of secreted and transmembrane proteins. Disruption of normal ER functions upon various physiological conditions faced by solid tumors such as hypoxia or glucose deprivation, leads to the accumulation of misfolded proteins and the subsequent activation of an evolutionarily conserved signaling pathway named the unfolded protein response (UPR) (Schröder and Kaufman, 2005). UPR signaling induces translation attenuation and activation of specific gene expression programs aiming at reducing the protein load in the ER and at increasing ER folding and clearance capacity, respectively. As part of this mechanism, IRE1α, which is an ER stress sensor and an ER-resident kinase/endoribonuclease, promotes the splicing of *Xbp1* mRNA, thereby resulting in the synthesis of a potent transcription factor, and the subsequent transcriptional activation of specific genes involved in restoring ER homeostasis (Calfon et al., 2002; Yoshida et al., 2003). Recently IRE1α has also been shown to contribute to mRNA degradation through a process named Regulated IRE1 Dependent Decay of mRNA (RIDD) (Hollien et al., 2009). Connections between UPR signaling and human diseases have been established for instance with pathologies such as diabetes or cancer (Marciniak and Ron, 2006; Moenner et al., 2007). An increasing body of evidences indicates a functional link between IRE1α and tumor growth/progression. Indeed, impairing IRE1α signaling in human glioma cells reduced tumor growth and angiogenesis both in vitro and in vivo through mechanisms dependent on ischemia-induced VEGF expression (Auf et al., 2010; Drogat et al., 2007). The IRE1α substrate *Xbp1* has been shown to be necessary for tumor growth in vivo without affecting VEGF expression, suggesting that IRE1α mediates its angiogenic properties independently of the XBP1 pathway (Romero-Ramirez et al., 2004). Moreover, several reports also showed that XBP1 is overexpressed in human cancers (Shuda et al., 2003) and that constitutive expression of its spliced form is sufficient to promote multiple myeloma in vivo (Carrasco et al., 2007). Recently, a large-scale sequencing analysis of somatic mutations present in the kinome of a wide variety of human cancers revealed a high prevalence of mutations in the IRE1α gene (Greenman et al., 2007). However, the precise mechanisms by which wild-type or mutant IRE1α contribute to cancer development/progression

Journal of Cell Science

Autocrine control of glioma cells adhesion and migration through IRE1α-mediated cleavage of SPARC mRNA

Nicolas Dejeans[1,2,‡], Olivier Pluquet[1,2,*,‡], Stéphanie Lhomond[1,2], Florence Grise[1,2], Marion Bouchecareilh[1,2], Amélie Juin[1,2], Maud Meynard-Cadars[1,2], Aurélien Bidaud-Meynard[1,2], Catherine Gentil[3], Violaine Moreau[1,2], Frédéric Saltel[1,2] and Eric Chevet[1,2,§]

[1]INSERM U1053, 146 rue Léo Saignat, 33076 Bordeaux, France
[2]Université Bordeaux-Segalen, 146 rue Léo Saignat, 33076 Bordeaux, France
[3]TIERS-MIP, Faculté de médecine de Purpan, 37 allées Jules Guesde, 31073 Toulouse, France

*Present address: Institut de Biologie de Lille, CNRS UMR8161/Universités Lille 1 et Lille 2/Institut Pasteur de Lille, 1, rue du Pr. Calmette, BP 447, 59021 Lille, France
‡These authors contributed equally to this work
§Author for correspondence (eric.chevet@u-bordeaux2.fr)

Accepted 28 May 2012
Journal of Cell Science 125, 4278–4287

doi: 10.1242/jcs.099291

Summary

The endoplasmic reticulum (ER) is an organelle specialized for the folding and assembly of secretory and transmembrane proteins. ER homeostasis is often perturbed in tumor cells because of dramatic changes in the microenvironment of solid tumors, thereby leading to the activation of an adaptive mechanism named the unfolded protein response (UPR). The activation of the UPR sensor IRE1α has been described to play an important role in tumor progression. However, the molecular events associated with this phenotype remain poorly characterized. In the present study, we examined the effects of IRE1α signaling on the adaptation of glioma cells to their microenvironment. We show that the characteristics of U87 cell migration are modified under conditions where IRE1α activity is impaired (DN_IRE1). This is linked to increased stress fiber formation and enhanced RhoA activity. Gene expression profiling also revealed that loss of functional IRE1α signaling mostly resulted in the upregulation of genes encoding extracellular matrix proteins. Among these genes, *Sparc*, whose mRNA is a direct target of IRE1α endoribonuclease activity, was in part responsible for the phenotypic changes associated with IRE1α inactivation. Hence, our data demonstrate that IRE1α is a key regulator of SPARC expression in vitro in a glioma model. Our results also further support the crucial contribution of IRE1α to tumor growth, infiltration and invasion and extend the paradigm of secretome control in tumor microenvironment conditioning.

Key words: IRE1, Cell adhesion, cell migration, Endoplasmic reticulum, SPARC

Introduction

The endoplasmic reticulum (ER) plays an essential role in maintaining the maturation and folding of secreted and transmembrane proteins. Disruption of normal ER functions upon various physiological conditions faced by solid tumors such as hypoxia or glucose deprivation, leads to the accumulation of misfolded proteins and the subsequent activation of an evolutionarily conserved signaling pathway named the unfolded protein response (UPR) (Schröder and Kaufman, 2005). UPR signaling induces translation attenuation and activation of specific gene expression programs aiming at reducing the protein load in the ER and at increasing ER folding and clearance capacity, respectively. As part of this mechanism, IRE1α, which is an ER stress sensor and an ER-resident kinase/endoribonuclease, promotes the splicing of *Xbp1* mRNA, thereby resulting in the synthesis of a potent transcription factor, and the subsequent transcriptional activation of specific genes involved in restoring ER homeostasis (Calfon et al., 2002; Yoshida et al., 2003). Recently IRE1α has also been shown to contribute to mRNA degradation through a process named Regulated IRE1 Dependent Decay of mRNA (RIDD) (Hollien et al., 2009). Connections between UPR signaling and human diseases have been established for instance with pathologies such as diabetes or cancer (Marciniak and Ron, 2006; Moenner et al., 2007). An increasing body of evidences indicates a functional link between IRE1α and tumor growth/progression. Indeed, impairing IRE1α signaling in human glioma cells reduced tumor growth and angiogenesis both in vitro and in vivo through mechanisms dependent on ischemia-induced VEGF expression (Auf et al., 2010; Drogat et al., 2007). The IRE1α substrate *Xbp1* has been shown to be necessary for tumor growth in vivo without affecting VEGF expression, suggesting that IRE1α mediates its angiogenic properties independently of the XBP1 pathway (Romero-Ramirez et al., 2004). Moreover, several reports also showed that XBP1 is overexpressed in human cancers (Shuda et al., 2003) and that constitutive expression of its spliced form is sufficient to promote multiple myeloma in vivo (Carrasco et al., 2007). Recently, a large-scale sequencing analysis of somatic mutations present in the kinome of a wide variety of human cancers revealed a high prevalence of mutations in the IRE1α gene (Greenman et al., 2007). However, the precise mechanisms by which wild-type or mutant IRE1α contribute to cancer development/progression

independently of the activation of other branches of the UPR, remains to be fully characterized. We have previously shown that IRE1α-deficient cell (DN_IRE1)-derived tumors had a different shape and spatial organization (Auf et al., 2010; Drogat et al., 2007). These changes were also accompanied by a decrease of the growth rate and a highly infiltrative and mesenchymal tumor phenotype. The goal of the present study was to better characterize the molecular pathways by which IRE1α can impact on glioma characteristics.

Herein, using different in vitro approaches, we have examined the effects of IRE1α inactivation on cell migration and cell adhesion in U87 glioma cells. We show that migration is increased in DN_IRE1 cells through the upregulation of the extracellular matrix protein SPARC. In addition, we demonstrate that IRE1α directly regulates *Sparc* mRNA expression at the post-transcriptional level, thereby contributing to auto/paracrine SPARC signaling in tumor cells. Our data reveal an emerging role of IRE1α in the control of tumor cell adhesion and migration.

Results

Loss of IRE1α activity correlates with changes in U87 glioma cells attachment and migration properties

To characterize the molecular and cellular mechanisms responsible for IRE1-dependent modulation of cancer cell proliferation and migration in vivo (Auf et al., 2010; Drogat et al., 2007), we tested the effect of the expression of a well characterized dominant negative form of IRE1α (DN_IRE1) (Auf et al., 2010; Drogat et al., 2007; Nguyên et al., 2004) (supplementary material Fig. S1A) on U87 cells proliferation, adhesion and invasion ability (Fig. 1). Alteration of IRE1α signaling was confirmed by the weak induction of *Xbp1* mRNA splicing in response to various ER stress inducers (Fig. 1A), as previously described (Drogat et al., 2007; Lee et al., 2002; Papandreou et al., 2011; Welihinda et al., 1998).

As expected, DN_IRE1 cells proliferation rate was lower than that of empty vector expressing cells (EV; Fig. 1B) and the number of migrating cells was significantly higher than in EV cells (Fig. 1C; supplementary material Fig. S1B). In addition, adhesion of DN_IRE1 cells was also increased on both collagen matrices and Matrigel (Fig. 1D). However, both cell lines exhibited similar invasion properties in Matrigel (supplementary material Fig. S1C). As the features of U87 cells characterized in the orthotopic tumor model (Auf et al., 2010; Drogat et al., 2007) presented some specificities that were not recapitulated in the experiments presented in Fig. 1, another model was developed to investigate cell adhesion and migration properties of DN_IRE1 cells. To this end, a neurosphere model was used to mimic the U87 EV and DN_IRE1 cells phenotypes previously described in vivo. As shown in Fig. 2A, the expression of DN_IRE1 resulted in a delay in neurosphere formation and in a decrease of the size they reached. This phenomenon was most likely due to differences in cell growth (Fig. 1B) and cell–cell adhesion properties existing between EV and DN_IRE1 cells. To further compare the migration properties of DN_IRE1 and EV cells, neurospheres of the same size were allowed to adhere, and both neurosphere dissociation and cell migration abilities were monitored across time. Cell number in both types of neurospheres plated on glass slides was also counted and was similar in EV and DN_IRE1 neurospheres (not shown). Forty-eight hours after seeding, EV neurospheres remained compact and homogenous whereas DN_IRE1 neurospheres appeared flattened and dissociated (Fig. 2B). Interestingly, the mode of cell migration appeared to be different for both cell lines. Indeed, DN_IRE1 cells presented a more collective and organized migration, in contrast to EV cells, which migrated in a stochastic/individual manner (Fig. 2B). Both the dissociation capacity of

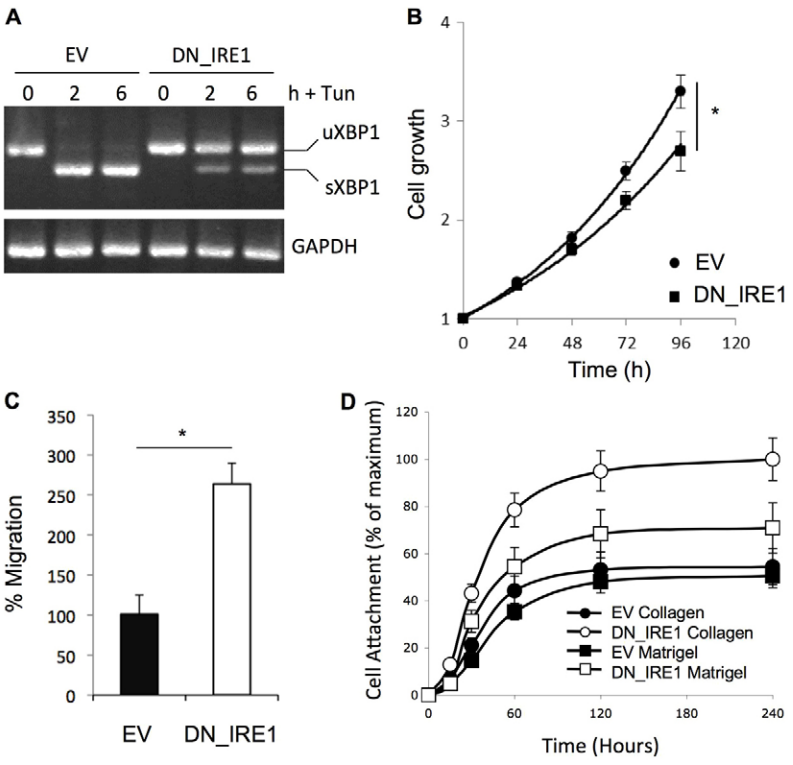

Fig. 1. Impairment of IRE1α signaling alters U87 cells migration, adhesion and proliferation properties. (**A**) Biochemical characterization of U87 cells expressing an empty vector (EV) or a dominant-negative form of IRE1α (DN_IRE1) for the splicing of *Xbp1* mRNA upon Tunicamycin (5 µg/ml)-induced ER stress. *Xbp1* mRNA splicing was evaluated by RT-PCR. The spliced (sXBP1) and unspliced (uXBP1) forms of XBP1 are indicated. (**B**) Cell growth was measured in normal serum conditions in EV and DN_IRE1 cells. (**C**) EV and DN_IRE1 cells were tested for migration in vitro in Transwell chambers as described in the Materials and Methods. The percentage of cells migrating through the Transwell inserts was determined. Results are expressed as percentage of the control (EV). (**D**) EV (closed symbols) and DN_IRE1 (open symbols) cells were assessed for their ability to attach to collagen (circles) or Matrigel (squares). After the indicated times, cell attachment was measured as a function of the absorbance (SRB assay at 492 nm). *$P<0.05$.

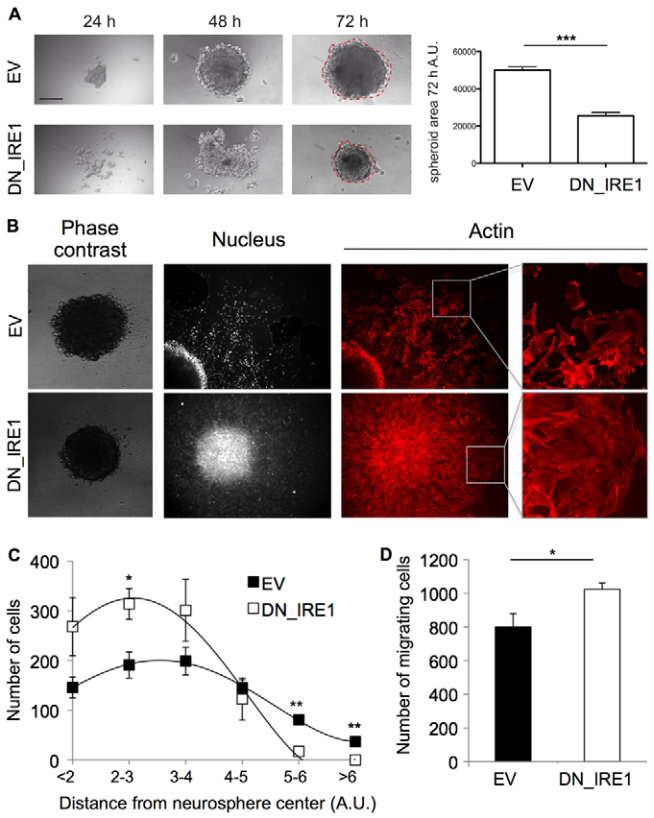

Fig. 2. Impairment of IRE1α signaling modulates neurosphere formation and migration capacity of U87 cells. (**A**) The ability of U87 cells expressing an empty vector (EV) or a dominant-negative form of IRE1α (DN_IRE1) to form neurospheres was evaluated as described in the Materials and Methods. 24, 48 and 72 h after seeding, photos were taken and after 72 h the neurosphere surface was measured using the ImageJ software. (**B**) EV and DN_IRE1 neurospheres of the same size and number of cells were allowed to adhere on a 22-mm glass coverslip and cell migration was studied for 48 h. Phase-contrast (4 h after neurosphere seeding) images and nuclear and F-actin stainings (48 h after seeding) are shown. (**C**) The distance achieve by all the cells escaping the neurosphere bulk was measured using nucleus staining and an ImageJ macro, and the number of cells travelling less than 2, 3–4, 4–5, 5–6 and more than 6 arbitrary unit (A.U.) was estimated. (**D**) Quantification of cells migrating from the neurosphere bulk (*P<0.05; **P<0.01).

DN_IRE neurospheres and the migration mode of the DN_IRE1 cells were reflected by the fact that more DN_IRE1 cells were migrating compared to EV cells, but the former appeared to migrate to a relatively shorter distance from the neurosphere center (Fig. 2C,D). Taken together, these data support the ability of IRE1α activity to regulate tumor cell features, including growth, migration and adhesion properties. Moreover, these data are consistent with those observed in vivo where DN_IRE1 cell-derived tumors were smaller, exhibited extensive tumor cell infiltration in the surrounding normal tissue than EV cell-derived tumors and were also tightly associated to the abluminal site of blood vessels without apparent penetration (Auf et al., 2010; Drogat et al., 2007).

As observed in Fig. 2B, the global organization of actin cytoskeleton was modified in DN_IRE1 cells. In this organization, stress fibers and focal adhesions constitute a contractile apparatus that allows cell attachment to the extracellular matrix through the plasma membrane and focal adhesions (Pellegrin and Mellor, 2007). Furthermore, these structures are known to constitute major cellular elements in the ability of cells to migrate. Considering these observations, we further examined the organization of the actin cytoskeleton and the associated adhesive contacts using immunofluorescence microscopy. We observed more actin stress fibers/cables in DN_IRE1 compared to control (EV) cells (Fig. 3A). This was accompanied by a gain of focal adhesions as illustrated by vinculin or paxillin staining (Fig. 3A; and quantified in Fig. 3B). In this context the small GTPase Rho represents one of the main regulators of actin stress fibers formation in adherent cells through activation of its effector protein Rho kinase (Ridley et al., 1999; Ridley et al., 1992). This led us to test whether RhoA activation was altered in DN_IRE1 cells compared to EV cells using commercially available kits (see Materials and Methods). Impairment of IRE1α activity led to significant basal activation of RhoA as assessed by using the G-LISA™ assay (Fig. 4A). The role of RhoA as the main regulator of stress fiber formation was then confirmed in DN_IRE1 cells using either the pharmacological Rho-kinase inhibitor Y-27632 or RhoA

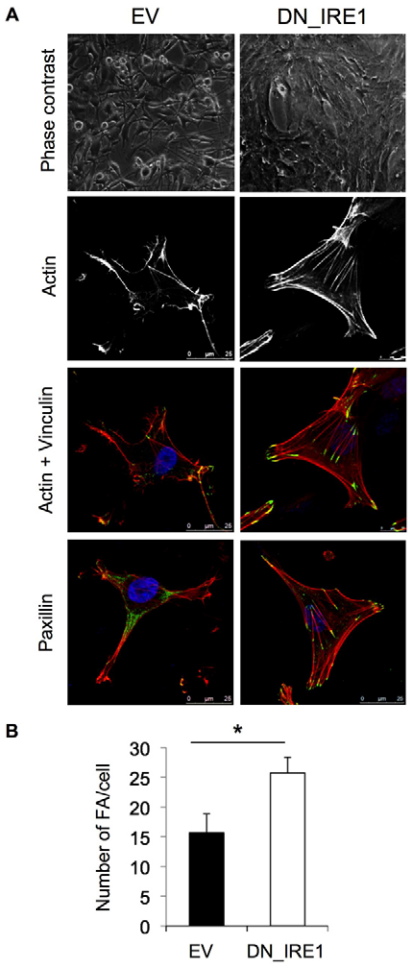

Fig. 3. Impairment of IRE1α signaling leads to F-actin cytoskeleton and cell architecture remodeling. (**A**) Phase-contrast analysis, phalloidin staining of F-actin and immunofluorescence analysis of vinculin and paxillin of EV and DN_IRE1 cells. (**B**) Measurement of focal adhesions (FA) in EV and DN_IRE1 cells as determined using vinculin staining (*P<0.05).

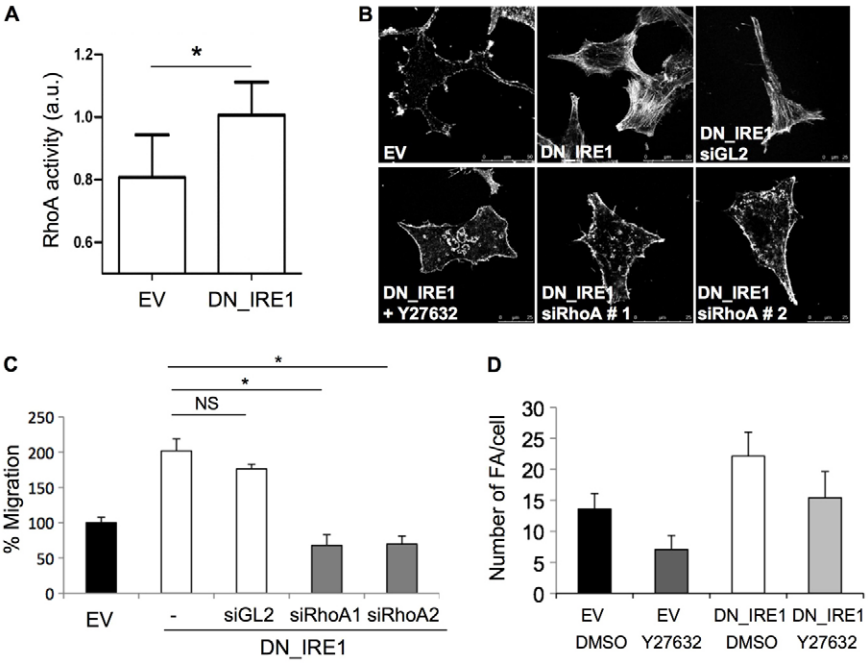

Fig. 4. Impairment of IRE1α signaling alters RhoA activation and cell adhesion properties in U87 cells. (**A**) RhoA activation in U87 EV and DN_IRE1 cells (measured as described in the Materials and Methods; *$P<0.05$). (**B**) EV and DN_IRE1 cells were either subjected to RhoA silencing by two different siRNAs (named no. 1 and no. 2) as well as a non-target luciferase siRNA (GL2) as a control, for 48 h or they were treated with the Rho Kinase inhibitor Y-27632 (10 μM) for 4 h. Fluorescence microscopy using phalloidin to stain F-actin was then performed on both cell lines. (**C**) Cells were subjected to RhoA silencing by the two different siRNAs as well as a non-target luciferase siRNA (GL2) as a control, for 48 h, and were tested for migration in vitro in Transwell assays. Migration was determined as in Fig. 1C (*$P<0.05$; NS, non-significant). (**D**) The number of focal adhesions was determined as described in the Materials and Methods in EV and DN_IRE1 cells treated with Y-27632 (10 μM) or DMSO for 24 h. A two-way ANOVA revealed a statistical difference between the DMSO and Y27632 conditions ($P<0.05$) and between the EV and DN_IRE1 cell types ($P<0.05$).

silencing strategies (supplementary material Fig. S2A) followed by immunofluorescence analyses. As shown in Fig. 4B, targeting RhoA signaling using either pharmacological or siRNA-based silencing strategies was sufficient to inhibit/prevent stress fiber formation in DN_IRE1 cells. This observation was also supported by the evaluation of the impact of RhoA silencing or Y-27632 treatment on U87 EV and DN_IRE1 cell migration capacity and focal adhesion number (Fig. 4C,D). In Fig. 4D, a two-way ANOVA statistical analysis revealed that both pharmacological treatment (Y27632) and expression of DN_IRE1 impacted on focal adhesion number per cell ($P<0.05$). These experiments showed that targeting RhoA expression or activity was sufficient to counteract DN_IRE1 cells migration ability and, in a same way, their increased focal adhesion number. This was also confirmed by measuring the impact of Y-27632 on the phosphorylation of the focal adhesion kinase (FAK), another focal adhesion marker (supplementary material Fig. S2B). Taken together, these results demonstrate that loss of IRE1α activity influences U87 cells attachment and migration properties by involving the small GTPase RhoA.

Gene expression profiling in EV and DN_IRE1 cells revealed differential expression of genes encoding extracellular matrix proteins

One of the major roles of IRE1α is to control the expression of membrane or secreted proteins coding genes through its capacities to splice the *Xbp1* mRNA or by directly cleaving a set of mRNA. Considering this, we hypothesized that DN_IRE1 cells might present modulations of the expression of mRNA encoding secretory or trans-membrane proteins in favor of an increase in adhesion and migration processes. To address this question, we compared mRNA expression profiles in control (EV; clone T1P5) and DN_IRE1 (clone 1C5) cells subjected or not to different ER stress inducing agents and thus IRE1α activators: glucose (−Glu) or glutamine (−Gln) deprivation, hypoxia (Hx) or tunicamycin (Tun) exposure. The data sets were deposited at the NCBI Gene Expression Omnibus GSE27306. Principal Component Analysis (PCA) was applied to visualize correlations in the control and DN_IRE1 transcriptional profiles. Fig. 5A illustrates that DN_IRE1 cells could be distinguished using the first two principal components, which account for 53% of total variation. DN_IRE1 cell populations were separated from control cells populations along the first principal component. We also noted that cultures performed under hypoxia (Hx) produced gene expression profiles that were separated from the other stress and basal culture conditions which showed intermediates positions along the second principal component. Other principal components did not display any information. This indicated that EV and DN_IRE1 populations subjected to Hx were associated with distinct transcriptional profiles, with some similarities in their gene expression. In contrast, the transcriptional profile of genes modulated in others control conditions showed very little overlap with profiles seen in others DN_IRE1 conditions.

To extract more information from these data, the PCA was applied by considering genes as individuals (Fig. 5B). The two first principal components accounted for 97% of the total variation. Fig. 5B shows genes that presented the most elevated mean between the different conditions along the first principal component and indicates the comparison of individual gene expression levels. The second principal component is built around genes that showed the biggest differences between samples from control and DN_IRE1 cells. PCA dimension 2 graphically shows the split between control and DN_IRE1 cells. The top 50 probe sets both positively and negatively regulated (corresponding to 40 genes; supplementary material Table S1) were subjected to functional annotation. The Kyoto Encyclopedia of Genes and Genome (KEGG), a compendium of genes annotated and organized by signaling pathway (Ogata et al., 1998), was used for this purpose (Fig. 5C). This revealed that both the ECM–receptor interaction and the focal adhesion signaling pathways were enriched in the DN_IRE1 signature, thus reinforcing our initial phenotypic observations.

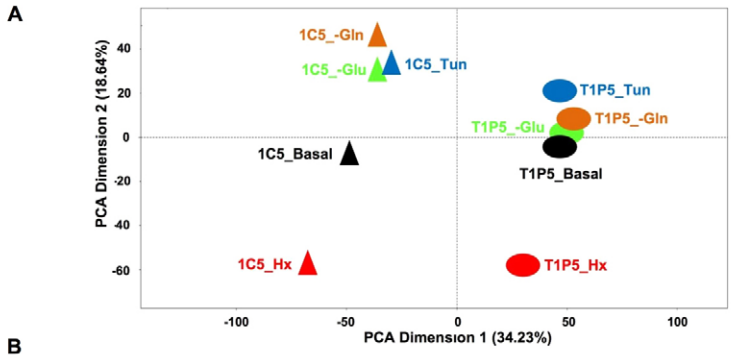

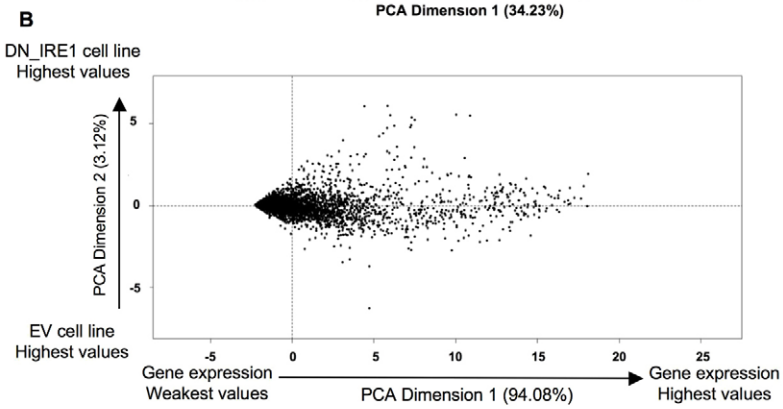

C

ID	Term	P value
4512	ECM-Receptor Interaction	0,00022
4510	Focal Adhesion	0,0058
4514	Cell Adhesion Molecules	0,086
0760	Nicotimide and nicotinamide metabolisms	0,086

Fig. 5. Transcriptional profiles of EV and DN_IRE1α cells revealed substantial differences in genes encoding extracellular matrix proteins. (**A**) Principal component analysis (PCA) of transcriptional profiles of EV (T1P5 clone) and DN_IRE1 cells (1C5 clone). The two-dimensional scatter plot shows the first two principal components of the analysis of 6078 genes. Data points from individual experimental conditions were represented using different shapes (triangles represent DN_IRE1 U87 cells, circles represent control U87 cells; Hx: hypoxia 0.1% for 16 h; -Glu: glucose deprivation for 16 h; -Gln: glutamine deprivation for 16 h; Tun: tunicamycin 1 μg/ml for 16 h). (**B**) Plot of individual genes that were significantly differentially expressed between EV and DN_IRE1 cells (all conditions combined). The top 50 probe-sets contributing the most to differences between EV and DN_IRE1 cells are listed in supplementary material Table S1. (**C**) Over-represented molecular pathways and functional annotation of the gene list in supplementary material Table S1 using KEGG pathway analysis.

IRE1α signaling regulates migration of U87 cells by downregulating Sparc mRNA expression

Based on the above-mentioned data, we further analyzed the list of genes identified through gene expression profiling (supplementary material Table S1) and selected genes that were i) overexpressed in DN_IRE1 cells, ii) involved in the modulation of cellular microenvironment and iii) functionally related to ER stress signaling. Based on these selection criteria, we selected SPARC. SPARC/Osteonectin is a matrix-associated protein that elicits changes in cell shape, inhibits cell-cycle progression and influences the synthesis of extracellular matrix (ECM) (Brekken and Sage, 2001; Chlenski and Cohn, 2010). Moreover, SPARC was a good candidate to explain the in vivo DN_IRE1 expressing tumor phenotype previously observed. Indeed, it was shown that SPARC overexpression delays tumor growth and promotes invasion in a rat glioma model (Kunigal et al., 2006; Rempel et al., 2001). Adding to that, *Sparc* mRNA was identified as a RIDD substrate that led to the repression of its expression through an internal cleavage (Hollien and Weissman, 2006). Using quantitative real-time PCR and semi-quantitative PCR we showed that SPARC mRNA was overexpressed in different clones of DN_IRE1 expressing cells compared to control cells under basal conditions and upon ER stress (Fig. 6A,B). As previously demonstrated (Hollien et al., 2009; Hollien and Weissman, 2006), we found that ER stress inducers (tunicamycin and dithiothreitol; DTT) were able to decrease *Sparc* mRNA in an IRE1α dependent manner in our glioma model (Fig. 6B). Moreover, siRNA-mediated IRE1α silencing in glioma cells led to increase *Sparc* mRNA expression (Fig. 6C; supplementary material Fig. S2C). A recent study identified a conserved consensus IRE1α cleavage sequence located in stem-loop structures on mRNA (Oikawa et al., 2010). Based on this information, we found only one potential IRE1α-cleavage site within *Sparc* mRNA using the M-FOLD program (Fig. 6D). We then investigated whether *Sparc* mRNA was cleaved by IRE1α using an in vitro RNA cleavage assay as previously reported (Bouchecareilh et al., 2011a). Total RNA from U87 cells was subjected to the in vitro cleavage assay in the presence of GST–IRE1α. RT-PCR using primers overlapping or not the putative cleavage site were then performed to determine the *Sparc* mRNA levels (Fig. 6E). In vitro results indicated a strong decrease in *Sparc* mRNA expression corresponding to the cleaved amplicon only (1499–1709) whereas another region of *Sparc* mRNA (278–479) remained intact (Fig. 6E). These data indicate that IRE1α is responsible of *Sparc* mRNA cleavage, which will lead inevitably to its exonuclease-mediated degradation in a cellular context.

We next sought to investigate the consequences of IRE1α-mediated alteration of SPARC expression in U87 cells. To modulate *Sparc* mRNA expression in U87 cells, a siRNA-based approach was undertaken and SPARC expression was indeed efficiently silenced in both control (EV) and DN_IRE1 cells at both RNA and protein levels (Fig. 7A; supplementary material Fig. S2D). This strategy allowed us to almost completely suppress SPARC secretion in the extracellular medium (supplementary material Fig. S3A). To identify if SPARC overexpression was associated with RhoA activation and focal adhesion/stress fiber regulation, we measured FAK phosphorylation and RhoA

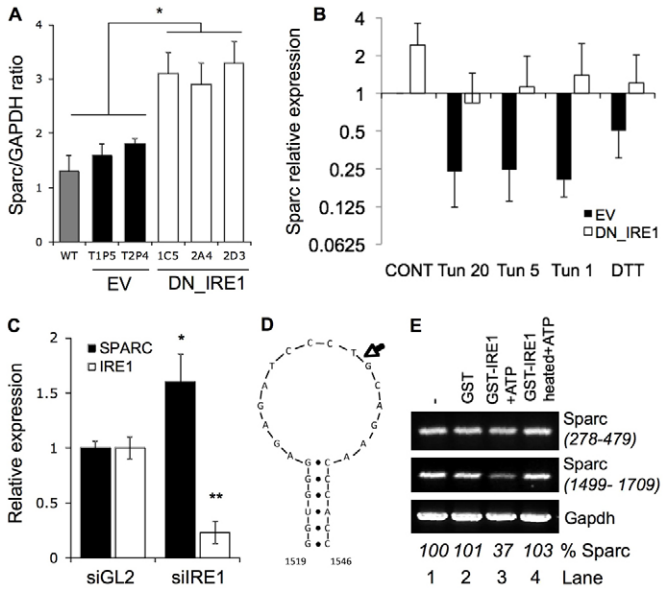

Fig. 6. IRE1α mediates the cleavage of *Sparc* mRNA. (**A**) *Sparc* mRNA expression in wild-type, EV (T1P5 and T2P4 clones) and DN_IRE1 (1C5, 2A4 and 2D3 clones) cells as quantified by quantitative RT-PCR. (**B**) *Sparc* mRNA levels were measured by quantitative RT-PCR and were normalized to beta-2 microglobulin (B2M) levels upon treatment with ER stress inducers including Tunicamycin (Tun, 20, 5 and 1 μg/ml, 24 h) or DTT (2 mM, 6 h). Results were normalized to the EV non-stressed condition. (**C**) siRNA-mediated attenuation of IRE1α expression (white bars) leads to enhanced *Sparc* mRNA expression (black bars). (**D**) Schematic representation of the IRE1α cleavage sites with secondary structures, predicted using M-FOLD. The cleavage site is indicated by an arrow. (**E**) In vitro RNA cleavage assay. Total RNA extracted from U87 cells was incubated with GST or GST–IRE1α-cyto in the presence of ATP for 2 h at 37℃. In the 'GST-IRE1 heated + ATP' condition, GST–IRE1α-cyto was heated to suppressed its activity, and used as a negative control. RT-PCR was then performed to determine *Sparc* and *Gapdh* mRNA levels. Quantifications are indicated as percentage of control (*P<0.05).

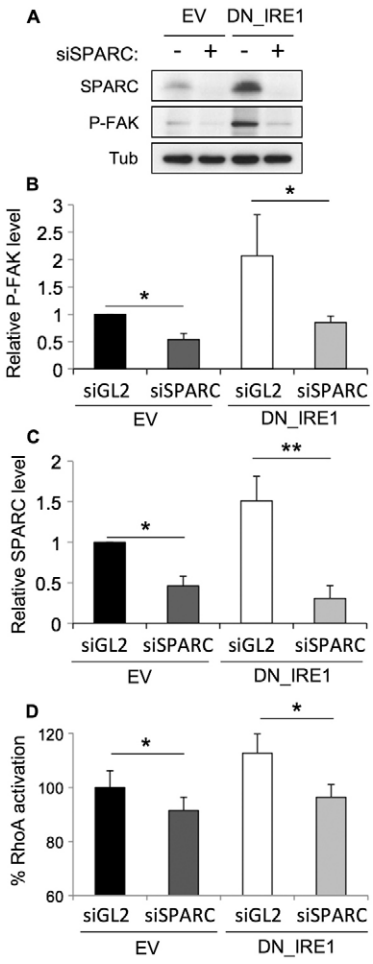

Fig. 7. IRE1α-mediated *Sparc* mRNA controls U87 architectural structure. (**A**) EV and DN_IRE1 cells were subjected to SPARC silencing by siRNA or non-target luciferase (GL2) silencing as a control. SPARC protein levels and FAK phosphorylation were evaluated by western blotting. Tubulin (Tub) was used as a loading control. (**B**,**C**). Relative quantification of SPARC protein levels and FAK phosphorylation. Values were normalized to tubulin levels. (**D**) EV and DN_IRE1 cells were subjected to SPARC silencing by siRNA or non-target luciferase (GL2) silencing as a control and were assessed for RhoA activation. (*P<0.05; **P<0.01).

activation in EV or DN_IRE1 cells silenced or not for SPARC (Fig. 7). As expected, SPARC expression correlated perfectly with P-FAK (Fig. 7A–C) and with RhoA activation (Fig. 7D). To further test whether SPARC-mediated RhoA activation and FAK phosphorylation were associated with the migration/proliferation phenotype observed for DN_IRE1 cells, the capacity of EV and DN_IRE1 cells to form neurospheres and to migrate in Transwell assays was then studied (Fig. 8). First and as anticipated, siRNA-mediated downregulation of *Sparc* mRNA expression significantly increased the size of neurospheres after 72 h (Fig. 8A). Second, SPARC silencing altered the migration capacity of both EV and DN_IRE1 cells (Fig. 8B). Third, the use of SPARC blocking antibodies (Sweetwyne et al., 2004) in the medium of cultured cells led to a similar observation with the reduction of cell migration, thus suggesting an autocrine/paracrine mechanism of action (Fig. 8C). This demonstrated that the process of IRE1α-mediated control of U87 cells was SPARC-dependent and most likely occurred in an autocrine/paracrine fashion.

Discussion

In the present study, using a combination of cellular and molecular approaches we correlate the inhibition of IRE1α activity in glioma with alteration of tumor cells/extracellular matrix interactions. We show that the structure of the actin cytoskeleton is affected in IRE1α signaling deficient cells compared to control cells (Figs 2, 3), thereby indicating an alteration of cell's architecture and demonstrating an increase in focal adhesions number. Moreover, at the molecular level, transcriptional profiles indicated substantial differences between control and DN_IRE1 cells. Indeed a majority of genes modulated in DN_IRE1 cells encoded secreted proteins associated to the extracellular matrix or to cell adhesion (Fig. 5) such as collagen or fibronectin (supplementary material Table S1). Based on these analyses, we identify *Sparc* mRNA as an IRE1α-endoribonuclease regulated transcript relevant of our glioma model. *Sparc* encodes a matrix secretory protein that regulates the interaction of tumor cells with the extracellular matrix and impacts on their adhesion/migration properties through, among others, the activation of RhoA signaling (Figs 7, 8). These data led us to propose a model in which ER stress-mediated control of

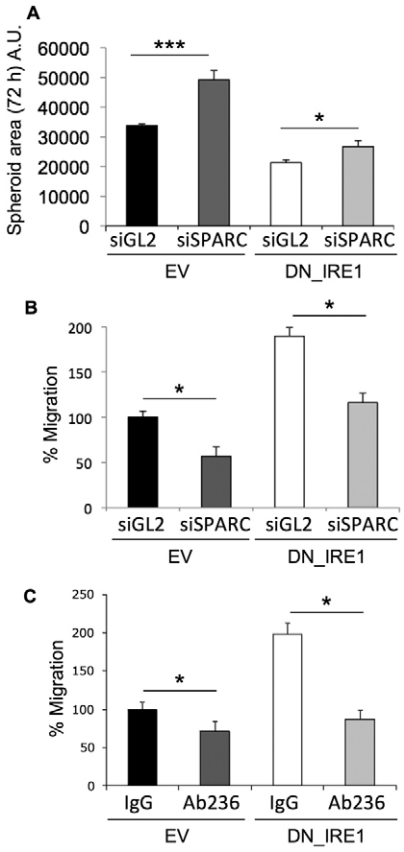

Fig. 8. Role of *Sparc* mRNA expression in DN_IRE1 cell migration and neurosphere formation. (**A**) Sizes of spheroids formed by incubating 2000 cells silenced or not for SPARC on an agar matrix for 72 h, as described in the Materials and Methods. (**B**) EV and DN_IRE1 cells were subjected to SPARC silencing by siRNA or non-target luciferase (GL2) silencing as a control and were tested for migration in vitro using Transwell assays. (**C**) EV and DN_IRE1 cells were exposed to SPARC blocking antibodies (ab236) added to the medium and were tested for migration in vitro using Transwell assays (*$P<0.05$; ***$P<0.001$).

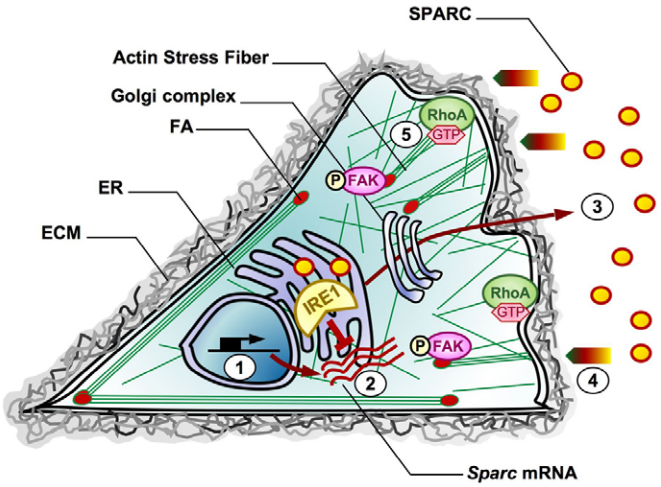

Fig. 9. Schematic representation of the mode of action of IRE1α signaling in gliomas leading to control of cell proliferation and migration. U87 wild-type cancer cells can still proliferate under challenging conditions through enhanced adaptability. In contrast, when IRE1α signaling is impaired, cell proliferation capacity is decreased, which is associated to the post-transcriptional derepression of *Sparc* mRNA expression (1 and 2). Secreted SPARC (3) will in turn, interact with the extracellular matrix (4) and consecutively enhanced cell migration, stress fiber formation and focal adhesion number through RhoA-dependent mechanisms (5). ECM, extracellular matrix; ER, endoplasmic reticulum; FA, focal adhesion.

Sparc mRNA expression could provide a selective advantage for tumor cells to adapt to challenging environments (Fig. 9).

Several reports have previously demonstrated that IRE1α mediates both the cleavage and the degradation of mRNA encoding secretory proteins independently of the *Xbp1* pathway (Hollien et al., 2009; Hollien and Weissman, 2006; Oikawa et al., 2010; Oikawa et al., 2007). Oikawa and colleagues identified a consensus sequence CU↓GCAG with IRE1α cleavage site present between the second and the third base and located in the loop portion of a stem loop structure, similar to those found in *Xbp1* mRNA (Yoshida et al., 2003; Yoshida et al., 2001). Interestingly, we found a sequence compatible with this consensus in *Sparc* mRNA and its in vitro cleavage by IRE1α was monitored by PCR (Fig. 6). Moreover, the *D. melanogaster* ortholog of *Sparc* mRNA was identified as an IRE1α substrate in a previous study (Hollien and Weissman, 2006). This reinforced the relevance of our observation and strongly suggested a link between ER stress signaling and tumor cells adhesion/migration processes.

High levels of *Sparc* mRNA have been correlated with cancer progression and poor prognosis, or in contrast, with tumor suppression depending of the cancer types (Podhajcer et al., 2008; Tai and Tang, 2008). As such, downregulation of SPARC by siRNA in invasive glioma cell lines, which were subsequently injected in an orthotopic mouse model, led to inhibition of infiltrating tumor cell dissemination (Seno et al., 2009). As well, in glioma, overexpression of SPARC inhibits cell proliferation both in vitro and in vivo (Podhajcer et al., 2008; Tai and Tang, 2008). When injected into immunodeficient rat brains, U87 cell-derived tumors overexpressing SPARC exhibited small tumor size with extensive tumor cell infiltrations compared to U87 control cell-derived tumors, which were bigger with a well delimited perimeter (Schultz et al., 2002). The latter phenotype presented therefore features similar to those observed in DN_IRE1 glioma cell-derived tumors (Auf et al., 2010; Drogat et al., 2007).

SPARC has been characterized as acting in matrix remodeling and cell migration processes. SPARC participates to survival, adhesion, migration, invasion in glioma cell lines (Arnold and Brekken, 2009). Both aggressiveness and migration capacity of cancer cells were shown to depend on SPARC concentration in the ECM, thereby making SPARC a target for therapies treating glioma invasion (Kunigal et al., 2006). Moreover, we observed an enhanced activation of RhoA in cells deficient for IRE1α signaling (Fig. 4). This is in agreement with data showing that RhoA is involved in the SPARC-induced migration of U87 cells (Kunigal et al., 2006) and is consistent with our previous work linking Rho GTPase signaling to the Unfolded Protein Response (Bouchecareilh et al., 2011b; Caruso et al., 2008). Moreover, SPARC expression has been previously described to increase U87 cell migration (Rempel et al., 2001). Furthermore, in our study, DN_IRE1 cells migration specific properties were also correlated with increased attachment to collagen and Matrigel

compared to EV cells (Fig. 1) and to the upregulation of the expression of extracellular matrix proteins (supplementary material Table S1). Interestingly Schultz and colleagues and Golembieski and Rempel found that the level of secreted SPARC controls the balance between tumor cells adherence and migration (Schultz et al., 2002; Golembieski and Rempel, 2002). They showed that, in contrast to low and high levels of SPARC expression, which promote tumor invasiveness, intermediate expression levels induce stronger adherence and a typical in vivo invasion as a bulk tumor along the corpus callosum. In our study, DN_IRE1 glioma cells presented some characteristics that could correspond to an intermediate level of SPARC expression. Indeed, DN_IRE1 expressing cells present elevated migration capacity, weak invasion ability and a migration profile more collective than that of EV expressing cells (Figs 1, 2; supplementary material Fig. S1).

SPARC downstream signaling regulating glioma migration was shown to involve HSP27 and p38MAPK (Golembieski et al., 2008) as well as the uPA–uPAR system (Kunigal et al., 2006), the TGF-beta (Francki et al., 2004) and integrins (Barker et al., 2005) signaling pathways or the SHC–RAF–ERK pathway (Thomas et al., 2010). As our initial phenotypic observations correlated with increased stress fiber formation and RhoA activity, we focused on this signaling pathway as a read out of SPARC secretion and activity. Our data suggest that secretion of SPARC and extracellular matrix proteins (collagen, fibronectin) may influence the local environment, resulting in enhanced glioma cell migration (supplementary material Table S1). Interestingly, we found that SPARC addition to the media (0.1 and 1 μg/ml, 24 h) was not sufficient to reproduce the DN_IRE1 effect on U87 cell migration or focal adhesion increase (not shown). However, we also found that SPARC blocking antibodies were sufficient to suppress the increase in DN_IRE1 expressing U87 cells migration capacity (Fig. 8C). With regard to these results, we might propose that SPARC overexpression is necessary but not sufficient to explain DN_IRE1 cells migration capacity. For instance, SPARC has been shown to enhance fibronectin-induced stress fiber formation and fibronectin matrix assembly (Barker et al., 2005). In our model, both fibronectin expression and SPARC levels were increased (supplementary material Table S1; Fig. 7A; supplementary material Fig. S3B), thereby suggesting a synergistic effect. We propose a model in which SPARC impacts on the cell interaction with its ECM and induces a range of signaling pathways to promote a general induction of stress fiber formation and increase in cell migration (Fig. 9).

Our data provide the first molecular connection between IRE1α signaling in the ER and tumor phenotypes. In Fig. 9, we propose a model that recapitulates our data in which impairing IRE1α signaling in glioma cells relieves the post-transcriptional repression of *Sparc* mRNA. This in turn leads to the modulation of cell migration properties through RhoA-dependent mechanisms. This model could be disease-relevant since *IRE1α* has been found mutated in a panel of human gliomas (Greenman et al., 2007; Parsons et al., 2008). Interestingly, two of these mutations, more precisely the Q780 (a stop mutant) and the S769F were recently found to result in the abrogation of IRE1α endoribonuclease activity (Xue et al., 2011). Hence, we propose that IRE1α activity may be modulated in these mutated human cancers, and therefore may contribute to tumor progression through, for instance, SPARC dependent processes.

Materials and Methods

Cell culture and treatments

U87 cells were grown in DMEM glutamax (Invitrogen, Carlsbad, CA, USA) supplemented with 10% FBS and antibiotics. U87 were stably transfected with pcDNA3/IRE1-NCK1, an expression vector encoding a cytoplasmic-defective IRE1α mutant). U87 cells were selected using 450 μg/ml G418 and several isolated clones were tested: T1P5 (referred as EV in the text) and T2P4 as empty vector and 1C5 (referred as DN_IRE1 in the text), 2A4 and 2D4 as IRE1 dominant negative expressing cell lines. For microarray experiments, tunicamycin (purchased from Calbiochem; Merck KGaA, Darmstadt, Germany) was used at 1 μg/ml for 16 h, hypoxic conditions were done at 1% in a Heraeus incubator BB-6060, glucose deprivation was performed by using DMEM F405 medium supplemented with 1% FBS and glutamine deprivation was done by using DMEM F405 medium supplemented with 1% FBS and glucose. RhoA inhibitor Y-27632 and DTT were purchased from Sigma (St Louis, MO, USA).

Western blotting

Antibodies against P-FAK and fibronectin were purchased from BD Transduction Laboratory (Oxford, UK), alpha-tubulin from Sigma (St Louis, MO, USA), RhoA from Santa Cruz Biotechnology (Santa Cruz, CA) and SPARC from Cell Signaling Technology (Danvers, MA). Anti-CNX antibodies were kindly given by John Bergeron (McGill University, Montreal, QC, Canada). SPARC extraction from cell culture media was performed by adding 75 μl of rehydrated Heparin Sepharose CL-6B (GE Healthcare, USA) to 5 ml of cell culture media containing 1% FBS. The solution was then incubated with agitation at 4℃ for 4 h. The gel was then recovered by centrifugation and mixed with Laemmli sample buffer before western blotting.

Small Interfering RNA

Small interfering (si) RNAs were chemically synthesized (MWG) and transfected into U87 cells and derivatives (50 nmol) using Lipofectamine™ RNAiMAX (Invitrogen, Carlsbad, CA, USA) for 72 hrs according to the protocol of the manufacturer. Small interfering RNAs were designed against RhoA mRNA (5′-AAGAAGTCAA-GCATTTCTGTC-3′ or purchased from Applied Biosystems, Ambion, Carlsbad, CA, USA), against SPARC mRNA (5′-GAAGAUCCAUGAGAAUGAG-3′; 5′-ACACACAUUGCAGCUUCAA-3′; 5′-ACAAGACCUUCGACUCUUC-3′) or IRE1 mRNA (5′-GCGUCUUUUACUACGUAAU-3′) or purchased (for IRE1) from Dharmacon (Lafayette, CO, USA). As a control we used the GL2 siRNA sequence (5′-CGUACGCGGAAUACUUCGATT-3′) designed to target the firefly luciferase.

RhoA activity assay

RhoGTPase protein activity assay was performed by using the G-LISA™ RhoA Activation Assay Biochem Kit™ (Cytoskeleton Inc., CO, USA) according to the manufacturer's instructions.

Attachment assays

Plates (96-well) were coated with a filtered solution of 400 μg/ml collagen in PBS (Sigma, St Louis, MO, USA) or with Matrigel as previously described (Kunigal et al., 2006; Rempel et al., 2001). Rat tail collagen I was purchased from BD Bioscience and was coated on culture plates as recommended by the manufacturer. EV and DN_IRE1 cells (25,000 cells) were plated for time points 0, 15 and 30 min and 1, 2 and 4 hours. Medium and unattached cells were aspirated. Wells were washed with PBS and attached cells were fixed in 3% paraformaldehyde for 30 min, rinsed with PBS three times, and stained with Sulforhodamine B (SRB assay kit, Sigma, St Louis, MO, USA). Data were quantified by spectrophotometry at 492 nm. At time 0, no cell was attached to the substratum.

Immunofluorescence analyses

Cells grown on 12-mm coverslip (Rempel et al., 2001) were treated as indicated, washed with PBS, fixed with 4% paraformaldehyde for 15 min at room temperature, and then blocked with 5% BSA, PBS, 0.1% Triton X-100 for 1 h. Filamentous actin was visualized using phalloidin–FITC as previously described (Liu et al., 1999). Cortactin, paxillin, vinculin, cells were visualized as previously described (Moreau et al., 2003). Cells were incubated with primary antibodies for 16 h at 4℃, washed with PBS, and incubated for 1 h with FITC/TRITC conjugated secondary antibodies (Invitrogen, Carlsbad, CA, USA). To visualize the nucleus, cells were counterstained with 1 μg/mL 4,6-diamidino-2-phenylindole (DAPI, Sigma, St Louis, MO, USA). After mounting, cells were analyzed with a SP5 confocal microscope (Leica Microsystems, Mannheim, Germany).

Focal adhesion quantification

Quantification of focal adhesion was adapted from the method of Juin and colleagues (Juin et al., 2012). Confocal images of isolated cells were obtained using a SP5 confocal microscope (Leica Microsystems, Mannheim, Germany) by using a 63×/NA 1.4 Plan Neo-Fluar objective. Cell surface area was measured upon phalloidin staining, and vinculin staining was used as a focal adhesion

marker. We developed a macro with ImageJ software that allowed measurement of all required parameters of focal adhesions: number/cells and cell size (using the Feret diameter, the longest distance between any two points). At least 2000 focal adhesions were counted for each condition in three independent experiments and in a total of 180 to 280 cells. The results were expressed as the mean of the three experiments.

Migration and invasion assays

Cells were tested for migration and invasion abilities in vitro using 8 μm pores Transwell inserts (BD BioCoat^{TM}). The upper side of the Transwell inserts with 8 mm pores was either uncoated (migration) or coated (invasion) with Matrigel. U87 cells were added to the upper chamber at 25,000 cells per well in serum free medium. The lower portion of the chamber contained 1% serum as chemo attractant. After incubation for 16 h, the cells at the upper side were removed with a cotton swab. Filters were fixed with paraformaldehyde 3% for 30 min, and then the cells at the lower side were stained with Crystal Violet 0.1%. The level of migration and invasion was determined by counting cells in five randomly areas under a light microscope.

Neurospheres

Neurosphere formation experiments were performed by incubating 2000 cells by well in a 96-well plate previously coated with 50 μl of 1.5% agar gel. For neurosphere dissociation/migration, neurospheres of the same size (obtained by incubating 3000 and 6000 of EV and DN_IRE1 expressing cells, respectively) were put on a 22-mm coverslip and incubated for 48 h. Then, neurosphere were fixed with 4% paraformaldehyde for 20 min at room temperature. Cell actin (phalloidin-546) and nucleus (Hoechst) were stained and visualized as described in the Immunofluorescence analyses section with some modifications: after blockage, neurosphere cells were incubated 1 h with Hoechst and phalloidin-546. After mounting, cells were analyzed using a Zeiss epifluorescence microscope.

RNA cleavage assay

Total RNA (10 μg) from U87 was incubated with the cytoplasmic domain of human GST–IRE1α (5 μg) at 37℃ for the indicated times in a 5× buffer containing 250 mM Tris pH 7.5, 600 mM NaCl, 5 mM $MgCl_2$, 5 mM $MnCl_2$, 25 mM β-mercaptoethanol, supplemented with or without 10 mM ATP. As control, we used GST–IRE1α denatured by heating 10 min at 100℃. RT-PCR was performed using SPARC primers and GAPDH as internal control. IRE1α cleaved or uncleaved RNAs were used as a template for reverse transcription and PCR was then performed using SPARC primers. Secondary structure of *Sparc* mRNA was predicted using M-FOLD (http://mobyle.pasteur.fr/cgi-bin/portal.py?form=mfold).

Microarray experiments and analyses

Microarray assay and preprocessing analysis were performed in the microarray core facility of the Research Institute for Biotherapy at Montpellier using the standard Affymetrix protocol. Total RNA was extracted using Trizol (Invitrogen). RNA integrity was verified on an Agilent 2100 Bioanalyzer. For each of the samples, total RNA was reverse transcribed into cDNA, followed by in vitro transcription and biotin labeling to generate cRNA (Enzo Biochem, Farmingdale, NY, USA). The fragmented, biotin-labeled cRNA was hybridized to Human Genome U133 2.0 oligonucleotide arrays (Affymetrix, Santa Clara, CA, USA) containing approximately 22,000 probes. Microarrays were stained with streptavidin antibody and streptavidin–phycoerythrin in an Affymetrix Fluidics station. Arrays were scanned using a 3000 7G scanner. Row data were analyzed and principal components analysis (PCA) was carried out to highlight potential expression profiles within and across cell lines using R software version 2.8.0 (Gentleman et al., 2004). Spots for which the gene expression values were too low or not statistically significant were removed (6078 probesets were selected). Principal Component Analysis (PCA) builds a new coordinate system, which maximizes the variance in the data. The Principal Components (PCs) are linear combinations of the original variables X1, X2, …, Xz, chosen in such a way that PCA dimension 1 describes the largest fraction of variation in the data, and subsequent PCs describe maximal portions of the remaining variation. An essential requirement is that all PCs should be orthogonal to each other. Thus, only the first few PCs need to be considered to get a good overview of the data. In our datasets, the variables X1, X2, …, Xz represent our different cell conditions. The data of n objects (gene expression), each measured at m treatments or cell lines, can be written as an n by m matrix X. Before mapping the data, the samples in X were centered by subtracting their means and a biplot was then constructed. The Kyoto encyclopedia of Genes and Genomes (KEGG), a compendium of genes annotated and organized by signaling pathway was used for annotations (Ogata et al., 1998).

Semi-quantitative PCR and quantitative real-time PCR

Total RNA was prepared using the Trizol reagent (Invitrogen, Carlsbad, CA, USA). Semi-quantitative analyses were carried out as previously described (Nguyên et al., 2004). PCR products were separated on 1% agarose gels. For real-time quantitative PCR, RNA was reverse transcribed with Superscript II (Promega, Charbonnières-les-Bains, France). All PCR reactions were performed with a Stratagene X4000 thermocycler (Stratagene, Amsterdam, The Netherlands) and the SYBR Green PCR Core reagents kit (Bio-Rad, Marnes-La-Coquette, France). Experiments were performed in triplicates for each data point. Each sample was normalized on the basis of its expression of the RLP0 or B2M genes (2ΔΔCt). For amplification, the following pairs were used: SPARC 278-479: 5′-GTGCAGAGGAAACCGAA-3′ (FWD) and 5′-AAGTGGCAGGAAGAGTCGAA-3′ (REV). SPARC 1499–1709: 5′-GGTTCAAACTTTTGGGAGCA-3′ (FWD) and 5′-CCGATTCACCAACTCCAC-3′ (REV). GAPDH: 5′-ACCACCATGGAGAAGGCTGG-3′ (FWD) and 5′-CTCAGTGTAGCCCAGGATGC-3′ (REV). RPL0: 5′-GGCGACCTGGAAGTCCAACT-3′ (FWD) and 5′-CCATCAGCACCACAGCCTTC-3′ (REV). IRE1α: 5′-GCCACCCTGCAAGAGTATGT-3′ (FWD) and 5′-ATGTTGAGGGAGTGGAGGTG-3′ (REV). B2M: 5′-GTGCTGTCTCCATGTTTGATGTATC-3′ (FWD) and 5′-CTAAGTTGCCAGCCCTCCTAGA-3′ (REV), XBP1: 5′-GGAACAGCAAGTGGTAGA-3′ (FWD) and 5′-CTGGAGGGGTGACAAC-3′ (REV).

Assay for cell growth (SRB)

The SRB assay was performed as previously described (Vichai and Kirtikara, 2006). Briefly, cells were seeded into 96-well plates in 100 μl at a density of 5000 cells/well. After cell inoculation, the plates were incubated at 37℃ for 24, to 96 h. Cell were then fixed in situ with trichloroacetic acid and stained with sulforhodamine B (Sigma, St Louis, MO, USA). Absorbance was measured at 510 nm.

Statistical analyses

Data are presented as means ± s.d. or s.e.m. of at least three experiments. Statistical significance ($P<0.05$ or less) was determined using a paired or unpaired t-test or ANOVA as appropriate and performed with GraphPad Prism software (GraphPad Software, San Diego, CA, USA).

Acknowledgements

We thank the Chevet lab for critical reading of the manuscript. We are indebted to Sebastien Marais (Bordeaux Imaging Center, Bordeaux, France) for help with the ImageJ program.

Funding

This work was supported by the Avenir program of Institut National de la Santé et de la Recherche Médicale; Institut national du cancer; Ligue Contre le Cancer to E.C.; the French Association pour la Recherche contre le Cancer to O.P.; La Ligue contre le Cancer to N.D.; and the Cancéropôle Grand Sud-Ouest to C.G.

Supplementary material available online at
http://jcs.biologists.org/lookup/suppl/doi:10.1242/jcs.099291/-/DC1

References

Arnold, S. A. and Brekken, R. A. (2009). SPARC: a matricellular regulator of tumorigenesis. *J. Cell Commun. Signal.* **3**, 255-273.

Auf, G., Jabouille, A., Guérit, S., Pineau, R., Delugin, M., Bouchecareilh, M., Magnin, N., Favereaux, A., Maitre, M., Gaiser, T. et al. (2010). Inositol-requiring enzyme 1alpha is a key regulator of angiogenesis and invasion in malignant glioma. *Proc. Natl. Acad. Sci. USA* **107**, 15553-15558.

Barker, T. H., Baneyx, G., Cardó-Vila, M., Workman, G. A., Weaver, M., Menon, P. M., Dedhar, S., Rempel, S. A., Arap, W., Pasqualini, R. et al. (2005). SPARC regulates extracellular matrix organization through its modulation of integrin-linked kinase activity. *J. Biol. Chem.* **280**, 36483-36493.

Bouchecareilh, M., Higa, A., Fribourg, S., Moenner, M. and Chevet, E. (2011a). Peptides derived from the bifunctional kinase/RNase enzyme IRE1{alpha} modulate IRE1{alpha} activity and protect cells from endoplasmic reticulum stress. *FASEB J.* **25**, 3115-3129.

Bouchecareilh, M., Marza, E., Caruso, M. E. and Chevet, E. (2011b). Small GTPase signaling and the unfolded protein response. *Methods Enzymol.* **491**, 343-360.

Brekken, R. A. and Sage, E. H. (2001). SPARC, a matricellular protein: at the crossroads of cell-matrix communication. *Matrix Biol.* **19**, 816-827.

Calfon, M., Zeng, H., Urano, F., Till, J. H., Hubbard, S. R., Harding, H. P., Clark, S. G. and Ron, D. (2002). IRE1 couples endoplasmic reticulum load to secretory capacity by processing the XBP-1 mRNA. *Nature* **415**, 92-96.

Carrasco, D. R., Sukhdeo, K., Protopopova, M., Sinha, R., Enos, M., Carrasco, D. E., Zheng, M., Mani, M., Henderson, J., Pinkus, G. S. et al. (2007). The differentiation and stress response factor XBP-1 drives multiple myeloma pathogenesis. *Cancer Cell* **11**, 349-360.

Caruso, M. E., Jenna, S., Bouchecareilh, M., Baillie, D. L., Boismenu, D., Halawani, D., Latterich, M. and Chevet, E. (2008). GTPase-mediated regulation of the

unfolded protein response in Caenorhabditis elegans is dependent on the AAA+ ATPase CDC-48. *Mol. Cell. Biol.* **28**, 4261-4274.

Chlenski, A. and Cohn, S. L. (2010). Modulation of matrix remodeling by SPARC in neoplastic progression. *Semin. Cell Dev. Biol.* **21**, 55-65.

Drogat, B., Auguste, P., Nguyen, D. T., Bouchecareilh, M., Pineau, R., Nalbantoglu, J., Kaufman, R. J., Chevet, E., Bikfalvi, A. and Moenner, M. (2007). IRE1 signaling is essential for ischemia-induced vascular endothelial growth factor-A expression and contributes to angiogenesis and tumor growth in vivo. *Cancer Res.* **67**, 6700-6707.

Francki, A., McClure, T. D., Brekken, R. A., Motamed, K., Murri, C., Wang, T. and Sage, E. H. (2004). SPARC regulates TGF-beta1-dependent signaling in primary glomerular mesangial cells. *J. Cell. Biochem.* **91**, 915-925.

Gentleman, R. C., Carey, V. J., Bates, D. M., Bolstad, B., Dettling, M., Dudoit, S., Ellis, B., Gautier, L., Ge, Y., Gentry, J. et al. (2004). Bioconductor: open software development for computational biology and bioinformatics. *Genome Biol.* **5**, R80.

Golembieski, W. A. and Rempel, S. A. (2002). cDNA array analysis of SPARC-modulated changes in glioma gene expression. *J. Neurooncol.* **60**, 213-226.

Golembieski, W. A., Thomas, S. L., Schultz, C. R., Yunker, C. K., McClung, H. M., Lemke, N., Cazacu, S., Barker, T., Sage, E. H., Brodie, C. et al. (2008). HSP27 mediates SPARC-induced changes in glioma morphology, migration, and invasion. *Glia* **56**, 1061-1075.

Greenman, C., Stephens, P., Smith, R., Dalgliesh, G. L., Hunter, C., Bignell, G., Davies, H., Teague, J., Butler, A., Stevens, C. et al. (2007). Patterns of somatic mutation in human cancer genomes. *Nature* **446**, 153-158.

Hollien, J. and Weissman, J. S. (2006). Decay of endoplasmic reticulum-localized mRNAs during the unfolded protein response. *Science* **313**, 104-107.

Hollien, J., Lin, J. H., Li, H., Stevens, N., Walter, P. and Weissman, J. S. (2009). Regulated Ire1-dependent decay of messenger RNAs in mammalian cells. *J. Cell Biol.* **186**, 323-331.

Juin, A., Billottet, C., Moreau, V., Destaing, O., Albiges-Rizo, C., Rosenbaum, J., Génot, E. and Saltel, F. (2012). Physiological type I collagen organization induces the formation of a novel class of linear invadosomes. *Mol. Biol. Cell* **23**, 297-309.

Kunigal, S., Gondi, C. S., Gujrati, M., Lakka, S. S., Dinh, D. H., Olivero, W. C. and Rao, J. S. (2006). SPARC-induced migration of glioblastoma cell lines via uPA-uPAR signaling and activation of small GTPase RhoA. *Int. J. Oncol.* **29**, 1349-1357.

Lee, K., Tirasophon, W., Shen, X., Michalak, M., Prywes, R., Okada, T., Yoshida, H., Mori, K. and Kaufman, R. J. (2002). IRE1-mediated unconventional mRNA splicing and S2P-mediated ATF6 cleavage merge to regulate XBP1 in signaling the unfolded protein response. *Genes Dev.* **16**, 452-466.

Liu, D. Y., Martic, M., Clarke, G. N., Dunlop, M. E. and Baker, H. W. (1999). An important role of actin polymerization in the human zona pellucida-induced acrosome reaction. *Mol. Hum. Reprod.* **5**, 941-949.

Marciniak, S. J. and Ron, D. (2006). Endoplasmic reticulum stress signaling in disease. *Physiol. Rev.* **86**, 1133-1149.

Moenner, M., Pluquet, O., Bouchecareilh, M. and Chevet, E. (2007). Integrated endoplasmic reticulum stress responses in cancer. *Cancer Res.* **67**, 10631-10634.

Moreau, V., Tatin, F., Varon, C. and Génot, E. (2003). Actin can reorganize into podosomes in aortic endothelial cells, a process controlled by Cdc42 and RhoA. *Mol. Cell. Biol.* **23**, 6809-6822.

Nguyên, D. T., Kebache, S., Fazel, A., Wong, H. N., Jenna, S., Emadali, A., Lee, E. H., Bergeron, J. J., Kaufman, R. J., Larose, L. et al. (2004). Nck-dependent activation of extracellular signal-regulated kinase-1 and regulation of cell survival during endoplasmic reticulum stress. *Mol. Biol. Cell* **15**, 4248-4260.

Ogata, H., Goto, S., Fujibuchi, W. and Kanehisa, M. (1998). Computation with the KEGG pathway database. *Biosystems* **47**, 119-128.

Oikawa, D., Tokuda, M. and Iwawaki, T. (2007). Site-specific cleavage of CD59 mRNA by endoplasmic reticulum-localized ribonuclease, IRE1. *Biochem. Biophys. Res. Commun.* **360**, 122-127.

Oikawa, D., Tokuda, M., Hosoda, A. and Iwawaki, T. (2010). Identification of a consensus element recognized and cleaved by IRE1 alpha. *Nucleic Acids Res.* **38**, 6265-6273.

Papandreou, I., Denko, N. C., Olson, M., Van Melckebeke, H., Lust, S., Tam, A., Solow-Cordero, D. E., Bouley, D. M., Offner, F., Niwa, M. et al. (2011). Identification of an Ire1alpha endonuclease specific inhibitor with cytotoxic activity against human multiple myeloma. *Blood* **117**, 1311-1314.

Parsons, D. W., Jones, S., Zhang, X., Lin, J. C., Leary, R. J., Angenendt, P., Mankoo, P., Carter, H., Siu, I. M., Gallia, G. L. et al. (2008). An integrated genomic analysis of human glioblastoma multiforme. *Science* **321**, 1807-1812.

Pellegrin, S. and Mellor, H. (2007). Actin stress fibres. *J. Cell Sci.* **120**, 3491-3499.

Podhajcer, O. L., Benedetti, L. G., Girotti, M. R., Prada, F., Salvatierra, E. and Llera, A. S. (2008). The role of the matricellular protein SPARC in the dynamic interaction between the tumor and the host. *Cancer Metastasis Rev.* **27**, 691-705.

Rempel, S. A., Golembieski, W. A., Fisher, J. L., Maile, M. and Nakeff, A. (2001). SPARC modulates cell growth, attachment and migration of U87 glioma cells on brain extracellular matrix proteins. *J. Neurooncol.* **53**, 149-160.

Ridley, A. J., Paterson, H. F., Johnston, C. L., Diekmann, D. and Hall, A. (1992). The small GTP-binding protein rac regulates growth factor-induced membrane ruffling. *Cell* **70**, 401-410.

Ridley, A. J., Allen, W. E., Peppelenbosch, M. and Jones, G. E. (1999). Rho family proteins and cell migration. *Biochem. Soc. Symp.* **65**, 111-123.

Romero-Ramirez, L., Cao, H., Nelson, D., Hammond, E., Lee, A. H., Yoshida, H., Mori, K., Glimcher, L. H., Denko, N. C., Giaccia, A. J. et al. (2004). XBP1 is essential for survival under hypoxic conditions and is required for tumor growth. *Cancer Res.* **64**, 5943-5947.

Schröder, M. and Kaufman, R. J. (2005). The mammalian unfolded protein response. *Annu. Rev. Biochem.* **74**, 739-789.

Schultz, C., Lemke, N., Ge, S., Golembieski, W. A. and Rempel, S. A. (2002). Secreted protein acidic and rich in cysteine promotes glioma invasion and delays tumor growth in vivo. *Cancer Res.* **62**, 6270-6277.

Seno, T., Harada, H., Kohno, S., Teraoka, M., Inoue, A. and Ohnishi, T. (2009). Downregulation of SPARC expression inhibits cell migration and invasion in malignant gliomas. *Int. J. Oncol.* **34**, 707-715.

Shuda, M., Kondoh, N., Imazeki, N., Tanaka, K., Okada, T., Mori, K., Hada, A., Arai, M., Wakatsuki, T., Matsubara, O. et al. (2003). Activation of the ATF6, XBP1 and grp78 genes in human hepatocellular carcinoma: a possible involvement of the ER stress pathway in hepatocarcinogenesis. *J. Hepatol.* **38**, 605-614.

Sweetwyne, M. T., Brekken, R. A., Workman, G., Bradshaw, A. D., Carbon, J., Siadak, A. W., Murri, C. and Sage, E. H. (2004). Functional analysis of the matricellular protein SPARC with novel monoclonal antibodies. *J. Histochem. Cytochem.* **52**, 723-733.

Tai, I. T. and Tang, M. J. (2008). SPARC in cancer biology: its role in cancer progression and potential for therapy. *Drug Resist. Updat.* **11**, 231-246.

Thomas, S. L., Alam, R., Lemke, N., Schultz, L. R., Gutiérrez, J. A. and Rempel, S. A. (2010). PTEN augments SPARC suppression of proliferation and inhibits SPARC-induced migration by suppressing SHC-RAF-ERK and AKT signaling. *Neuro-oncol.* **12**, 941-955.

Vichai, V. and Kirtikara, K. (2006). Sulforhodamine B colorimetric assay for cytotoxicity screening. *Nat. Protoc.* **1**, 1112-1116.

Welihinda, A. A., Tirasophon, W., Green, S. R. and Kaufman, R. J. (1998). Protein serine/threonine phosphatase Ptc2p negatively regulates the unfolded-protein response by dephosphorylating Ire1p kinase. *Mol. Cell. Biol.* **18**, 1967-1977.

Xue, Z., He, Y., Ye, K., Gu, Z., Mao, Y. and Qi, L. (2011). A conserved structural determinant located at the interdomain region of mammalian inositol-requiring enzyme 1alpha. *J. Biol. Chem.* **286**, 30859-30866.

Yoshida, H., Matsui, T., Yamamoto, A., Okada, T. and Mori, K. (2001). XBP1 mRNA is induced by ATF6 and spliced by IRE1 in response to ER stress to produce a highly active transcription factor. *Cell* **107**, 881-891.

Yoshida, H., Matsui, T., Hosokawa, N., Kaufman, R. J., Nagata, K. and Mori, K. (2003). A time-dependent phase shift in the mammalian unfolded protein response. *Dev. Cell* **4**, 265-271.

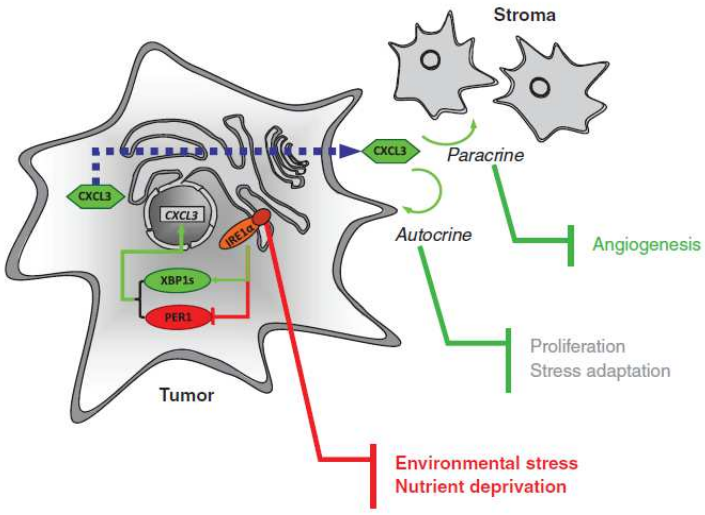

Figure 15: Schéma récapitulatif du rôle d'IRE1α et de PER1 dans les U-87 MG.

ARTICLE 4

Molecular and Cellular Pathobiology

Cancer Research

Posttranscriptional Regulation of *PER1* Underlies the Oncogenic Function of IREα

Olivier Pluquet[1,2], Nicolas Dejeans[1,2], Marion Bouchecareilh[1,2], Stephanie Lhomond[1,2], Raphael Pineau[2,3], Arisa Higa[1,2], Maylis Delugin[2,3], Chantal Combe[1,2], Sandrine Loriot[1,2], Gaelle Cubel[1,2], Nathalie Dugot-Senant[2], Anne Vital[2,4], Hugues Loiseau[2,5], Sara J.C. Gosline[6], Said Taouji[1,2], Michael Hallett[6], Jann N. Sarkaria[7], Keith Anderson[8], Wenting Wu[8], Fausto J. Rodriguez[9], Jean Rosenbaum[1,2], Frédéric Saltel[1,2], Martin E. Fernandez-Zapico[10], and Eric Chevet[1,2]

Abstract

Growing evidence supports a role for the unfolded protein response (UPR) in carcinogenesis; however, the precise molecular mechanisms underlying this phenomenon remain elusive. Herein, we identified the circadian clock *PER1* mRNA as a novel substrate of the endoribonuclease activity of the UPR sensor IRE1α. Analysis of the mechanism shows that IRE1α endoribonuclease activity decreased *PER1* mRNA in tumor cells without affecting PER1 gene transcription. Inhibition of IRE1α signaling using either siRNA-mediated silencing or a dominant-negative strategy prevented *PER1* mRNA decay, reduced tumorigenesis, and increased survival, features that were reversed upon *PER1* silencing. Clinically, patients showing reduced survival have lower levels of *PER1* mRNA expression and increased splicing of *XBP1*, a known IRE-α substrate, thereby pointing toward an increased IRE1α activity in these patients. Hence, we describe a novel mechanism connecting the UPR and circadian clock components in tumor cells, thereby highlighting the importance of this interplay in tumor development. *Cancer Res; 73(15); 4732–43. ©2013 AACR.*

Introduction

The tumor microenvironment, and in particular, hypoxia and nutrient limitation, can lead to perturbations of endoplasmic reticulum functions, thereby resulting in the activation of an adaptive response named the unfolded protein response (UPR; refs. 1, 2). The UPR primarily provides tumor cells with the ability to cope with stress and to adapt for survival. In addition to its role in cellular adaptation, the UPR, and in particular IRE1α signaling, have been proposed to play significant roles during tumor development. This was supported by the identification of somatic mutations in the *IRE1* gene (3) or the dysregulation of endoplasmic reticulum stress targets in various cancers (4–6). Moreover, the RNAse activity of IRE1α and the XBP1 transcription factor, whose mRNA is spliced by the combined action of IRE1α RNAse activity and a yet unknown ligase, have also been found to be necessary for tumor formation and growth in multiple myeloma, glioblastoma, and transformed embryonic fibroblast (7–9). Although our data have pointed toward a role for IRE1α signaling in tumor biology, IRE1α-dependent signaling pathways involved in such process still remain unclear.

In the present study, using glioblastoma as a model, we show that IRE1α endoribonuclease unexpectedly cleaves the mRNA encoded by the core circadian clock gene, *PER1*, thereby leading to its degradation. As PER1 is not a secretory protein but rather localizes to the cytosol/nucleus, this could therefore contribute to the regulation of a central signaling pathway and to an endoplasmic reticulum-dependent control of tumor growth. Collectively, we define a novel interplay between IRE1α and *PER1* regulating tumor growth and angiogenesis, an observation consistent with the emerging role of *PER1* in cancer (10, 11). Moreover, the analysis of clinical samples revealed that low *PER1* mRNA expression and high *XBP1* mRNA splicing correlated with poorer prognoses. These results identify IRE1α as a master regulator of cellular homeostasis in tumors, and provide the rationale for the development of IRE1α-targeted therapies in cancer cells.

Authors' Affiliations: [1]Inserm U1053; [2]University of Bordeaux; [3]Inserm U1029; Departments of [4]Pathology and [5]Neurosurgery, CHU Pellegrin, Bordeaux, France; [6]McGill Centre for Bioinformatics, McGill University, Montreal, Quebec, Canada; and Departments of [7]Radiation Oncology, [8]Biostatistics, [9]Anatomic Pathology and Laboratory Medicine, and [10]Center for Novel Therapeutics, Mayo Clinic, Rochester, Minnesota

Note: Supplementary data for this article are available at Cancer Research Online (http://cancerres.aacrjournals.org/).

Current address for O. Pluquet: Institut de Biologie de Lille, CNRS UMR8161/Universités Lille 1 et Lille 2/Institut Pasteur de Lille, 1, rue du Pr. Calmette, BP 447, 59021 Lille, France; current address for F.J. Rodriguez, Department of Pathology, Division of Neuropathology, Johns Hopkins University, Baltimore, Maryland.

M. Bouchecareilh, S. Lhomond, and R. Pineau contributed equally to this work.

Corresponding Author: Eric Chevet, Inserm U1053, University of Bordeaux, 146 rue Leo Saignat, 33076 Bordeaux Cedex, France. Phone: 335-5757-9253; Fax: 335-5651-4077; E-mail: eric.chevet@inserm.fr

doi: 10.1158/0008-5472.CAN-12-3989

Published OnlineFirst June 10, 2013; DOI: 10.1158/0008-5472.CAN-12-3989

Cancer Research

Posttranscriptional Regulation of *PER1* Underlies the Oncogenic Function of IRE α

Olivier Pluquet, Nicolas Dejeans, Marion Bouchecareilh, et al.

Cancer Res 2013;73:4732-4743. Published OnlineFirst June 10, 2013.

Published OnlineFirst June 10, 2013; DOI: 10.1158/0008-5472.CAN-12-3989

Posttranscriptional Regulation of *PER1* Underlies the Oncogenic Function of IREα

Olivier Pluquet[1,2], Nicolas Dejeans[1,2], Marion Bouchecareilh[1,2], Stephanie Lhomond[1,2], Raphael Pineau[2,3], Arisa Higa[1,2], Maylis Delugin[2,3], Chantal Combe[1,2], Sandrine Loriot[1,2], Gaelle Cubel[1,2], Nathalie Dugot-Senant[2], Anne Vital[2,4], Hugues Loiseau[2,5], Sara J.C. Gosline[6], Said Taouji[1,2], Michael Hallett[6], Jann N. Sarkaria[7], Keith Anderson[8], Wenting Wu[8], Fausto J. Rodriguez[9], Jean Rosenbaum[1,2], Frédéric Saltel[1,2], Martin E. Fernandez-Zapico[10], and Eric Chevet[1,2]

Abstract

Growing evidence supports a role for the unfolded protein response (UPR) in carcinogenesis; however, the precise molecular mechanisms underlying this phenomenon remain elusive. Herein, we identified the circadian clock *PER1* mRNA as a novel substrate of the endoribonuclease activity of the UPR sensor IRE1α. Analysis of the mechanism shows that IRE1α endoribonuclease activity decreased *PER1* mRNA in tumor cells without affecting PER1 gene transcription. Inhibition of IRE1α signaling using either siRNA-mediated silencing or a dominant-negative strategy prevented *PER1* mRNA decay, reduced tumorigenesis, and increased survival, features that were reversed upon *PER1* silencing. Clinically, patients showing reduced survival have lower levels of *PER1* mRNA expression and increased splicing of *XBP1*, a known IRE-α substrate, thereby pointing toward an increased IRE1α activity in these patients. Hence, we describe a novel mechanism connecting the UPR and circadian clock components in tumor cells, thereby highlighting the importance of this interplay in tumor development. *Cancer Res; 73(15); 4732–43. ©2013 AACR.*

Introduction

The tumor microenvironment, and in particular, hypoxia and nutrient limitation, can lead to perturbations of endoplasmic reticulum functions, thereby resulting in the activation of an adaptive response named the unfolded protein response (UPR; refs. 1, 2). The UPR primarily provides tumor cells with the ability to cope with stress and to adapt for survival. In addition to its role in cellular adaptation, the UPR, and in particular IRE1α signaling, have been proposed to play significant roles during tumor development. This was supported by the identification of somatic mutations in the *IRE1* gene (3) or the dysregulation of endoplasmic reticulum stress targets in various cancers (4–6). Moreover, the RNAse activity of IRE1α and the XBP1 transcription factor, whose mRNA is spliced by the combined action of IRE1α RNAse activity and a yet unknown ligase, have also been found to be necessary for tumor formation and growth in multiple myeloma, glioblastoma, and transformed embryonic fibroblast (7–9). Although our data have pointed toward a role for IRE1α signaling in tumor biology, IRE1α-dependent signaling pathways involved in such process still remain unclear.

In the present study, using glioblastoma as a model, we show that IRE1α endoribonuclease unexpectedly cleaves the mRNA encoded by the core circadian clock gene, *PER1*, thereby leading to its degradation. As PER1 is not a secretory protein but rather localizes to the cytosol/nucleus, this could therefore contribute to the regulation of a central signaling pathway and to an endoplasmic reticulum-dependent control of tumor growth. Collectively, we define a novel interplay between IRE1α and *PER1* regulating tumor growth and angiogenesis, an observation consistent with the emerging role of *PER1* in cancer (10, 11). Moreover, the analysis of clinical samples revealed that low *PER1* mRNA expression and high *XBP1* mRNA splicing correlated with poorer prognoses. These results identify IRE1α as a master regulator of cellular homeostasis in tumors, and provide the rationale for the development of IRE1α-targeted therapies in cancer cells.

Authors' Affiliations: [1]Inserm U1053; [2]University of Bordeaux; [3]Inserm U1029; Departments of [4]Pathology and [5]Neurosurgery, CHU Pellegrin, Bordeaux, France; [6]McGill Centre for Bioinformatics, McGill University, Montreal, Quebec, Canada; and Departments of [7]Radiation Oncology, [8]Biostatistics, [9]Anatomic Pathology and Laboratory Medicine, and [10]Center for Novel Therapeutics, Mayo Clinic, Rochester, Minnesota

Note: Supplementary data for this article are available at Cancer Research Online (http://cancerres.aacrjournals.org/).

Current address for O. Pluquet: Institut de Biologie de Lille, CNRS UMR8161/Universités Lille 1 et Lille 2/Institut Pasteur de Lille, 1, rue du Pr. Calmette, BP 447, 59021 Lille, France; current address for F.J. Rodriguez, Department of Pathology, Division of Neuropathology, Johns Hopkins University, Baltimore, Maryland.

M. Bouchecareilh, S. Lhomond, and R. Pineau contributed equally to this work.

Corresponding Author: Eric Chevet, Inserm U1053, University of Bordeaux, 146 rue Leo Saignat, 33076 Bordeaux Cedex, France. Phone: 335-5757-9253; Fax: 335-5651-4077; E-mail: eric.chevet@inserm.fr

doi: 10.1158/0008-5472.CAN-12-3989

Published OnlineFirst June 10, 2013; DOI: 10.1158/0008-5472.CAN-12-3989

Materials and Methods

Recombinant protein expression

IRE1cyto cDNA (AA 470–977) was cloned from human liver cDNAs using the Gateway technology (Invitrogen Corp.) into either pGEX-2TK or pDEST17. IRE1cyto cDNA devoid of ATG, was amplified by PCR using the Platinum Taq DNA Polymerase High Fidelity (Invitrogen Corp.) and the following amplification scheme: denaturation at 94°C for at 40 seconds, annealing at 60°C for 40 seconds, elongation at 68°C for 2 minutes, 35 cycles. The PCR products were precipitated using PEG8000 and recombined into pDONR201 using the Gateway BP clonase (Invitrogen Corp.). The plasmids were then transformed into competent DH5α cells and positive clones selected and sequenced. Positive clones were recombined into destination vectors using LR clonase (Invitrogen Corp.). Five individual colonies were selected and pooled and plasmid DNA was amplified and subsequently transformed into competent BL21 bacterial cells. Recombinant protein expression in BL21 cells was induced using 1 mmol/L IPTG for 3 hours. Bacteria were then collected by centrifugation, lysed, and recombinant proteins purified as recommended by the manufacturer (Gibco BRL). The resulting purified proteins were concentrated and dialyzed using Amicon ultra centrifugal filters (cutoff = 20,000 Da; Millipore Corp.), followed by functional testing as previously described (12, 13).

Animal experiments, intracranial injections, tumor size, and blood capillary measurements

The protocol used was as previously described (14, 15) and was approved by the local animal committee. Cell implantations (2×10^5 cells) in Nude mice were at 2 mm lateral to the bregma and 3 mm in depth using empty vector and IRE1_DN cells stably expressing pGIPZ-GFP-shPer1 or pGIPZ-GFP alone. Twenty-eight days postinjection, brain sections were observed for GFP fluorescence and stained using hematoxylin and eosin for visualization of tumor masses. Tumor volume was then estimated by measuring the length (L) and width (W) of each tumor and was calculated using the following formula ($L \times W^2 \times 0.5$). CD31-positive vessels and Ki-67–positive cells were numerated after immunohistologic staining using rat antibodies against CD31 (PharMingen), mouse antibody against Ki-67 (Clone MIB1, Dako), and secondary antibodies coupled to HRP (Dako). Imaging was carried out using a Nikon E600 microscope equipped with a digital camera DMX1200.

Microarray analysis

Microarray assay and preprocessing analysis were conducted in the microarray core facility of the Research Institute for Biotherapy at Montpellier using the standard Affymetrix protocol. Total RNA was extracted using TRIzol reagent (Invitrogen). RNA integrity was verified on an Agilent 2100 Bioanalyzer. For each of the samples, total RNA was reverse transcribed into cDNA, followed by *in vitro* transcription and biotin labeling to generate cRNA (Enzo Biochem). The fragmented, biotin-labeled cRNA was hybridized to the Human Genome U133 2.0 oligonucleotide arrays (Affymetrix) containing approximately 22,000 probes. Microarrays were stained with streptavidin antibodies and streptavidin–phycoerythrin in an Affymetrix Fluidics station. Arrays were scanned using a 3000 7G scanner. Raw data were processed into R/Bioconductor by using the Limma package (16). To determine genes whose expression increased when IRE1α is inactivated, probe set intensities were obtained by means of Gene Chip Robust Multiarray Averaging and were selected by using a corrected P value threshold of 0.05 and fold change threshold of $|\log2(fc)| \geq 2.5$ as previously described in ref. 15. The regulated genes are listed in Supplementary Table S1. Data are accessible on the NCBI Geo portal with the reference number GSE27306.

RNA isolation, reverse transcription PCR, and quantitative PCR analyses

Total RNA was prepared using the TRIzol reagent (Invitrogen Corp.). Semiquantitative analyses were carried out as previously described (17). The primers used were designed using Primer depot software (18) and are listed in Supplementary Table S4. The PCR products were resolved on 1% to 3% agarose gels. For real-time quantitative PCR (qPCR), RNA was reverse transcribed with Superscript II (Promega). All PCR reactions were carried out with a Stratagene ×4000 thermocycler (Stratagene) and the SYBR Green PCR Core Reagents Kit (Bio-Rad). Experiments were conducted in triplicate for each data point. Each sample was normalized toward the expression of the *Rplp0* gene.

RNA cleavage assay

Total RNA (10 μg) from U87 or HepG2 was incubated with the cytoplasmic domain of human GST-IRE1α (5 μg) at 37°C for the indicated amounts of time in a buffer containing 250 mmol/L Tris pH 7.5, 600 mmol/L NaCl, 5 mmol/L MgCl2, 5 mmol/L MnCl2, 25 mmol/L β-mercaptoethanol, supplemented with or without 10 mmol/L ATP as previously described (12). As control, we used heat-denatured GST-IRE1α. Reverse transcriptase (RT)-PCR was then conducted using *Per1* primers and *Gapdh* as internal control. The pcDNA3.1-hPer1 expression vector was linearized by using SspI and used as a template for *in vitro* transcription by using T7 polymerase (Promega) in the presence of dNTP and 32PαdUTP. *In vitro* transcribed radiolabeled RNA was incubated in kinase buffer (50 mmol/L Tris-HCl, pH 7.5, 150 mmol/L NaCl, 1 mmol/L MgCl2, 1 mmol/L MnCl2, 5 mmol/L 2-mercaptoethanol, and 2 mmol/L ATP) with the cytoplasmic domain of human GST-IRE1α at 37°C for increasing amounts of time. Fragments resulting from the enzymatic reaction were resolved by Tris Borate EDTA-Urea electrophoresis and visualized by radioautography on X-ray films. Secondary structure of *Per1* mRNA was predicted using M-FOLD (19). For actinomycin D pulse-chase experiments, actinomycin D was applied to 50% confluent empty vector or IRE1_DN cells at a final concentration of 5 μg/mL for the indicated amounts of time. Total RNA was then extracted and reverse transcribed before qPCR analysis using the following primers targeting Per1: forward 5′-ctcagtggctgtctccttcc and reverse 5′-gagccaggagctcagagaag (fragment 898–1016) or forward 5′- ggatgtgcatctggtgaagc and reverse 5′- ccttgaacgtgcctgtagca (fragment 1891–1991).

Published OnlineFirst June 10, 2013; DOI: 10.1158/0008-5472.CAN-12-3989

Lentiviral transduction and PER1 knockdown by shRNA

For Per1 knockdown experiments, we used the pGIPZ-GFP-lentiviral vectors expressing Per1 short-hairpin RNA (shRNA) as previously described (Open Biosystems). Lentivirus-containing supernatant was collected 48 hours after transfection in LTA-HEK293T cells, 0.2 μm filtered, and snap frozen at −80°C. U87 cells were infected with lentivirus at low multiplicity according to the manufacturer's instructions. Cells were selected in puromycin (2.5 μg/mL) and polyclonal populations were expanded and analyzed.

Luciferase reporter gene assay

The human Per1 promoter luciferase reporter gene construct was kindly provided by U. Albrecht (Freiburg, Switzerland). The hPer1-Luc plasmid was generated as previously described (20). Following transfection, cells were incubated for 24 hours and stimulated or not with drugs for an additional 16 hours. Luciferase activity was measured using the dual luciferase kit (Promega) according the manufacturer's instructions. Light emission was measured in a luminometer (Lumistar).

RNA interference

siRNA were designed using Greg Hannon's webtool and listed in Supplementary Table S5. Cells were transfected by using the siRNAi Max Lipofectamine reagent (Invitrogen Corp.). Following incubation for 48 to 72 hours, total RNA was extracted and used for semi-quantitative RT-PCR.

Colony formation assay

Cells were plated at density of 104 per well in 12-well plates and cell proliferation rate was measured by cell counting (Beckman Coulter). For colony formation, 2,500 cells were seeded in 6-well plates. Twenty-four hours later, fresh medium was added and the cells were allowed to form colonies. After 2 weeks, the colonies were stained with 0.1% crystal violet and counted. The experiments were carried out at least twice in triplicate.

Antibody-based analyses

Total protein extracts and immunoblotting were conducted as previously described (14). Antibodies against PER1 and tubulin were purchased from Cogenics and Santa Cruz Biotechnology. Proteins were detected using secondary antibodies coupled to HRP (Dako) and immunoblots revealed using enhanced chemiluminescence and radioautography. For immunohistochemistry, analyses were carried out as previously described (15) using an antibody that was raised against the protein translated from *Xbp1s* mRNA (21).

Cell culture, transfections, and treatments

HepG2 and U87 cells were grown in Dulbecco's Modified Eagle Medium, supplemented with 10% FBS, L-glutamine, and antibiotics. U87 and HepG2 cells were stably transfected with pcDNA3/IRE1-NCK-1, an expression vector encoding a cytoplasmic-defective IRE1α mutant (17). U87 cells were transiently transfected with pED-IRE1 WT or mutant K599A (22) expression vectors. Transfections were conducted using Lipofectamine (Invitrogen Corp.) according to the manufacturer's recommendations. Actinomycin D were purchased from Sigma and used as indicated.

Statistical analyses

Data are presented as means ± SD. Statistical significance ($P < 0.05$ or lower) was determined using the Student t test 2-tailed distribution, assuming equal variance for the samples (GraphPad Prism). For *in vivo* studies, Kaplan–Meier curves and log-rank analysis were conducted using GraphPad 5.0.

Human samples

A total of 29 human glioblastoma samples were collected from The Bordeaux Tumor Bank and 31 + 20 samples from the Mayo Clinic. Twelve samples from normal or peritumoral brain tissues were also collected. Samples were collected according to the recommendations of the local ethics committees and informed consent was systematically obtained.

Results

IRE1α loss-of-function results in PER1 mRNA posttranscriptional upregulation

Using global expression profiles of U87 cells stably transfected with an empty vector or a well-established dominant-negative (DN)-IRE1α vector (IRE1_DN; ref. 17), we identified *PER1* mRNA as a potential target of IRE1α signaling (Supplementary Table S1). *PER1* mRNA expression was increased in both IRE1_DN cells and IRE1α-silenced cells, whereas XBP1 silencing had no effect (Fig. 1A). This indicates that *PER1* mRNA expression regulation is dependent on IRE1α activity but not on XBP1. Similar results were obtained in additional empty vector or IRE1_DN (Supplementary Fig. S1A) HepG2 stable transfected cells (Supplementary Fig. S1B), thus ruling out any clonal or cell line-specific effects. Changes were specific of *PER1*, as *PER2* mRNA levels were not altered in these conditions (Fig. 1A). To further investigate the relationship between IRE1α activity and *PER1* mRNA expression, parental U87 cells were transiently transfected with increasing amounts of IRE1αWT or kinase dead mutant IRE1αK599A (22, 23). *PER1* mRNA expression was reduced in cells overexpressing IRE1αWT in a dose-dependent manner (Fig. 1B; compare lanes 2 and 3 to lane 1). In contrast, *PER1* mRNA accumulated in cells overexpressing IRE1αK599A (Fig. 1B; compare lanes 4 and 5 to lane 1). The impact of IRE1α activity inhibition on *PER1* mRNA was also concomitant with an increase in PER1 protein levels in IRE1_DN cells (Fig. 1C).

PER1 mRNA expression was previously found to be under the control of UPR-regulated transcription factor ATF6 (24). To determine whether the observed IRE1α-dependent regulation of *PER1* mRNA occurred at the transcriptional level, empty vector and IRE1_DN cells were transfected with a *PER1* promoter reporter construct containing the −1,500 bp upstream of the transcriptional start site. These experiments were carried out under control conditions (CTL) or upon overexpression of spliced XBP1 (XBP1) or the circadian clock regulator BMAL1 that is known to control *PER1* expression (as a positive control). *PER1* promoter activity remained unchanged in IRE1_DN or IRE1α-silenced cells, whereas it doubled in BMAL1-overexpressing cells and remained unchanged in cells

Published OnlineFirst June 10, 2013; DOI: 10.1158/0008-5472.CAN-12-3989

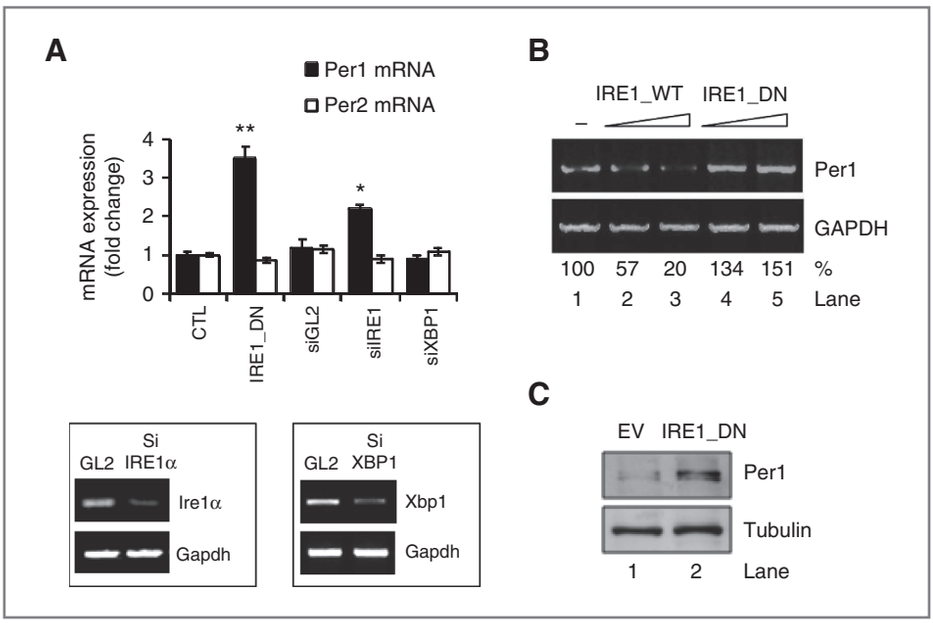

Figure 1. Impaired IRE1α activity leads the upregulation of *PER1* mRNA. A, expression of *PER1* and *PER2* mRNA was measured by PCR in control (EV) and IRE1_DN U87 cells as well as U87 cells subjected to IRE1α silencing, XBP1 silencing, or luciferase silencing as control (GL2) by siRNA for 72 hours (insets). *PER1* and *PER2* mRNA levels were normalized to *RPLP0* levels (*t* test; *, $P < 0.05$; **, $P < 0.001$). B, U87 cells were transiently transfected with increasing concentrations of plasmids encoding for WT-IRE1α or DN K599A IRE1α, followed by mRNA extraction. The expression of *PER1* and *Gapdh* was assessed by RT-PCR. C, PER1 and tubulin protein levels in empty vector and IRE1_DN cells.

overexpressing XBP1s (Fig. 2B). These results indicate that the increase in *PER1* mRNA in the absence of functional IRE1α may occur posttranscriptionally and independently of XBP1s. We then tested whether *PER1* mRNA expression increase in IRE1_DN cells was associated with an increase in *PER1* mRNA half-life. This was assessed using an actinomycin D pulse-chase experiment followed by qRT-PCR (Fig. 2C). Under these conditions, *PER1* mRNA half-life was significantly prolonged going from 2.3 hours in empty vector cells to 3.5 hours in IRE1_DN cells. Together, these data identify *PER1* mRNA as an IRE1α-regulated target in cancer cells and provide a novel role for IRE1α activity on *PER1* mRNA stability.

PER1 mRNA is cleaved by IRE1α

Next, as IRE1α was shown to control mRNA levels through direct cleavage (25), we examine whether *PER1* mRNA was a direct target of IRE1α endoribonuclease activity. We studied the effects of IRE1α activity on *PER1* mRNA regulation through internal cleavage sites. *PER1* mRNA potential cleavage fragments amounts were measured upon siRNA-mediated silencing of the ribonucleases XRN1/2 and SKI2, which respectively contribute to RNA degradation 5′-3′ and 3′-5′, as previously described (26). We confirmed that treatment with XRN1/2 or SKI2 siRNAs specifically reduced the expression of target mRNAs without affecting the expression of endogenous *Ire1α* mRNA (Supplementary Fig. S2). Treatment with XRN1/2 or SKI2 siRNA did not affect *PER1* mRNA sequences corresponding to 5′ (exons 4–8) and 3′ (exon 23) mRNA ends in IRE1_DN cells (Fig. 2D), showing that no *PER1* mRNA cleavage fragments were present in these cells. In empty vector cells, SKI2 knockdown led to the accumulation of the 5′ *PER1* mRNA sequence corresponding to the exons 4 to 8, and thus located upstream of potential IRE1α cleavage sites. In contrast, the fragment located downstream of these sites (exon 23) did not accumulate when compared with control irrelevant siRNA (GL2; Fig. 2D). Conversely, treatment with siRNA targeting the 5′ to 3′ exonucleases XRN1/2 only led to the increase of the fragment, downstream of this site (exon 23; Fig. 2D).

Sequence analysis revealed that five IRE1α consensus cleavage sites were present on human *PER1* mRNA (Fig. 3A). Moreover, these cleavage sites were associated with P-loops structures, thereby creating potential cleavage sites for IRE1α endoribonuclease (Supplementary Fig. S3A). We then tested whether IRE1α could directly cleave *PER1* mRNA. Total RNA from U87 cells was subjected to an *in vitro* IRE1α-mediated cleavage assay (12). This reaction was followed by RT-PCR to monitor *PER1* mRNA levels (Fig. 3B). A strong decrease in *PER1* mRNA level was observed when total RNA was incubated with IRE1α and ATP, whereas mRNA levels of the housekeeping genes *ORP150* or *GAPDH* were unchanged (Fig. 3B). A positive control for IRE1α endoribonuclease activity was obtained using *XBP1* mRNA as a substrate (Supplementary Fig. S3B). These results show that IRE1α cleaves *PER1* mRNA *in vitro*. Then, to identify the cleavage products resulting from *PER1* mRNA, *in vitro* transcribed and radiolabeled *PER1* mRNA was subjected to IRE1α cleavage as described above. These experiments showed a major radiolabeled fragment of approximately 4 kb corresponding to the mRNA transcribed from the *PER1* cDNA. In addition, three bands corresponding to entities of, respectively, 2.7, 1.7, and 1 kb were also present in the original transcription reaction (Fig. 3C, lane 2). All the radiolabeled material was RNA as shown by RNase

Published OnlineFirst June 10, 2013; DOI: 10.1158/0008-5472.CAN-12-3989

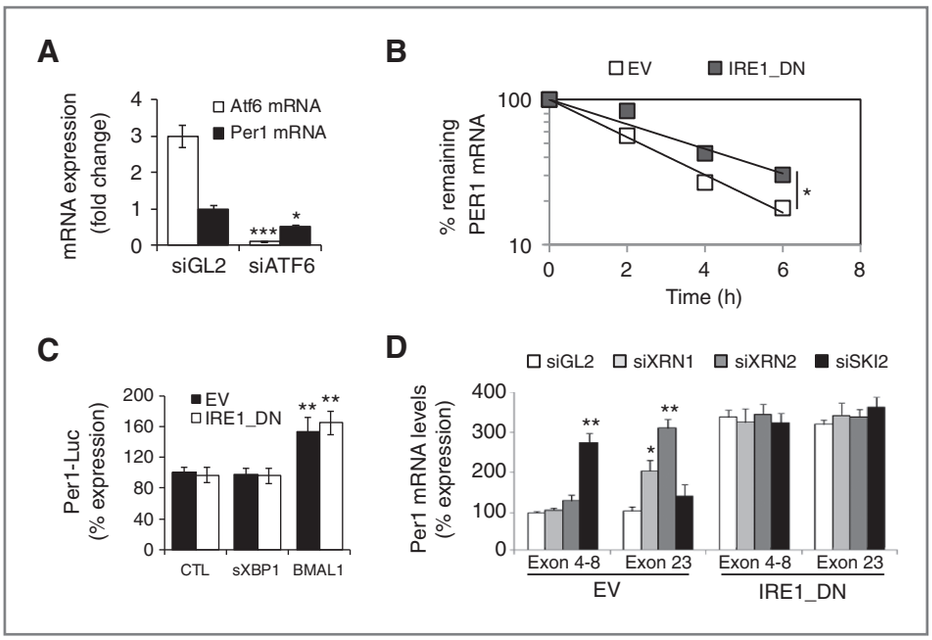

Figure 2. IRE1α-mediated posttranscriptional control of *PER1* mRNA in cultured cells. A, *PER1* (closed) and *ATF6* (open) mRNA expression as determined by quantitative RT-PCR in cells transfected with siRNA against luciferase (siGL2) and ATF6 (siATF6). Experiments were carried out in triplicate and the mean ± SD, statistical significance (Student *t* test) is indicated (*, $P < 0.05$; ***, $P < 0.01$). B, empty vector and IRE1_DN cells were cotransfected with control plasmid (pCMV-rL) or PER1 promoter-dependent luciferase reporter and either an empty pCDNA3 vector, a pCDNA3-sXBP1 vector, or a pCDNA3-BMAL1 vector. Cells were then lysed and lysates analyzed with the Dual-Luciferase Reporter Kit (Promega). Results were normalized against pCMV-*Renilla* luciferase (*t* test, **$P < 0.05$). C, actinomycin D pulse-chase was carried out as described in Materials and Methods. Total mRNA was extracted and quantitative RT-PCR experiments were conducted using *PER1* mRNA-specific primer pairs. The experiment was repeated 3 times and data are presented as mean ± SD. Statistical significance was determined using Student *t* test, *, $P < 0.03$. D, empty vector and IRE1_DN cells were transfected with siRNA against XRN1/2 or SKI2. RNA was isolated after 48 hours and was used to amplify different regions of *PER1* mRNA. Experiments were carried out in triplicate and the mean ± SD, statistical significance (Student *t* test) is indicated (*, $P < 0.05$; **, $P < 0.01$).

A-mediated degradation (Fig. 3C, lane 1). In the presence of GST-IRE1α-cyto, a band of approximately 2 kb (Fig. 3C, lanes 3–5) appeared across time and could correspond to the product generated following IRE1α-mediated cleavage at nucleotide 1920 (Site 3, Supplementary Table S2), thus suggesting that IRE1α cleaves *PER1* mRNA at least at the cleavage site #3. To determine whether IRE1α can also cleave *PER1* mRNA at others sites, the five putative sites were mutated by insertion of a single mutation with the site CUGCAC where G was replaced by A. Mutated cDNA were *in vitro* transcribed and subjected to IRE1-mediated cleavage as above. Site-specific PCR amplification was then carried out for each reaction (Fig. 3D). This revealed that out of the 5 potential cleavage sites identified, only 3, namely 1920, 3197, and 3378 were cleaved by IRE1α *in vitro* (Fig. 3D). Taken together, these data are consistent with an IRE1α-dependent cleavage of *PER1* mRNA.

IRE-dependent PER1 degradation modulates cancer cell survival and tumor progression *in vivo*

To determine the biologic significance of *PER1* mRNA cleavage by IRE1α on tumor cell growth, *PER1* mRNA expression was attenuated using lentiviral-mediated delivery of GFP-shPER1 in empty vector and IRE1_DN cells (or GFP empty vector as control). We first confirmed that pGIPZ-GFP-shPER1 viral particles effectively reduced *PER1* mRNA and protein expression in U87 cells using RT-PCR and immunoblotting (Fig. 4A and S4). Using these cells, the impact of *PER1* regulation by IRE1α anchorage-independent cell growth was investigated. After 2 weeks, the IRE1_DN cells showed a reduced ability to form colonies compared with empty vector cells (Fig. 4B). We then investigated the effects of *PER1* silencing on tumor growth using our previously described *in vivo* orthotopic glioblastoma model (14). Fluorescence microscopy analysis of the tumors revealed GFP expression in tumor cells, thereby further confirming successful and stable lentiviral transduction in tumor cells up to 28 days postinjection (Fig. 4C). This also revealed that low PER1 expression in an IRE1α wild-type background neither impacted on tumor volume (Fig. 4C and D), tumor shape (Fig. 4C and D), nor on the number of tumor proliferating cells (Fig. 3D). IRE1_DN cell-derived tumors were smaller ($P < 0.001$) with extensive tumor cell infiltration in surrounding parenchyma (Fig. 4D; $P < 0.001$). Interestingly, at 28 days postinjection, the size of IRE1_DNsh-PER1 cell-derived tumors was comparable with that of IRE1_DN cell-derived tumors (Fig. 4D), however, with reduced tumor cell infiltrates (Fig. 4D) and better-delimited perimeters as compared with empty vector-derived tumors. This phenotype was accompanied by a marked restoration of proliferation within the tumor (Fig. 4D). These results confirm a role of IRE1α signaling in tumor growth *in vivo* and show the involvement of the IRE1α/*PER1* axis in this process. Moreover, tumor

Published OnlineFirst June 10, 2013; DOI: 10.1158/0008-5472.CAN-12-3989

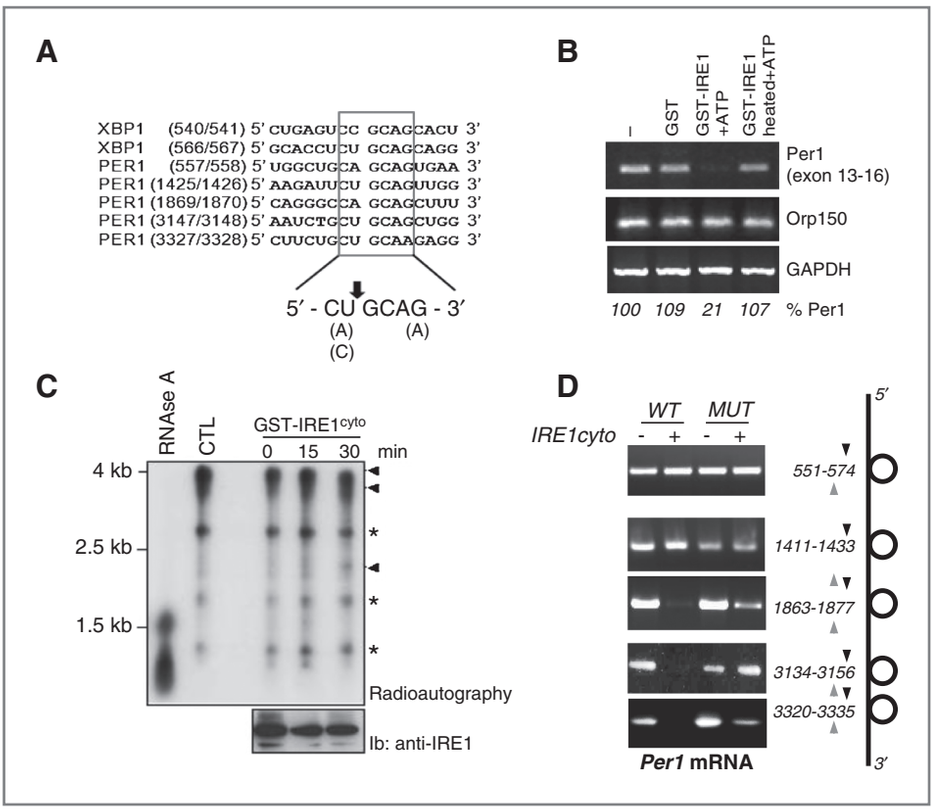

Figure 3. IRE1α-mediated posttranscriptional control of *PER1* mRNA *in vitro*. A, sequence alignment of *XBP1* mRNA IRE1α-mediated cleavage sites with similar regions in *PER1* mRNAs. B, *in vitro* RNA cleavage assay. Total RNA extracted from U87 cells was incubated with GST or GST-IRE1α-cyto in the presence of ATP for 2 hours at 37°C. RT-PCR was then conducted to determine *PER1*, *ORP150*, and *GAPDH* mRNA levels. C, PER1 cDNA sequence cloned into the pCDNA3 vector was used as template for *in vitro* transcription using the T7 Ribomax kit (Promega) in the presence of 32P-UTP. The resulting radiolabeled riboprobe was then incubated or not with dephosphorylated GST-hIRE1cyto for the indicated periods of time or with RNase A for 15 minutes at room temperature. The reaction products were resolved by PAGE and revealed by radioautography on X-ray films. The amount of recombinant GST-IRE1cyto added to the reaction is shown in the bottom blot using immunoblot with anti-IRE1 antibodies. *, nonspecific bands; Arrowheads, full and cleaved *PER1* mRNA products. D, *PER1* mRNA wild-type and mutated on each potential IRE1α cleavage sites were transcribed *in vitro* and subjected to *in vitro* cleavage with GST-hIRE1cyto as in F. Reaction products were then subjected to RT-PCR with specific primers flanking each cleavage site.

angiogenesis, which is abnormal in IRE1_DN-derived tumors (14, 15), was investigated in *PER1*-silenced cells using CD31 immunostaining (Fig. 4C). High vascular density was apparent in empty vector and EVshPER1 cell-derived tumors (Fig. 4C). Tumor vascularization was partially restored in IRE1_DNshPER1-derived tumors (Fig. 4C and D). These results establish that the loss of cancer cell proliferation and tumor vascularization due to impairment of IRE1α activity is in part mediated by increased PER1 expression and suggest a potential role for PER1 in tumor angiogenesis. As the IRE1α/*PER1* axis impacts on tumor growth capacity and angiogenesis, we then measured the consequences of its alteration on mouse survival following orthotopic injection (Fig. 5A). IRE1α signaling inhibition (IRE1_DN cell-derived tumors) increased the survival of tumor-bearing mice compared with those bearing empty vector cell-derived tumors. This survival advantage was lost in *PER1* knocked-down tumors (Fig. 5A), thereby reinforcing the existence of functional interplay between IRE1α and *PER1* underlying IREα.

Next, we sought to define mediating IRE1α/*PER1* axis, to this end we identified the genes controlled by this axis and potentially involved in the control of tumor growth/angiogenesis. mRNA expression profiles in IRE1_DN and subjected or not to known endoplasmic reticulum stress inducers such as glucose or glutamine deprivation, hypoxia or Tun exposure were compared with those obtained in empty vector cells. These experimental conditions are also known to recapitulate microenvironmental stresses. We identified the top 50 genes up and downregulated all conditions included (Fig. 6A). As PER1 has been defined as a transcriptional repressor, we focused our attention on the genes downregulated in IRE1_DN cells, which were found to be enriched in both cytokine–cytokine receptor interaction and chemokine signaling pathways. To further explore the IRE1α/*PER1*–dependent cytokine and chemokine regulatory networks upon endoplasmic reticulum stress, validation of potential target genes was carried out using RT-qPCR. The proangiogenic chemokine *CXCL3* was the most significant gene that showed restoration of its expression in IRE1_DNshPER1 cells upon glucose deprivation (Fig. 6B). We postulated

Published OnlineFirst June 10, 2013; DOI: 10.1158/0008-5472.CAN-12-3989

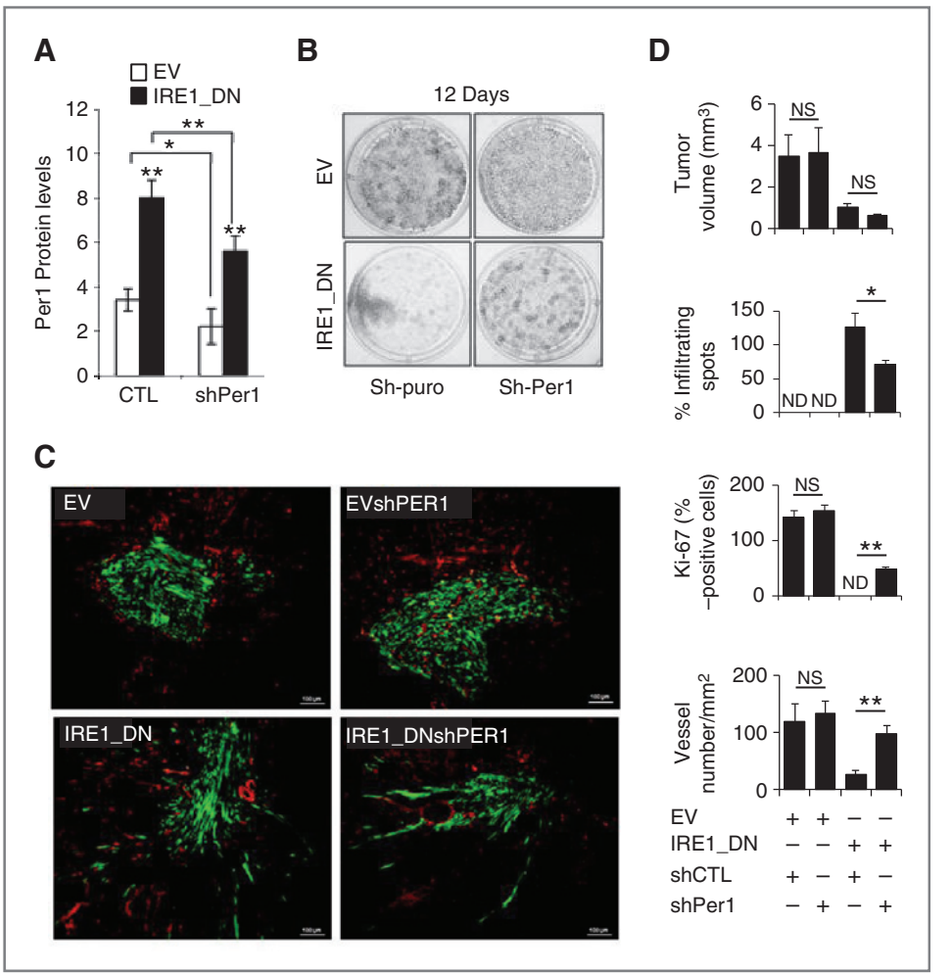

Figure 4. Impact of *PER1* mRNA expression levels on IRE1_DN cell-derived tumors. A, the expression of PER1 was monitored using immunoblot analysis in empty vector and IRE1_DN cells silenced or not for PER1 (shPER1). Quantification of 3 independent experiments is represented as the mean ± SD. B, empty vector (EV) and IRE1_DN cells and their shPER1 counterparts were seeded in 6-well plates at equal densities. Cells were allowed to form colonies for 12 days. The colonies were stained with crystal violet 0.1%. C, intracranial implantation of U87 cells expressing either the IRE1_DN or the empty vector in the presence of pGIPZ-GFP-shPER1 or pGIPZ-GFP lentiviral vector was done in nude mice ($n = 16$). Immunohistochemical staining of tumor and surrounding tissue was done using anti-CD31 antibodies (red). Scale bar, 100 μm. D, quantification of implanted tumors' features. Intracerebral tumor volume was determined. Four independent tumors were measured for each clone. Infiltrating spots were estimated by counting tumor field at ×5 magnification for each condition (*t* test, ns, nonsignificant; *, $P < 0.05$). The percentage of dividing cells (Ki-67 positive) in the 4 types of tumors was estimated by counting 5 different fields at ×40 magnification for each experiment. The mean Ki-67 intensity per condition is plotted with error bars representing SD. Significant differences are indicated between each empty vector and IRE1_DN pairs, and between empty vector compared with IRE1_DN. Vascular density was quantified by counting vessels from 5 randomly chosen fields per animal ($n = 4$ animals per conditions) and normalized to the tumor surface. Significant differences are indicated between each empty vector and IRE1_DN pairs, and between empty vector compared with IRE1_DN (*t* test, NS, nonsignificant; ***, $P < 0.0005$; **, $P < 0.001$; *, $P < 0.05$).

that this might be due to the coordinated regulation of *CXCL3* expression by XBP1 that was already proposed by Gargalovic and colleagues (27) and the downregulation of PER1, which in this context would play a repressor role. As anticipated from our model, U87 cells transiently silenced for XBP1 and/or overexpressing PER1 and exposed or not to endoplasmic reticulum stress induced by Glc deprivation showed an attenuation of *CXCL3* mRNA expression increase mediated by Glc deprivation (Fig. 6C). This shows that XBP1s increase and PER1 downregulation both contribute to the regulation of *CXCL3* mRNA expression. Hence, integrated IRE1α signaling specifically controls chemokine expression upon stress.

Low levels of PER1 gene correlates with poor survival in patients

To investigate whether the IRE1α/*PER1* axis was of clinical relevance, human glioblastoma samples from 2 independent sources (CHU Bordeaux and Mayo Clinic) were analyzed for *PER1* mRNA expression by qPCR. This revealed that both cohorts presented an expression of *PER1* mRNA lower in tumors than that observed in normal or nontumoral tissues (red/Bordeaux; black/Mayo, Fig. 5B). To evaluate the impact of low *PER1* expression on prognosis, postsurgery survival of 60 patients with glioblastoma was followed (Fig. 5C). These patients were classified into 2 groups in which *PER1* expression

Published OnlineFirst June 10, 2013; DOI: 10.1158/0008-5472.CAN-12-3989

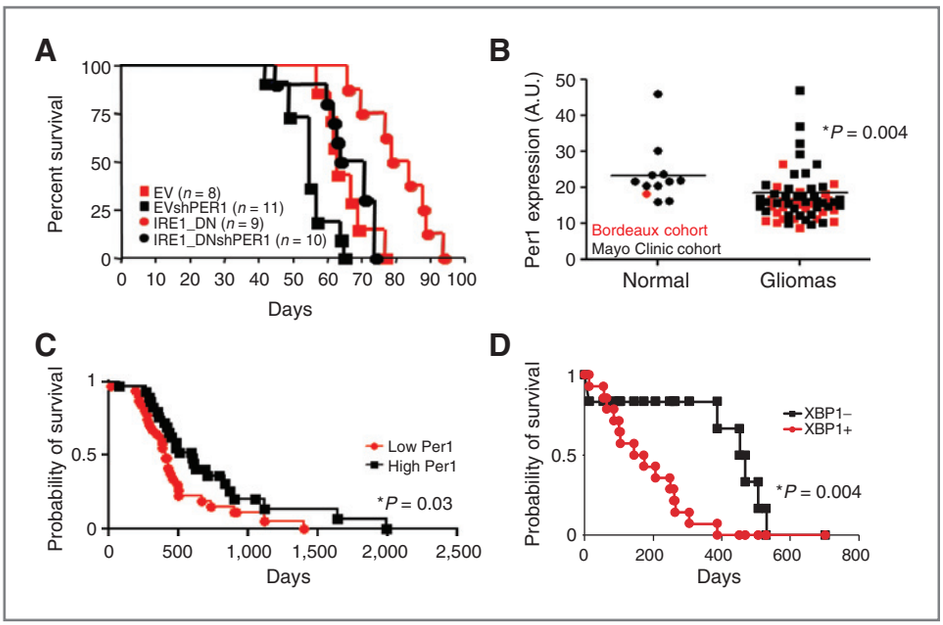

Figure 5. IRE1/*PER1* signaling axis in tumor growth. A, overall survival of mice subjected to intracranial implantation of empty vector and IRE1_DN cells and their shPER1 counterparts was reported in Kaplan–Meier survival curves. (EV vs. IRE1_DN, $P < 0.001$; IRE1_DN vs. IRE1_DNshPER1, $P < 0.001$; EV vs. IRE1_DNshPER1, $P =$ NS; log-rank test). B, qPCR analysis of *PER1* mRNA expression in 60 glioblastoma cancer samples and 12 normal brain tissues. Bordeaux cohort is indicated in red, Mayo Clinic cohort in black. The results are expressed in arbitrary units as a ratio of *PER1* transcripts to *Rplp0* transcripts. The *P* value is indicated. C, high ($n = 31$) and low ($n = 29$) *PER1* mRNA level correlates with patient survival. Values were plotted in Kaplan–Meier survival curves. Statistical difference between the 2 groups is indicated. Statistical difference between the 2 groups in indicated $P = 0.03$; log-rank test. D, Kaplan–Meier survival curves of patients displaying negative sXBP1 staining (6; XBP1−) or positive sXBP1 staining (14; XBP1+). $P = 0.004$; log-rank test.

was either lower or higher than average *PER1* mRNA. The low *PER1* group contained 31 patients and the high PER1 group contained 29 patients. Interestingly, high *PER1* expression significantly correlated with increased survival with a median of 599 days compared with 411 days in the low *PER1* group ($P = 0.03$; Fig. 5C). This result is in agreement with those obtained in *in vitro* and *in vivo* tumor models showing that *PER1* differentially affects patient outcome and strongly supports a specific role for the IRE1α/*PER1* axis in the pathogenesis of glioblastoma. To confirm that low *PER1* levels are associated with high IRE1α activity, we investigated whether the tumors contained the translation product of *Xbp1s* mRNA (XBP1s protein). To this end, paraffin-embedded specimens from 20 other glioblastoma samples (Supplementary Table S3) were analyzed for the presence of XBP1s protein using immunohistochemistry with a monoclonal antibody specific to XBP1s (Supplementary Fig. S5 and Supplementary Table S3; 21). XBP1s protein expression was then correlated with patient survival. The data were represented as Kaplan–Meier plots discriminating between 2 populations that exhibited either a positive or a negative XBP1s staining (Fig. 5D). This showed that the absence of/low XBP1s staining significantly correlated with enhanced survival. Together with data obtained with the expression of *PER1* mRNA, these results suggested that IRE1α signaling activation in glioblastoma correlated with low patient survival. Finally, we tested the relevance of *CXCL3* to glioblastoma outcome using the Rembrandt database (28). High expression of *CXCL3* mRNA seemed to correlate with low patient survival (not shown). Interestingly and as expected, in our cohort of human tumors, expression of *CXCL3* mRNA negatively correlated with that of *PER1* mRNA (Fig. 6D). This further reinforced the instrumental role of an IRE1α-dependent pathway in tumor aggressiveness. Taken together, these data further support a specific and important role for IRE1α signaling in human glioblastoma and show that PER1 is a genuine signaling intermediate in glioblastoma progression. Moreover, these results suggest that IRE1α may be a suitable therapeutic target for patients with this disease.

Discussion

Our results identify *PER1* mRNA as a novel and atypical substrate (coding for a cytosolic/nuclear protein) of RIDD contributing to cancer development. As PER1 is a core gene of the circadian clock, our observation could also be placed in the perspective of a previous report (29) that shows the significance of the UPR/circadian clock connection in the control of hepatic metabolism. In addition, another study showed that a connection between the eIF2α-dependent transcription factor ATF4 and the circadian clock transcription systems plays an important role in multidrug resistance in tumor cells (30). In this context, IRE1α-mediated *PER1* mRNA decay could also represent another pathway in the well-described posttranscriptional regulation mechanisms of the circadian clock (31), whose relevance to cancer still remains to be investigated.

Published OnlineFirst June 10, 2013; DOI: 10.1158/0008-5472.CAN-12-3989

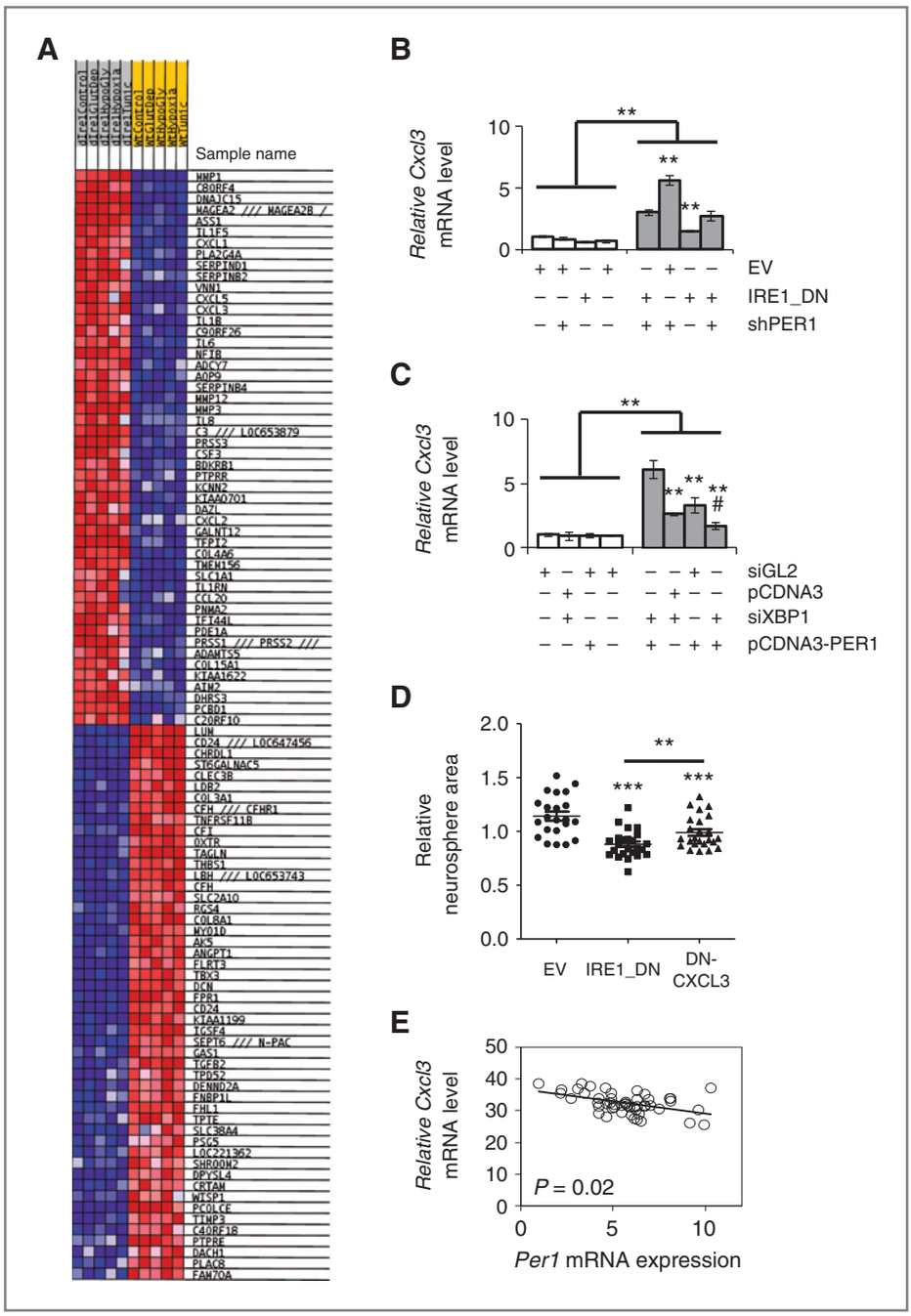

Figure 6. Relevance of IRE1 signaling in cancer. A, heatmap for microarray results. Blue, upregulation; Red, downregulation. B, U87 cells-expressing or not functional IRE1α and silenced or not for PER1 were starved or not of glucose for 16 hours in presence of dialyzed serum; CXCL3 mRNA abundance was measured by qPCR. Messenger RNA levels were normalized to those of RPLP0 and to untreated control. Error bars represent the SDs of at least 3 independent experiments. (*t* test, NS, nonsignificant; *, $P < 0.05$). C, U87 cells were transfected with siXBP1 for 72 hours and/or with pcDNA3PER1 for 24 hours before glucose deprivation for additional 16 hours. Total RNA was purified from these cells and analyzed by qRT-PCR for CXCL3 expression (using GAPDH as internal reference). The experiment was carried out in triplicate and is presented as the mean ± SD. Statistical significance was determined using the Student *t* test. *, $P < 0.06$; ***, $P < 0.01$; #, $P < 0.03$. D, sixty-two human glioblastoma samples (24 Bordeaux cohort; 38 Mayo cohort) were analyzed for *Per1* and *Cxcl3* mRNA expression using qRT-PCR. Three technical replicates were conducted. Data indicate a negative correlation (slope = −0.75) with statistical significance ($P = 0.0208$).

The findings included in this report show a direct clinical relevance of this newly identified IREα/Per1 axis as we have determined that *PER1* mRNA may be a useful marker for predicting patient survival (Fig. 5). In addition to its role in the control of the circadian clock, PER1 has also directly been involved in cell stress response, through interactions with ATM and Chk2 to participate in γ-irradiation–induced apoptosis (11). Moreover, low *PER1* mRNA expression was observed in a variety of cancers (10, 11, 32, 33), thereby suggesting its involvement in cancer development. Our data show that low PER1 together with high XBP1s expression are significantly associated with lower glioma patient survival. These observations point toward an instrumental role of IRE1α in glioma development. This was also supported by the suggested driver role of IRE1α mutations in cancer including glioma (3), however, the functional implication of these mutations remains to be shown.

IRE1α RNAse-dependent signaling in tumor could on the one hand regulate *XBP1* mRNA splicing thereby leading to previously shown induction of proinflammatory cytokines as

Published OnlineFirst June 10, 2013; DOI: 10.1158/0008-5472.CAN-12-3989

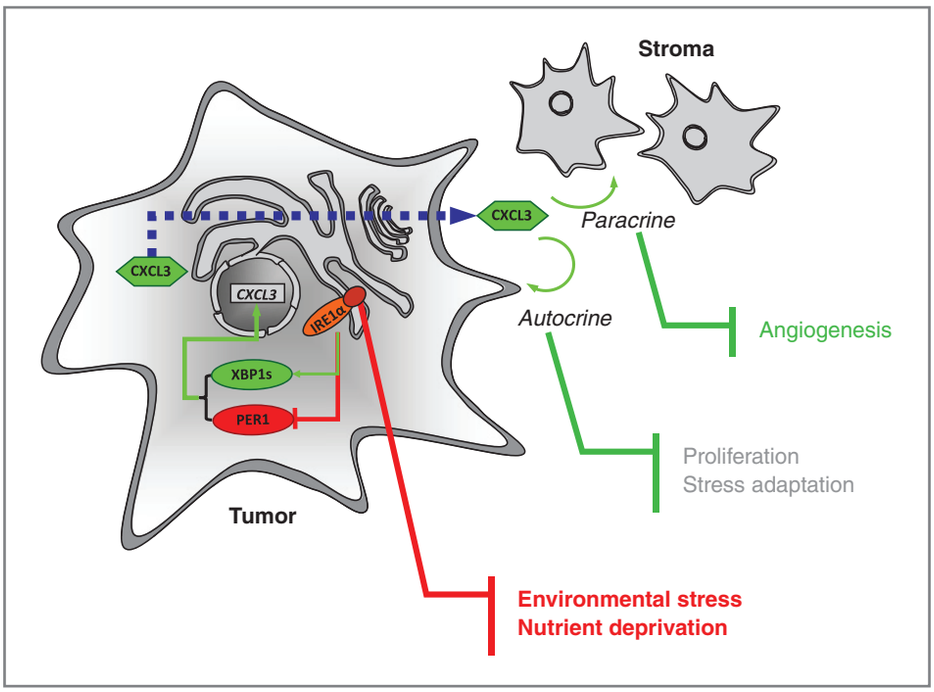

Figure 7. Schematic representation of the IRE1α-dependent activation loop that controls tumor cell adaptation. Tumor cell is presented in light gray and stromal cells in dark gray. Proteins are represented by circles; green, upregulation; red, downregulation. Connections following stress-mediated activation of IRE1α are presented in green for activation and red for inhibition. The dashed blue line represents the traffic of CXCL3 protein through the secretory pathway.

reported in many instances (27, 34–36) and in parallel enhance this effect by repressing PER1 expression, which in turn could act as derepression of cytokine expression, as illustrated for other core circadian genes (37–39). Mutually exclusive phenotypic changes in glioma observed upon impairement of IRE1α signaling from massive/angiogenic to diffuse/avascular could either result from the IRE1α-dependent activation of a cell-autonomous proinflammatory/angiogenic phenotype or from the coordinated posttranscriptional stabilization of specific mRNA (RIDD substrates), thereby leading to major changes in tumor cell–microenvironment interactions.

As such, our study shows that *CXCL3* mRNA is *per se* an IRE1α/XBP1s/PER1-dependent target in our model as determined in Fig. 6. These data are also consistent with the emerging role of CXCL3 as a key player in cancer development (27, 40) that also applies to glioblastoma (41, 42). Consequently, we identify here an IRE1α-dependent mechanism that coincidentally activates *XBP1* mRNA splicing and *PER1* mRNA decay. This provides a molecular link between IRE1α activation and tumor cell adaptation, and directly links IRE1α activity to proinflammatory/angiogenic phenotypes (Fig. 7).

Taken together, these data further support a specific and important role for IRE1α signaling in human glioblastoma and show that PER1 is a genuine signaling intermediate in glioblastoma progression. Moreover, these results suggest that IRE1α may constitute a suitable therapeutic target for patients with this disease. As a consequence, this suggests that controlling the interplay between UPR signaling and the circadian clock component might also be a suitable strategy to slow down cancer progression; our results may consequently define a model for novel therapeutic option for cancers.

Disclosure of Potential Conflicts of Interest

J.N. Sarkaria has a commercial research grant from Genentech, Basilea, Sanofi, and Merck. E. Chevet has a commercial research grant from Servier. No potential conflicts of interest were disclosed by the other authors.

Authors' Contributions

Conception and design: O. Pluquet, N. Dejeans, M.E. Fernandez-Zapico, E. Chevet

Development of methodology: O. Pluquet, N. Dejeans, M. Bouchecareilh, R. Pineau, A. Higa, S. Loriot, S. Taouji, F. Saltel, E. Chevet

Acquisition of data (provided animals, acquired and managed patients, provided facilities, etc.): O. Pluquet, S. Lhomond, R. Pineau, A. Higa, C. Combe, N. Dugot-Senant, A. Vital, H. Loiseau, J.N. Sarkaria, F.J. Rodriguez, E. Chevet

Analysis and interpretation of data (e.g., statistical analysis, biostatistics, computational analysis): O. Pluquet, N. Dejeans, A. Vital, S.J.C. Gosline, S. Taouji, F. Saltel, M. Hallett, K. Anderson, W. Wu, E. Chevet

Writing, review, and/or revision of the manuscript: O. Pluquet, N. Dejeans, M. Bouchecareilh, A. Higa, A. Vital, J.N. Sarkaria, W. Wu, F.J. Rodriguez, J. Rosenbaum, M.E. Fernandez-Zapico, E. Chevet

Administrative, technical, or material support (i.e., reporting or organizing data, constructing databases): M. Bouchecareilh, R. Pineau, M. Delugin, G. Cubel, F.J. Rodriguez

Study supervision: N. Dejeans, E. Chevet

Acknowledgments

The authors thank M. Moenner (Université Bordeaux 1, Bordeaux, France) for precious help and fruitful discussions, S. Manié (UMR CNRS 5286, INSERM 1052, Cancer Research Center of Lyon, Lyon, France), and the Chevet lab for critical reading of the manuscript. The authors also thank Dr S. Gery (University of California, Los Angeles, CA) for the gift of pcDNA3.1-hPER1 expression vector and Dr U. Albrecht (Freiburg, Switzerland) for providing us with the pPER1-Luc vector.

Grant Support

This work was supported by an Avenir program (INSERM), grants from the Institut National du Cancer (INCa), Ligue contre le cancer, a Marie Curie International Reintegration Grant (E. Chevet), a grant from the Mayo Clinic Cancer Centre (M.E. Fernandez-Zapico), a grant from Institut Fédératif de Recherche 66 (O. Pluquet). O. Pluquet was supported by fellowships from INSERM and Association pour la Recherche contre le Cancer. M. Bouchecareilh was supported from a fellowship from le Conseil Régional d'Aquitaine and la

Published OnlineFirst June 10, 2013; DOI: 10.1158/0008-5472.CAN-12-3989

Fondation pour la Recherche Française (FRM). Human glioblastoma samples were collected through the Bordeaux Tumor Bank (JP Merlio, CHU Bordeaux, France) funded by the Cancéropôle Grand Sud-Ouest and by a CEREPEG project grant (PHRC 2003; H. Loiseau) or through the Mayo Clinic Department of Clinical Pathology and funded by the Mayo Clinic SPORE in Brain Cancer P50 CA108961 (Rochester).

The costs of publication of this article were defrayed in part by the payment of page charges. This article must therefore be hereby marked *advertisement* in accordance with 18 U.S.C. Section 1734 solely to indicate this fact.

Received October 19, 2012; revised April 19, 2013; accepted May 3, 2013; published OnlineFirst June 10, 2013.

References

1. Moenner M, Pluquet O, Bouchecareilh M, Chevet E. Integrated endoplasmic reticulum stress responses in cancer. Cancer Res 2007;67:10631–4.
2. Schroder M, Kaufman RJ. The mammalian unfolded protein response. Annu Rev Biochem 2005;74:739–89.
3. Greenman C, Stephens P, Smith R, Dalgliesh GL, Hunter C, Bignell G, et al. Patterns of somatic mutation in human cancer genomes. Nature 2007;446:153–8.
4. Bifulco G, Miele C, Di Jeso B, Beguinot F, Nappi C, Di Carlo C, et al. Endoplasmic reticulum stress is activated in endometrial adenocarcinoma. Gynecol Oncol 2012;125:220–5.
5. Davies MP, Barraclough DL, Stewart C, Joyce KA, Eccles RM, Barraclough R, et al. Expression and splicing of the unfolded protein response gene XBP-1 are significantly associated with clinical outcome of endocrine-treated breast cancer. Int J Cancer 2008;123:85–8.
6. Dejeans N, Glorieux C, Guenin S, Beck R, Sid B, Rousseau R, et al. Overexpression of GRP94 in breast cancer cells resistant to oxidative stress promotes high levels of cancer cell proliferation and migration: implications for tumor recurrence. Free Radic Biol Med 2012;52:993–1002.
7. Papandreou I, Denko NC, Olson M, Van Melckebeke H, Lust S, Tam A, et al. Identification of an Ire1alpha endonuclease specific inhibitor with cytotoxic activity against human multiple myeloma. Blood 2011;117:1311–4.
8. Romero-Ramirez L, Cao H, Nelson D, Hammond E, Lee AH, Yoshida H, et al. XBP1 is essential for survival under hypoxic conditions and is required for tumor growth. Cancer Res 2004;64:5943–7.
9. Romero-Ramirez L, Cao H, Regalado MP, Kambham N, Siemann D, Kim JJ, et al. X box-binding protein 1 regulates angiogenesis in human pancreatic adenocarcinomas. Transl Oncol 2009;2:31–8.
10. Chen ST, Choo KB, Hou MF, Yeh KT, Kuo SJ, Chang JG. Deregulated expression of the PER1, PER2 and PER3 genes in breast cancers. Carcinogenesis 2005;26:1241–6.
11. Gery S, Koeffler HP. The role of circadian regulation in cancer. Cold Spring Harb Symp Quant Biol 2007;72:459–64.
12. Bouchecareilh M, Caruso ME, Roby P, Parent S, Rouleau N, Taouji S, et al. AlphaScreen-based characterization of the bifunctional kinase/RNase IRE1alpha: a novel and atypical drug target. J Biomol Screen 2010;15:406–17.
13. Bouchecareilh M, Higa A, Fribourg S, Moenner M, Chevet E. Peptides derived from the bifunctional kinase/RNase enzyme IRE1{alpha} modulate IRE1{alpha} activity and protect cells from endoplasmic reticulum stress. FASEB J 2011;25:3115–29.
14. Drogat B, Auguste P, Nguyen DT, Bouchecareilh M, Pineau R, Nalbantoglu J, et al. IRE1 signaling is essential for ischemia-induced vascular endothelial growth factor-A expression and contributes to angiogenesis and tumor growth in vivo. Cancer Res 2007;67:6700–7.
15. Auf G, Jabouille A, Guerit S, Pineau R, Delugin M, Bouchecareilh M, et al. Inositol-requiring enzyme 1alpha is a key regulator of angiogenesis and invasion in malignant glioma. Proc Natl Acad Sci U S A 2010;107:15553–8.
16. Gentleman RC, Carey VJ, Bates DM, Bolstad B, Dettling M, Dudoit S, et al. Bioconductor: open software development for computational biology and bioinformatics. Genome Biol 2004;5:R80.
17. Nguyen DT, Kebache S, Fazel A, Wong HN, Jenna S, Emadali A, et al. Nck-dependent activation of extracellular signal-regulated kinase-1 and regulation of cell survival during endoplasmic reticulum stress. Mol Biol Cell 2004;15:4248–60.
18. Cui W, Taub DD, Gardner K. qPrimerDepot: a primer database for quantitative real time PCR. Nucleic Acids Res 2007;35:D805–9.
19. Zuker M. Mfold web server for nucleic acid folding and hybridization prediction. Nucleic Acids Res 2003;31:3406–15.
20. Motzkus D, Maronde E, Grunenberg U, Lee CC, Forssmann W, Albrecht U. The human PER1 gene is transcriptionally regulated by multiple signaling pathways. FEBS Lett 2000;486:315–9.
21. Bouchecareilh M, Marza E, Caruso ME, Chevet E. Small GTPase signaling and the unfolded protein response. Methods Enzymol 2011;49:343–60.
22. Tirasophon W, Welihinda AA, Kaufman RJ. A stress response pathway from the endoplasmic reticulum to the nucleus requires a novel bifunctional protein kinase/endoribonuclease (Ire1p) in mammalian cells. Genes Dev 1998;12:1812–24.
23. Welihinda AA, Tirasophon W, Green SR, Kaufman RJ. Protein serine/threonine phosphatase Ptc2p negatively regulates the unfolded-protein response by dephosphorylating Ire1p kinase. Mol Cell Biol 1998;18:1967–77.
24. Wu J, Rutkowski DT, Dubois M, Swathirajan J, Saunders T, Wang J, et al. ATF6alpha optimizes long-term endoplasmic reticulum function to protect cells from chronic stress. Dev Cell 2007;13:351–64.
25. Hollien J, Lin JH, Li H, Stevens N, Walter P, Weissman JS. Regulated Ire1-dependent decay of messenger RNAs in mammalian cells. J Cell Biol 2009;186:323–31.
26. Iqbal J, Dai K, Seimon T, Jungreis R, Oyadomari M, Kuriakose G, et al. IRE1beta inhibits chylomicron production by selectively degrading MTP mRNA. Cell Metab 2008;7:445–55.
27. Gargalovic PS, Gharavi NM, Clark MJ, Pagnon J, Yang WP, He A, et al. The unfolded protein response is an important regulator of inflammatory genes in endothelial cells. Arterioscler Thromb Vasc Biol 2006;26:2490–6.
28. Madhavan S, Zenklusen JC, Kotliarov Y, Sahni H, Fine HA, Buetow K. Rembrandt: helping personalized medicine become a reality through integrative translational research. Mol Cancer Res 2009;7:157–67.
29. Cretenet G, Le Clech M, Gachon F. Circadian clock-coordinated 12 Hr period rhythmic activation of the IRE1alpha pathway controls lipid metabolism in mouse liver. Cell Metab 2010;11:47–57.
30. Igarashi T, Izumi H, Uchiumi T, Nishio K, Arao T, Tanabe M, et al. Clock and ATF4 transcription system regulates drug resistance in human cancer cell lines. Oncogene 2007;26:4749–60.
31. Kojima S, Shingle DL, Green CB. Post-transcriptional control of circadian rhythms. J Cell Sci 2011;124:311–20.
32. Lin YM, Chang JH, Yeh KT, Yang MY, Liu TC, Lin SF, et al. Disturbance of circadian gene expression in hepatocellular carcinoma. Mol Carcinog 2008;47:925–33.
33. Ye J, Rawson RB, Komuro R, Chen X, Dave UP, Prywes R, et al. ER stress induces cleavage of membrane-bound ATF6 by the same proteases that process SREBPs. Mol Cell 2000;6:1355–64.
34. Kaser A, Martinez-Naves E, Blumberg RS. Endoplasmic reticulum stress: implications for inflammatory bowel disease pathogenesis. Curr Opin Gastroenterol 2012;26:318–26.
35. Miani M, Colli ML, Ladriere L, Cnop M, Eizirik DL. Mild endoplasmic reticulum stress augments the proinflammatory effect of IL-1beta in pancreatic rat beta-cells via the IRE1alpha/XBP1s pathway. Endocrinology 2010;153:3017–28.
36. Villeneuve J, Lepreux S, Mulot A, Berard AM, Higa-Nishiyama A, Costet P, et al. A protective role for CD154 in hepatic steatosis in mice. Hepatology 2010;52:1968–79.
37. Hashiramoto A, Yamane T, Tsumiyama K, Yoshida K, Komai K, Yamada H, et al. Mammalian clock gene Cryptochrome regulates arthritis via proinflammatory cytokine TNF-alpha. J Immunol 2011;184:1560–5.

Published OnlineFirst June 10, 2013; DOI: 10.1158/0008-5472.CAN-12-3989

38. Lee JH, Sancar A. Regulation of apoptosis by the circadian clock through NF-kappaB signaling. Proc Natl Acad Sci U S A 2012;108:12036–41.
39. Narasimamurthy R, Hatori M, Nayak SK, Liu F, Panda S, Verma IM. Circadian clock protein cryptochrome regulates the expression of proinflammatory cytokines. Proc Natl Acad Sci U S A 2012;109:12662–7.
40. Marotta LL, Almendro V, Marusyk A, Shipitsin M, Schemme J, Walker SR, et al. The JAK2/STAT3 signaling pathway is required for growth of CD44CD24 stem cell-like breast cancer cells in human tumors. J Clin Invest 2011;121:2723–35.
41. Bruyere C, Mijatovic T, Lonez C, Spiegl-Kreinecker S, Berger W, Kast RE, et al. Temozolomide-induced modification of the CXC chemokine network in experimental gliomas. Int J Oncol 2011;38:1453–64.
42. Kammerer R, Buchner A, Palluch P, Pongratz T, Oboukhovskij K, Beyer W, et al. Induction of immune mediators in glioma and prostate cancer cells by non-lethal photodynamic therapy. PLoS ONE 2011;6:e21834.

WT (**ARTICLE 5, Figure 3**), aucune déstabilisation n'est observée pour deux autres cibles du RIDD: SPARC et PDGFRB (données non montrées).

En outre, les quatre mutations étudiées affectent différemment chacun des substrats PER1, COL6A1 et SCARA3. Par exemple pour la mutation A414T, la dégradation de l'ARNm de PER1 est accentuée alors que celle de COL6A1 est légèrement diminuée, et que celle de SCARA3 est abolie, cet ARNm étant même stabilisé par rapport à la condition contrôle U87-EV.

L'injection intracrânienne de cellules tumorales U-87 MG surexprimant ces formes mutées d'IRE1α dans un modèle murin a permis de définir qu'aucune des deux mutations définies comme initiatrices de tumeurs (S739F et Q780*) ne semblent conférer de gain d'agressivité aux tumeurs cérébrales.

De façon intéressante, nous avons montré que la mutation gain de fonction P336L abroge totalement les capacités d'implantation des cellules tumorales dans le cerveau des souris.

Au contraire, la mutation gain de fonction A414T identifiée par notre équipe augmente significativement la croissance et la vascularisation des tumeurs cérébrales, entraînant rapidement la mort des souris.

De plus amples études restent à mener pour définir les mécanismes moléculaires pouvant expliquer les phénotypes observés lors de la surexpression de ces mutations, en particulier pour les mutations P336L et A414T.

ARTICLE 5

Functional impact of IRE1alpha somatic mutations in glioblastoma

Stéphanie Lhomond[1], Nicolas Dejeans[1], Saïd Taouji[1], Néstor Pallares-Lupon[1], Raphaël Pineau[2], Olga Papadodima[3], Hugues Loiseau[4], Olivier Pluquet[1,6], Arisotelis Chatziioannou[3], and Eric Chevet[1,5*]

[1]INSERM U1053, Avenir, Université Bordeaux-Segalen, Bordeaux, France. [2]Université Bordeaux 1, Bordeaux, France. [3]Institute of Biology, Medicinal Chemistry & Biotechnology, NHRF, 48 Vassileos Constantinou Ave., Athens, Greece. [4]Department of Neurosurgery, CHU Pellegrin, Bordeaux, France. [5]Centre Régional de Lutte Contre le Cancer Eugène Marquis, Rennes, France.

*Correspondance to : Eric Chevet, INSERM U1053, Université de Bordeaux-Segalen, 146 rue Léo Saignat, 33076 Bordeaux, France. Phone : 33 (0)5 57 57 92 53. Fax : 33 (0)5 56 51 40 77. Email : eric.chevet@inserm.fr

[4]Present address: Institut de Biologie de Lille, CNRS UMR8161/Universités Lille 1 et Lille 2/Institut Pasteur de Lille, 1, rue du Pr. Calmette, BP 447, 59021 Lille, France.

Functional impact of IRE1alpha somatic mutations in glioblastoma

Stéphanie Lhomond[1], Nicolas Dejeans[1], Saïd Taouji[1], Néstor Pallares-Lupon[1], Raphaël Pineau[2], Olga Papadodima[3], Hugues Loiseau[4], Olivier Pluquet[1,6], Arisotelis Chatziioannou[3], and Eric Chevet[1,5*]

[1]INSERM U1053, Avenir, Université Bordeaux-Segalen, Bordeaux, France. [2]Université Bordeaux 1, Bordeaux, France. [3]Institute of Biology, Medicinal Chemistry & Biotechnology, NHRF, 48 Vassileos Constantinou Ave., Athens, Greece. [4]Department of Neurosurgery, CHU Pellegrin, Bordeaux, France. [5]Centre Régional de Lutte Contre le Cancer Eugène Marquis, Rennes, France.

*Correspondance to : Eric Chevet, INSERM U1053, Université de Bordeaux-Segalen, 146 rue Léo Saignat, 33076 Bordeaux, France. Phone : 33 (0)5 57 57 92 53. Fax : 33 (0)5 56 51 40 77. Email : eric.chevet@inserm.fr

[4]Present address: Institut de Biologie de Lille, CNRS UMR8161/Universités Lille 1 et Lille 2/Institut Pasteur de Lille, 1, rue du Pr. Calmette, BP 447, 59021 Lille, France.

ABSTRACT

Glioblastoma multiforme (GBM) is the most lethal form of glioma with an overall survival at 5 years nearly null (< 5%). This mainly results from acquired resistances to therapies. To understand the mechanisms underlying this phenomenon, current studies aim at deciphering key signaling pathways involved in tumor growth and treatment escape. Increasing evidences point towards IRE1alpha as a central player in GBM development, particularly in cancer cell invasion and tumor vascularization. Recent studies have unraveled the presence of somatic mutations on the IRE1alpha gene in GBM that could play a driver role but without providing any functional information. Herein, we identified a new somatic mutation: A414T in human GBM which increased aggressiveness of U-87 MG derived tumors in mice. This mutation stabilized IRE1alpha oligomers and thus increased IRE1alpha signaling in tumor, leading to a late induction of proliferative and pro-angiogenic pathways.

Significance: **This study provides the first mechanistic example of how a somatic mutation in the IRE1alpha gene can provide adaptive advantages to glioblastoma cells.**

Keywords: Endoplasmic reticulum, cancer, stress, ERN1, XBP1, RIDD, angiogenesis

INTRODUCTION

Glioblastoma multiforme (GBM) is one of the most lethal adult cancers, as most patients die within 15 months after diagnosis [1]. GBM is an aggressive, incurable glioma (stade IV astrocytoglioma, WHO classification) due to great heterogeneity of cell subtypes within the tumor and to the presence of invasive spot that cannot be easily cured by surgical resection or targeted radiation [2]. To limit tumor recurrences from invasive cells, chemotherapy (temolozomide (TMZ)) was added to surgery and radiation [3]. Although TMZ has demonstrated some efficiency, it only increases patient's survival from 12.1 to 14.6 months. Understanding biological processes of GBM progression and treatment resistance is thus a major issue to develop more effective therapies. To decipher the molecular mechanisms involved in GBM development, and therefore identifying new target for GBM diagnosis, prognosis or therapy, large scale sequencing studies on human cancer biopsies was led by The Cancer Genome Atlas (TCGA) [4, 5]. Five majors GBM markers were identified: EGFR, PTEN, TP53, NF1 and IDH1 [4] and clinical trials are ongoing. In addition to these highly mutated genes, more potential targets have been identified by the potential oncogenic power of the carried mutations. In this idea, the Endoplasmic Reticulum (ER) stress sensor IRE1alpha was defined as the fifth most oncogenic mutated kinase in human cancers, as it was shown to carry six somatic mutations defined as driver [6]. Two of those potentially driver mutations, S769F and Q780*, were identified in GBM samples, as well as a third mutation, P336L, identified in a TCGA study [5]. Apart from the sequencing data, little is known about the functional impact of those mutations, even if a previous study aimed to understand their structural impact [7].

IRE1alpha is a major component of ER stress signaling. Indeed upon ER stress, misfolded proteins accumulate in ER lumen, triggering activation of the adaptive Unfolded Protein Response (UPR) which is transduced by three ER transmembrane proteins, PERK, ATF6 and IRE1alpha [8]. Once activated, the serine/threonine kinase and RNase IRE1alpha oligomerises, activating three major downstream pathways including the phosphorylation of targeted proteins leading to the activation of JNK1 [9, 10], the splicing of XBP1 mRNA [11, 12] and the degradation of targeted mRNA also called RNA regulated IRE1 dependent decay (RIDD) [13, 14]. By its central role in cell homeostasis control, IRE1alpha signaling has been involved in tumor development [15]. Our previous studies determined that IRE1alpha role in mRNA degradation was critical for GBM growth and vascularization [16, 17]. To further characterize the roles of IRE1alpha in glioma, we sequenced GBM samples and identified a new somatic mutation that differs from those previously described, on residu A414. Adding this mutation to the three ones previously described, we characterize herein the impact of these four mutations on GBM cells U-87 MG in vitro and in vivo.

RESULTS

Identification of a novel somatic mutation on IRE1alpha in GBM – Previous tumor sequencing studies identified six mutations of IRE1alpha that were defined as driver mutations in various cancers [6]. As IRE1alpha plays a key role in cancer development, in particular in GBM [5, 6, 15-18], we sequenced IRE1alpha gene exons on twenty-three GBM samples and identified a fourth IRE1alpha mutation in one GBM human sample: the A414T mutation (**Figure 1A**). This A414T mutation came from an aggressive, mesenchymal like GBM developed in a 70-year old female. Immunohistochemistry staining revealed that this tumor was also highly vascularized (CD31 staining) and IRE1alpha over activated, as indicated by the strong XBP1s staining observed using immunohistochemistry (**Figure 1B**). Added to the three mutations previously described in literature, it brought to four the number

of IRE1alpha mutations identified so far in GBM patients. A sequence alignment demonstrated that whereas the mutations P336L, S769F and Q780* affect conserved amino acid in various species, the mutation identified in our sequencing study altered an apparently less conserved amino acid (**Figure S1**). This lability could explain why this A414T mutation, previously described in GBM samples, has been excluded from further analyses, as it was considered as a SNP or a secondary acquired mutation [4, 5].

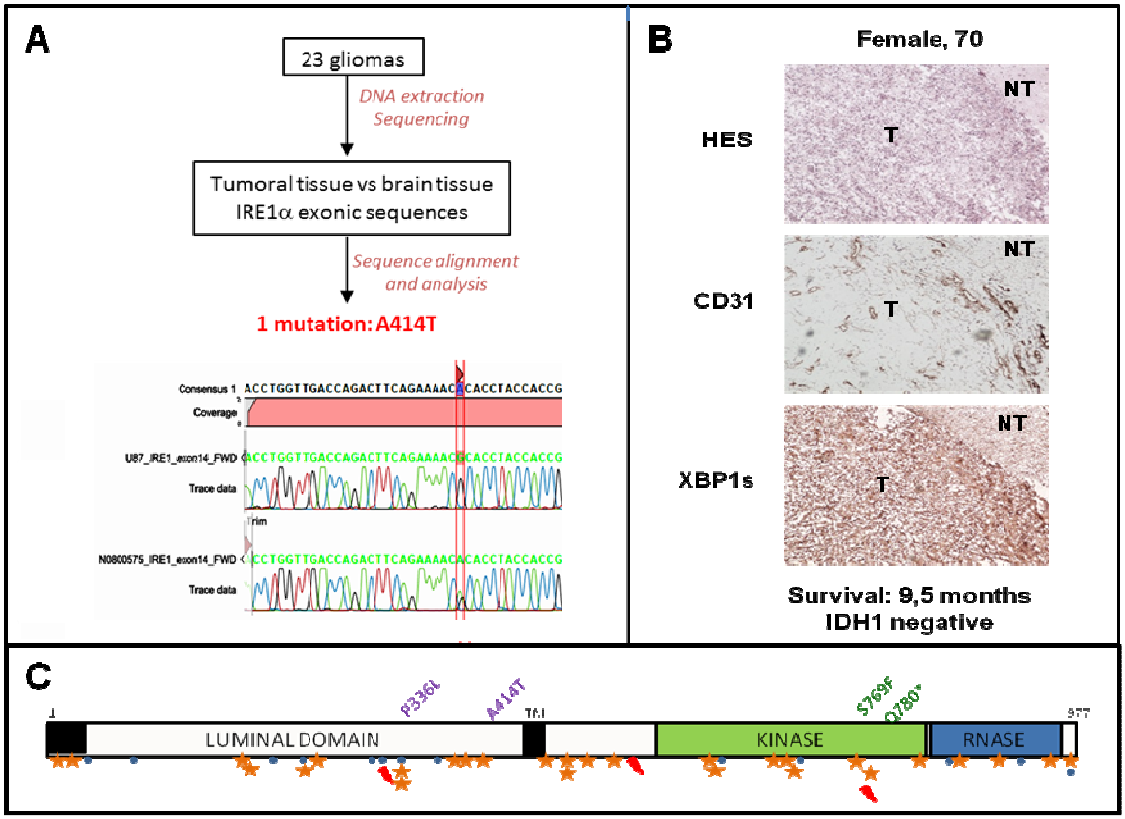

Figure 1: Identification of an IRE1alpha somatic mutation in a human glioblastoma tumor. *A. Specific IRE1alpha exons sequencing flowchart: DNA was extracted from 23 gliomas samples provided by the Bordeaux Tumor Bank and IRE1alpha exons sequences were compared to normal brain tissue IRE1alpha sequence. One of the 23 samples showed a novel IRE1alpha mutation, as indicated by the red arrow on DNA sequence representation. B. Tumor characterization from the female, 70 year-old patient presenting the A414T mutation. Imunohistochemistry staining revealed a mesenchymal-like encapsulated tumor (Hematoxylin and eosin stain: HES), highly vascularized as indicated by CD31 staining of endothelial cells. IRE1alpha activation within the tumor is visible by overexpression of the spliced form of XBP1 (XBP1s) in the tumoral tissue (T) compared to the non-tumoral tissue (NT). C. Overview of mutations identified to date in the IRE1alpha gene in various cancer samples, including nonsense mutations (red), missense mutations (orange stars) and synonymous mutations (blue circles). The four mutations identified in GBM are located above a schematic representation of the IRE1alpha protein. TM: transmembrane domain.*

IRE1alpha mutations impact kinase and RNAse functions

IRE1alpha is a bifunctional protein that contains a kinase and a RNase domain (**Figure 1C**) involved in three downstream signaling pathways including i) the phosphorylation of targeted proteins leading to JNK1 activation, ii) the degradation of targeted mRNA (RIDD) and iii) the

unconventional splicing of XBP1 mRNA. Around fifty mutations were identified all along IRE1alpha gene in various cancers, among which only three were identified in GBM: the missense mutations P336L and S769F and the nonsense mutation Q780* (**Figure 1C**). The localization of those mutations in IRE1alpha secondary structure revealed no apparent clustering of the mutations, not even into IRE1alpha catalytic domains. However, the cytosolic mutations S769F and Q780* are located in the kinase domain of the protein whereas the luminal mutations P336L and A414T appear to be located in alpha-helix domains potentially involved in IRE1alpha interaction domains with ER partners (data not shown).

To measure the potential impact of the four mutations found in GBM, we overexpressed either the wild type (WT) or the mutated forms of IRE1alpha in U-87 MG cells, in a normal endogenous IRE1alpha background (**Figure 2A**). The four mutations bearing proteins were overexpressed in U-87 MG cells using a lentivirus system and as anticipated the stop mutation Q780* leads to overexpression of a shorter IRE1alpha protein (80 kDa instead of 110 kDa). Immunofluorescent staining of IRE1alpha co-localized this protein with the ER resident protein KDEL and thereby confirmed that mutations did not affect IRE1alpha localization to the ER (**Figure 2B**).

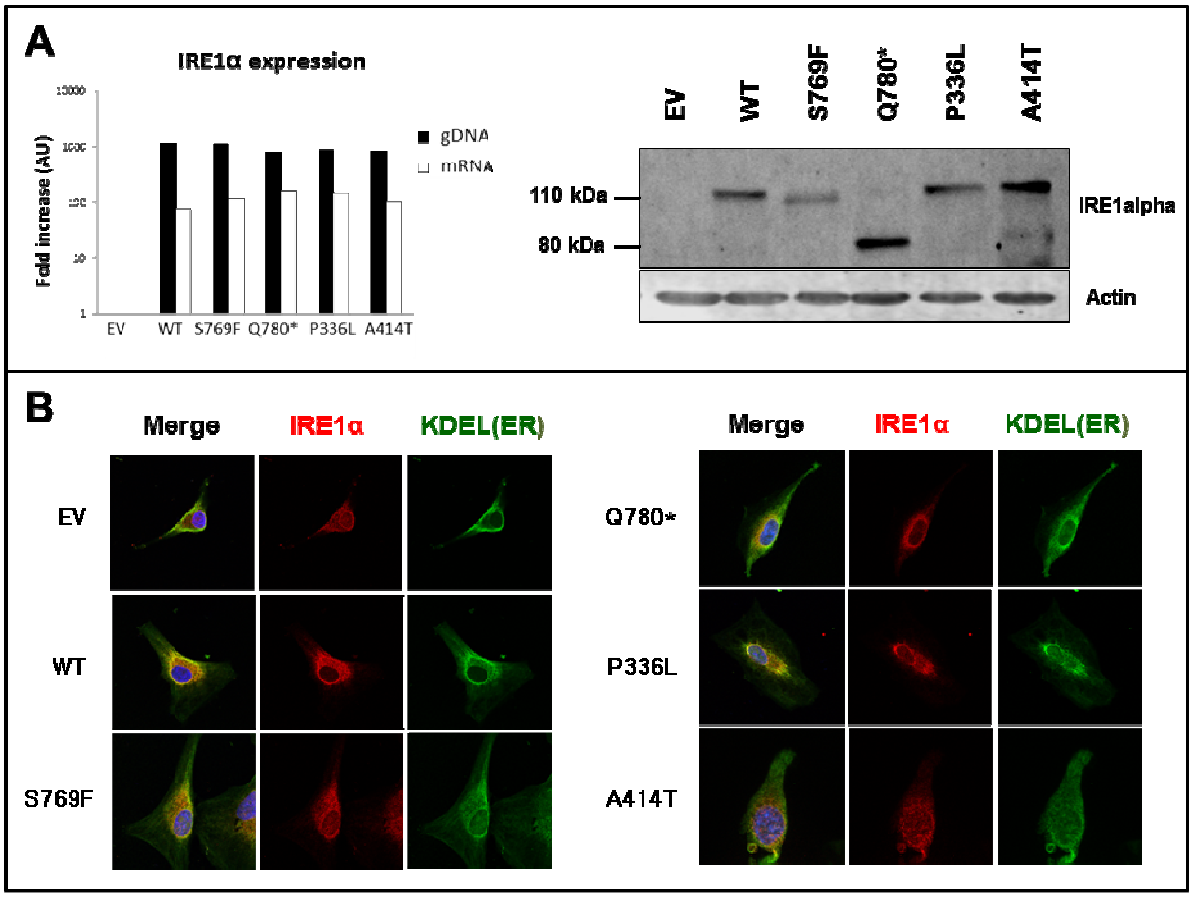

Figure 2: Overexpression of IRE1alpha wild-type or mutated forms in U-87 MG cells. *A. U-87 MG were transduced with empty pCDH lentivector (EV) or with pCDH lentivector containing the WT (WT) or the mutated (S769F, Q780*, P336L, A414T) IRE1alpha coding sequence. PCR and RT-PCR were respectively performed on genomic DNA (gDNA) and messenger RNA (mRNA) indicated a 1000-fold gDNA increase corresponding to a 100-fold mRNA increase. Immunoblot (anti-IRE1alpha and anti-actin) revealed a 10-fold over expression of full length (100kDa) IRE1alpha protein in WT, S769F, P336L and A414T conditions and over expression of a truncated (80kDa) IRE1alpha protein in Q780* condition.*

C. Confocal immunofluorescence studies performed with U-87 cells expressing these variant proteins showed co-localization of WT or mutated IRE1alpha (red) with the ER marker KDEL (green).

As reported in other cellular system [10], the overexpression of the WT form in U-87 MG was sufficient to activate IRE1alpha in basal conditions compared to the control empty-vector (EV) expressing cells, as indicated by IRE1alpha basal oligomerization and phosphorylation, as well as XBP1 mRNA basal splicing (**Figure 3**). As expected, we showed that Q780* corresponded to a loss-of-function mutation. Indeed the loss of the last part of the kinase domain and the entire RNase and C-terminus domains did not affect IRE1alpha oligomerization but impaired the resulting trans-autophosphorylation (**Figure 3A, Figure S2**) as well as XBP1 mRNA splicing (**Figure 3A-3B**) and RIDD activity (**Figure 3C**). It is important to note that this mutation was not dominant-negative as did not prevent XBP1 splicing by endogenous IRE1alpha upon tunicamycin treatment (**Figure S2B**).

In the other part, P336L and A414T mutations increased IRE1alpha oligomerization capacities, leading to IRE1alpha over phosphorylation and enhanced XBP1 splicing (**Figure 3A-3B**). Interestingly this over activation of proximal IRE1alpha signaling was not associated with a significant increase in XBP1 transcriptional activity (**Figure 3B, Figure S2**), global RIDD activity (**Figure 3C**) or UPR activation (**Figure S2**). Moreover, no significant impact of these mutations was measured on U-87 MG proliferation rate nor adhesion and migration abilities (**Figure S3**) *in vitro*. It is important to note that whereas WT-IRE1alpha over expression efficiently increased RIDD activity on PERIOD1 (PER1), COL6A1 and SCARA3, the four mutations had different effects depending on the targeted mRNA (**Figure 3C**). No IRE1alpha over expression (WT or mutants) seemed to decrease SPARC and PDGFRB mRNA levels (data not shown). This selectivity can be explained by modifications in IRE1alpha binding to luminal or cytosolic partners due to IRE1alpha over expression or mutations. We also hypothesized that IRE1alpha mutations induced transcriptomic changes which could impact on mRNA addressing to IRE1alpha.

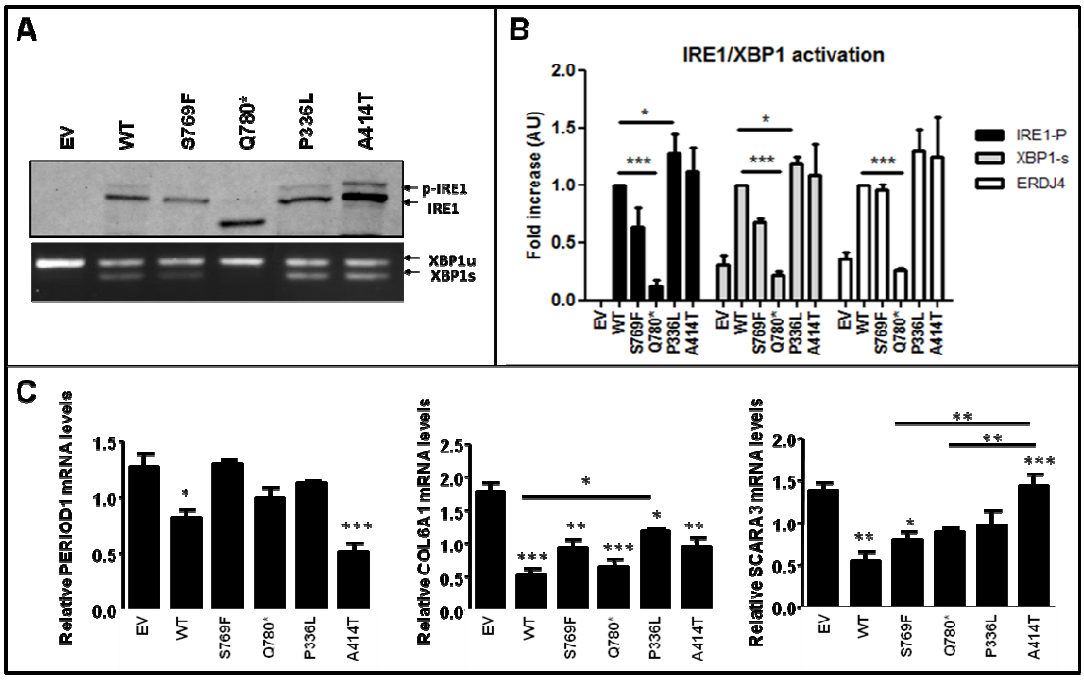

Figure 3: Impact of somatic mutations on IRE1alpha signaling. *A. Anti-IRE1alpha Phostag immunoblot showing both phosphorylated (p-IRE1) and non phosphorylated (IRE1) IRE1alpha proteins revealed IRE1alpha phosphorylation in basal conditions due to over expression of WT, P336L and A414T but not S769F nor Q780* forms of IRE1alpha. EtBr-stained agarose gel of XBP1 cDNA amplicons corresponding to unspliced (XBP1u) and spliced (XBP1s) forms of XBP1 mRNA revealed XBP1 splicing in basal conditions due to over expression of WT, S769F, P336L and A414T but not Q780* forms of IRE1alpha. B. Bar graph representing the quantification of 3 levels of IRE1/XBP1 activation: IRE1alpha phosphorylation (p-IRE1/IRE1) and XBP1 mRNA splicing (XBP1s/(XBP1u+XBP1s)) measured as indicated in A., completed by qPCR quantification of ERDJ4, a transcriptional target of XBP1s. Three independent biological samples were used. Data are means +/− SD. P-values: * <0.05 and *** <0.002. C. Analysis of mRNA expression (normalized to 18S) after 2-hrs Actinomycin D (ActD) treatment to inhibit de novo transcription. COL6A1: Collagen, type VI, alpha 1; SCARA3: scavenger receptor class A, member 3. Three independent biological samples were used. Data are means +/− SD. P-values: * <0.05, ** <0.01 and *** <0.002.*

IRE1alpha over expression promotes tumor development *in vivo*

To measure the impact of IRE1alpha over expression on tumor development we implanted control U-87 MG or cells expressing WT and mutated forms of IRE1alpha into mouse brain, as previously described [15, 17]. Fifteen days post-implantation, five mice of each group were sacrificed and brains were isolated for immunofluorescence (IF) staining of tumor cells (vimentin) and vessels (CD31). As expected, IF staining highlighted that IRE1alpha over expression enhanced tumor growth and vascularization, whereas impairment of IRE1alpha signaling (DN) reduced both size and vascularization of tumors (**Figure 4C-4D**). Moreover, DN significantly promoted mouse survival after U-87 MG implantation, whereas IRE1alpha over expression dramatically reduced it (**Figure 4A**) by developing massive and well-encapsulated tumors (**Figure 4B**). An exception of this tumorigenic effect of IRE1alpha was observed with the P336L mutation. Indeed, this mutation prevented U-87 MG engraftment in mouse brain, leading to a complete absence of tumor formation (data not shown) and had no lethal impact on mouse survival (**Figure 4A**). A possible explanation for this unexpected result is that the mutation affected downstream IRE1alpha signaling, leading to an over activation of tumor suppressors like p53. Even if we indeed measured a p53 over expression in P336L expressing U-87 MG cells, no increase in p53 activity was observed (**Figure S4**), so mechanisms of tumor suppression by P336L remains to be elucidated.

A414T mutation leads to pro angiogenic and proliferative phenotypes

Among the four mutations, the loss-of-function mutations S769F and Q780* seemed to have little effects on mouse survival (**Figure 4A**) whereas the Q780* mutation seemed to accelerate the early steps of tumor growth (**Figure 4C**). However the P336L and A414T mutations did not have a similar gain-of-function impact on IRE1alpha *in vitro*, their impact on *in vivo* tumor development was diametrically opposed. Indeed, whereas P336L totally blocked tumor formation, A414T shortened mouse survival (**Figure 4A**), by promoting tumor growth and vascularization (**Figure 4B**). The pro-angiogenic effects of A414T mutation not only increased the number of vessels associated with the tumor mass, but also increased the size of those vessels (**Figure 4A-4B**), an effect that was much less visible in early step of tumorigenesis (**Figure 4C-4D**). Even if this mutation did not lead to *in vivo* XBP1s overexpression (**Figure 4B**), it seemed to selectively increased RIDD activity, as indicated by increased degradation of PER1 mRNA but not others tested RIDD targets (**Figure 3C**).

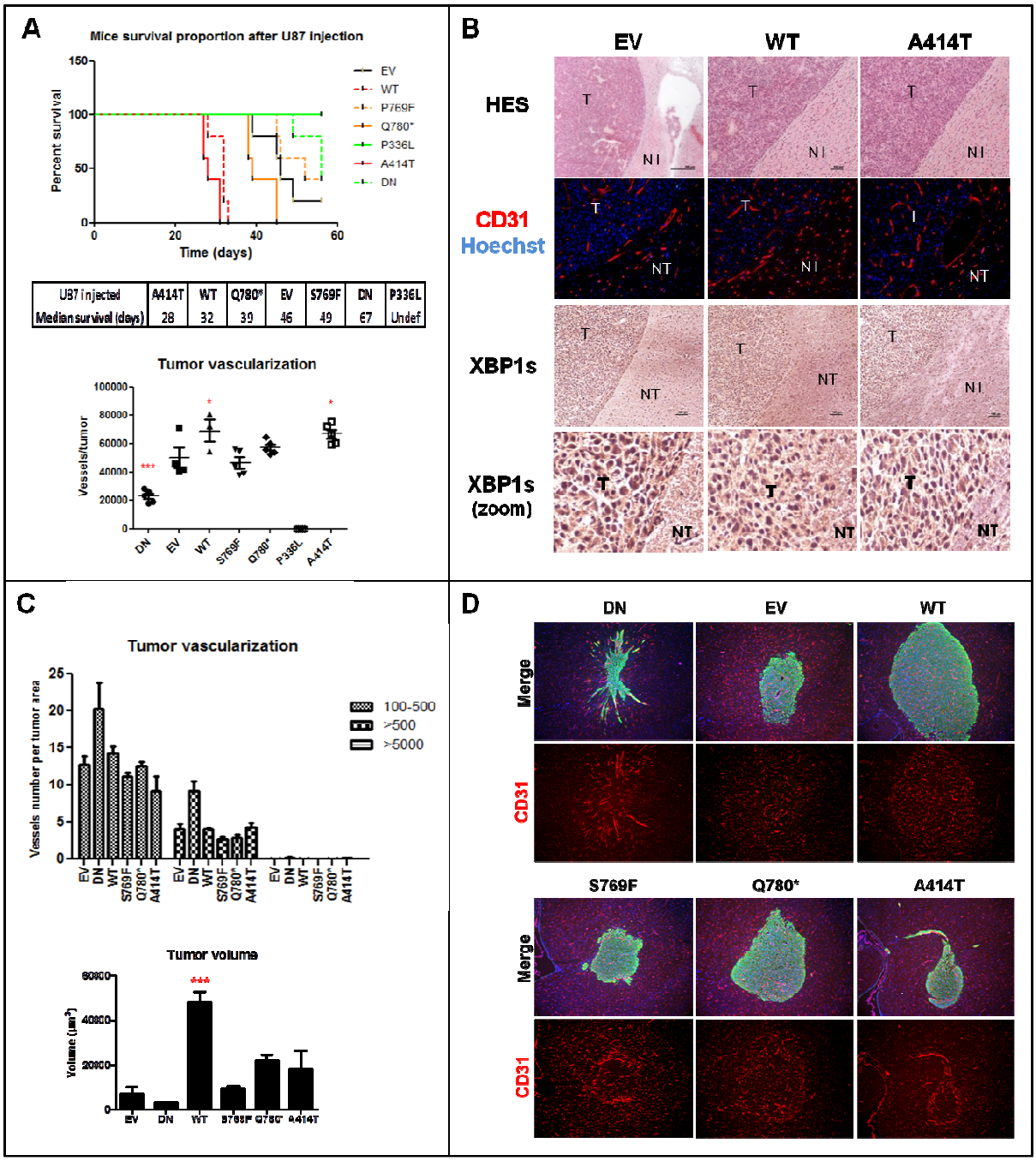

Figure 4: Impact of IRE1alpha somatic mutations on tumor development after orthotopic graft of U-87 MG in mice. *A. Tumor cells (U-87 MG) were injected into the brain of recipient mice (Rag-γ 2C). Animals were sacrificed at first clinical sights of tumor development and each sacrifice was reported in the Kaplan-Meyer curve, indicating a gain of lethality for tumors formed in WT or A414T conditions. Brains were collected and analyzed by immunostaining as described in B. Graphic representation of vessel number and size for each tumor indicated that tumors derived from U87-WT or U87-A414T were highly vascularized compare to other conditions. B. Representative immunofluorescence imaging of tumors formed from EV, WT or A414T U-87, showing tumor vascularization (red, CD31 staining; blue: nucleus staining). T: tumoral tissue; NT: non-tumoral tissue. Representative imaging of tumor phenotype (HES) and XBP1s did not revealed significant differences in term of tumor*

*encapsulation, tumor size or tumoral induced IRE1alpha. C. Tumor cells (U-87 MG) were injected into the brain of recipient mice (Rag-γ 2C). Animals were sacrificed fifteen days post-injection. Brains were collected and analyzed by immunostaining as described in B. Graphic representation of vessel number and size for each tumor as well as tumor size indicated that tumors derived from U87-WT grown more rapidly than all other conditions, with an associated angiogenesis. D. Representative fluorescence imaging of tumors showing tumor vascularization (red, CD31 staining), tumor phenotype (green: vimentin (cancer cells); blue: nucleus). T: tumoral tissue; NT: non-tumoral tissue. Quantification of vessels associated to each tumor are reported in C. For animal experimentation, data shown are mean ± SEM of five mice per experiment. *, P <0.05 and ***, P < 0.002 (two-way ANOVA with Bonferroni post-test).*

DISCUSSION

Our results identified a novel mutation in IRE1alpha: the A414T mutation. Our work represents the first characterization of the functional evidence of a role of IRE1alpha somatic mutation on tumor development. The proliferative and angiogenic effects of the A414T mutation can be explained in part by the increased degradation of Per1 mRNA (**Figure 3C**), as our previous studies highlighted the role of PER1 in IRE1alpha associated tumor development and vascularization. However, it is interesting to note that IRE1alpha mutation A414T did not induce significant difference in vessel number of 15-days formed tumors (**Figure 4C**). However, vessels remodeling at day 15 was more important in tumors formed from U87-DN or U87-A414T cells than in other conditions, as we could observed long vessels along which tumors cells seemed to migrate by co-option. Interestingly, only U87-DN tumors evolved in mesenchymal tumors, as previously described [15], whereas U87-A414T tumors evolved in encapsulated massive tumors presenting many large intra-tumoral vessels, which could indicate a delayed switch on proliferative and angiogenic phenotype in this condition.

Surprisingly, the P336L mutation is so far the only IRE1alpha mutation that was identified in more than one tumor sample and even in more than one cancer type (one in glioma [5] and two in intestine cancers [19]) so the role of this mutation should probably not be restricted to these anti-tumoral effects. We hypothesized that the oncogenic potential of this mutation could need particular cancer context, for instance acquired mutation in key genes for GBM development highlighted by TCGA project (EGFR, PTEN, TP53, NF1 and IDH1), as no previous study defined P336L as a driver mutation. In this idea, we measured TP53 expression and identified an over expression of TP53 resulting of the P336L IRE1alpha over expression, but without any functional impact on TP53 activity (**Figure S3**) so P336L mutation could allow stabilization of mutated TP53, emphasizing the pro-tumoral role of such mutations of TP53. Moreover, recent work reported a direct role of the IRE1alpha kinase target JNK in stabilizing EGFR ligand epiregulin (EREG) and consequently an autocrine activation loop of EGFR, which should provide proliferative advantage of GBM cells in which EGFR signaling was already altered by mutations [20]. This hypothesis could also explain the proliferative effects of A414T mutation and experiments should be led to involve EGFR or other key GBM proteins in IRE1alpha dependant GBM growth, as both P336L and A414T mutations seemed to stabilize IRE1alpha kinase and RNases activities.

Taken together, the results acquired so far did not explain the potential role of mutations S769F and Q780*, which were predicted to have a driver role in GBM development. However, complementary studies are needed to determine if those mutations present a selective advantage in initiating emergence of cancer cells in a healthy tissue context. As far as we could guess from this study, IRE1alpha mutation described here are more likely

secondary mutations, which can be enhanced cancer cell survival in precise background including acquired mutations or resistance to chemotherapy induced cell death.

Previous work highlighted a potential interest in measure of IRE1alpha activation in GBM as correlative studies linked IRE1alpha downstream targets PER1 and XBP1 to GBM aggressiveness [17]. Thus, establishing IRE1alpha mutation status in GBM should provide a pertinent tool to adapt therapeutic treatments to a "in kind" care of GBM patients.

MATERIALS AND METHODS

DNA sequencing and patient data **-** All tumors were frozen after surgical resection. These tumors were clinically and genetically characterized in the department of neurosurgery of the Pellegrin Hospital (Bordeaux, France) and informed consent was obtained in accordance with French legislation. GBM were classified according to i) the presence of IDH1, OLIGO2 and TP53 expression and ii) tumor phenotype (size and form of tumor cells, hyperplasia, necrosis, proliferation indice). IRE1alpha exons sequencing was performed by Beckman Coulter Genomics (Takeley, UK) using specific primers flanking exonic regions of IRE1alpha . The presence of IRE1alpha mutation was detected using nucleotide sequence alignment software. Tumor in which IRE1alpha mutation was identified presented classical GBM characteristic with endothelial hyperplasia and MIB1 proliferation index of 15%, and was IDH1 negative, with 5% of OLIG2 and 5% of TP53 positive cells.

Cloning and site-directed mutagenesis - Selected punctual mutations were introduced on IRE1alpha exonic sequence using QuickChange Directed Mutagenesis kit with the following primers:

Mutation (AA)	Sens	Primer sequence (5'-3')
S769F	FWD	GCGTCTTTTACTACGTAATCTTTGAGGGCAGCCACCCTTTTGGC
	REV	GCCAAAAGGGTGGCTGCCCTCAAAGATTACGTAGTAAAAGACGC
Q780*	FWD	CCCTTTTGGCAAGTCCCTGTAGCGGCAGGCCAACATCC
	REV	GGATGTTGGCCTGCCGCTACAGGGACTTGCCAAAAGGG
P336L	FWD	ACAAGGGGGAGTGTGTGATCACGCTCAGCACGGACGTCAA
	REV	TTGACGTCCGTCCTGAGCGTGATCACACACTCCCCCTTGT
A414T	FWD	CCAGACTTCAGAAAACACACCTACCACCGTGTCTCGGGA
	REV	TCCCGAGACACGGTGGTAGGTGTGTTTTCTGAAGTCTGG

The wild-type or mutated sequences were then cloned in the multicloning site of the expression lentivector pCDH-CMV-MCS-EF1-Puro-copGFP (System biosciences). The presence of only mutations of interest was checked by a minimum two-X cover sequencing (Beckman Coulter Genomics).

Cell culture, treatments, antibodies - U87-MG cells were grown in DMEM glutamax (Invitrogen, Carlsbad, CA, USA) supplemented with 10% FBS. U-87 MG were stably transfected at MOI = 0.3 with pCDH-CMV-MCS-EF1-Puro-copGFP (System biosciences) empty vector (EV), or pCDH-CMV-MCS-EF1-Puro-copGFP containing IRE1alpha wild-type sequence (WT) or mutated sequence (P336L, A414T, S769F or Q780*). U-87 MG cells were selected using 2µg/mL puromycin and polyclonal populations were tested for GFP expression. For microarray experiments, tunicamycin (purchased from Calbiochem (Merck KGaA, Darmstadt, Germany)) was used at 0.5 µg/mL for 16 hrs. Actinomycin D were purchased from Sigma (StLouis, MO, USA) and used as indicated.

Semi-quantitative PCR and Quantitative real-time PCR - Total RNA was prepared using the Trizol reagent (Invitrogen, Carlsbad, CA, USA). Semi-quantitative analyses were carried out as previously described [16, 17]. PCR products were separated on 4% agarose gels. All RNAs were reverse transcribed with Maxima Reverse Transcriptase (Thermo Scientific, Waltham, MA, USA), according to manufacturer protocol. All PCR reactions were performed with a MJ Mini thermal cycler from Biorad (Hercules, CA, USA) and qPCR with a StepOnePlus™

Real-Time PCR Systems from Applied Biosystems and the SYBR Green PCR Core reagents kit (Bio-Rad). Experiments were performed with at least triplicates for each data point. Each sample was normalized on the basis of its expression of the 18S gene. For quantitative PCR the following pairs of primer were used:

	Sense	Primer sequence (5'-3')		Sense	Primer sequence (5'-3')
BiP	FWD	GCTTATGGCCTGGATAAGAGG	Herpud	FWD	CTATTCCGCCTTCCTTGTAGC
	REV	CCACAACTTCGAAGACACCAT		REV	CCTCTTGGGTCAGCAATTACA
Chop	FWD	ATTGACCGAATGGTGAATCTGC	Orp150	FWD	GAAGATGCAGAGCCCATTTC
	REV	AGCTGAGACCTTTCCTTTTGTCTA		REV	TCTGCTCCAGGACCTCCTAA
Col6A1	FWD	CCCTCGTGGACAAAGTCAAG	Pdgfrb	FWD	TCCATCCCTCTGTTCTCCTG
	REV	GTTTCGGTCACAGCGGTAGT		REV	CTGCCCTCTCCCAGTTATCA
Edem	FWD	AGTCATCAACTCCAGCTGGAA	Per1	FWD	TATACCCTGGAGGAGCTGGA
	REV	AACCATCTGGTCAATCTGTCG		REV	AGGAAGGAGACAGCCACTGA
Erdj4	FWD	TGGTGGTTCCAGTAGACAAAGG	Scara3	FWD	CGCTGCCAGAAGAACCTATC
	REV	CTTCGTTGAGTGACAGTCCTGC		REV	AACCAGAGAGGCCAACACAG
Grp94	FWD	TCCTCCTCCTGACGTTGTAAA	Sparc	FWD	GGCCTGGATCTTCTTTCTCC
	REV	TGCTCGCCATCTAGTACATCC		REV	CCACCACCTCTGTCTCATCA

Western blotting – Antibodies against IRE1alpha, ERK and PDGFRb were purchased from Santa Cruz Biotechnology (Santa Cruz, CA) and p21, p-ERK, AKT, p-AKT from Cell Signaling Technology (Danvers, MA). Anti-CNX antibodies were kindly given by John Bergeron (McGill University, Montreal, Qc, Canada). Proteins were extracted from U-87 cells using a RIPA buffer (Sigma).

Immunofluorescence analyses - Cells grown on 22-mm coverslip were washed with PBS, fixed with 4% paraformaldehyde for 10 min at room temperature, and then blocked with 5% BSA, PBS, 0.1% Triton X-100 for 1 h. ER was stained using anti-KDEL antibody (Enzo) and over expressed IRE1alpha was stained using anti-IRE1alpha antibody (SantaCruz). Cells were incubated with primary antibodies for 1 h at room temperature, washed with PBS, and incubated for 45 min with Donkey anti-mouse and Donkey anti-rabbit antibodies (Invitrogen). To visualize the nucleus, cells were counterstained with 1 µg/mL 4,6-diamidino-2-phenylindole (DAPI, Sigma). After mounting, cells were analyzed with a SP5 confocal microscope (Leica Microsystems, Mannheim, Germany).

Cell attachment assays - Plates (96-well) were plated at 5000 cells per well (96-well plate) for 0 min, 7 min, 15 min or 30 min. Medium and unattached cells were aspirated. Attached cells were fixed in 3% paraformaldehyde for 10 min, rinsed with PBS three times, and stained with SulfoRhodamine B (SRB assay kit, Sigma). Data were quantified by spectrophotometry at 492 nm. At time 0, no cell was attached.

Sphere formation and migration - Sphere formation experiments were performed by incubating 5000 cells by well in a 96-wells plate previously coated with 50 µl of 1.5% agar gel. For sphere dissociation/migration, spheres of the same size (obtained by incubating 5000 of each cell types for 48 hrs) were put on a 22-mm coverslip (Rempel et al., 2001) and incubated for 48 hrs. Then, spheres were fixed with 4% paraformaldehyde for 20 min at room temperature. Cell actin (phalloidin-FITC) and nucleus (Hoechst) were thus stained and visualized as previously described (Dejeans et al, 2012). To parameters were measured: the

size of the resulting sphere after 48 hrs of cell migration from the sphere, and the migrating distance of cells from the center of each sphere.

Intracranial injections, tumor size, and blood capillary measurements - Two independent sets of experiments were carried out using Rag ɣ mice. The protocol used was as previously described ([15]). Cell implantations were at 2 mm lateral to the bregma and 3 mm in depth using seven different sets of cells for U87-EV cells, U87-WT cells, U87-S769F cells, U87-Q780* cells, U87-P336L cells, U87-A414T cells and U87 IRE1.NCK DN cells. Fifteen days post injection, or at first clinical signs, mice were sacrificed, brains were frozen and sliced using a cryostat. Brain sections were stained using H&E staining or Anti-vimentin antibodies (Interchim) for visualization of tumor masses. Tumor volume was then estimated by measuring the length (L) and width (W) of each tumor and was calculated using the following formula ($L \times W^2 \times 0.5$). CD31-positive vessels were numerated after immunohistologic staining of the vascular bed using rat antibodies against CD31 (PharMingen) and fluorescent secondary antibodies (Interchim). Imaging was carried out using a Axioplan 2 epifluorescent microscope (Zeiss) equipped with a digital camera Axiocam (Zeiss). Blood vessels were quantified by two independent investigators. Vessels number was measured in 12 to 20 thresholded images per condition using ImageJ software. This quantification was made three times for each image and three vessels size (surface) were reported: between 100 pixel² and 500 pixels², more than 500 pixel² or more than 5000 pixel² (1 pixel = 0.67112477 µm). The average of vessel number of each size was calculated per brain. Experiments were repeated on five Rag-gamma mice for each condition.

Biomass analysis (SRB) - The SRB assay was performed as previously described (Vichai and Kirtikara, 2006). Briefly, cells were seeded into 96-well plates in 100 µL at a density of 5000 cells/well. After cell inoculation, the plates were incubated at 37°C with 5% CO2 for 24, to 96 hrs. Cell were then fixed *in situ* with trichloroacetic acid and stained with sulforhodamine B (Sigma). Absorbance was measured at 510 nm.

Soft-agar colony-forming assay - IRE1 mutant or wild-type (WT)–expressing cells or control cells (20,000) were plated onto six-well plates in DMEM containing 10% FBS and 0.2% agar (overlay) onto the top of an agar underlay (DMEM containing 10% FBS and 0.4% agar). Cells were fed after 5 days with 1.5 mL of overlay, and the colonies were counted after 10 days of incubation under a light microscope at ×20 magnification. Twenty different fields were scored from each well by two independent investigators. Assays were carried out in duplicate and the results were expressed as mean ± SD.

Statistical analyses - Data are presented as mean ± SD or SEM. Statistical significance ($p<0.05$ or less) was determined using a paired or unpaired t test or ANOVA as appropriate and performed with GraphPad Prism software (GraphPad Software, San Diego, CA, USA).

ACKNOWLEDGEMENTS

This work was funded by grants from Institut National du Cancer (INCa), Inserm (Avenir), and Ligue Contre le Cancer (Comité des Landes, LARGE project) to EC. SL was funded by a PhD scholarship from the French government and by a scholarship from the Fondation pour la Recherche Médicale. ND was funded by a post-doctoral fellowship from the Fondation de France. The French tumorothèque graciously gave GBM tumor samples.

Figure S1

Sequence alignment of IRE1 proteins reveals that Pro[336] and Ser[769] residues but not Ala[414] are well conserved in IRE1 proteins. Numbers refer to residue positions in human IRE1α protein (ERN1); D. melanogaster, fly; C. elegans, worm; S. cerevisiae, yeast.

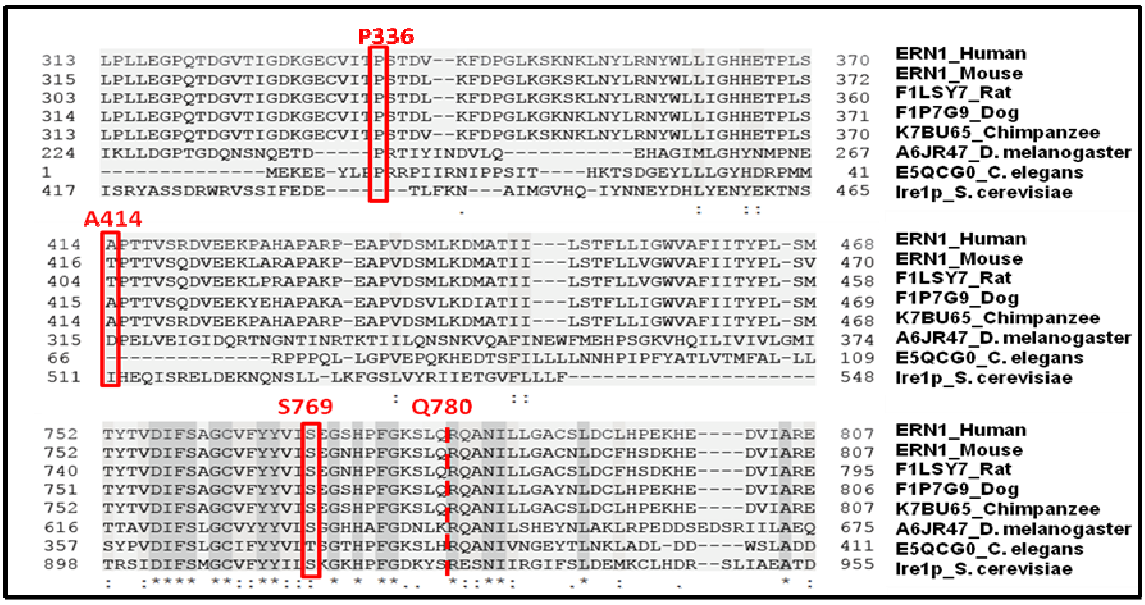

Figure S2

A. DSP-mediated in vivo cross-linking of IRE1 proteins in mutant expressing U87 cells. Anti-IRE1alpha immunoblot under both reduced (top) and non reduced (bottom) revealed IRE1alpha oligomerization in basal conditions due to over expression of WT, P336L and A414T but not S769F nor Q780 IRE1alpha variant proteins. B. EtBr-stained agarose gel of XBP1 cDNA amplicons corresponding to unspliced (XBP1u) and spliced (XBP1s) forms of XBP1 mRNA revealed XBP1 splicing in basal conditions or upon tunicamycin treatment (TUN, 5µg/mL for 6 hrs). C. Analysis of mRNA expression in U87 cells expressing mutant IRE1alpha proteins (normalized to 18S). CHOP: C/EBP homologous protein; ORP150: Oxygen-regulated protein 150; GRP94: Glucose related protein of 94 kDa; BiP(GRP98): Binding immunoglobulin protein. Two independent biological samples were used. Data are means +/− SD.*

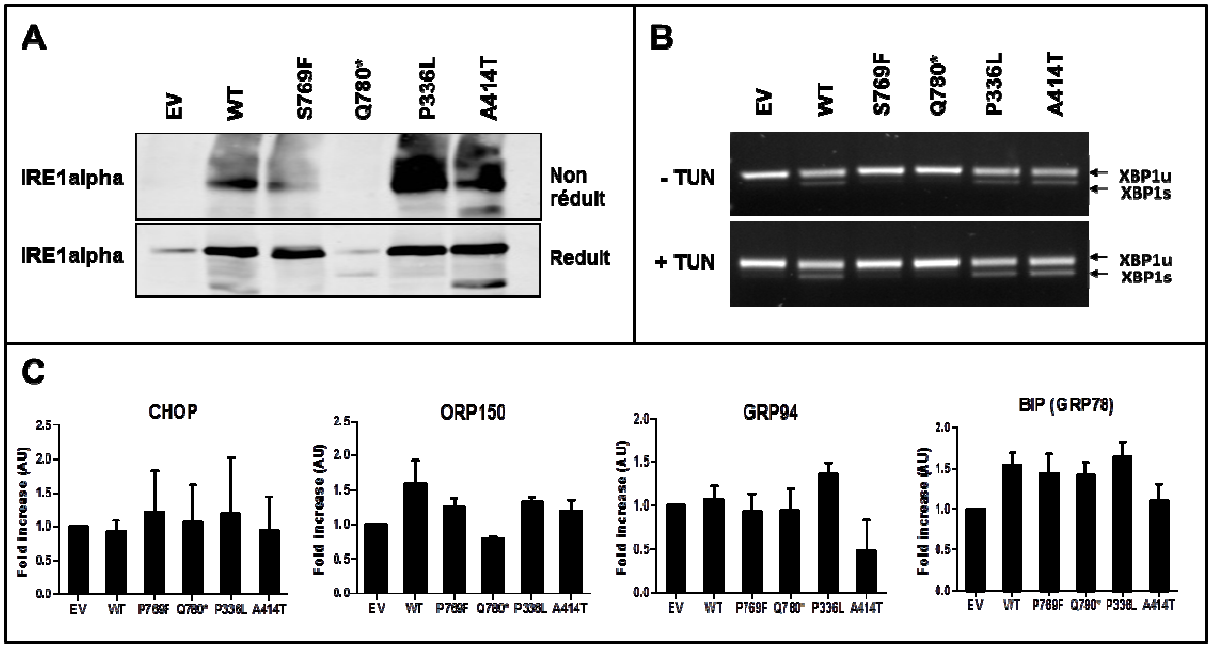

Figure S3

A. Bar graph representing the doubling time of U-87 MG population for each condition. B. Bar graph representing cells' adhesion rate established by measuring number of adherent cells at 0 min, 7 min, 15 min and 30 min post-seeding. C. Representative imaging of the neurosphere phenotypes at 6 hrs and 48 hrs post-seeding in agar coated well of a 96-well plate. The curve representation of the neurosphere size along 48 hrs did not reveal any significant differences in terms of cell aggregation and adhesion. Bar graphs represent neuroshere size at 6 hrs post-seeding (top) and of the rate of neurosphere formation (bottom). All data shown are mean ± SEM of at least three bio logical replicates.

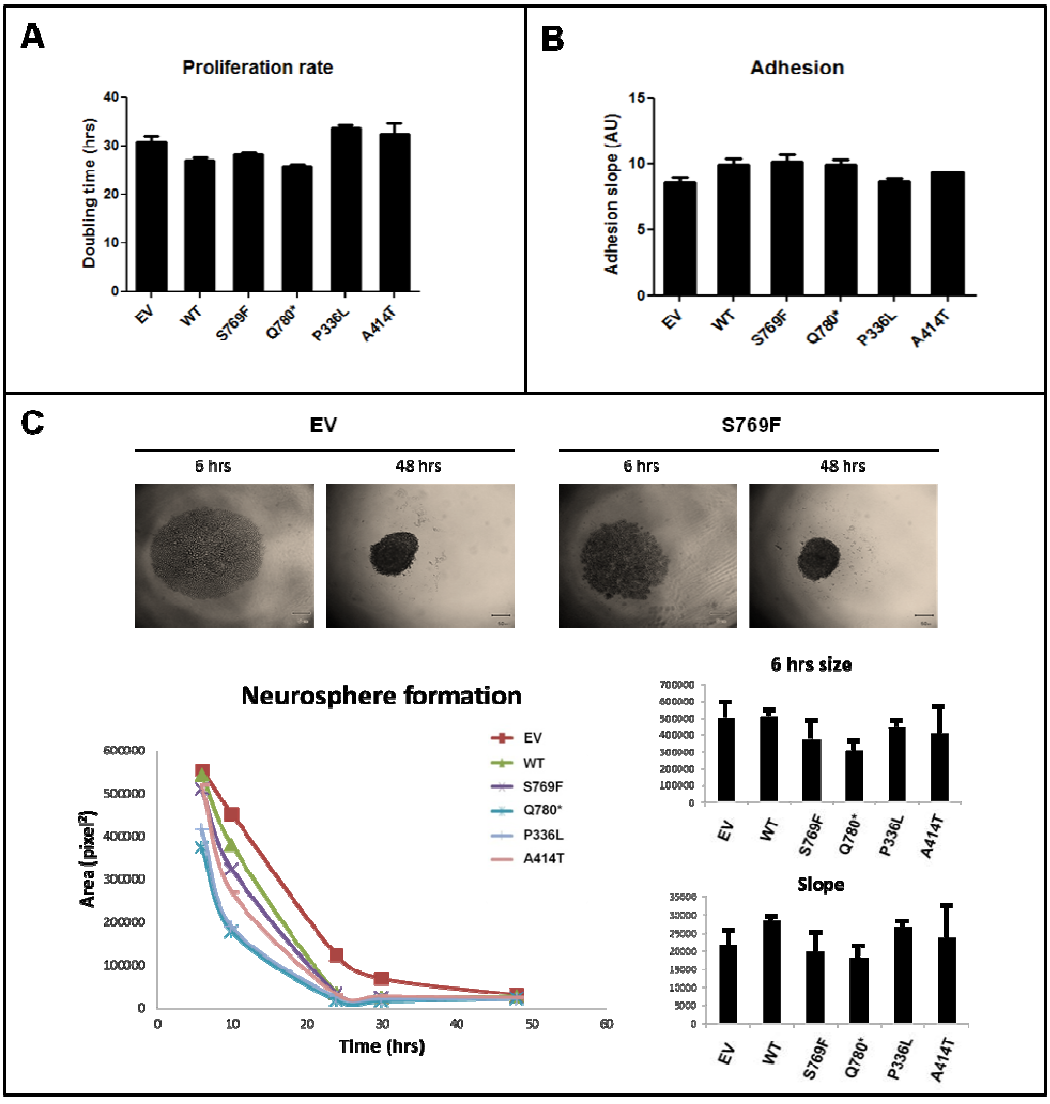

Figure S4:

A. KEGG representation of the glioma specific signaling pathways. Yellow boxes represent actors of glioma specific signaling(regulated by IRE1alpha. B. Immunoblot analysis performed on U87 cells expressing IRE1alpha variants lysates revealed PDGFRb and p53 but not pERK, ERK, pAKT, AKT nor p21 overexpression induced by P336L mutation. Calnexin (CANX) is used as loading control. C. Luminescent reporter of p53 (Qiagen) revealed p53 inactivation by P336L-IRE1α overexpression. Data are represented as means ±SD of at least three independent replicates.

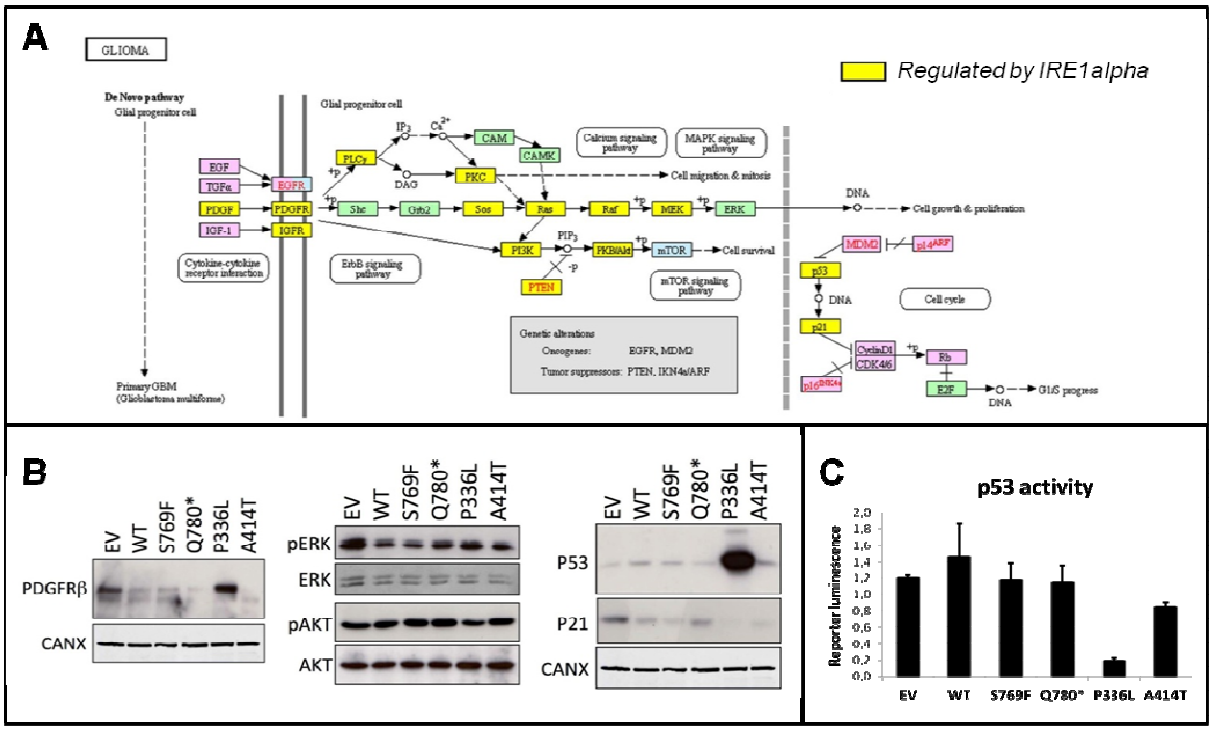

REFERENCES

1. Anton, K., J.M. Baehring, and T. Mayer, *Glioblastoma multiforme: overview of current treatment and future perspectives.* Hematol Oncol Clin North Am, 2012. **26**(4): p. 825-53.
2. Louis, D.N., et al., *The 2007 WHO classification of tumours of the central nervous system.* Acta Neuropathol, 2007. **114**(2): p. 97-109.
3. Stupp, R., et al., *Radiotherapy plus concomitant and adjuvant temozolomide for glioblastoma.* N Engl J Med, 2005. **352**(10): p. 987-96.
4. (TCGA), T.C.G.A., *Comprehensive genomic characterization defines human glioblastoma genes and core pathways.* Nature, 2008. **455**(7216): p. 1061-8.
5. Parsons, D.W., et al., *An integrated genomic analysis of human glioblastoma multiforme.* Science, 2008. **321**(5897): p. 1807-12.
6. Greenman, C., et al., *Patterns of somatic mutation in human cancer genomes.* Nature, 2007. **446**(7132): p. 153-8.
7. Xue, Z., et al., *A conserved structural determinant located at the interdomain region of mammalian inositol-requiring enzyme 1alpha.* J Biol Chem, 2011. **286**(35): p. 30859-66.
8. Ron, D. and P. Walter, *Signal integration in the endoplasmic reticulum unfolded protein response.* Nat Rev Mol Cell Biol, 2007. **8**(7): p. 519-29.
9. Urano, F., et al., *Coupling of stress in the ER to activation of JNK protein kinases by transmembrane protein kinase IRE1.* Science, 2000. **287**(5453): p. 664-6.
10. Han, D., et al., *IRE1alpha kinase activation modes control alternate endoribonuclease outputs to determine divergent cell fates.* Cell, 2009. **138**(3): p. 562-75.
11. Calfon, M., et al., *IRE1 couples endoplasmic reticulum load to secretory capacity by processing the XBP-1 mRNA.* Nature, 2002. **415**(6867): p. 92-6.
12. Yoshida, H., et al., *XBP1 mRNA is induced by ATF6 and spliced by IRE1 in response to ER stress to produce a highly active transcription factor.* Cell, 2001. **107**(7): p. 881-91.
13. Hollien, J., et al., *Regulated Ire1-dependent decay of messenger RNAs in mammalian cells.* J Cell Biol, 2009. **186**(3): p. 323-31.
14. So, J.S., et al., *Silencing of lipid metabolism genes through IRE1alpha-mediated mRNA decay lowers plasma lipids in mice.* Cell Metab. **16**(4): p. 487-99.
15. Auf, G., et al., *Inositol-requiring enzyme 1alpha is a key regulator of angiogenesis and invasion in malignant glioma.* Proc Natl Acad Sci U S A, 2010. **107**(35): p. 15553-8.
16. Dejeans, N., et al., *Autocrine control of glioma cells adhesion and migration through IRE1alpha-mediated cleavage of SPARC mRNA.* J Cell Sci, 2012. **125**(Pt 18): p. 4278-87.
17. Pluquet, O., et al., *Posttranscriptional regulation of PER1 underlies the oncogenic function of IREalpha.* Cancer Res, 2013. **73**(15): p. 4732-43.
18. Drogat, B., et al., *IRE1 signaling is essential for ischemia-induced vascular endothelial growth factor-A expression and contributes to angiogenesis and tumor growth in vivo.* Cancer Res, 2007. **67**(14): p. 6700-7.
19. database, N.g., *ERN1 endoplasmic reticulum to nucleus signaling 1 [Homo sapiens (human)]*. 2013, NCBI gene database.
20. Auf, G., et al., *High epiregulin expression in human U87 glioma cells relies on IRE1alpha and promotes autocrine growth through EGF receptor.* BMC Cancer, 2013. **13**: p. 597.

activités RNase d'IRE1α soit l'activité RIDD, l'épissage de XBP1 et la dégradation de miR. Deux procédés ont été particulièrement pertinents pour découpler ces activités: l'utilisation d'inhibiteurs sélectifs [7, 118, 162] ou la caractérisation de mutation dirigées [119, 163, 164] ou naturelles [165].

L'ensemble de ces résultats confirment l'implication d'IRE1α dans le développement des GBM, mais ils soulignent également la complexité du rôle joué par IRE1α dans ce type de cancer.

❖ Impact des mutations sur la structure d'IRE1α

Trois mutations somatiques présentes sur le gène IRE1α dans les GBM ont été décrites dans la littérature, dont deux mutations prédites pour avoir un effet initiateur de tumeur (S769F et Q780*) [159] et la troisième (P336L) exclue de l'étude sur le caractère initiateur de tumeur car étant survenue dans une tumeur préalablement traitées par chimiothérapie (TMZ) [154, 159]. Nous avons pu identifier une quatrième mutation somatique dans les GBM, la mutation A414T, en analysant la séquence des exons du gène codant pour IRE1α dans 23 GBM humains (**ARTICLE 5, Figure 1**). Cette fréquence d'environ 4% d'échantillons qui contiennent des mutations d'IRE1α a également été retrouvée dans d'autres études de séquençage massif de l'ADN génomique de tumeurs, qui ont permis de mettre en évidence d'autres mutations d'IRE1α [156]. Ainsi, des études de séquençage d'IRE1α à plus grande échelle devraient permettre l'identification de nouvelles mutations d'IRE1α et ainsi fournir de nouvelles pistes entre IRE1α et GBM. Afin d'augmenter la pertinence de notre approche nous proposons aussi de séquencer les exons du gène codant pour IRE1α dans 25 lignées primaires de glioblastome humain (obtenues gracieusement grâce au Dr V. Quillien, Rennes).

Les mutations étudiées ici concernant des mutations substituant à l'acide aminé d'origine un acide aminé aux propriétés différentes, voire une mutation tronquante, nous pouvons penser qu'elles induisent des modifications structurelles importantes. Leur localisation dans une modélisation de la structure d'IRE1α est représentée ci-dessous (**Figure 16**).

La mutation stop Q780* est la mutation dont l'effet structurel est le plus facile à anticiper. En effet, le codon stop se forme dans le dernier tiers du domaine kinase, ce qui provoque la perte de la boucle de régulation de l'activité kinase (P830, [165]), la perte du domaine d'activité RNase et la perte du domaine C-terminal, site potentiel d'interaction de constituants de l'UPRosome.

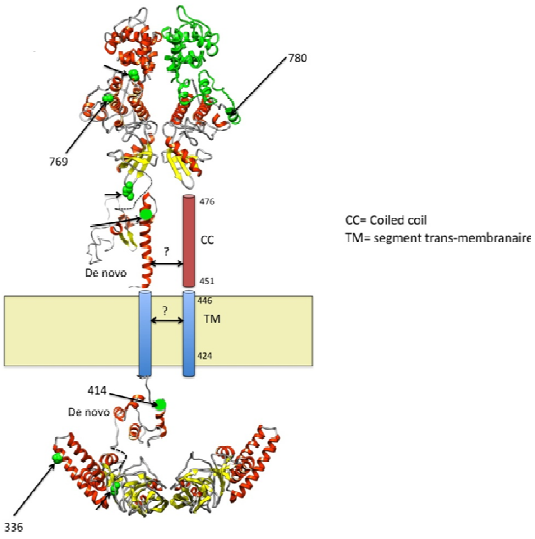

Figure 16: Modélisation de la structure d'un dimère IRE1α
Les mutations sont localisées par des points verts. Modèle par Rémi Fronzes.

La deuxième mutation qui provoque une altération dans le domaine cytosolique d'IRE1α induit le remplacement d'une sérine en phénylalanine, soit l'introduction d'un acide aminé hydrophile phosphorylable à la place d'un acide aminé aromatique hyprophobe, ce qui peut entraîner des changements conformationels importants. Bien que cet acide aminé ne soit pas situé près des éléments clés du domaine kinase (K599: site de liaison à l'ATP et D688: accepteur de proton), cette modification pourrait altérer la conformation de la poche de fixation du nucléotide importante pour **i)** les activités kinase et RNase, par un enchainement de changements de conformation [118] et **ii)** l'oligomérisation [166]. Une étude précédente a modélisé cette mutation et conclu que celle-ci affectait probablement la stabilité et l'activation du domaine kinase [165].

La mutation P336L entraîne le changement d'une proline en leucine, donc bien que ce soit la seule mutation impliquant deux acides aminés assez semblables (hydrophobes, aliphatiques) elle devrait induire des changements de conformation majeurs, du fait que la proline induit un coude qui modifie l'axe de la protéine. En outre, un acide aminé proche, la cystéine C332, a été impliquée dans la formation de ponts disulfures qui contribuent à la stabilisation des oligomères IRE1α [167]. L'oligomérisation d'IRE1α étant l'étape préliminaire à l'activation de ses domaines kinase et RNase (**Figure 17**), cela implique que cette mutation P336L semble située dans un domaine clé de régulation de l'activité IRE1α et qu'elle puisse moduler la stabilité des oligomères. Cette hypothèse que la mutation P336L intervient dans une zone clé de la régulation d'IRE1α est étayée par le fait que c'est la seule mutation qui ait

été identifiée à ce jour dans plusieurs échantillons de tumeurs, provenant de patients atteints de cancers différents, soit deux cancers intestinaux et un GBM [90].

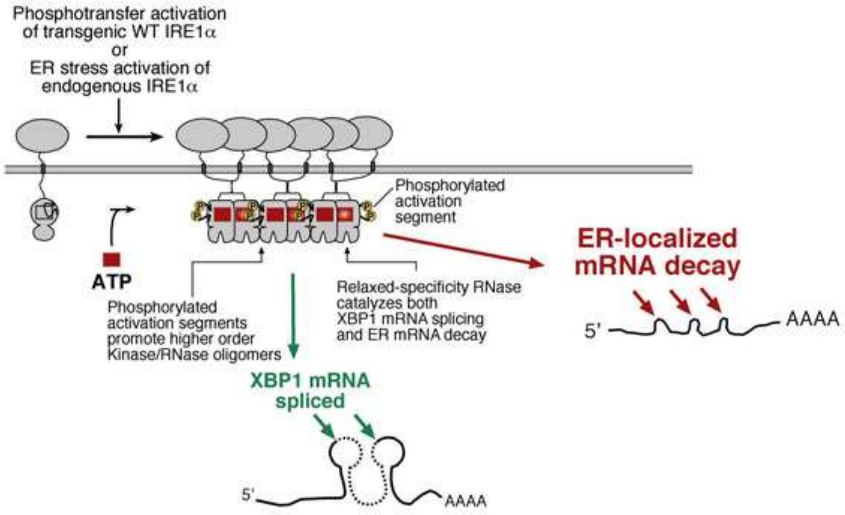

Figure 17: Schéma de l'activation par oligomérisation d'IRE1α
Han et al, 2009 [7].

La deuxième mutation identifiée dans le domaine luminal d'IRE1α, A414T, pourrait induire des modifications de structure importantes, puisqu'elle provoque le changement d'une alanine (aliphatique hydrophobe) en thréonine (hydrophile).

Bien que ces deux mutations cytosoliques P336L et A414T ne semblent pas faire partie du domaine fonctionnel d'oligomérisation [168], ou du site de liaison avec la protéine chaperonne BiP (acides aminés 307-334) [94, 167], elles pourraient toutes deux altérer la formation et la stabilité des oligomères IRE1α **i)** en modifiant les propriétés physiques du domaine d'oligomérisation, **ii)** en déstabilisant la liaison avec les partenaires luminaux qui empêchent cette oligomérisation (BiP) et **iii)** en favorisant la liaison avec les éventuels partenaires luminaux qui stabilisent les complexes oligomériques d'IRE1α. Ces partenaires luminaux pourraient être des protéines mal conformées, comme cela a été montré dans le cas de Ire1p (levure) [169] (**Figure 18 A**) ou d'IRE1β (ERN2) [170], isoforme d'IRE1α (ERN1) dont l'expression est restreinte aux tissus intestinaux. L'alignement de séquence entre ces deux isoformes permet d'ailleurs de constater que la proline P336 est localisée dans un domaine conservé (**Figure 18 B**), qui pourrait éventuellement lier les protéines mal conformées.

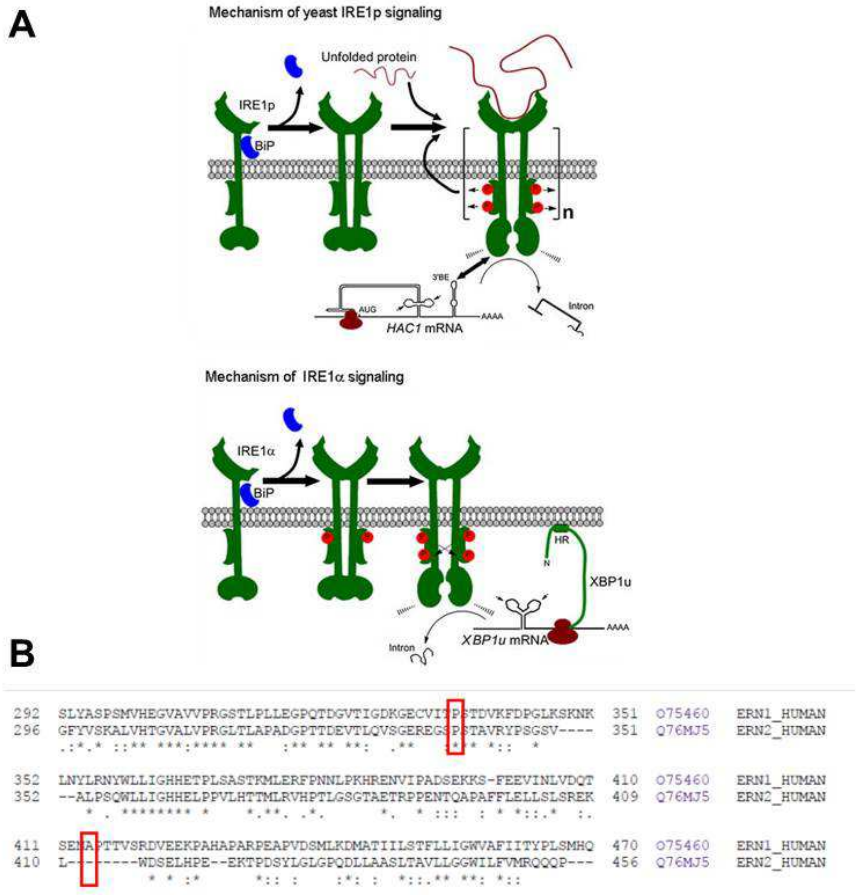

Figure 18: Ire1p et IRE1β peuvent lier les protéines mal conformées.
A. Schéma comparatif de l'activation d'IRE1 chez la levure et chez l'Homme. *Hetz, 2012 [8]*.
B. Alignement de la séquence des domaines luminaux d'IRE1α (ERN1) et IRE1β (ERN2).
Les encadrés rouges indiquent les acides aminés P336 et A414 d'IRE1α.

En plus de ces quatre mutations, une mutation silencieuse a été identifiée dans un prélèvement de GBM, la mutation P319P [153]. Bien que nous ayons choisi ici de focaliser notre étude sur la caractérisation des mutations non silencieuses, le nombre croissant de mutations silencieuses identifiées dans le gène d'IRE1α suggère aussi qu'elles pourraient avoir un rôle dans la fonctionnalité d'IRE1α, comme cela a été établie pour d'autres protéines [171], et ainsi dans le développement des GBM.

❖ <u>Impact des mutations sur la signalisation IRE1α</u>

Comme nous l'avons vu précédemment, la surexpression de la protéine IRE1α sauvage suffit à induire son activation (**Figure 17,** [7]) et la présence des mutations étudiées a un impact sur la signalisation proximale d'IRE1α: les mutations cytosoliques S769F et Q780*

diminuent significativement l'activation basale d'IRE1α induite dans notre modèle de surexpression, tandis que les mutations P336L et A414T semblent potentialiser cette activation basale (**ARTICLE 5, Figure 3**), notamment en favorisant la formation ou la stabilité des oligomères d'IRE1α. Ces effets peuvent d'ailleurs être dus soit à un effet sur la stabilité et donc l'expression d'IRE1α, soit modifier les propriétés d'IRE1α sans altérer son expression ou sa localisation. De ces données, nous pouvions anticiper que les mutations S769F et Q780* étaient des mutations entraînant une perte de fonction d'IRE1α, tandis que les mutations P336L et A414T semblaient être au contraire des mutations entraînant un gain de fonction. Cependant, si les résultats obtenus pour l'épissage de XBP1 sont cohérents avec cette hypothèse, les résultats sur la mesure de l'activité RIDD nous obligent à modérer ce schéma. En effet, la surexpression même d'IRE1α, dans notre modèle, n'a pas le même impact sur toutes les cibles du RIDD, sous-entendant que cette surexpression entraîne bien une activation d'IRE1α (Figure 17, [7]) mais qui semble différente de l'activation d'IRE1α endogène par un stress du RE, au moins en ce qui concerne la sélectivité des ARNm dégradés par le RIDD (**Figure 19**). Ces résultats apportent donc un nouvel exemple du découplage qui existe entre les différentes activités RNases d'IRE1α, et dont les études menées chez la levure soulignent l'importance. En effet, si la caractérisation de l'épissage de l'équivalent levure de XBP1, HAC1, a pu être mis en évidence chez *S. cerevisae*, il n'a pas lieu chez *S. pombe*, alors qu'à l'inverse, le RIDD mis en évidence chez *S. pombe* n'est pas présent chez *S. cerevisae*.

Figure 19: Variations d'expression de substrats du RIDD
Représentation en cluster de l'effet des mutations sur la stabilité des ARNm de substrats du RIDD (qPCR) après traitement à l'actinomycine D. Cette représentation permet d'apprécier l'ensemble des variations, significatives ou non, de la stabilité des substrats du RIDD dans nos différentes conditions. Nous pouvons constater que la surexpression d'IRE1α-WT ou des mutants a toujours tendance à déstabiliser ces substrats par rapport aux conditions contrôles (EV), sauf pour quelques substrats (SCARA3 et PDGFRβ pour le mutant A414T, et SPARC et PER1 pour le mutant P336L).

De plus, pour les substrats du RIDD affectés par la surexpression d'IRE1α, les mutations ont des effets sélectifs: une même mutation peut avoir un effet opposé sur deux substrats du RIDD. C'est le cas par exemple de la mutation A414T qui stabilise l'ARNm de SCARA3 et favorise au contraire la dégradation de l'ARNm de PER1. Les mécanismes d'adressage des ARNm cibles à la membrane du RE, et en particulier à IRE1α sont à ce jour méconnus. L'hypothèse la plus répandue est que cet adressage se fasse peut après la synthèse des ARNm, soit directement lors de leur export au niveau des pores nucléaires [106, 107], soit lors de leur traduction au niveau des ribosomes attachés à la membrane du RE (pour les protéines de la voie de sécrétion). Il est également probable que des partenaires protéiques encore inconnus soient impliqués dans l'adressage de ces ARNm à IRE1α, facteurs dont par exemple la liaison à IRE1α pourrait expliquer la sélectivité de dégradation de certains ARNm. Dans cette idée, les mutations pourraient altérer la liaison de ces partenaires à IRE1α, soit par une modification de l'accessibilité du site de liaison, soit par une altération de ce site. Il est également possible que cet adressage dépende de l'abondance relative de chacun des ARNm cibles, abondance qui pourrait, dans notre cas, être modifiée par l'activation d'IRE1α. Ainsi, en altérant les voies de signalisation en aval d'IRE1α, en particulier la cinétique d'activation de cibles transcriptionnelles, elles pourraient modifier l'abondance de substrats du RIDD et ainsi leur clivage par IRE1α et donc leur stabilité. Des études transcriptomique sont en cours de réalisation, qui pourraient nous permettre de mieux comprendre les mécanismes de régulation de cette dégradation sélective de substrats du RIDD dans notre modèle. Des molécules et des mutations ont été identifiées qui permettent l'inhibition sélective de l'épissage de XBP1 ou du RIDD [6, 7]. Il serait intéressant d'utiliser ces inhibiteurs afin de découpler les activités RNase d'IRE1α et de caractériser pour chaque mutation l'effet de l'épissage de XBP1 indépendamment de l'effet sur le RIDD, et vice versa.

Des expériences sont en cours de réalisation qui nous permettront de définir l'impact des mutations sur la signalisation en aval de l'activité kinase d'IRE1α (phosphorylation de JNK, ERK) ainsi que sur les signalisations clés de la croissance tumorale et de l'angiogenèse (EREG, VEGF) dépendantes d'IRE1α.

- ❖ Impact des mutations sur la formation des tumeurs dans un modèle de greffe orthotopique chez la souris

Une greffe orthotopique chez la souris de cellules de GBM contrôle (U87-EV) ou dont la signalisation d'IRE1α a été bloquée (U87-DN) constitue un modèle intéressant pour caractériser l'impact de la signalisation IRE1α sur la formation et le développement de

tumeurs cérébrales [157]. La greffe de U-87 MG exprimant de façon stable les formes sauvage (U87-WT) ou mutées (U87-S769F, U87-Q780*, U87-P336L ou U87-A414T) d'IRE1α a permis de déterminer que les mutations P336L et A414T ont un effet très important sur le développement tumoral par rapport à la condition contrôle mais également par rapport à la surexpression de la forme sauvage d'IRE1α, effet développé ci-après. Les mutations S769F et Q780*, pour lesquelles nous avons mesuré une diminution de la phosphorylation d'IRE1α et de l'épissage de XBP1 par rapport à la condition WT *in vitro*, abrogent l'effet de la surexpression d'IRE1α, puisque **i)** les tumeurs formées 15 jours après la greffe ont une taille est une vascularisation similaires aux tumeurs contrôles (**ARTICLE 5, Figure 4**), et que **ii)** les souris ayant reçues les U87-EV, les U87-S769F et les U87-Q780* ne présentent pas de différences significatives de survie, ni de différences de phénotype des tumeurs développées (**ARTICLE 5, Figure 4**). Il est surprenant que ces deux mutations, qui comprennent pourtant une mutation tronquante (Q780*) donc un effet visible sur les domaines catalytiques d'IRE1α, n'aient pas d'effets significatifs sur la progression tumorale dans notre étude. Ceci pourrait refléter les limites de notre modèle d'étude. En effet, ces mutations, tout comme la mutation P336L, peuvent avoir des effets pro-tumoraux dans un contexte bien particulier. Elles peuvent, par exemple, conférer un avantage sélectif aux cellules tumorales soumises aux traitements anti-cancéreux comme la radiothérapie ou la chimiothérapie, comme le suggère les expériences préliminaires de résistance à la mort induite par le TMZ (**Figure 20**). Ainsi, ces mutations pourraient augmenter les capacités d'adaptation de ces cellules à un stress aigu du RE.

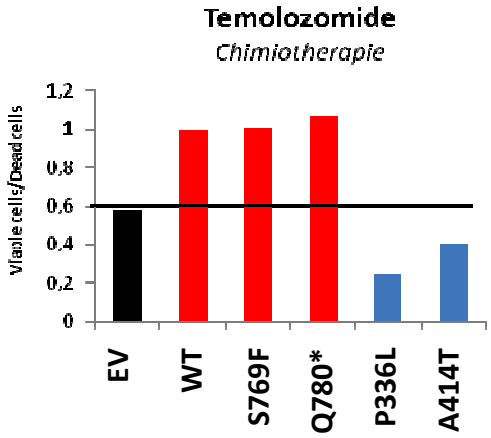

Figure 20: Impact des mutations d'IRE1α sur la résistance au TMZ
Les cellules sont traitées pendant 24h avec du DMSO (contrôle) ou du TMZ (150 µM) puis la viabilité et la cytotoxicité sont mesurées simultanément (kit multitox, Promega). Le ratio viabilité/cytotoxicité nous informe que la surexpression d'IRE1α WT ou des mutants S769F et Q780* confère une résistance à la mort induite par le TMZ.

Lors de l'implantation des U87-P336L dans le cerveau des souris, aucune tumeur n'est formée, ce qui suggère que cette mutation altère le potentiel tumorigène *in vivo* des U-87 MG. Des recherches complémentaires seront nécessaires pour comprendre l'impact de cette mutation sur la formation de tumeurs, mais nous pouvons d'ores et déjà faire l'hypothèse que cette mutation affecte particulièrement la capacité des U-87 MG à s'implanter dans le cerveau des souris. Ceci pourrait notamment être dû à des modifications de facteurs remodelant la matrice extracellulaire et donc le cytosquelette et les adhésions intercellulaires. Les effets de cette mutation ne sont pour l'instant que mesurables *in vivo*, puisque les tests effectués *in vitro*, soit par un modèle de formation de neurosphères et de migration à partir de ces sphères, soit par la mesure d'attachement au substrat, ne nous ont pas permis de mettre en évidence des différences significatives entre les U87-EV, les U87-WT et les U87-P336L (**ARTICLE 5, Figure S3**). Cette mutation n'ayant pas été définie comme initiatrice de tumeur, elle pourrait également ne fournir un avantage sélectif aux cellules tumorales que dans le contexte d'autres mutations, par exemple de l'EGFR [115], ou se révéler avantageuse en induisant des mécanismes de résistance aux chimiothérapies [154].

Une autre explication possible serait l'augmentation de l'expression dans ces cellules d'un facteur suppresseur de tumeur, comme par exemple p53. En effet, si de nombreuses études relatent les dérégulations pro-oncogéniques des cibles d'IRE1α (NFkB, PTEN, etc., **ARTICLE 1**), de plus en plus de travaux avancent un rôle anti-tumoral de l'UPR, vraisemblablement dû au dépassement d'un seuil de stress cellulaire qui fait basculer l'UPR d'une réponse pro-survie à une réponse pro-mort. Nous avons effectivement mesuré une augmentation de p53 dans les cellules U87-P336L, mais la participation de cette surexpression (ou stabilisation) de p53 au phénotype observé reste à définir, puisqu'elle n'entraîne pas une augmentation de l'activité de p53 (**ARTICLE 5, Figure S4**).

Les données de la littérature suggèrent que la mutation P336L pourrait perturber de façon critique le fonctionnement de la protéine IRE1α et conférer ainsi un avantage sélectif aux cellules cancéreuses. Or, de façon intéressante, nos travaux montrent que l'expression de cette mutation semble modifier le phénotype de ces cellules, avec l'acquisition d'un phénotype pseudo-épithélial (données non montrées), qui reste à caractériser. La modification des propriétés d'organisation de ces cellules pourraient expliquer en partie les effets constatés *in vivo*.

La mutation A414T, quant à elle, n'avait jamais été mise en évidence comme une mutation somatique: bien qu'identifiée dans les analyses précédemment réalisées, elle avait été définie comme SNP (Single nucleotide polymorphism) [153, 154]. Cependant, la

comparaison avec un tissu sain nous a permis de mettre en évidence cette mutation dans notre étude, mutation qui semble pertinente puisque nos travaux ont révélé que cette mutation apporte un avantage sélectif aux cellules tumorales *in vivo*, en induisant une croissance plus rapide des tumeurs issues des U-87 MG chez les souris, ainsi qu'une vascularisation plus importante dans ces tumeurs comparé aux tumeurs formées à partir des U87-WT (**ARTICLE 5, Figure 4**). Ceci aboutit à une mortalité plus importante des souris après l'implantation de ces cellules U87-A414T, et les vaisseaux développés au sein de ces tumeurs ont une taille bien plus importante que les vaisseaux mesurés dans les autres conditions. Il semblerait que l'effet de cette mutation passe dans ce cas par une augmentation de la signalisation pro-angiogénique qui confèrerait un avantage prolifératif aux tumeurs U87-A414T, plus qu'une réelle augmentation des capacités de prolifération, puisqu'aucune augmentation de la prolifération de ces cellules n'a été mesuré *in vitro* (**ARTICLE 5, Figure S3**). Cette hypothèse est également étayée par le fait que les tumeurs formées à partir des U87-A414T à jour 15 (J15) après la greffe orthotopique ne présentent pas d'augmentation de taille significative par rapport aux conditions contrôles, ni un nombre plus important de vaisseaux. Nous avons toutefois constaté que ces tumeurs présentent un remodelage important des vaisseaux sanguins, avec l'apparition de longs vaisseaux fins sur lesquelles les cellules tumorales co-optent (**ARTICLE 5, Figure 4**), formant une excroissance qui ressemble aux prémices de la migration observée dans les tumeurs formées à partir des U87-DN (**ARTICLE 5, Figure 4**; [157]).

La plupart des tumeurs ont, à J15, un phénotype différent de celui présent lors du sacrifice des animaux donc lors de l'apparition des signes cliniques. En effet, les tumeurs développées jusqu'aux signes cliniques sont des tumeurs de forme sphérique dont le contour est régulier. La seule condition pour laquelle le phénotype des tumeurs est de type infiltrant ou mésenchymateux est la condition DN. Au contraire, à J15, les tumeurs sont majoritairement sous forme d'ellipsoïdes irréguliers, avec quelques fois la présence de points d'infiltration très proches de la tumeur principale. Toutefois, ces pseudo-infiltrats ne sont pas présents dans toutes les coupes de tumeurs observées. Cette grande variabilité dans la taille, la forme et l'infiltration des tumeurs développées 15 jours après l'implantation des cellules ne permet pas de conclure quant au rôle des mutations dans l'acquisition d'un phénotype précoce particulier, et nécessiterait une étude plus globale des tumeurs formées, par exemple en marquant l'ensemble de la tumeur en trois dimensions par des billes d'or.

❖ Conclusions et perspectives

De façon intéressante, on peut noter que sur les quatre mutations somatiques qui ont fait l'objet de notre étude, ce sont les mutations localisées dans le domaine luminal d'IRE1α dont l'impact a pu être mesuré ici.

Bien que ces résultats ne permettent pas de confirmer le rôle initiateur de tumeur des mutations prédites comme telles par des analyses bioinformatiques, ils ne permettent pas non plus d'infirmer cette prédiction. En effet, deux expériences clés restent à réaliser pour compléter ces résultats: l'expression inductible de ces mutants, ainsi que l'expression de ces mutants dans des cellules non cancéreuses.

En effet, le potentiel oncogénique des mutants réside par définition dans les capacités de ces mutations à faire basculer la cellule d'une cellule non transformée à une cellule cancéreuse. Leur expression dans des cellules cérébrales immortalisées mais non transformées comme par exemple des astrocytes humains normaux immortalisées (NHA-TS) [172] permettrait de déterminer si ces mutations promeuvent la carcinogenèse. Du fait de problèmes techniques, je n'ai pas eu la possibilité de mener ces expériences et ainsi conclure quant au rôle initiateur de tumeur de ces mutations. Cependant, j'ai pu réaliser des expériences préliminaires indiquant que les mutations S769F, Q780*, P336L et A414T peuvent être exprimées de façon stable dans un tel modèle cellulaire.

En outre, une surexpression inductible des mutants permettrait d'étudier l'effet des mutations à un instant donné, sans que les cellules ne se soient adaptées à ces mutations, et permettrait de mesurer l'impact précoce de ces mutations sur la fonctionnalité de la cellule.

De même, il serait intéressant de répéter ces études non plus dans un contexte de surexpression d'IRE1α qui aboutit à une activation basale de la protéine, mais dans un contexte de mutation mono-allélique par des expériences d'édition du génome (TALEN ™, CRISPR/Cas9) qui mimeraient plus fidèlement le contexte de mutation hétérozygote dans lequel toutes les mutations d'IRE1α ont été identifiées.

Ce travail sera complété par des études de migration avec des techniques d'imagerie individuelle des cellules (IBIDI) ainsi que par des études transcriptomiques permettant de déterminer les cibles et les voies de signalisation altérées par la présence de mutations d'IRE1α et ainsi établir une signature propre à chaque mutation, expériences qui sont en cours de réalisation.

Le modèle murin de formation des GBM a été très utile pour établir l'importance de la signalisation d'IRE1α dans ces tumeurs [156], cependant il présente des limites majeures. En effet, l'injection intracrânienne, donc la greffe orthotopique, de cellules dérivées de GBM

humain, les U-87 MG, entraîne la formation d'une tumeur dont les caractéristiques sont bien plus pertinentes qu'une tumeur formée à partir de ces mêmes cellules lors d'une greffe hétérotopique sous-cutanée. Cependant, il est intéressant de noter que les tumeurs formées dans le cerveau des souris (greffe orthotopique) à partir des U-87 MG présentent un phénotype particulier qui diffère de celui des tumeurs retrouvées chez les patients. Ainsi, peu de patients sont diagnostiqués avec des GBM bien encapsulés et richement vascularisés, deux caractéristiques qui feraient de ces tumeurs des tumeurs facilement opérables. Ainsi, dans le cas du modèle murin que nous utilisons, les tumeurs formées et la mortalité qui en résulte dépendent de facteurs tels que la vitesse de prolifération des cellules cancéreuses alors que la létalité des GBM chez l'Homme dépend principalement de la réponse au traitement, donc de la capacité des cellules à **i)** former des infiltrats dans le cerveau des patients, et **ii)** résister à la mort induite par les traitements (chimiothérapie). Ainsi, l'étude réalisée ici sur l'impact des mutations sur la formation de tumeurs après une greffe orthotopique chez la souris sont informatifs lorsqu'on les compare aux tumeurs formées dans les conditions contrôles (EV et WT), notamment sur l'impact de ces mutations sur la prolifération et l'angiogenèse au niveau de la masse tumorale, mais ne suffisent pas à comprendre l'effet que ces mutations peuvent avoir chez les patients. Pour compléter ces résultats, nous pourrions par exemple implanter nos différentes lignées de U-87 MG selon le protocole utilisé ici, attendre que la tumeur se développe (quinze jours environ), puis appliquer aux souris le même protocole thérapeutique que celui habituellement appliqué aux patients (chirurgie, radiothérapie/chimiothérapie [151]) et suivre l'échappement des cellules cancéreuses aux traitements curatifs. Nous pourrions également étudier l'impact de ces mutations sur des modèles animaux formant de façon spontanée des tumeurs, ce qui nous permettrait de définir le rôle de ces mutations dans les étapes initiales de la tumorigenèse.

Le séquençage systématique des tumeurs des patients et l'identification de mutations d'IRE1α dans ces tumeurs reste en tout cas un excellent moyen de découvrir des mutations pertinentes d'IRE1α, et de déchiffrer les mécanismes dépendants de la signalisation IRE1α mis en jeu lors du développement de ces tumeurs.

Ces mutations sont également des outils puissants pour essayer d'éclaircir deux grandes inconnues de la signalisation IRE1α: **i)** sa régulation par des protéines cytosoliques et luminales et **ii)** son potentiel en tant que cible thérapeutique.

i) De nombreuses études menées chez la levure ont permis de déterminer comment l'activation de la protéine Ire1p est régulée en conditions basales et en situation de stress. Cependant, un nombre croissant de travaux relatent des différences importantes entre les

mécanismes d'activation d'Ire1p chez la levure et d'IRE1α chez l'Homme, notamment en ce qui concerne leurs modulateurs [8]. Bien que les interactants cytosoliques d'IRE1α, parmi lesquels nous pouvons citer BI-1, NCK, HSP90, TRAF2, ASK1 et IKK, soient de mieux en mieux caractérisés, les régulateurs luminaux d'IRE1α sont peu connus. Ainsi, la caractérisation de l'interactome des protéines IRE1α portant les mutations luminales P336L et A414T, qui semblent avoir un effet de gain de fonction, permettra de mieux définir les mécanismes luminaux de régulation d'IRE1α, en conditions de stress du RE comme en conditions basales.

ii) De plus, nous pourrons compléter ces études par des criblages de molécules inhibitrices d'IRE1α ou de molécules utilisés en chimiothérapie. Pour tester l'impact de la présence de mutations sur IRE1α dans le GBM, nous proposons non seulement d'évaluer l'activation des voies de stress du RE dans les cellules U-87 MG exprimant ou non ces mutants en réponse à des agents inducteurs du stress du RE tels que la tunicamycine (inhibiteur de la N-glycosylation) ou la thapsigargine (inhibiteur de la pompe calcique SERCA2b), mais aussi de mesurer la résistance/sensibilité de ces cellules à la mort cellulaire induite par le stress du RE. Qui plus est nous proposons de mesurer la résistance/sensibilité de ces cellules à des chimiothérapies traditionnellement utilisées contre les GBM. impliquant la signalisation IRE1α et jouant un rôle dans le développement des GBM (**Figure 20**). Une meilleure connaissance de ces mécanismes permettra non seulement de justifier des approches thérapeutiques visant à moduler l'activité IRE1α mais aussi de classer les tumeurs humaines en fonction de leur statut d'activation de cette voie de signalisation. La combinaison de ces différentes approches pourrait permettre de cibler sélectivement certains types de tumeurs avec des molécules modulant l'activité IRE1α pour soit les sensibiliser à des agents chimiothérapeutiques classiques (comme par exemple le TMZ) soit pour directement en limiter la croissance, l'angiogenèse ou l'invasion.

IRE1α ayant été associé à un rôle moteur dans l'oncogenèse [159], ses mutations représentent un outil pertinent pour tester notre hypothèse que la protéine IRE1α est un interrupteur moléculaire entre les phénotypes angiogénique versus invasif et qu'elle pourrait ainsi être envisagée comme **i)** marqueur moléculaire des tumeurs humaines qui restent encore, à ce jour, mal classifiées et **ii)** cible thérapeutique pour contourner la résistance évasive associée à ces tumeurs.

En effet, nos travaux pourraient permettre d'associer une signature transcriptomique à chaque modulation d'IRE1α (suractivation (U87-WT), inactivation (U87-DN), etc.) et surtout d'associer ces signatures à des effets biologiques et cliniques particuliers tels qu'une augmentation de la prolifération tumorale, une augmentation de l'angiogenèse, une résistance

accrue aux traitements ou encore un phénotype invasif qui répond mal à la chirurgie. L'ensemble de ces données permettrait donc dans l'idéal d'associer à chaque tumeur une signature transcriptomique liée à l'état d'activation des voies dépendantes d'IRE1α et cette signature constituerait alors un facteur prédictif puissant de l'évolution de la tumeur et de la réponse aux traitements que cette tumeur est susceptible d'avoir, que ce soit à la chimiothérapie, à la radiothérapie ou à la chirurgie, et ainsi permettre aux cliniciens d'adapter au mieux le traitement pour améliorer la durée de vie ou au moins le confort de vie des patients atteints de GBM.

De plus, la compréhension des mécanismes par lesquels IRE1α est dérégulé dans les GBM, que ce soit directement par des mutations ou par une perturbation plus globale de la cellule cancéreuse (activation longue durée de l'UPR, mutation d'effecteurs des voies adaptatrices, etc.), permettrait d'affiner la recherche d'inhibiteurs d'IRE1α. En effet, la découverte d'inhibiteurs capables de cibler sélectivement une seule des quatre activités d'IRE1α (activité RIDD, activité d'épissage de l’ARNm codant pour XBP1, activité de dégradation de pré-miR ou activité kinase) permettrait de rétablir une réponse IRE1α pro-mort dans les cellules cancéreuses pour lesquelles la réponse IRE1α est devenue une réponse pro-survie par le découplage de ses activités. De telles molécules existent comme le montre les travaux de Han et al [7]. Ainsi, la corrélation de l'expression de différents marqueurs de la signalisation IRE1α comme PER1 [161], XBP1s [161], EREG [115] ou miR-17 [106] chez un même patient pourrait aiguiller le traitement vers tel ou tel inhibiteur d'IRE1α.

CONCLUSION GÉNÉRALE

L'ensemble de mes travaux de thèse renforcent le rôle essentiel de la protéine IRE1α dans la biologie des glioblastomes, que ce soit au niveau de la croissance, de la migration, de l'implantation des cellules tumorales, ou encore de l'angiogenèse.

En effet, l'inactivation de la signalisation IRE1α par une stratégie de dominant-négatif ou de siRNA compromet la capacité des cellules de glioblastomes à former des tumeurs massives et hautement vascularisées, phénotype principalement dû à la perte de la fonction RIDD, et à la stabilisation subséquente de protéines cruciales dans le développement des tumeurs. Nous assistons alors à une bascule d'un profil de tumeurs angiogéniques à un profil de tumeurs invasives.

Ainsi, la perte du RIDD conduit **i)** à une surexpression de la protéine SPARC, ce qui a pour conséquence de favoriser la migration des cellules cancéreuses et **ii)** à une surexpression de la protéine PER1, ce qui altère la vascularisation de la tumeur et la prolifération des cellules cancéreuses.

Cependant, le rôle d'IRE1α dans les glioblastomes ne se limite pas à l'épissage de XBP1 ou au RIDD, comme le suggère l'étude des mutations. Bien que ces mutations soulignent la complexité de la signalisation d'IRE1α dans les cellules tumorales, elles représentent aussi un outil puissant pour déchiffrer les mécanismes moléculaires qui régissent le rôle d'IRE1α dans le cancer.

Ces résultats confortent l'importance de l'UPR et en particulier d'IRE1α dans le développement des cancers, et la pertinence qu'il y a à envisager IRE1α comme outil de pronostic et de diagnostic, ainsi que de la recherche de traitements anticancéreux ciblant IRE1α.

BIBLIOGRAPHIE

1. Alberts, B., Johnson, A., Lewis, J., Raff, M., Roberts, K., and Walter, P. (2002). Molecular biology of the cell, Forth edn (New York, Garland Science).
2. Olzmann, J.A., R.R. Kopito, and J.C. Christianson, *The mammalian endoplasmic reticulum-associated degradation system.* Cold Spring Harb Perspect Biol, 2013. **5**(9).
3. Budnik, A. and D.J. Stephens, *ER exit sites--localization and control of COPII vesicle formation.* FEBS Lett, 2009. **583**(23): p. 3796-803.
4. DiMauro, S., et al., *The clinical maze of mitochondrial neurology.* Nat Rev Neurol, 2013. **9**(8): p. 429-44.
5. Wiseman, R.L., et al., *An adaptable standard for protein export from the endoplasmic reticulum.* Cell, 2007. **131**(4): p. 809-21.
6. Hetz, C., *The unfolded protein response: controlling cell fate decisions under ER stress and beyond.* Nat Rev Mol Cell Biol, 2012. **13**(2): p. 89-102.
7. Han, D., et al., *IRE1alpha kinase activation modes control alternate endoribonuclease outputs to determine divergent cell fates.* Cell, 2009. **138**(3): p. 562-75.
8. Hetz, C. and L.H. Glimcher, *Fine-tuning of the unfolded protein response: Assembling the IRE1alpha interactome.* Mol Cell, 2009. **35**(5): p. 551-61.
9. Dejeans, N., et al., *Addicted to secrete - novel concepts and targets in cancer therapy.* Trends Mol Med, 2014.
10. Palade, G., *Intracellular aspects of the process of protein synthesis.* Science, 1975. **189**(4206): p. 867.
11. Mizushima, N., *Autophagy: process and function.* Genes Dev, 2007. **21**(22): p. 2861-73.
12. Feng, Y., et al., *The machinery of macroautophagy.* Cell Res, 2014. **24**(1): p. 24-41.
13. Bernales, S., K.L. McDonald, and P. Walter, *Autophagy counterbalances endoplasmic reticulum expansion during the unfolded protein response.* PLoS Biol, 2006. **4**(12): p. e423.
14. Wang, C.W. and D.J. Klionsky, *The molecular mechanism of autophagy.* Mol Med, 2003. **9**(3-4): p. 65-76.
15. Lavoie, C. and J. Paiement, *Topology of molecular machines of the endoplasmic reticulum: a compilation of proteomics and cytological data.* Histochem Cell Biol, 2008. **129**(2): p. 117-28.
16. Shimizu, Y. and L.M. Hendershot, *Organization of the functions and components of the endoplasmic reticulum.* Adv Exp Med Biol, 2007. **594**: p. 37-46.
17. Berridge, M.J., M.D. Bootman, and H.L. Roderick, *Calcium signalling: dynamics, homeostasis and remodelling.* Nat Rev Mol Cell Biol, 2003. **4**(7): p. 517-29.
18. Rizzuto, R., et al., *Mitochondria as sensors and regulators of calcium signalling.* Nat Rev Mol Cell Biol, 2012. **13**(9): p. 566-78.
19. Berridge, M.J., *The endoplasmic reticulum: a multifunctional signaling organelle.* Cell Calcium, 2002. **32**(5-6): p. 235-49.
20. Coe, H. and M. Michalak, *Calcium binding chaperones of the endoplasmic reticulum.* Gen Physiol Biophys, 2009. **28 Spec No Focus**: p. F96-F103.
21. Mori, T., et al., *Sigma-1 receptor chaperone at the ER-mitochondrion interface mediates the mitochondrion-ER-nucleus signaling for cellular survival.* PLoS One, 2013. **8**(10): p. e76941.

22. Marchi, S., S. Patergnani, and P. Pinton, *The endoplasmic reticulum-mitochondria connection: One touch, multiple functions.* Biochim Biophys Acta, 2014. **1837**(4): p. 461-469.
23. McPherson, P.S. and K.P. Campbell, *The ryanodine receptor/Ca2+ release channel.* J Biol Chem, 1993. **268**(19): p. 13765-8.
24. Lytton, J., et al., *Functional comparisons between isoforms of the sarcoplasmic or endoplasmic reticulum family of calcium pumps.* J Biol Chem, 1992. **267**(20): p. 14483-9.
25. Helenius, J., et al., *Translocation of lipid-linked oligosaccharides across the ER membrane requires Rft1 protein.* Nature, 2002. **415**(6870): p. 447-50.
26. Baumann, O. and B. Walz, *Endoplasmic reticulum of animal cells and its organization into structural and functional domains.* Int Rev Cytol, 2001. **205**: p. 149-214.
27. Fagone, P. and S. Jackowski, *Membrane phospholipid synthesis and endoplasmic reticulum function.* J Lipid Res, 2009. **50 Suppl**: p. S311-6.
28. Achleitner, G., et al., *Association between the endoplasmic reticulum and mitochondria of yeast facilitates interorganelle transport of phospholipids through membrane contact.* Eur J Biochem, 1999. **264**(2): p. 545-53.
29. Pichler, H., et al., *A subfraction of the yeast endoplasmic reticulum associates with the plasma membrane and has a high capacity to synthesize lipids.* Eur J Biochem, 2001. **268**(8): p. 2351-61.
30. Underwood, K.W., et al., *Evidence for a cholesterol transport pathway from lysosomes to endoplasmic reticulum that is independent of the plasma membrane.* J Biol Chem, 1998. **273**(7): p. 4266-74.
31. Wirtz, K.W., *Phospholipid transfer proteins: from lipid monolayers to cells.* Klin Wochenschr, 1991. **69**(3): p. 105-11.
32. Wang, X., et al., *SREBP-1, a membrane-bound transcription factor released by sterol-regulated proteolysis.* Cell, 1994. **77**(1): p. 53-62.
33. Sakai, J., et al., *Sterol-regulated release of SREBP-2 from cell membranes requires two sequential cleavages, one within a transmembrane segment.* Cell, 1996. **85**(7): p. 1037-46.
34. Brown, M.S. and J.L. Goldstein, *The SREBP pathway: regulation of cholesterol metabolism by proteolysis of a membrane-bound transcription factor.* Cell, 1997. **89**(3): p. 331-40.
35. Brown, M.S. and J.L. Goldstein, *A proteolytic pathway that controls the cholesterol content of membranes, cells, and blood.* Proc Natl Acad Sci U S A, 1999. **96**(20): p. 11041-8.
36. Radhakrishnan, A., et al., *Switch-like control of SREBP-2 transport triggered by small changes in ER cholesterol: a delicate balance.* Cell Metab, 2008. **8**(6): p. 512-21.
37. Pai, J.T., M.S. Brown, and J.L. Goldstein, *Purification and cDNA cloning of a second apoptosis-related cysteine protease that cleaves and activates sterol regulatory element binding proteins.* Proc Natl Acad Sci U S A, 1996. **93**(11): p. 5437-42.
38. Wang, X., et al., *Cleavage of sterol regulatory element binding proteins (SREBPs) by CPP32 during apoptosis.* Embo J, 1996. **15**(5): p. 1012-20.
39. Sato, R., *SREBPs: protein interaction and SREBPs.* Febs J, 2009. **276**(3): p. 622-7.
40. Shimano, H., *Sterol regulatory element-binding proteins (SREBPs): transcriptional regulators of lipid synthetic genes.* Prog Lipid Res, 2001. **40**(6): p. 439-52.
41. Pikuleva, I.A., *Cytochrome P450s and cholesterol homeostasis.* Pharmacol Ther, 2006. **112**(3): p. 761-73.
42. Payne, A.H. and D.B. Hales, *Overview of steroidogenic enzymes in the pathway from cholesterol to active steroid hormones.* Endocr Rev, 2004. **25**(6): p. 947-70.

43. Rone, M.B., J. Fan, and V. Papadopoulos, *Cholesterol transport in steroid biosynthesis: role of protein-protein interactions and implications in disease states.* Biochim Biophys Acta, 2009. **1791**(7): p. 646-58.
44. Sonnino, S. and A. Prinetti, *Membrane domains and the "lipid raft" concept.* Curr Med Chem, 2013. **20**(1): p. 4-21.
45. Porter, K.R. and G.E. Palade, *Studies on the endoplasmic reticulum. III. Its form and distribution in striated muscle cells.* J Biophys Biochem Cytol, 1957. **3**(2): p. 269-300.
46. Nebert, D.W., K. Wikvall, and W.L. Miller, *Human cytochromes P450 in health and disease.* Philos Trans R Soc Lond B Biol Sci, 2013. **368**(1612): p. 20120431.
47. Gorlich, D., et al., *A mammalian homolog of SEC61p and SECYp is associated with ribosomes and nascent polypeptides during translocation.* Cell, 1992. **71**(3): p. 489-503.
48. Gorlich, D. and T.A. Rapoport, *Protein translocation into proteoliposomes reconstituted from purified components of the endoplasmic reticulum membrane.* Cell, 1993. **75**(4): p. 615-30.
49. Kalies, K.U., D. Gorlich, and T.A. Rapoport, *Binding of ribosomes to the rough endoplasmic reticulum mediated by the Sec61p-complex.* J Cell Biol, 1994. **126**(4): p. 925-34.
50. Raden, D., W. Song, and R. Gilmore, *Role of the cytoplasmic segments of Sec61alpha in the ribosome-binding and translocation-promoting activities of the Sec61 complex.* J Cell Biol, 2000. **150**(1): p. 53-64.
51. Cheng, Z., et al., *Identification of cytoplasmic residues of Sec61p involved in ribosome binding and cotranslational translocation.* J Cell Biol, 2005. **168**(1): p. 67-77.
52. Heinrich, S.U., et al., *The Sec61p complex mediates the integration of a membrane protein by allowing lipid partitioning of the transmembrane domain.* Cell, 2000. **102**(2): p. 233-44.
53. Hessa, T., et al., *Recognition of transmembrane helices by the endoplasmic reticulum translocon.* Nature, 2005. **433**(7024): p. 377-81.
54. Benham, A.M., *Protein secretion and the endoplasmic reticulum.* Cold Spring Harb Perspect Biol, 2012. **4**(8): p. a012872.
55. Parodi, A.J., *Protein glucosylation and its role in protein folding.* Annu Rev Biochem, 2000. **69**: p. 69-93.
56. Okuda-Shimizu, Y. and L.M. Hendershot, *Characterization of an ERAD pathway for nonglycosylated BiP substrates, which require Herp.* Mol Cell, 2007. **28**(4): p. 544-54.
57. Stephens, D.J., *De novo formation, fusion and fission of mammalian COPII-coated endoplasmic reticulum exit sites.* EMBO Rep, 2003. **4**(2): p. 210-7.
58. Hobman, T.C., et al., *Immunoisolation and characterization of a subdomain of the endoplasmic reticulum that concentrates proteins involved in COPII vesicle biogenesis.* Mol Biol Cell, 1998. **9**(6): p. 1265-78.
59. Jarosch, E., U. Lenk, and T. Sommer, *Endoplasmic reticulum-associated protein degradation.* Int Rev Cytol, 2003. **223**: p. 39-81.
60. McCracken, A.A. and J.L. Brodsky, *Recognition and delivery of ERAD substrates to the proteasome and alternative paths for cell survival.* Curr Top Microbiol Immunol, 2005. **300**: p. 17-40.
61. Bernasconi, R., et al., *Stringent requirement for HRD1, SEL1L, and OS-9/XTP3-B for disposal of ERAD-LS substrates.* J Cell Biol, 2010. **188**(2): p. 223-35.
62. Christianson, J.C., et al., *Defining human ERAD networks through an integrative mapping strategy.* Nat Cell Biol, 2011. **14**(1): p. 93-105.
63. Harding, H.P., Y. Zhang, and D. Ron, *Protein translation and folding are coupled by an endoplasmic-reticulum-resident kinase.* Nature, 1999. **397**(6716): p. 271-4.

64. Vattem, K.M. and R.C. Wek, *Reinitiation involving upstream ORFs regulates ATF4 mRNA translation in mammalian cells.* Proc Natl Acad Sci U S A, 2004. **101**(31): p. 11269-74.
65. Jiang, H.Y., et al., *Activating transcription factor 3 is integral to the eukaryotic initiation factor 2 kinase stress response.* Mol Cell Biol, 2004. **24**(3): p. 1365-77.
66. Novoa, I., et al., *Feedback inhibition of the unfolded protein response by GADD34-mediated dephosphorylation of eIF2alpha.* J Cell Biol, 2001. **153**(5): p. 1011-22.
67. Cullinan, S.B. and J.A. Diehl, *PERK-dependent activation of Nrf2 contributes to redox homeostasis and cell survival following endoplasmic reticulum stress.* J Biol Chem, 2004. **279**(19): p. 20108-17.
68. Cullinan, S.B., et al., *Nrf2 is a direct PERK substrate and effector of PERK-dependent cell survival.* Mol Cell Biol, 2003. **23**(20): p. 7198-209.
69. Harding, H.P., et al., *An integrated stress response regulates amino acid metabolism and resistance to oxidative stress.* Mol Cell, 2003. **11**(3): p. 619-33.
70. Haze, K., et al., *Mammalian transcription factor ATF6 is synthesized as a transmembrane protein and activated by proteolysis in response to endoplasmic reticulum stress.* Mol Biol Cell, 1999. **10**(11): p. 3787-99.
71. Shen, J., et al., *ER stress regulation of ATF6 localization by dissociation of BiP/GRP78 binding and unmasking of Golgi localization signals.* Dev Cell, 2002. **3**(1): p. 99-111.
72. Nadanaka, S., H. Yoshida, and K. Mori, *Reduction of disulfide bridges in the lumenal domain of ATF6 in response to glucose starvation.* Cell Struct Funct, 2006. **31**(2): p. 127-34.
73. Sato, Y., et al., *Luminal domain of ATF6 alone is sufficient for sensing endoplasmic reticulum stress and subsequent transport to the Golgi apparatus.* Cell Struct Funct, 2011. **36**(1): p. 35-47.
74. Schindler, A.J. and R. Schekman, *In vitro reconstitution of ER-stress induced ATF6 transport in COPII vesicles.* Proc Natl Acad Sci U S A, 2009. **106**(42): p. 17775-80.
75. Chen, X., J. Shen, and R. Prywes, *The luminal domain of ATF6 senses endoplasmic reticulum (ER) stress and causes translocation of ATF6 from the ER to the Golgi.* J Biol Chem, 2002. **277**(15): p. 13045-52.
76. Ye, J., et al., *ER stress induces cleavage of membrane-bound ATF6 by the same proteases that process SREBPs.* Mol Cell, 2000. **6**(6): p. 1355-64.
77. Yoshida, H., et al., *ATF6 activated by proteolysis binds in the presence of NF-Y (CBF) directly to the cis-acting element responsible for the mammalian unfolded protein response.* Mol Cell Biol, 2000. **20**(18): p. 6755-67.
78. Adachi, Y., et al., *ATF6 is a transcription factor specializing in the regulation of quality control proteins in the endoplasmic reticulum.* Cell Struct Funct, 2008. **33**(1): p. 75-89.
79. van Huizen, R., et al., *P58IPK, a novel endoplasmic reticulum stress-inducible protein and potential negative regulator of eIF2alpha signaling.* J Biol Chem, 2003. **278**(18): p. 15558-64.
80. Yoshida, H., et al., *XBP1 mRNA is induced by ATF6 and spliced by IRE1 in response to ER stress to produce a highly active transcription factor.* Cell, 2001. **107**(7): p. 881-91.
81. Yamamoto, K., et al., *Transcriptional induction of mammalian ER quality control proteins is mediated by single or combined action of ATF6alpha and XBP1.* Dev Cell, 2007. **13**(3): p. 365-76.
82. Reimold, A.M., et al., *An essential role in liver development for transcription factor XBP-1.* Genes Dev, 2000. **14**(2): p. 152-7.
83. Urano, F., et al., *Coupling of stress in the ER to activation of JNK protein kinases by transmembrane protein kinase IRE1.* Science, 2000. **287**(5453): p. 664-6.

84. Zhang, K., et al., *The unfolded protein response sensor IRE1alpha is required at 2 distinct steps in B cell lymphopoiesis.* J Clin Invest, 2005. **115**(2): p. 268-81.
85. Zinszner, H., et al., *CHOP is implicated in programmed cell death in response to impaired function of the endoplasmic reticulum.* Genes Dev, 1998. **12**(7): p. 982-95.
86. Tanaka, T., et al., *Targeted disruption of ATF4 discloses its essential role in the formation of eye lens fibres.* Genes Cells, 1998. **3**(12): p. 801-10.
87. Zhang, P., et al., *The PERK eukaryotic initiation factor 2 alpha kinase is required for the development of the skeletal system, postnatal growth, and the function and viability of the pancreas.* Mol Cell Biol, 2002. **22**(11): p. 3864-74.
88. Harding, H.P., et al., *Diabetes mellitus and exocrine pancreatic dysfunction in perk-/- mice reveals a role for translational control in secretory cell survival.* Mol Cell, 2001. **7**(6): p. 1153-63.
89. Mori, K., *Signalling pathways in the unfolded protein response: development from yeast to mammals.* J Biochem, 2009. **146**(6): p. 743-50.
90. database, N.g., *ERN1 endoplasmic reticulum to nucleus signaling 1 [Homo sapiens (human)]*. 2013, NCBI gene database.
91. Bertolotti, A., et al., *Dynamic interaction of BiP and ER stress transducers in the unfolded-protein response.* Nat Cell Biol, 2000. **2**(6): p. 326-32.
92. Credle, J.J., et al., *On the mechanism of sensing unfolded protein in the endoplasmic reticulum.* Proc Natl Acad Sci U S A, 2005. **102**(52): p. 18773-84.
93. Kimata, Y., et al., *A role for BiP as an adjustor for the endoplasmic reticulum stress-sensing protein Ire1*. J Cell Biol, 2004. **167**(3): p. 445-56.
94. Zhou, J., et al., *The crystal structure of human IRE1 luminal domain reveals a conserved dimerization interface required for activation of the unfolded protein response.* Proc Natl Acad Sci U S A, 2006. **103**(39): p. 14343-8.
95. Marcu, M.G., et al., *Heat shock protein 90 modulates the unfolded protein response by stabilizing IRE1alpha.* Mol Cell Biol, 2002. **22**(24): p. 8506-13.
96. Calfon, M., et al., *IRE1 couples endoplasmic reticulum load to secretory capacity by processing the XBP-1 mRNA.* Nature, 2002. **415**(6867): p. 92-6.
97. Uemura, A., et al., *Unconventional splicing of XBP1 mRNA occurs in the cytoplasm during the mammalian unfolded protein response.* J Cell Sci, 2009. **122**(Pt 16): p. 2877-86.
98. Yoshida, H., et al., *pXBP1(U) encoded in XBP1 pre-mRNA negatively regulates unfolded protein response activator pXBP1(S) in mammalian ER stress response.* J Cell Biol, 2006. **172**(4): p. 565-75.
99. Lee, A.H., N.N. Iwakoshi, and L.H. Glimcher, *XBP-1 regulates a subset of endoplasmic reticulum resident chaperone genes in the unfolded protein response.* Mol Cell Biol, 2003. **23**(21): p. 7448-59.
100. Yoshida, H., et al., *A time-dependent phase shift in the mammalian unfolded protein response.* Dev Cell, 2003. **4**(2): p. 265-71.
101. Oikawa, D., et al., *Identification of a consensus element recognized and cleaved by IRE1 alpha.* Nucleic Acids Res, 2010. **38**(18): p. 6265-73.
102. Hollien, J. and J.S. Weissman, *Decay of endoplasmic reticulum-localized mRNAs during the unfolded protein response.* Science, 2006. **313**(5783): p. 104-7.
103. Hollien, J., et al., *Regulated Ire1-dependent decay of messenger RNAs in mammalian cells.* J Cell Biol, 2009. **186**(3): p. 323-31.
104. Oikawa, D., M. Tokuda, and T. Iwawaki, *Site-specific cleavage of CD59 mRNA by endoplasmic reticulum-localized ribonuclease, IRE1.* Biochem Biophys Res Commun, 2007. **360**(1): p. 122-7.
105. Tirasophon, W., et al., *The endoribonuclease activity of mammalian IRE1 autoregulates its mRNA and is required for the unfolded protein response.* Genes Dev, 2000. **14**(21): p. 2725-36.

106. Upton, J.P., et al., *IRE1alpha cleaves select microRNAs during ER stress to derepress translation of proapoptotic Caspase-2.* Science, 2012. **338**(6108): p. 818-22.
107. Hassler, J., S.S. Cao, and R.J. Kaufman, *IRE1, a double-edged sword in pre-miRNA slicing and cell death.* Dev Cell, 2012. **23**(5): p. 921-3.
108. Maurel, M., et al., *MicroRNA-1291-mediated silencing of IRE1alpha enhances Glypican-3 expression.* Rna, 2013. **19**(6): p. 778-88.
109. Puthalakath, H., et al., *ER stress triggers apoptosis by activating BH3-only protein Bim.* Cell, 2007. **129**(7): p. 1337-49.
110. Nakagawa, T., et al., *Caspase-12 mediates endoplasmic-reticulum-specific apoptosis and cytotoxicity by amyloid-beta.* Nature, 2000. **403**(6765): p. 98-103.
111. Yoneda, T., et al., *Activation of caspase-12, an endoplastic reticulum (ER) resident caspase, through tumor necrosis factor receptor-associated factor 2-dependent mechanism in response to the ER stress.* J Biol Chem, 2001. **276**(17): p. 13935-40.
112. Saleh, M., et al., *Differential modulation of endotoxin responsiveness by human caspase-12 polymorphisms.* Nature, 2004. **429**(6987): p. 75-9.
113. Lerner, A.G., et al., *IRE1alpha induces thioredoxin-interacting protein to activate the NLRP3 inflammasome and promote programmed cell death under irremediable ER stress.* Cell Metab, 2012. **16**(2): p. 250-64.
114. Oslowski, C.M., et al., *Thioredoxin-interacting protein mediates ER stress-induced beta cell death through initiation of the inflammasome.* Cell Metab, 2012. **16**(2): p. 265-73.
115. Auf, G., et al., *High epiregulin expression in human U87 glioma cells relies on IRE1alpha and promotes autocrine growth through EGF receptor.* BMC Cancer, 2013. **13**: p. 597.
116. Lin, J.H., et al., *IRE1 signaling affects cell fate during the unfolded protein response.* Science, 2007. **318**(5852): p. 944-9.
117. Lin, J.H., et al., *Divergent effects of PERK and IRE1 signaling on cell viability.* PLoS One, 2009. **4**(1): p. e4170.
118. Han, D., et al., *A kinase inhibitor activates the IRE1alpha RNase to confer cytoprotection against ER stress.* Biochem Biophys Res Commun, 2008. **365**(4): p. 777-83.
119. Eletto, D., et al., *Protein Disulfide Isomerase A6 Controls the Decay of IRE1a Signaling via Disulfide-Dependent Association.* Molecular Cell, 2014. **53**: p. 1-15.
120. Zhang, B., et al., *Genotype-phenotype correlation in combined deficiency of factor V and factor VIII.* Blood, 2008. **111**(12): p. 5592-600.
121. Chung, K.T., Y. Shen, and L.M. Hendershot, *BAP, a mammalian BiP-associated protein, is a nucleotide exchange factor that regulates the ATPase activity of BiP.* J Biol Chem, 2002. **277**(49): p. 47557-63.
122. Lagier-Tourenne, C., et al., *Homozygosity mapping of Marinesco-Sjogren syndrome to 5q31.* Eur J Hum Genet, 2003. **11**(10): p. 770-8.
123. De Praeter, C.M., et al., *A novel disorder caused by defective biosynthesis of N-linked oligosaccharides due to glucosidase I deficiency.* Am J Hum Genet, 2000. **66**(6): p. 1744-56.
124. Drumm, M.L., et al., *Chloride conductance expressed by delta F508 and other mutant CFTRs in Xenopus oocytes.* Science, 1991. **254**(5039): p. 1797-9.
125. Riordan, J.R., et al., *Identification of the cystic fibrosis gene: cloning and characterization of complementary DNA.* Science, 1989. **245**(4922): p. 1066-73.
126. Jensen, T.J., et al., *Multiple proteolytic systems, including the proteasome, contribute to CFTR processing.* Cell, 1995. **83**(1): p. 129-35.
127. Ward, C.L. and R.R. Kopito, *Intracellular turnover of cystic fibrosis transmembrane conductance regulator. Inefficient processing and rapid degradation of wild-type and mutant proteins.* J Biol Chem, 1994. **269**(41): p. 25710-8.

128. Lomas, D.A. and R. Mahadeva, *Alpha1-antitrypsin polymerization and the serpinopathies: pathobiology and prospects for therapy.* J Clin Invest, 2002. **110**(11): p. 1585-90.
129. Rudnick, D.A. and D.H. Perlmutter, *Alpha-1-antitrypsin deficiency: a new paradigm for hepatocellular carcinoma in genetic liver disease.* Hepatology, 2005. **42**(3): p. 514-21.
130. Wang, Y. and D.H. Perlmutter, *Targeting intracellular degradation pathways for treatment of liver disease caused by alpha1-antitrypsin deficiency.* Pediatr Res, 2014. **75**(1-2): p. 133-9.
131. Liu, Y., et al., *Oligosaccharide modification in the early secretory pathway directs the selection of a misfolded glycoprotein for degradation by the proteasome.* J Biol Chem, 1999. **274**(9): p. 5861-7.
132. Carrell, R.W. and D.A. Lomas, *Alpha1-antitrypsin deficiency--a model for conformational diseases.* N Engl J Med, 2002. **346**(1): p. 45-53.
133. Senderek, J., et al., *Mutations in SIL1 cause Marinesco-Sjogren syndrome, a cerebellar ataxia with cataract and myopathy.* Nat Genet, 2005. **37**(12): p. 1312-4.
134. Jaeken, J. and G. Matthijs, *Congenital disorders of glycosylation: a rapidly expanding disease family.* Annu Rev Genomics Hum Genet, 2007. **8**: p. 261-78.
135. Delepine, M., et al., *EIF2AK3, encoding translation initiation factor 2-alpha kinase 3, is mutated in patients with Wolcott-Rallison syndrome.* Nat Genet, 2000. **25**(4): p. 406-9.
136. Julier, C. and M. Nicolino, *Wolcott-Rallison syndrome.* Orphanet J Rare Dis, 2010. **5**: p. 29.
137. Harding, H.P. and D. Ron, *Endoplasmic reticulum stress and the development of diabetes: a review.* Diabetes, 2002. **51 Suppl 3**: p. S455-61.
138. Thomas, S.E., et al., *Diabetes as a disease of endoplasmic reticulum stress.* Diabetes Metab Res Rev, 2010. **26**(8): p. 611-21.
139. Wang, S. and R.J. Kaufman, *The impact of the unfolded protein response on human disease.* J Cell Biol, 2012. **197**(7): p. 857-67.
140. Cao, S.S. and R.J. Kaufman, *Targeting endoplasmic reticulum stress in metabolic disease.* Expert Opin Ther Targets, 2013. **17**(4): p. 437-48.
141. Kaser, A., et al., *XBP1 links ER stress to intestinal inflammation and confers genetic risk for human inflammatory bowel disease.* Cell, 2008. **134**(5): p. 743-56.
142. Matus, S., et al., *The stress rheostat: an interplay between the unfolded protein response (UPR) and autophagy in neurodegeneration.* Curr Mol Med, 2008. **8**(3): p. 157-72.
143. Huber, A.L., et al., *p58(IPK)-mediated attenuation of the proapoptotic PERK-CHOP pathway allows malignant progression upon low glucose.* Mol Cell, 2013. **49**(6): p. 1049-59.
144. Bissell, M.J. and W.C. Hines, *Why don't we get more cancer? A proposed role of the microenvironment in restraining cancer progression.* Nat Med, 2012. **17**(3): p. 320-9.
145. Oue, N., et al., *Signal peptidase complex 18, encoded by SEC11A, contributes to progression via TGF-alpha secretion in gastric cancer.* Oncogene, 2013.
146. Mathew, R., et al., *Autophagy suppresses tumorigenesis through elimination of p62.* Cell, 2009. **137**(6): p. 1062-75.
147. Powers, E.T., et al., *Biological and chemical approaches to diseases of proteostasis deficiency.* Annu Rev Biochem, 2009. **78**: p. 959-91.
148. Lakkaraju, A.K. and F.G. van der Goot, *Calnexin controls the STAT3-mediated transcriptional response to EGF.* Mol Cell, 2013. **51**(3): p. 386-96.
149. Atkins, C., et al., *Characterization of a novel PERK kinase inhibitor with antitumor and antiangiogenic activity.* Cancer Res, 2013. **73**(6): p. 1993-2002.

150. Louis, D.N., et al., *The 2007 WHO classification of tumours of the central nervous system.* Acta Neuropathol, 2007. **114**(2): p. 97-109.
151. Anton, K., J.M. Baehring, and T. Mayer, *Glioblastoma multiforme: overview of current treatment and future perspectives.* Hematol Oncol Clin North Am, 2012. **26**(4): p. 825-53.
152. Stupp, R., et al., *Radiotherapy plus concomitant and adjuvant temozolomide for glioblastoma.* N Engl J Med, 2005. **352**(10): p. 987-96.
153. (TCGA), T.C.G.A., *Comprehensive genomic characterization defines human glioblastoma genes and core pathways.* Nature, 2008. **455**(7216): p. 1061-8.
154. Parsons, D.W., et al., *An integrated genomic analysis of human glioblastoma multiforme.* Science, 2008. **321**(5897): p. 1807-12.
155. Nguyen, D.T., et al., *Nck-dependent activation of extracellular signal-regulated kinase-1 and regulation of cell survival during endoplasmic reticulum stress.* Mol Biol Cell, 2004. **15**(9): p. 4248-60.
156. Drogat, B., et al., *IRE1 signaling is essential for ischemia-induced vascular endothelial growth factor-A expression and contributes to angiogenesis and tumor growth in vivo.* Cancer Res, 2007. **67**(14): p. 6700-7.
157. Auf, G., et al., *Inositol-requiring enzyme 1alpha is a key regulator of angiogenesis and invasion in malignant glioma.* Proc Natl Acad Sci U S A, 2010. **107**(35): p. 15553-8.
158. Kunigal, S., et al., *SPARC-induced migration of glioblastoma cell lines via uPA-uPAR signaling and activation of small GTPase RhoA.* Int J Oncol, 2006. **29**(6): p. 1349-57.
159. Greenman, C., et al., *Patterns of somatic mutation in human cancer genomes.* Nature, 2007. **446**(7132): p. 153-8.
160. Dejeans, N., et al., *Autocrine control of glioma cells adhesion and migration through IRE1alpha-mediated cleavage of SPARC mRNA.* J Cell Sci, 2012. **125**(Pt 18): p. 4278-87.
161. Pluquet, O., et al., *Posttranscriptional regulation of PER1 underlies the oncogenic function of IREalpha.* Cancer Res, 2013. **73**(15): p. 4732-43.
162. Papa, F.R., et al., *Bypassing a kinase activity with an ATP-competitive drug.* Science, 2003. **302**(5650): p. 1533-7.
163. Tirasophon, W., A.A. Welihinda, and R.J. Kaufman, *A stress response pathway from the endoplasmic reticulum to the nucleus requires a novel bifunctional protein kinase/endoribonuclease (Ire1p) in mammalian cells.* Genes Dev, 1998. **12**(12): p. 1812-24.
164. Iwawaki, T., et al., *Translational control by the ER transmembrane kinase/ribonuclease IRE1 under ER stress.* Nat Cell Biol, 2001. **3**(2): p. 158-64.
165. Xue, Z., et al., *A conserved structural determinant located at the interdomain region of mammalian inositol-requiring enzyme 1alpha.* J Biol Chem, 2011. **286**(35): p. 30859-66.
166. Bouchecareilh, M., et al., *Peptides derived from the bifunctional kinase/RNase enzyme IRE1alpha modulate IRE1alpha activity and protect cells from endoplasmic reticulum stress.* Faseb J, 2011. **25**(9): p. 3115-29.
167. Liu, C.Y., Z. Xu, and R.J. Kaufman, *Structure and intermolecular interactions of the luminal dimerization domain of human IRE1alpha.* J Biol Chem, 2003. **278**(20): p. 17680-7.
168. Liu, C.Y., M. Schroder, and R.J. Kaufman, *Ligand-independent dimerization activates the stress response kinases IRE1 and PERK in the lumen of the endoplasmic reticulum.* J Biol Chem, 2000. **275**(32): p. 24881-5.
169. Gardner, B.M. and P. Walter, *Unfolded proteins are Ire1-activating ligands that directly induce the unfolded protein response.* Science, 2011. **333**(6051): p. 1891-4.

170. Oikawa, D., et al., *Direct association of unfolded proteins with mammalian ER stress sensor, IRE1beta.* PLoS One, 2012. **7**(12): p. e51290.
171. Kimchi-Sarfaty, C., et al., *A "silent" polymorphism in the MDR1 gene changes substrate specificity.* Science, 2007. **315**(5811): p. 525-8.
172. Sasai, K., et al., *O6-methylguanine-DNA methyltransferase is downregulated in transformed astrocyte cells: implications for anti-glioma therapies.* Mol Cancer, 2007. **6**: p. 36.

ANNEXE : ARTICLE 6

Endoplasmic reticulum stress-activated transcription factor ATF6α requires the disulfide isomerase PDIA5 to modulate chemoresistance

Arisa Higa[1,6], Said Taouji[1], Stéphanie Lhomond[1], Devon Jensen[2], Martin E. Fernandez-Zapico[3], Jeremy C Simpson[4], Jean-Max Pasquet[5], Randy Schekman[2] and Eric Chevet[1]

[1]INSERM U1053, Université Bordeaux Segalen, Bordeaux, France. [2]Department of Molecular and Cell Biology, University of California at Berkeley, Berkeley, CA, USA. [3]Schulze Center for Novel Therapeutics, Division of Oncology Research, Mayo Clinic, Rochester, MN, USA. [4]School of Biology & Environmental Science and Conway Institute of Biomolecular & Biomedical Research, University College Dublin, Belfield, Dublin 4, Ireland. [5]INSERM U1035, Université Bordeaux Segalen, Bordeaux, France.

Correspondence to Eric Chevet, Inserm U1053, Université Bordeaux Segalent, 146 rue Léo Saignat, 33000 Bordeaux, France. Tel. +33(0)557579253; email eric.chevet@inserm.fr

[6]Present address: Medical Industry Translational Research Centre, Fukushima Medical University, 1 Hikarigaoka, Fukushima, 960-1295

Endoplasmic reticulum stress-activated transcription factor ATF6α requires the disulfide isomerase PDIA5 to modulate chemoresistance

Arisa Higa[1,6], Said Taouji[1], Stéphanie Lhomond[1], Devon Jensen[2], Martin E. Fernandez-Zapico[3], Jeremy C Simpson[4], Jean-Max Pasquet[5], Randy Schekman[2] and Eric Chevet[1]

[1]INSERM U1053, Université Bordeaux Segalen, Bordeaux, France. [2]Department of Molecular and Cell Biology, University of California at Berkeley, Berkeley, CA, USA. [3]Schulze Center for Novel Therapeutics, Division of Oncology Research, Mayo Clinic, Rochester, MN, USA. [4]School of Biology & Environmental Science and Conway Institute of Biomolecular & Biomedical Research, University College Dublin, Belfield, Dublin 4, Ireland. [5]INSERM U1035, Université Bordeaux Segalen, Bordeaux, France.

Correspondence to Eric Chevet, Inserm U1053, Université Bordeaux Segalent, 146 rue Léo Saignat, 33000 Bordeaux, France. Tel. +33(0)557579253; email eric.chevet@inserm.fr

[6]Present address: Medical Industry Translational Research Centre, Fukushima Medical University, 1 Hikarigaoka, Fukushima, 960-1295

ATF6α, a membrane-anchored transcription factor from the endoplasmic reticulum (ER), modulating the cellular response to stress as an effector of the Unfolded Protein Response (UPR) is a key player in the development of tumor of different origin. ATF6α activation has been linked to oncogenic transformation and tumor maintenance, however the mechanism(s) underlying this phenomenon remains elusive. Here, using a phenotypic siRNA screening, we identified a novel role for ATF6α in chemoresistance and defined the protein disulfide isomerase A5 (PDIA5) as necessary for ATF6α activation upon ER stress. PDIA5 contributed to disulfide bond rearrangement in ATF6α under stress conditions thereby leading to ATF6α export from the ER and activation of its target genes. Further analysis of the mechanism demonstrate that PDIA5 promotes ATF6α packaging into COPII vesicles and that the PDIA5/ATF6α activation loop is essential to confer cancer cells chemoresistance. Genetic and pharmacological inhibition of the PDIA5-ATF6α axis restored sensitivity to the drug treatment. This work defines the mechanisms underlying the role of ATF6α activation to carcinogenesis and chemoresistance, furthermore it identifies PDIA5 as a key regulator ATF6α-mediated cellular functions in cancer.

Keywords: Cancer, endoplasmic reticulum stress, ATF6α, PDIA5, chemoresistance

Introduction

Protein folding in the Endoplasmic Reticulum (ER) can be particularly affected by the presence of mutation(s) in secretory proteins or by dynamic changes in the cellular microenvironment, events, which are often encountered in cancers. In the ER, these events are sensed by specific sensors, which in turn trigger select signaling pathways, collectively named the Unfolded Protein Response (UPR) (21). The UPR is an adaptive response that either allows the cells to overcome the stress or promote cell death in the case of overwhelming burden (21). Three ER resident proteins, namely the protein kinase PKR-like ER kinase (PERK), the inositol-requiring protein-1 alpha (IRE1α) and the activating transcription factor-6 alpha (ATF6α) have been identified as the major transducers of the UPR in mammals. They display an ER-luminal domain that senses misfolded proteins and are activated by a common mechanism involving the dissociation of the ER chaperone BiP/GRP78. PERK is responsible for translational attenuation through the phosphorylation of the alpha subunit of the eukaryotic translation initiation factor-2 (eIF2α) (7). IRE1α mediates the unconventional splicing of X-box binding protein-1 (*Xbp1*) mRNA (26) as well as mRNA expression levels through Regulated IRE1α-Dependent mRNA Decay (RIDD; (13)) and controls the activation of the c-jun N-terminal kinase (JNK) pathway. The third arm of the UPR is controlled by ATF6α. This membrane-anchored transcription factor is a type II transmembrane protein regulated by intra-membrane proteolysis by the Golgi apparatus localized Site-1 and Site-2 proteases (S1P and S2P) upon ER stress (8). Indeed upon ER stress, BiP dissociates from the luminal domain of ATF6α thereby unmasking both Golgi localization signals (24) and disulfide bonds between two conserved cysteine residues (18, 19). Although ATF6α has been linked to cancer development (2, 15) or tumor dormancy (22), the precise underlying mechanisms

remain unclear. To better characterize the ER molecular mechanisms underlying ATF6α activation processes in the ER and evaluate their role(s) in cancer, we developed a functional ATF6α activation screen using small interfering RNA (siRNA) targeting a panel of well-established cancer relevant ER foldases (5, 16). We identify PDIA5 as an essential ER localized regulator of ATF6α activation allowing this transcription factor export from the ER upon stress. Moreover, using leukemia cells as model, we show a novel role of this ATF6α–PDIA5 axis regulating resistance to Imatinib. Collectively, our results identify a novel signaling pathway mediating chemoresistance in cancer cells, this knowledge may help the tailoring of future clinical studies.

Materials and Methods

Cell Culture and Transfection - HeLa cells were cultured in Dulbecco's modified Eagle's medium (DMEM) supplemented with 10% fetal bovine serum (FBS) and penicillin-streptomycin (100 U/ml and 100 μg/ml, respectively) at 37°C in a 5% CO_2 incubator. HeLa cells stably expressing 3xFLAG-ATF6α (HeLa-ATF6α) were generated and maintained as previously described (23). K562 and LAMA (R= Imatinib resistant; S= Imatinib sensitive) cells were maintained in RPMI1640 medium containing 10% FBS and antibiotics. HeLa cells were transiently transfected with FLAG-ATF6α or FLAG-ATF6α-p50 using Lipofectamine and PLUS reagents (Invitrogen) according to the manufacturer's protocols.

Antibodies and Chemicals - Mouse monoclonal anti-FLAG M2 antibody was obtained from Sigma-Aldrich. Mouse monoclonal anti-ATF6α antibody was from BioAcademia. Rabbit polyclonal anti-ERK1 antibody was from Santa Cruz Biotechnologies. Rabbit polyclonal anti-Giantin antibody was purchased from Abcam. Mouse monoclonal anti-PDIA5 and mouse monoclonal anti-KDEL were from Abnova and Stressgen, respectively. Rabbit anti-CNX antibodies were a kind gift from Dr. John Bergeron (McGill University, Montreal, Qc, Canada). Polyclonal anti-ERGIC53, anti-Ribophorin I and anti-Sec22b antibodies were generated as described previously (23). Fluorescent-conjugated secondary antibodies were from Molecular Probes (Life Technologies). Imatinib mesylate (Gleevec®, Novartis, Basel, Switzerland) was dissolved in DMSO at a stock concentration of 250 mM, stored at -20°C, and subsequently diluted with serum-free culture medium prior to use. The PDI inhibitor 16F16 was purchased from Sigma (Sigma, StLouis, MO, USA)

RNA Interference - siRNAs were obtained from RNAi Co. and Ambion. The sequences of siRNAs used in this study are described in **Table S1**. siRNA was delivered into HeLa, HeLa-ATF6α or K562 cells by reverse transfection using Lipofectamine RNAiMAX (Invitrogen) at a siRNA concentration of 12.5 or 25 nM.

***In Vitro* Budding Assay** - HeLa-ATF6α cells were transfected with siRNAs against PDIA5 or control. Seventy-two hours after, cells were permeabilized with 40 μg/ml digitonin for 5 min on ice. Cells were then washed and incubated with ATP regenerating system (ATPr; 1 mM ATP, 40 mM creatine phosphate, 200 μg/ml creatine phosphokinase, 50 μM GDP-mannose), 3 mM GTP and 4 mg/ml rat liver cytosol in KHM buffer (110 mM KOAc, 2 mM $Mg(OAc)_2$ and 20 mM Hepes pH 7.2) for 1 h at 30°C. Rat liver cytosol was prepared as described previously (14). The vesicle fraction was separated from the donor microsome fraction by centrifugation at 12,000 rpm for 10 min. The supernatants were then centrifuged at 55,000 rpm for 25 min at 4°C to collect the vesicles. The pellets were solubilized with Buffer C (10 mM Tris-HCl pH 7.6, 100 mM NaCl and 1% Triton X-100) and analyzed by immunoblotting using antibodies against mouse monoclonal anti-ATF6α (1:1,000), rabbit polyclonal anti-ERGIC53 (1:10,000), anti-Ribophorin I (1:10,000) and anti-Sec22b (1:10,000).

Plasmids - Human ATF6α cDNA was amplified by PCR from human liver total cDNA and cloned into p3xFLAG-CMV7.1 vector within the *HindIII* /*SalI* restriction sites. The FLAG-ATF6α-p50 construct was derived from the above-mentioned plasmid. Human ATF6α cDNA was digested with *PvuII* and ligated subsequently in the p3xFLAG vector. The resulting translation product corresponded to a FLAG-tagged ATF6α-p50 protein. The dominant negative Sar1 (Sar1(DN)) plasmid was a kind gift from Dr.

Lippincott-Schwartz (NIH, Bethesda, USA). To construct a siRNA resistant PDIA5 cDNA (PDIA5r), the human PDIA5 cDNA was amplified by PCR subcloned in pGEM-Teasy plasmid. Silent mutations were introduced by in vitro site-directed mutagenesis using the Stratagen QuikChange® II XL Site-Directed Mutagenesis Kit in the regions that are targeted by siRNAs (sequence PDIA5 5'-AGGATGATGCCGCAT replaced by 5'-AGAATGATGCCACAC). The insert was then sub-cloned into pcDNA3 and sequence verified.

Indirect immunofluorescence - HeLa cells were plated on coverslips and transfected with FLAG-ATF6α. Twenty-four hours post transfection, cells were fixed in methanol at -20°C for 5 min and blocked with 3% BSA in immunofluorescence buffer (0.15 M NaCl, 2 mM EGTA, 1 mM $MgCl_2$ and 10 mM PIPES-Na pH 7.2) for 30 min at room temperature. Then cells were incubated with primary (anti-FLAG, 1:500; anti-CNX, 1:500 or anti-Giantin, 1:1,000) and secondary (Alexa-488 labeled anti-mouse IgG or Alexa-568 labeled anti-rabbit IgG, 1:250, respectively) antibodies for 1 h. DNA was stained using Hoechst 33342 (Invitrogen) for 15 min. Coverslips were mounted on microscope slides using Fluoromount-G (SouthernBiotech) and observed using a Leica TCS SP5 confocal microscope with 63x oil immersion objective for fluorescence detection.

Immunoprecipitation/immunoblotting - To prepare whole-cell extracts, cells were washed twice with PBS and then incubated with RIPA buffer (25 mM Tris-HCl pH 7.5, 150 mM NaCl, 1% NP-40, 1% sodium deoxycholate and 0.1% SDS) for 30 min on ice. Lysates were sonicated and centrifuged at 13,000 rpm for 20 min at 4°C. For immunoprecipitation, cells were rinsed twice and collected in ice-cold PBS. Cell

pellets were then incubated with Lysis buffer (50 mM Tris-HCl pH 7.5 and 1% TritonX-100) for 30 min on ice and clarified by centrifugation at 13,000 rpm for 20 min at 4°C. For co-immunoprecipitation of ATF6α with BiP, cells were transfected with Sar1(DN) after siRNA transfection and were lysed using Lysis buffer. After pre-clearing using protein A or protein G Sepharose (GE Healthcare Bio-Sciences), lysates were incubated overnight with anti-FLAG (1:200) antibodies at 4°C. The beads were then added to the immune complexes and precipitated for 1 h at 4°C with gentle rotation and washed five times with Lysis buffer. Immunoprecipitates were eluted with Laemmli sample buffer containing 50 mM DTT for 10 min at 70°C. The proteins were analyzed by immunoblotting and detected using LumiGLO chemiluminescent substrate system (Kirkegaard & Perry Laboratories). Dilutions of primary antibodies used for immunoblotting were as follows: anti-ATF6α, 1:1,000; anti-CNX, 1:2,000; anti-ERK, 1:1,000; anti-FLAG, 1:1,000; anti-KDEL, 1:1,000; anti-PDIA5, 1:500.

Quantitative RT-PCR - Total RNA was extracted from 48 h post siRNA transfection cells using TRIZOL reagent (Invitrogen) according to the manufacturer's instructions. cDNA was synthesized from the total RNA using SuperScript First-Strand Synthesis System (Invitrogen) or Reverse Transcription System (Promega) with Oligo(dT) primer and amplified with Taq DNA polymerase (Invitrogen). For quantitative RT-PCR (q-PCR), cDNA was analyzed with B-R SYBR Green SuperMix (Quanta Bioscience) in StepOnePlus™ system (Applied Biosystems). The primer sequences used for this experiment are shown in **Table S2.**

Mass spectrometry analyses and peptide quantification - HeLa-ATF6α cells were transfected with siRNA against PDIA5 or control in 150 mm diameter dishes. Seventy-two hours post transfection, cells were lysed in the presence of *N*-ethylmaleimide (NEM) using 25 mM Tris-HCl pH 7.5, 150 mM NaCl, 1% NP-40, 1% sodium deoxycholate and 0.3% SDS. Clarified lysates were then immunoprecipitated with anti-FLAG antibodies. Immunoprecipitates were eluted using a FLAG peptide and the eluates were then resolved by non-reducing (NR) SDS-PAGE and the gel stained with Coomassie Blue. The band corresponding to ATF6α was excised and digested sequentially with trypsin and GluC. The extracted peptides were then analyzed and quantified by LTQ-Orbitrap (Thermo-Fisher) mass spectrometry as previously described using a label-free approach (17). Normalization was achieved by using three ATF6α peptides systematically found in the experiments.

Cytotoxicity and apoptosis assays - Flow cytometry-based analysis of cell apoptosis was performed following staining of the cells with Annexin V-FITC and propidium iodide (PI) using the Annexin V-FITC kit (Beckman Coulter). The extent of apoptosis was quantified as the percentage of Annexin V–positive cells. The extent of Imatinib-induced apoptosis was assessed using the following formula: percent specific apoptosis = (test - control) x 100 / (100 - control). Cell death was assessed using Annexin V-fluorescein isothiocyanate–propidium iodide (Annexin-V FITC Apoptosis Kit**,** Beckman Coulter) according to the manufacturer's protocol. Sulforhodamine B assays were performed as previously described (6).

Statistical analyses - Data are presented as mean ± SEM of three separate experiments and compared using one-way analysis of variance (ANOVA) followed by

Dunnett's multiple comparison tests. The level of significance was set at $P<0.05$. All statistical analyses were performed using GraphPad Prism (version 5) statistical software (GraphPad Software; San Diego, CA).

Results

ER-Resident Proteins regulate the activation of ATF6α in response to ER Stress. To study the mechanism regulating ATF6α export from the ER to the Golgi apparatus and subsequent transport to the nucleus upon ER stress, we transiently expressed FLAG-tagged human ATF6α (FLAG-ATF6α) in Hela cells and determined the localization of ATF6α by immunofluorescence using anti-FLAG antibodies. To examine ATF6α activation under ER stress we used four known ER stress-inducing chemicals, Dithiothreitol (DTT, a reducing agent), Thapsigargin (Tg, a SERCA pump inhibitor), Azetidine-2-carboxylic acid (Azc, a proline analog) or Tunicamycin (Tun, a *N*-glycosylation inhibitor). As expected, ATF6α was exported from the ER to the Golgi apparatus within 30 min and reached the nucleus after 2 h of DTT treatment. As shown in Figure 1A, under basal conditions, ATF6α co-localized with the ER marker Calnexin (CNX) and following 1 h DTT treatment, co-localized with the Golgi complex marker Giantin (**Fig. 1A**). Tg and Tun also induced the translocation of ATF6α (**Fig. S1**), however translocation kinetics was slower compared to DTT treatment. Azc also promotes ATF6α export but had the weakest effect on the trafficking of this transcription factor among the ER inducers used in the screening. Next, to confirm the activation of ATF6α, we examined the cleavage of endogenous ATF6α upon ER stress, an established marker for the activation of molecule. Consistent with immunofluorescence data (**Fig. 1A**), immunoblot analysis showed DTT was the strongest inducer of ATF6α activation (**Fig. 1B** and **1C**).

It has been reported a reduction of intra- and inter-molecular disulfide bonds in ATF6α luminal domain as an underlying molecular event leading to its ER export during ER stress (18). As a consequence, we designed a cell-based siRNA assay against ER resident protein disulfide isomerases (PDIs) and thioredoxins and

foldases to identify the enzyme(s) involved in disulfide bond formation and/or remodeling that are required for ATF6α activation upon ER stress (**Fig. S2A**). Forty-eight hours post-siRNA transfection, the cells were further transfected with the FLAG-ATF6α. Twenty-four hours later, the cells were treated with DTT to induced ER stress for 2 h. These cells were then immuno-stained using anti-FLAG and anti-CNX or anti-Giantin antibodies. Cells expressing FLAG-ATF6α protein (number of cells counted ranged from 350 and 6300; **Fig. 2A**) were analyzed for the presence of tagged-ATF6α in the ER, Golgi complex and nucleus. The percentage of cells displaying both Golgi and nuclear localization of FLAG-ATF6α in each siRNA-transfected cell population was determined and compared to the control siRNA-transfected cells (**Fig. 2A**). Both primary and validation screens revealed that only PDIA5 silencing led to altered export of ATF6α to the Golgi complex upon DTT treatment (**Fig. 2B**). In order to confirm the effect of both PDIA5 siRNAs on their cognate target, we transfected each siRNA into HeLa cells and examined PDIA5 expression using immunoblot (**Fig. S2B**). Transfection of each siRNA (siRNA-1 and siRNA-2) led to significant decrease in PDIA5 expression compared to control siRNA. Both siRNAs neither impacted CNX nor ERK1 expression used as loading standards (**Fig. S2B**).

ER stress-induced ATF6α activation was also monitored using immunoblotting in HeLa cells. This revealed that silencing of PDIA5 using siRNAs used in screen decreased ATF6α cleavage upon DTT treatment (**Fig. 2C** and **Fig. S4A**; white arrowheads), thus confirming the immunofluorescence data. Moreover, the effect of PDIA5 siRNA on ATF6α cleavage was also observed in cells treated with the ER stress inducers Tg and Tun (**Fig. S3** and **Fig S4A**). Furthermore, silencing of PDIA3 or PDIA4 (**Fig. S4C**), two of the most abundant PDIs in the ER, did not affect ATF6α

activation upon DTT treatment (**Fig. S4B**), thus reinforcing the specificity of PDIA5 in this process.

PDIA5 silencing impairs ATF6α transcriptional activity. To confirm the effect of PDIA5 silencing on ATF6α activation and the subsequent impact on the transcriptional activation of ATF6α target genes, we measured mRNA expression levels of ATF6α target genes in control and PDIA5-silenced cells following DTT treatment (1 mM) using quantitative RT-PCR (q-PCR). First, we confirmed that the expression of *Pdia5* mRNA was attenuated by siRNA (**Fig. 3A** and **Fig. S5A**). Then we analyzed the expression of four ATF6α *bona fide* target genes (*Ero1Lβ*, *Grp94*, *Orp150* and *Herpud1*) (1, 25) and three UPR target genes (spliced form of *Xbp1* (*Xbp1s*) and *Xbp1* (*Xbp1u*), *Chop*, *Gadd34*) upon DTT (**Fig. 3A**), Tg or Tun (**Fig S5B**)-induced stress and/or silencing of PDIA5. This revealed that PDIA5 silencing prevented the induction of ATF6α target genes upon ER stress without affecting the induction of the UPR targets, *Chop* and *Gadd34* (**Fig. 3A, C** and **Fig. S5B**). The total amount of *Xbp1*s mRNA decreased upon PDIA5 silencing (data not shown). However, this may account for the fact that ATF6α also regulates the expression of *Xbp1* mRNA (26). This was confirmed by the fact that the induction of *Xbp1* mRNA splicing efficiency upon ER stress remained identical in control and PDIA5-silenced cells (**Fig. 3B**). These results established of the requirement for an intact PDIA5 for the ATF6α activation upon ER stress. To further ensure that the observed effect was effectively due to the absence of PDIA5, a rescue approach was undertaken. To this end a siRNA resistant form of PDIA5 (PDIA5r) was expressed in Hela cells silenced or not for PDIA5 and the expression of PDIA5 evaluated by immunoblot (**Fig. 3D**). As expected, endogenous PDIA5 was silenced upon transfection with the siRNA to

PDIA5 (**Fig. 3D**, lane 2) and the expression of the protein rescued when co-transfecting with the siRNA resistant form (**Fig. 3D,** lane 3). To test whether rescuing PDIA5 expression impacted on ATF6α signaling, DTT-induced expression of *Ero1Lβ* and *Herpud1* mRNA was monitored in cells knocked down for PDIA5 and rescued or not for the expression of this protein (**Fig. 3E**). Again, as shown in Figures S5 and 3A, PDIA5 silencing led to attenuated induction of *Ero1Lβ* and *Herpud1* mRNA expression upon DTT exposure and expression of PDIA5r in the silenced background restored the DTT-mediated induction of both mRNAs (**Fig. 3E**), thereby confirming PDIA5 dependency for ATF6α signaling in Hela cells. Interestingly, overexpression of PDIA5 alone was not sufficient to induce further expression of ATF6α target genes, suggesting that endogenous PDIA5 is not limiting. Finally, the impact of PDIA5 silencing on the expression of BiP protein, whose encoding gene is a major target of ATF6α, was evaluated in response to ER stress. When PDIA5 expression was knocked-down in the cells, the induction of BiP upon ER stress was significantly attenuated compared to control siRNA (**Fig. 4A** and **Fig. S6**), thus indicating that PDIA5 might be indeed required for ATF6α activation and subsequent signaling.

PDIA5-dependent activation of ATF6α is independent of the association with BiP. As BiP has also been shown to control ATF6α export from the ER through a dissociation mechanism (24), we sought to examine if there was any functional interplay between BiP dissociation in PDIA5 effect on ATF6α, to this end the ATF6α/BiP interaction was tested by co-immunoprecipitation. To prevent the export of ATF6α from the ER, and therefore its cleavage, the experiments were carried out in HeLa cells transfected with a dominant negative Sar1 (Sar1DN) construct, a mutant GTPase that prevents ER-to-Golgi traffic (20). Under those circumstances,

BiP associated with ATF6α under basal conditions and released from ATF6α upon DTT treatment (**Fig. 4B**). The same phenomenon was observed in PDIA5-silenced cells, although to a lesser extend (**Fig. 4B** and **C**). This suggests that dissociation of BiP from ATF6α might represent an early step in the ATF6α activation process but not completely sufficient to allow ATF6α export to the Golgi complex.

Modulation of disulfide bonds underlies PlAD5 activation of ATF6α. Since our results showed that the export of ATF6α from the ER was regulated by PDIA5 upon ER stress and since its activation is in part controlled by modulation of disulfide bonds (18), we then evaluated the oligomerization of ATF6α using Non-Reducing (NR) SDS-PAGE and immunoblot (**Fig. 4D**). This revealed that DTT treatment altered dramatically ATF6α oligomeric profile in control cells (**Fig. 4D**, left panel), whereas in PDIA5 siRNA-transfected cells, the high molecular weight forms remained present throughout the stress (**Fig. 4D**, right panel and **Fig. S7**). To evaluate the impact of PDIA5 silencing on the formation of disulfide bond in ATF6α, FLAG-ATF6α was immunoprecipitated and the reduced cysteine-containing peptides C1 and C2 (**Fig. 4E**, left panel) were quantified by mass spectrometry (**Fig. 4E**, right panel). This revealed that both peptides C1 and C2 were found in equivalent amounts in all experimental conditions. However, the amount of C1 and C2 was dramatically decreased in PDIA5-silenced cells (**Fig. 4E**, right panel). This suggests that PDIA5 impacts on ATF6α luminal domain content in reduced cysteines, thereby contributing to its activation process upon ER stress.

PDIA5 modulates ATF6α packaging into COPII vesicles. The coat protein complex II (COPII) is required for packaging of ATF6α and its trafficking from the ER

to the Golgi complex upon ER stress (23). We therefore examined if PDIA5 silencing impacted on ATF6α packaging into COPII vesicles. As previously reported (23) ATF6α budded poorly in the standard control reaction (**Fig. 5A, lane 7**). When DTT (5 mM) was added into the budding reactions, ATF6α packaging into COPII vesicles was enhanced (**Fig. 5A**, **lane 8**), a phenomenon that was greatly suppressed in PDIA5-silenced cells (**Fig. 5A, lane 10**). In control experiments, DTT did not affect ERGIC-53 or Sec22b budding, and did not cause significant Ribophorin-I release, as previously reported in the initial assay (23). Collectively, these results indicate that PDIA5 plays an instrumental role for ATF6α packaging to COPII vesicles. To further reinforce the functional link between PDIA5 and ATF6α, we first evaluated whether the silencing of these two genes impacted on cell's sensitivity to ER stress. As such both PDIA5 and ATF6α silencing increased Tun toxicity with a similar order of magnitude (**Fig S8**). Moreover we tested whether overexpression of the cytosolic part of ATF6α (ATF6α-p50), a constitutively activated form of ATF6α independent of disulfide bond reduction, would rescue PDIA5 silencing-mediated ER stress sensitivity. HeLa cells were transfected with an empty vector or FLAG-ATF6α-p50, and treated with 5 µg/ml Tun or vehicle control for 36 h. The expression of FLAG-ATF6α-p50 was monitored using immunoblot with anti-FLAG antibodies (**Fig. 5B,** bottom panel). The same experiment was repeated in PDIA5- or ATF6α-silenced cells. The results presented in Fig. 5C, show ATF6α-p50 rescued partially stress Tun sensitivity induced upon PDIA5 or ATF6α silencing. These results further support the functional link existing between these two proteins in the UPR.

PDIA5/ATF6α axis modulates sensitivity to Imatinib. ATF6α and PDIA5 have been associated with cell survival and chemoresistance in different tumor types (3, 4).

Using leukemia as a model, we sought to determine the role of this newly identified axis in chemoresistance, a well-defined ER stress inducer. We initially examined the expression of *Pdia5* mRNA in leukemia cell lines, K562 and LAMA (S; sensitive to Imatinib, R; resistant to Imatinib), respectively. Expression of *Pdia5* mRNA was significantly higher in resistant cells than in sensitive cells (**Fig. 6A**) and that it was not induced upon Imatinib treatment (**Fig. 6B**). To evaluate the impact of PDIA5 expression on the resistance phenotype, PDIA5 expression was silenced or not in K562R cells, which were then subjected to Imatinib treatment. Interestingly, PDIA5 silencing in K562R cells partially restored cells' sensitivity to Imatinib to a level comparable to that observed in sensitive cells (**Fig. 6C**). Furthermore this effect was mimicked when using a pharmacological inhibitor of PDI (16F16) (**Fig. 6D**). To test whether overexpression of PDIA5 was functionally linked to ATF6α activation in K562R cells ATF6α expression was knocked-down using siRNA and the subsequent impact on Imatinib sensitivity evaluated. Interestingly, ATF6α silencing partially restored the sensitivity of K562R cells to Imatinib (**Fig. 7A**) and a pharmacological inhibitor of PDI blocked the proteolytic cleavage of ATF6α in those cells, which was found to be constitutive otherwise (**Fig. 7B**). Finally, the co-silencing of PDIA5 and ATF6α further enhanced the sensitivity of K562R cells to Imatinib (**Fig. 7C**), thereby demonstrating the functional relationship of these proteins in the chemoresistance mechanism. This observation was also confirmed in CD34+ leukemia cells from 2 patients (**Fig. 7D**) in which Imatinib sensitivity was enhanced using 16F16, thereby reinforcing the pathophysiological and translational relevance of the PDIA5/ATF6α axis in cancer.

Discussion

The biological role of the UPR in oncogenesis, cancer development and resistance to chemotherapies is well established, however the roles of the three UPR sensors remain unequally documented. In particular the role of ATF6α is yet to be characterized. To define the activation mechanisms of ATF6α in cancer, we designed a siRNA screen aiming at identifying the proteins controlling ATF6α export from the ER. The subsequent results defined a novel ER stress inducible regulatory axis that depends on PDIA5-mediated activation of ATF6α. In this context, and to follow up on our initial aim, we investigated the relevance of this axis to cancer cell phenotypes. Interestingly, PDIA5 was found to be overexpressed in numerous cancers and to be part of a predictive signature of tumor cell resistance to chemotherapy (3, 4), however the mechanisms underlying this observation remain poorly understood. Since ATF6α had previously been associated with tumor cell dormancy (22), a hallmark of chemotherapy resistance, we investigated the role of the PDIA5/ATF6α axis in cancer cell resistance to Imatinib. We showed that genetically or pharmacologically impairing PDIA5 activity restored Imatinib sensitivity in Imatinib-resistant leukemia K562 cells (**Fig. 6** and **7**) and this through an ATF6α dependent mechanism (**Fig. 7** and **Fig. 8**). Thus our data demonstrated the role of the PDIA5/ATF6α signaling axis in leukemia cells resistance to Imatinib. One can anticipate that such results might also be observable in other models of drug resistance in cancer cells.

We further elaborated on the molecular mechanisms underlying this phenomenon. Indeed it is currently accepted that the export of ATF6α to the Golgi apparatus upon ER stress is controlled by the dissociation from ER chaperone BiP (24) and that the remodelling of intra- and intermolecular disulfide bonds formed in the luminal domain

405 of ATF6α is also involved in its activation process (18, 19). We found that PDIA5
406 silencing caused the retention of ATF6α in the ER under stress, thereby indicating
407 that PDIA5 is involved in the ATF6α activation mechanism upon ER stress. Silencing
408 of PDIA5 did not significantly affect the activation of the other arms of the UPR.
409 These results suggest possible mechanisms of PDIA5-dependent reduction of ATF6α
410 including (i) direct reduction that could be further evaluated by the detection of a
411 mixed-disulfide ATF6α-PDIA5 species, or alternatively by *in vitro* catalysis of ATF6α
412 reduction using a reconstituted system, (ii) indirect reduction via hypo-oxidizing ER
413 conditions, which could be assessed by measuring the thiol-disulfide milieu in the ER
414 in control or PDIA5-silenced cells.

415 It has been clearly demonstrated in previous reports that select protein
416 complexes were essential to the fine regulation of IRE1 signaling (10). This protein
417 platform, named the UPRosome, is essential for controlling IRE1-dependent cell fate
418 decisions upon ER stress (9, 11). In view of the results presented herein, one can
419 propose the emergence of the UPRosome as a general concept to regulate the ER
420 stress sensors and consequently the cellular outcome resulting from their activation.
421 In the case of ATF6α, the complex(es) formed with PDIA5 (the present study) and
422 BiP (24) in the ER might represent the first examples of an expanding family of
423 UPRosome platforms controlling UPR function.

424 In the present study, we also show that ATF6α dissociation from BiP, the first
425 event occurring in response to ER stress, is necessary but not sufficient for ATF6α
426 export. Interestingly the BiP binding site on ATF6α on amino acids 467-475 (24) also
427 encompasses a cysteine residue (peptide C2, **Fig. 5D**) that is important for ATF6α
428 activation process ((24) and the present study). The dissociation from BiP could
429 therefore represent an early/upstream event in the process that could occur in

conjunction with cysteine oxidation to favor its activation. Finally, the expression of exogenous ATF6α-p50 is sufficient to rescue the activation deficiency observed upon PDIA5 silencing and the resulting increased sensitivity of cells to ER stress (**Fig. 5**).

In conclusion, our result shed light on novel mechanisms responsible for the control of ATF6α activation through redox mechanisms and contribute to specific ER stress-induced signaling loops (12), and link this mechanism to the yet incompletely understood mechanisms of resistance to chemotherapy. Moreover, this study, by expanding the repertoire of molecular intermediates involved in the regulation of ER stress signaling provides additional druggable targets to bypass resistance to chemotherapy in cancer cells.

Acknowledgements

We thank Dr K. Dejgaard (McGill University, Montreal, Qc, Canada) and the Bordeaux Proteomics Platform for mass spectrometry sequencing. This work was supported by grants from INSERM (Avenir), Ligue contre le Cancer (comité des landes) and Institut National du Cancer (INCa) to EC, a Ulysses/IRCSET grant to EC and JCS, and funds from the Howard Hughes Medical Institute to RS. S.L. was supported by a PhD scholarship from the French government. The author's declare no conflict of interest.

References

1. **Adachi, Y., K. Yamamoto, T. Okada, H. Yoshida, A. Harada, and K. Mori.** 2008. ATF6 is a transcription factor specializing in the regulation of quality control proteins in the endoplasmic reticulum. Cell Struct Funct **33:**75-89.
2. **Arai, M., N. Kondoh, N. Imazeki, A. Hada, K. Hatsuse, F. Kimura, O. Matsubara, K. Mori, T. Wakatsuki, and M. Yamamoto.** 2006. Transformation-associated gene regulation by ATF6alpha during hepatocarcinogenesis. FEBS Lett **580:**184-90.
3. **Beesley, A. H., M. J. Firth, D. Anderson, A. L. Samuels, J. Ford, and U. R. Kees.** 2013. Drug-gene modeling in pediatric T-cell acute lymphoblastic leukemia highlights importance of 6-mercaptopurine for outcome. Cancer Res **73:**2749-59.
4. **Burguillo, F. J., J. Martin, I. Barrera, and W. G. Bardsley.** 2010. Meta-analysis of microarray data: The case of imatinib resistance in chronic myelogenous leukemia. Comput Biol Chem **34:**184-92.
5. **Chevet, E., P. H. Cameron, M. F. Pelletier, D. Y. Thomas, and J. J. Bergeron.** 2001. The endoplasmic reticulum: integration of protein folding, quality control, signaling and degradation. Curr Opin Struct Biol **11:**120-4.
6. **Dejeans, N., O. Pluquet, S. Lhomond, F. Grise, M. Bouchecareilh, A. Juin, M. Meynard-Cadars, A. Bidaud-Meynard, C. Gentil, V. Moreau, F. Saltel, and E. Chevet.** 2012. Autocrine control of glioma cells adhesion and migration through IRE1alpha-mediated cleavage of SPARC mRNA. J Cell Sci **125:**4278-87.
7. **Harding, H. P., Y. Zhang, and D. Ron.** 1999. Protein translation and folding are coupled by an endoplasmic-reticulum-resident kinase. Nature **397:**271-4.
8. **Haze, K., H. Yoshida, H. Yanagi, T. Yura, and K. Mori.** 1999. Mammalian transcription factor ATF6 is synthesized as a transmembrane protein and activated by proteolysis in response to endoplasmic reticulum stress. Mol Biol Cell **10:**3787-99.
9. **Hetz, C.** 2012. The unfolded protein response: controlling cell fate decisions under ER stress and beyond. Nat Rev Mol Cell Biol **13:**89-102.
10. **Hetz, C., and L. H. Glimcher.** 2009. Fine-tuning of the unfolded protein response: Assembling the IRE1alpha interactome. Mol Cell **35:**551-61.
11. **Hetz, C., F. Martinon, D. Rodriguez, and L. H. Glimcher.** 2011. The unfolded protein response: integrating stress signals through the stress sensor IRE1alpha. Physiol Rev **91:**1219-43.
12. **Higa, A., and E. Chevet.** 2012. Redox signaling loops in the unfolded protein response. Cell Signal **24:**1548-55.
13. **Hollien, J., J. H. Lin, H. Li, N. Stevens, P. Walter, and J. S. Weissman.** 2009. Regulated Ire1-dependent decay of messenger RNAs in mammalian cells. J Cell Biol **186:**323-31.
14. **Kim, J., S. Hamamoto, M. Ravazzola, L. Orci, and R. Schekman.** 2005. Uncoupled packaging of amyloid precursor protein and presenilin 1 into coat protein complex II vesicles. J Biol Chem **280:**7758-68.
15. **Malhi, H., and R. J. Kaufman.** 2011. Endoplasmic reticulum stress in liver disease. J Hepatol **54:**795-809.

16. **Moenner, M., O. Pluquet, M. Bouchecareilh, and E. Chevet.** 2007. Integrated endoplasmic reticulum stress responses in cancer. Cancer Res **67:**10631-4.
17. **Mouton-Barbosa, E., F. Roux-Dalvai, D. Bouyssie, F. Berger, E. Schmidt, P. G. Righetti, L. Guerrier, E. Boschetti, O. Burlet-Schiltz, B. Monsarrat, and A. Gonzalez de Peredo.** 2010. In-depth exploration of cerebrospinal fluid by combining peptide ligand library treatment and label-free protein quantification. Mol Cell Proteomics **9:**1006-21.
18. **Nadanaka, S., T. Okada, H. Yoshida, and K. Mori.** 2007. Role of disulfide bridges formed in the luminal domain of ATF6 in sensing endoplasmic reticulum stress. Mol Cell Biol **27:**1027-43.
19. **Nadanaka, S., H. Yoshida, and K. Mori.** 2006. Reduction of disulfide bridges in the lumenal domain of ATF6 in response to glucose starvation. Cell Struct Funct **31:**127-34.
20. **Nakano, A., H. Otsuka, M. Yamagishi, E. Yamamoto, K. Kimura, S. Nishikawa, and T. Oka.** 1994. Mutational analysis of the Sar1 protein, a small GTPase which is essential for vesicular transport from the endoplasmic reticulum. J Biochem **116:**243-7.
21. **Ron, D., and P. Walter.** 2007. Signal integration in the endoplasmic reticulum unfolded protein response. Nat Rev Mol Cell Biol **8:**519-29.
22. **Schewe, D. M., and J. A. Aguirre-Ghiso.** 2008. ATF6alpha-Rheb-mTOR signaling promotes survival of dormant tumor cells in vivo. Proc Natl Acad Sci U S A **105:**10519-24.
23. **Schindler, A. J., and R. Schekman.** 2009. In vitro reconstitution of ER-stress induced ATF6 transport in COPII vesicles. Proc Natl Acad Sci U S A **106:**17775-80.
24. **Shen, J., X. Chen, L. Hendershot, and R. Prywes.** 2002. ER stress regulation of ATF6 localization by dissociation of BiP/GRP78 binding and unmasking of Golgi localization signals. Dev Cell **3:**99-111.
25. **Yamamoto, K., T. Sato, T. Matsui, M. Sato, T. Okada, H. Yoshida, A. Harada, and K. Mori.** 2007. Transcriptional induction of mammalian ER quality control proteins is mediated by single or combined action of ATF6alpha and XBP1. Dev Cell **13:**365-76.
26. **Yoshida, H., T. Matsui, A. Yamamoto, T. Okada, and K. Mori.** 2001. XBP1 mRNA is induced by ATF6 and spliced by IRE1 in response to ER stress to produce a highly active transcription factor. Cell **107:**881-91.

Figure legends

Fig. 1. ATF6α activation assay. (*A*) HeLa cells transfected with FLAG-ATF6α plasmid for 24 h and treated with 1 mM DTT for the indicated time. Cells were then immunostained with anti-FLAG and anti-CNX (for ER) or anti-Giantin (for Golgi) antibodies. Cells were analyzed by confocal microscope. Bars, 10 μm. (*B*) Cleavage of endogenous ATF6α in HeLa cells exposed to DTT (1 mM), Tg (500 nM), Azc (10 mM), Tun (5 μg/ml) as analyzed by immunoblot using anti-ATF6α antibodies. Full length (ATF6α-p90) and cleaved form (ATF6α-p50) of ATF6α indicates as black and white arrowheads, respectively. The asterisk shows the non-glycosylated form of ATF6α. Anti-CNX was used as loading control. (*C*) Time course quantification of ATF6α-p90 and ATF6α-p50 upon treatment with the indicated ER stressor.

Fig. 2. Small interfering RNA screen. (*A*) siRNA-based assay in HeLa cells. Following transfection with siRNAs (25 nM) and FLAG-ATF6α plasmid, the cells were treated with DTT (1 mM) for 2 h and co-stained with antibodies against FLAG and CNX or Giantin. The number of cells with Golgi apparatus and nuclear staining was counted using confocal or epifluorescence microscopes. The percentage of Golgi apparatus and nuclear localization in siRNA-transfected cells was calculated and compared with that in control siRNA-trasnfected cells. Data represented are the mean ±SEM of triplicate experiments (*$p<0.05$ and **$p<0.01$, as compared with control). (n), number of cells counted for each siRNA experiment. (*B*) Secondary screen using alternative siRNA against targets identified in the primary screen. (*C*) siRNAs against PDIA5 were transfected into HeLa cells. Seventy-two hours after transfection, cells were treated with DTT (1 mM) for the indicated periods of time. Cell lysates were analyzed by immunoblotting using anti-ATF6α antibody. ATF6α-p90 and

ATF6α-p50 are indicated with black and white arrowheads, respectively. The white diamond shows a nonspecific protein recognized by anti-ATF6α antibodies. Time course quantification of ATF6α-p90 (left) and ATF6α-p50 (right) upon treatment are shown in lower graphs.

Fig. 3. Effects of PDIA5 silencing on ATF6α target genes and UPR signaling. (*A*) Heat map representation of the expression of ATF6α target genes upon silencing of PDIA5 using siRNA (25 nM) in HeLa cells. Forty-eight hours after transfection cells were treated with 1 mM DTT, 500 nM Tg or 5 µg/ml Tun for 2 h. Total RNA was isolated and analyzed by q-PCR using specific primers for ATF6α target genes (*Ero1Lβ*, *Grp94*, *Herpud1* and *Orp150*). Each mRNA expression was normalized to *Gapdh* mRNA. *(B*) HeLa cells were transfected with siRNA and treated with DTT, Tg or Tun and the splicing of *Xbp1* mRNA was evaluated using RT-PCR. *(C)* RNA was extracted from control or PDIA5-silenced and ER stressed-treated HeLa cells and analyzed by q-PCR using the specific primers *Gadd34*, *Chop* and *Gapdh*. Data of q-PCR are the mean ± SD of three independent experiments (*D*) Hela cells were transfected with siRNA (control (Ctl) or to PDIA5) and further transfected with pcDNA3-PDIA5r or not. Forty-eight hours later, lysates were analyzed by immunoblotting using either anti-PDIA5 or anti-CNX antibodies. The arrowhead shows PDIA5 and the asterisk indicates a non-specific band. (*E*) Cells transfected as in (D) were then treated or not with 1 mM DTT for 2h. RNA was then extracted and the expression of *Ero1Lβ* and *Herpud1* was evaluated by RT-qPCR. Data are presented as the average of three independent experiments ±SEM, *P<0.05.

584 **Fig. 4. Effects of PDIA5 silencing on ATF6α signaling.** (*A*) Seventy-two hours
585 after PDIA5 siRNA transfection, HeLa cells were treated with 1 mM DTT for the
586 indicated periods of time. BiP protein expression was analyzed by immunoblotting
587 using anti-KDEL antibody (upper panels). Anti-CNX antibodies were used as loading
588 control. BiP expression was normalized to CNX expression and quantified as a
589 percentage of the signal at time 0 (right panels, *p<0.05 and **p<0.01, as compared
590 to the signal at time 0). (*B*) HeLa-ATF6α cells were transfected with PDIA5 siRNA for
591 72 h and with Sar1(DN) for 24 h. Cell lysates were prepared from the cells treated
592 with or without DTT (1 mM for 1 h) and immunoprecipitated using anti-FLAG antibody.
593 Immunoprecipitates were resolved by SDS-PAGE and immunoblotted using anti-
594 KDEL and anti-FLAG antibodies. (*C*) Quantification of BiP and FLAG-ATF6α. Mean
595 ±SEM of triplicate experiments is shown (# p<0.03, as compared with control). (*D*)
596 Analysis of ATF6α redox state under conditions of PDIA5 silencing and ER stress.
597 The black diamond shows nonspecific protein. (*E*) Left panel: Schematic
598 representation of ATF6α including the cytosolic domain containing the DNA binding
599 site, the transmembrane domain and the luminal domain with the BiP binding site. In
600 the luminal domain the two cysteine containing peptides as generated by trypsin and
601 GluC proteolytic cleavage are indicated (peptide C1 and C2). Right panel:
602 Quantification of peptide C1 and C2 in HeLa-ATF6α cells transfected with siRNA
603 against PDIA5 under basal conditions. Normalization was performed using three
604 other ATF6α cysteine free peptides identified and quantified in the same
605 experimental conditions.
606
607 **Fig. 5. ATF6α export and PDIA5-mediated sensitivity to ER stress.** (*A*) ATF6α
608 export reconstitution assay. Vesicular fractions obtained in control siRNA-treated

HeLa-ATF6α cells and in cells silenced for PDIA5 for 72 h were analyzed by immunoblotting using anti-ATF6α, anti-Ribophorin I, anti-ERGIC53 and anti-Sec22b antibodies. (*B*) HeLa cells were transfected with empty pcDNA3 vector or pcDNA3-FLAG-ATF6α-p50. Twenty-four hours post transfection, cells were treated with Tun (5 µg/ml) for 36 h. Cell lysates were extracted and analyzed by immunoblot using anti-FLAG antibody. CNX was used as loading control. (*C*) Empty pcDNA3 or pcDNA3-FLAG-ATF6α-p50 were transiently transfected in HeLa cells as in (B). Twenty-four hours post-transfection, cells were treated with 5 µg/ml Tun for 36 h and cell toxicity assay based on SRB staining was performed. Data is shown as the mean of three independent experiments ± SEM (*p<0.05). ns, no significant difference.

Fig. 6: Expression and function of PDIA5 in Imatinib-sensitive and -resistant leukaemia cells. *(A)* Expression of *Pdia5* mRNA in K562 and LAMA cells either sensitive (white bars) or resistant (grey bars) to Imatinib as determined by q-PCR. Data are presented as the average of three independent experiments ±SEM (*p<0.05 and **p<0.01). (*B*) *Pdia5* mRNA expression in Imatinib sensitive (white bars) or resistant (grey bars) K562 cells subjected to Imatinib (10 µM) treatment. Data are presented as the average of three independent experiments ±SD. (*C*) Cell viability in response to 10 µM Imatinib treatment was determined in Imatinib sensitive K562 cells (K562S; white bars) or in Imatinib resistant K562 cells (K562R; black bars) transfected with a control siRNA (siCTL) or with a siRNA against PDIA5 (siPDIA5). Data are presented as the average of three independent experiments ±SEM (**p<0.01). (*D*) Impact of PDIA5 pharmacological inhibition with increasing concentrations of 16F16 on K562R cells' sensitivity to Imatinib. Data are presented as the average of three independent experiments ±SEM.

Fig. 7: Genetic and pharmacological disruption of the PDIA5/ATF6α signalling axis in K562 and patients'-derived leukaemia cells. (*A*) Impact of ATF6α siRNA-mediated silencing on K562R cells' sensitivity to Imatinib. Seventy-two hours after transfection, cells were treated with the indicated concentration of Imatinib for 48 h. Data are presented as the average of three independent experiments ±SEM. *(B)* Impact of PDIA5 pharmacological inhibition with 16F16 on ATF6α proteolytic processing in K562R cells subjected to Imatinib and/or DTT treatment as assessed by immunoblot using anti-ATF6α antibodies. *(C)* Impact of ATF6α and/or PDIA5 siRNA-mediated silencing on K562R cells' sensitivity to Imatinib. Data are presented as the average of three independent experiments ±SEM. *(D)* Impact of PDIA5 pharmacological inhibition with 16F16 on Imatinib sensitivity in three patients'-derived leukaemia lines either sensitive (IMS, CD34-) or resistant (IMR, CD34+) to Imatinib.

Fig. 8: Schematic representation of the role of the PDIA5/ATF6α signalling axis in chemoresistance in leukaemia cells. Arrows represent activation pathways whereas inhibitory mechanisms are represented by T-bars. Dotted lines represent pathways with uncharacterized mechanisms.

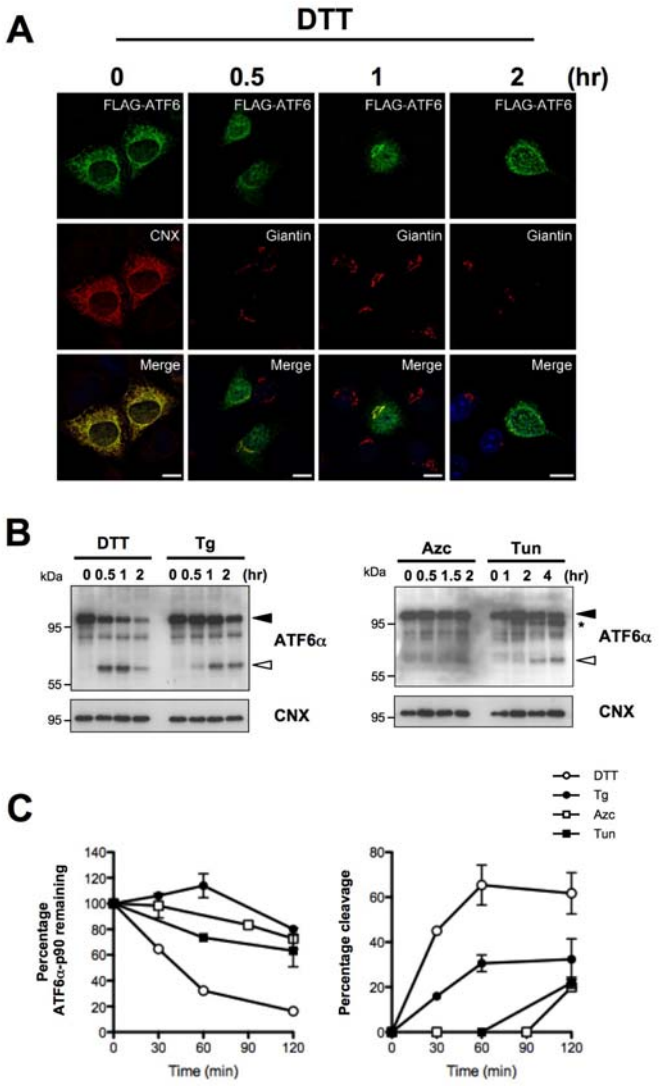

Higa et al._Fig. 1

653

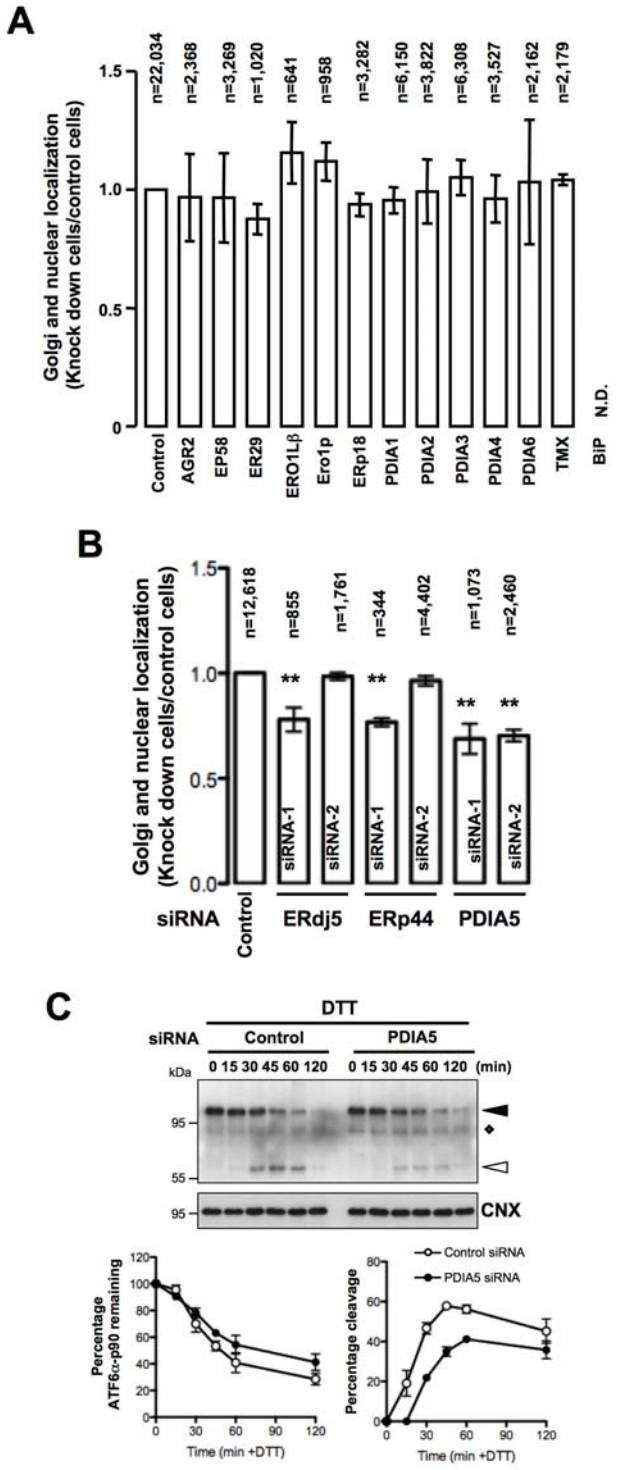

Higa et al._Fig 2

654

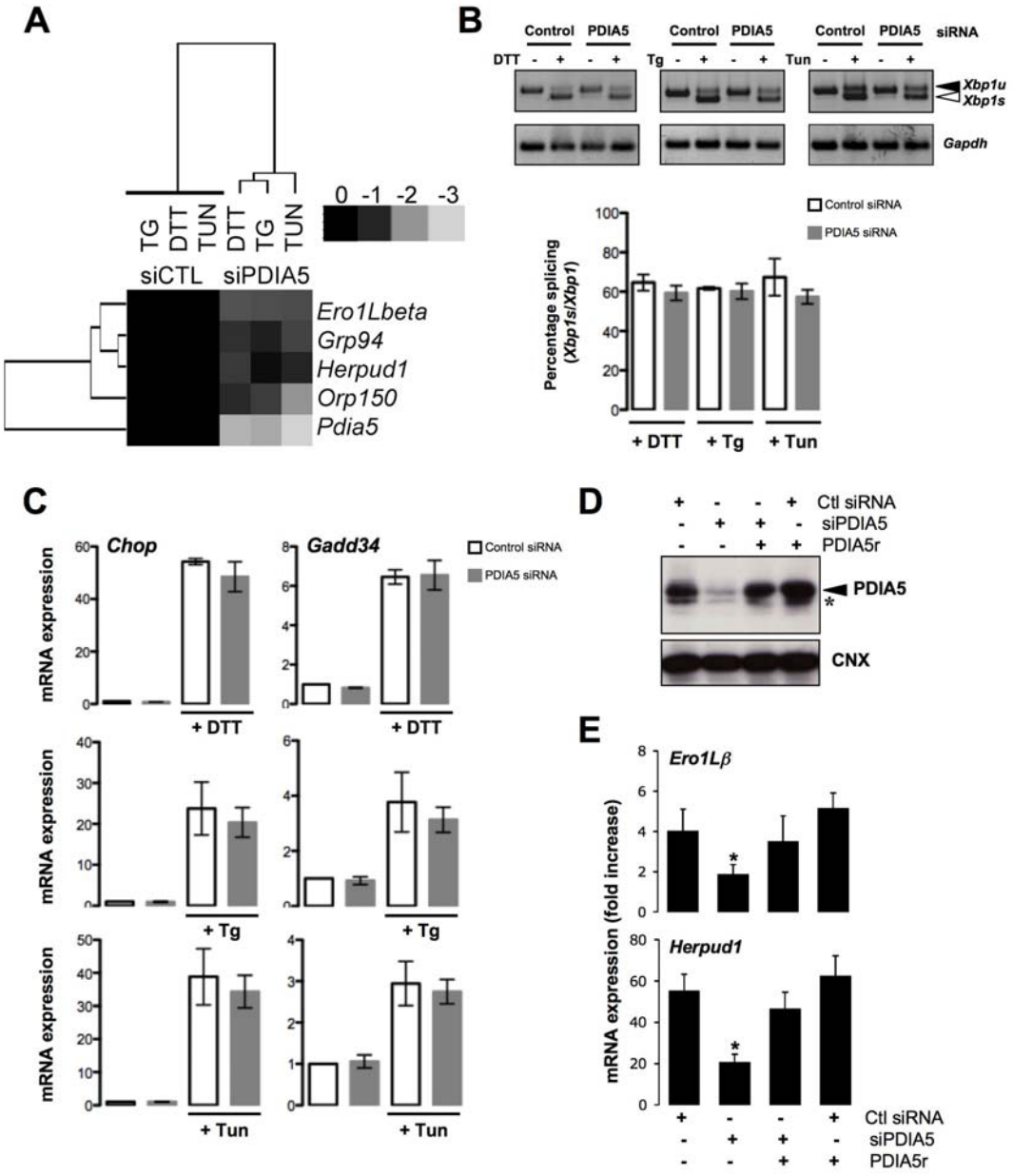

Higa et al._Fig 3

655

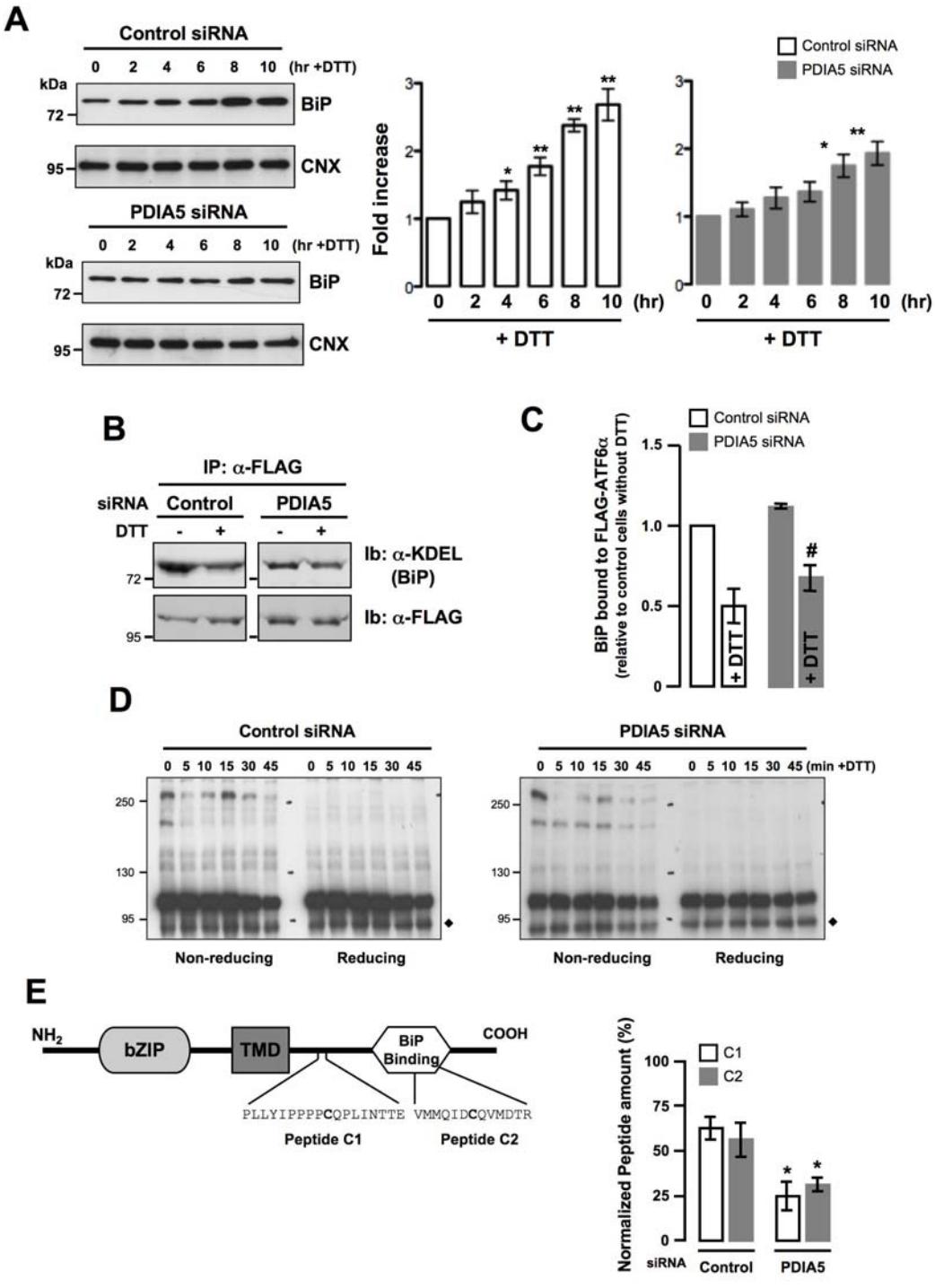

Higa et al._Fig 4

656

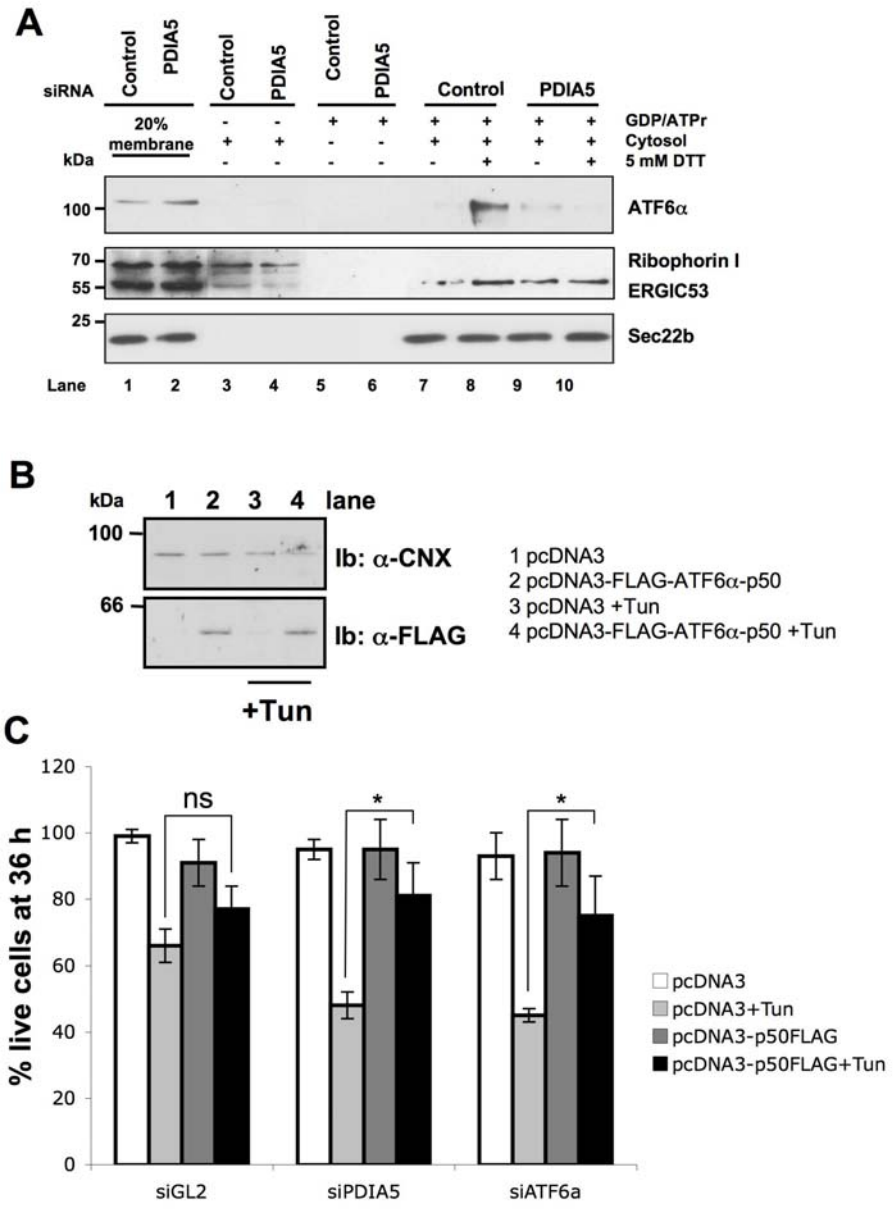

Higa et al._Fig 5

657

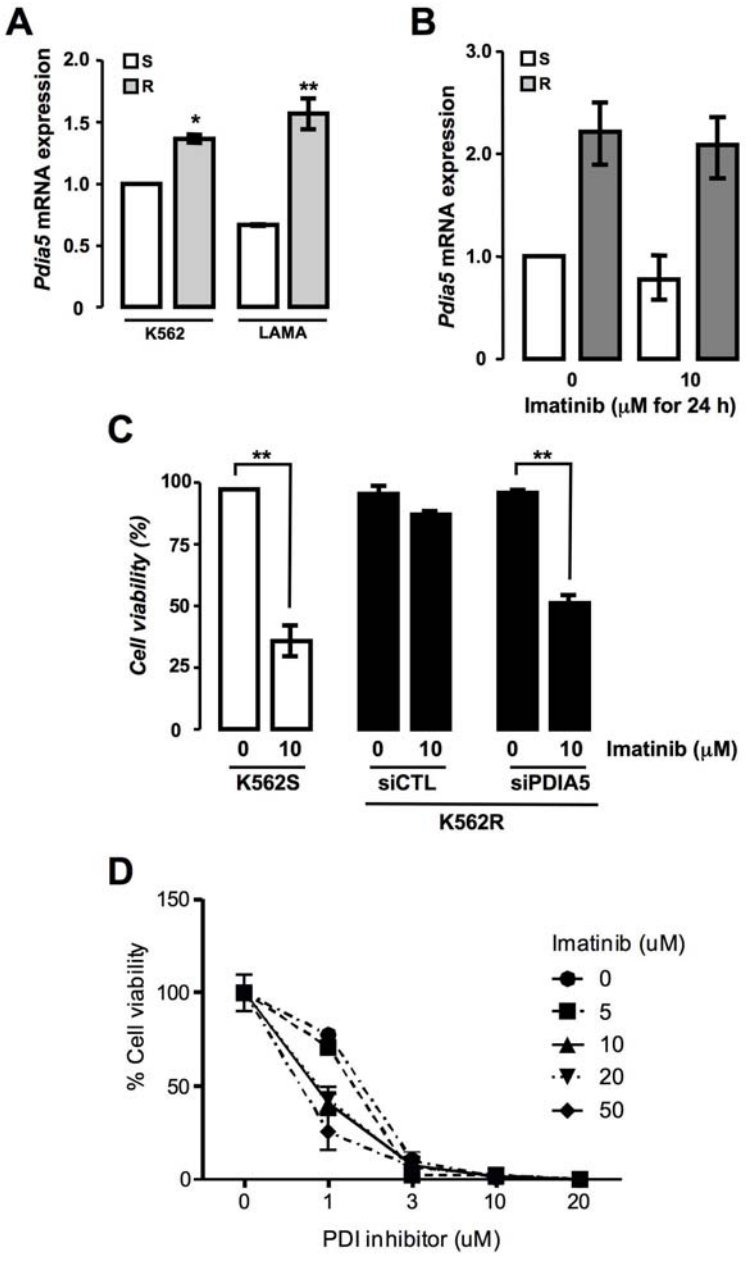

Higa et al._Fig 6

658

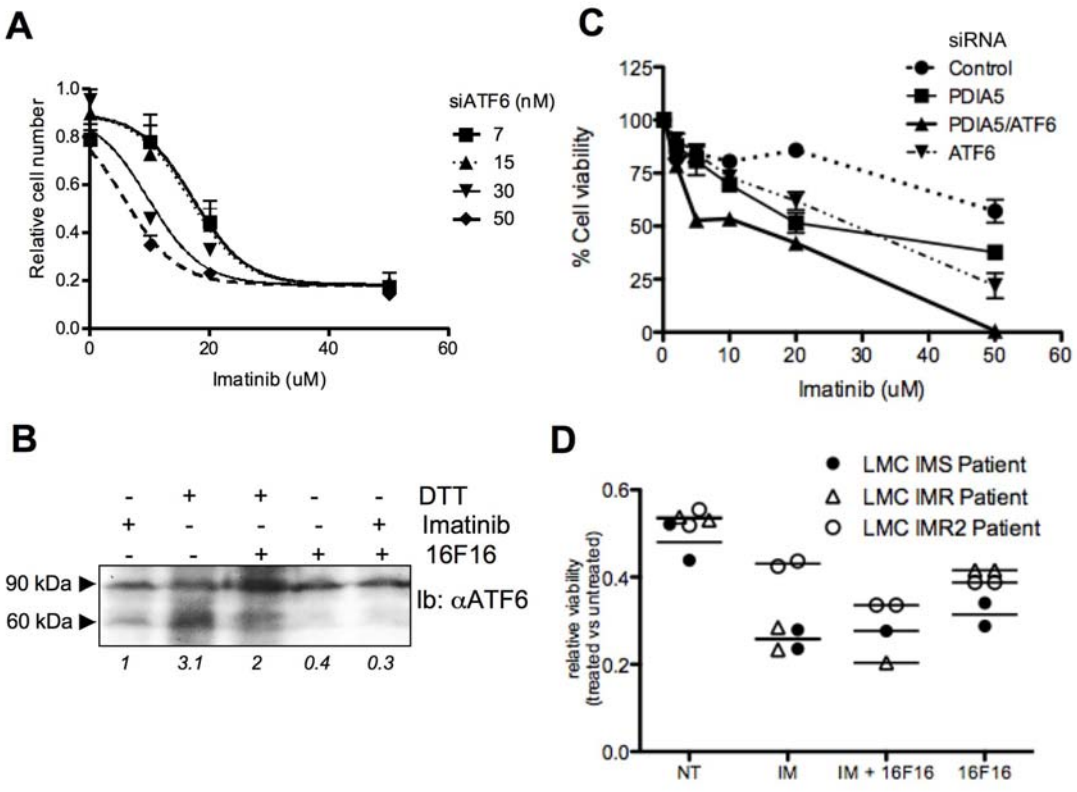

Higa et al._Fig 7

659

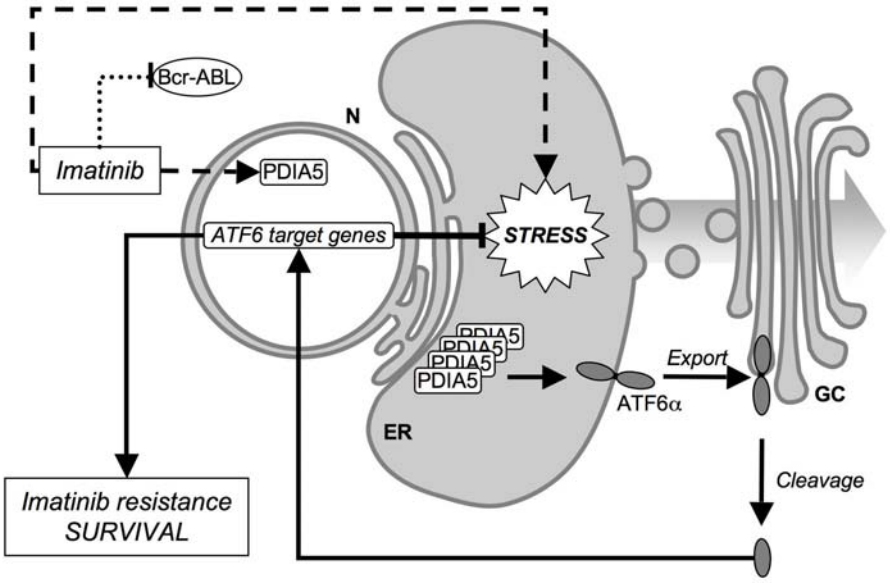

Higa et al._Fig 8

660

661

662